

SHAPING MEAT ANALOGUES

ingredients & texture

Miek Schlangen

SHAPING MEAT ANALOGUES ingredients & texture

Miek Schlangen



Propositions

1. The term "heterogeneous" lacks meaning without specifying a corresponding length scale when describing a product
(this thesis)
2. Concrete knowledge improves meat analogues
(this thesis)
3. A research visit abroad should be a mandatory part of the PhD program
4. To reach a sustainable food system, reducing overconsumption of protein is as important as replacing animal protein by plant protein
5. "*Man serves the interests of no creature except himself*" – George Orwell, is the main explanation for climate change
6. The use of animal products for human consumption is always unethical

Propositions belonging to the thesis, entitled

Shaping meat analogues: ingredients & texture

Miek Schlangen

Wageningen, 26 March 2024

Shaping meat analogues

Ingredients & texture

Miek Schlangen

Thesis committee

Promotor

Prof. Dr A.J. van der Goot

Personal chair at the Laboratory of Food Process Engineering

Wageningen University & Research

Other members

Prof. Dr E. van der Linden, Wageningen University & Research, Wageningen

Prof. Dr K. Schwarz, Christian-Albrechts-Universität, Kiel, Germany

Dr C. Terenzi, Wageningen University & Research, Wageningen

Dr M. Mellema, International Flavors & Fragrances, Hilversum

This research was conducted under the auspices of VLAG Graduate School
(Biobased, Biomolecular, Chemical, Food, and Nutrition sciences)

Shaping meat analogues

Ingredients & texture

Miek Schlangen

Thesis

submitted in fulfilment of the requirements for the degree of doctor

at Wageningen University

by the authority of the Rector Magnificus,

Prof. Dr. C. Kroeze,

in the presence of the

Thesis Committee appointed by the Academic Board

to be defended in public

on Tuesday 26 March 2024

at 1:30 p.m. in the Omnia Auditorium

Miek Schlangen

Shaping meat analogues: ingredients & texture

202 pages

PhD thesis, Wageningen University, Wageningen, the Netherlands (2024)

With references, with summary in English

ISBN 978-94-6447-179-3

DOI <https://doi.org/10.18174/645498>

Table of contents

Chapter 1	General introduction	10
Chapter 2	Dry fractionation to produce functional fractions from mung bean, yellow pea, and, cowpea flour	22
Chapter 3	Mechanical and rheological effects of transglutaminase treatment on dense plant protein blends	48
Chapter 4	How fractionation procedure of mung bean protein affects transglutaminase crosslinking	78
Chapter 5	Quantitative characterizations of visual fibrousness in meat analogues using automated image analysis	106
Chapter 6	Advanced tensile testing as a new tool to quantify properties of food	128
Chapter 7	General discussion	154
	References	176
	Summary	190
	Acknowledgements	194
	About the author	198

In the context of sustainable and ethical food production, we find ourselves in a pressing race against time, where the stakes are high, and the consequences of failure could be severe.



1

Chapter 1

General introduction

Protein-rich foods originating from animals are the major contributor to the environmental impact of food (Aiking, 2014; Aiking & de Boer, 2020). This impact explains the search for alternative food solutions. The research described in this thesis draws inspiration from the need to explore alternatives and focusses on the analysis of ingredients and texture of meat analogues.

This introduction starts with a deep dive into the history of meat analogues. Then, we discuss how the ingredients can be obtained that are required to produce today's meat analogues and how these ingredients should be modified to fit specific applications. Last, we elaborate on the texture of meat analogues and how to quantify those textures.

1.1 The history of meat analogues – from the ‘*first and finest vegetable entree*’ to fibrous, meat-like products

The first commercial meat analogue was produced from a combination of peanut butter and wheat gluten. This innovative canned product, known as Protose, was the brainchild of John Harvey Kellogg, the man behind cornflakes (US Patent No. 670283, 1901). The development of this first meat analogue in the 1890's was driven by the prediction that the increasing world population would ultimately lead to an increase in the price of meat. Besides, Kellogg strongly believed that eating animals was wrong, which further drove his ambition to develop meat-replacing products. Protose

“Combine equal parts peanut butter and wheat gluten, double the amount of water, and a dash of salt, yeast extract, and peanut oil. Steam this dough for approximately three hours and you will have produced the very first commercial meat analogue.”

– Inspired by patent no 670283

gained popularity for its potential to serve as a nutritious alternative to meat, especially during times when meat was scarce or expensive. It is quite remarkable to note that well over a century ago, entrepreneurs like Kellogg were already trying to develop meat analogues driven by partly similar motivations to those we see today. While Kellogg called it “*the first and finest vegetable entree ever developed*”, the question remains whether a canned protein product would be considered tasty or in any way resembled meat following today's standards. Nevertheless, Kellogg's Protose marked an important milestone in the history of meat analogues, acting as a precursor to the development of a new industry of meat analogues.

The history of meat analogues actually started earlier. The first documented reference to a meat analogue dates back to the year 965 (Shurtleff & Aoyagi, 2013) (Figure 1.1). This meat analogue consisted of tofu, which was proposed as a replacement for lamb in China. While this meat analogue was soy-based, the first documented mention of a wheat gluten-based meat analogue was in 1301 (Shurtleff & Aoyagi, 2013). Here, wheat gluten was recommended as the main ingredient to prepare mock lung sausage and mock eel. Additionally, Chinese culinary traditions included recipes for meat analogues using yuba, also known as tofu skin. While these products were referred to as meat analogues, they may not have mimicked animal meat in terms of texture. In this time period, protein intake was most likely more important than texture. These historical references show that meat analogues are not a recent invention, but have been created and consumed for centuries in Asia.

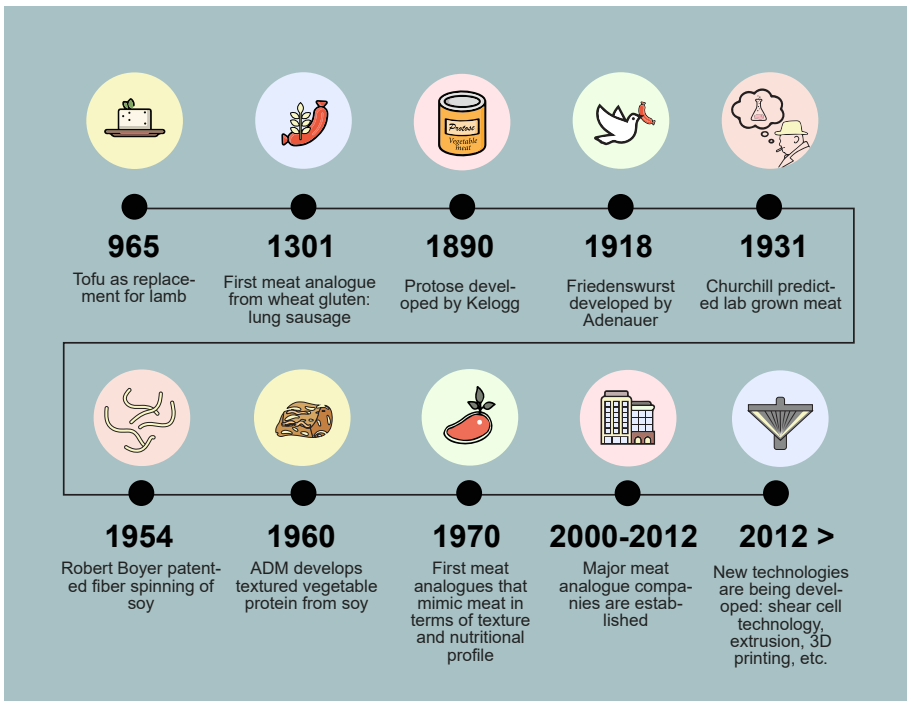


FIGURE 1.1 Schematic illustration of the history of meat analogues

As the 20th century progressed, more individuals and institutions began to investigate the possibilities of meat analogues (Figure 1.1). Konrad Adenauer, who served as the first Chancellor of West Germany, developed the “Friedenswurst” to fight the shortage of food during and after the first World War when he was mayor in Cologne. The sausage was based on mixing minced meat and soy flour. In 1931, Winston Churchill predicted that chicken meat would be lab-grown in the future (Churchill, 1931). During

the second World War, many nations faced severe shortages of meat due to rationing efforts. The scarcity drove governments and food scientists to explore alternatives to meat as a protein source (Warhawk Air Museum, 2019). This time period was therefore crucial for the idea of meat analogues to gain significant attention and investment.

However, it was in the post-war decades of the 1950s and 1960s that the development of meat analogues truly gained momentum (Figure 1.1). It was specifically this time period that texture started to become important and this was intertwined with technological innovations. In 1954, Robert Boyer issued a patent for texturizing soy proteins through fibre spinning, which process was inspired by the creation of textile fibres (US Patent No. 2682466, 1954). This period also saw the birth of textured vegetable protein (TVP) invented by the food processing company Archer Daniels Midland (ADM) in the 1960s (Shurtleff & Aoyagi, 2013). ADM extruded TVP from soy protein in the shape of rods or tubes. Production started in a small pilot plant and was sold to a small number of customers for use in chilli. The product only became successful when it was approved for use in the school lunch programme in 1971. In the 1970s, companies like Quorn and MorningStar Farms started to develop meat analogues that not only resembled meat in terms of taste and texture, but also offered improved nutritional profiles. Innovation in technology therefore opened up the possibility to produce meat analogues with a texture similar to real meat.

Technology has bloomed ever since. Currently, new technologies are being developed to create meat analogues, such as high moisture extrusion cooking (with innovations in die designs (Snel, Bellwald, van der Goot, & Beyrer, 2022) and micro-foaming (Zink, Zeneli, & Windhab, 2023)), shear cell technology (Grabowska, Tekidou, Boom, & van der Goot, 2014), mixing & coagulation (Dobson, Stobbs, Laredo, & Marangoni, 2023), 3D printing (Qiu *et al.*, 2023), and even cell culture (Hubalek, Post, & Moutsatsou, 2022). Technological innovation further bloomed due to Silicon Valley dynamics. Current major players in the meat analogue field, like Beyond Meat and Impossible Foods, were established in 2009 and 2011, respectively (Figure 1.1).

The development of meat analogues from Kellogg's early Protose to the modern plant-based meat analogues demonstrates the drive and innovation in this field. It has not only led to the creation of convincing meat analogues, but has also sustained interest and innovations in the ingredients to produce those products.

1.2 Fractionation of meat analogue ingredients

1

The production of meat analogues requires ingredients, and those ingredients are sourced from plants mostly. Given the objective of producing meat analogues abundant in protein, plants that are relatively high in protein content are mostly considered. Examples of such plants are soy, pea, beans, and lentils. These crops consist of a multitude of valuable components next to protein, such as fats, fibre, and starch. To extract the protein from the other components, fractionation methods can be employed.

Traditionally, the protein is extracted from plants employing wet fractionation processes mostly and is then used in meat analogues as a highly refined protein isolate (>80 wt.% protein on dry matter basis) or a protein concentrate (>60 wt.% protein on dry matter basis). Examples of protein ingredients are soy protein isolate produced from soy and pea protein isolate produced from (yellow) pea. These protein isolates have excellent ingredient functionality for meat analogue applications (Chantanuson, Nagamine, Kobayashi, & Nakagawa, 2022; Dekkers, Nikiforidis, & van der Goot, 2016; Osen, Toelstede, Wild, Eisner, & Schweiggert-Weisz, 2014; Schreuders *et al.*, 2019). Recently, more crops have been explored for their proteins. Mung beans are increasingly regarded as promising plant protein candidates, due to their high protein content and nutritional value. Mung bean protein isolate has already been successfully processed into a textured product through extrusion (Brishti *et al.*, 2021).

The use of highly refined protein isolates and concentrates may sound very promising, but there is a downside to the use of these ingredients. The process required to produce those isolates and concentrates, wet fractionation, can be both costly and environmentally burdening due to its heavy reliance on water, energy, and chemicals (Schutyser & van der Goot, 2011). The exact wet fractionation process depends on the type of raw material processed. Oil seeds are processed differently than starch-bearing crops. In the case of oilseeds, like soy bean, sunflower seed, and canola, the initial step involves removing oil through pressing and solvent extraction. This process yields a press cake containing approximately 30-50 wt.% protein. To further refine the protein in the press cake, an additional purification step using aqueous or alkaline extraction is often employed. This fractionation route typically yields protein isolates with protein contents exceeding 80 wt.% on dry matter basis (Rivera, Siliveru, & Li, 2022). Starch-bearing crops, such as legumes and cereals, are processed following a different wet fractionation approach. After milling, the material is dispersed in water and the starch granules are separated using a hydrocyclone. Next, alkaline extraction and/or acid precipitation are used to purify the protein fraction by removing other components (Boye, Zare, & Pletch, 2010). For oilseed as well as starch-bearing crops, the extracted protein remains in dispersion, introducing the need for a drying step to yield a dry

powder. Usually spray drying is used for this purpose, despite being an energy-intensive process (Lie-Piang, Braconi, Boom, & van der Padt, 2021). Furthermore, the production of protein isolates not only demands significant energy and water consumption, but also generates by-product streams, making it resource-inefficient. Previous studies demonstrated that use of protein isolates leads to protein losses during fractionation of up to 40-50% protein (Tamayo Tenorio, Kyriakopoulou, Suarez-Garcia, van den Berg, & van der Goot, 2018). Thus, the use of protein isolates obtained through wet fractionation exerts a negative influence on the sustainability of meat analogues produced from those ingredients. Hence, there is a need for the development of novel fractionation methods for more effective use of raw materials.

Fractionation tailored for specific end use is a key factor to make a next step in the development of meat analogues. Recent research revealed that complete isolation of protein is not always necessary (Grabowska *et al.*, 2016; Jia, Curubeto, Rodríguez-alonso, Keppler, & van der Goot, 2021; Saldanha do Carmo *et al.*, 2021). The formation of a fibrous texture in meat analogues, for example, requires a multiphase mixture (van der Sman & van der Goot, 2023). Additionally, from a health perspective, meat analogues serve as a source of protein, but could also deliver fat and fibres. The latter are all naturally present in pulses and legumes. Thus, partial fractionation, through process combinations such as milling, sieving, and/or air classification, might be sufficient instead of full purification by wet fractionation.

Protein in starch-bearing crops can be extracted through partial fractionation procedures, such as dry fractionation. Dry fractionation has been successfully applied to extract proteins from legumes (Assatory, Vitelli, Rajabzadeh, & Legge, 2019; de Angelis, 2021; Rivera *et al.*, 2022; Saldanha do Carmo *et al.*, 2020; Schutyser, Pelgrom, van der Goot, & Boom, 2015; Xing *et al.*, 2020) and cereals (Hernández-Álvarez, Mondor, & Nosworthy, 2023; Silventoinen, Rommi, Holopainen-Mantila, Poutanen, & Nordlund, 2019; Silventoinen, Sipponen, Holopainen-Mantila, Poutanen, & Sozer, 2018). Dry fractionation is done in several ways, but the first step is always milling of the raw materials. During milling, the matrix is broken up into smaller fragments and starch granules are liberated from the matrix (Möller, van der Padt, & van der Goot, 2021). The milling step is then followed by a fractionation step, such as sieving, air classification, or electrostatic separation. Sieving is based on particle size separation only. In air classification, an air flow induces centrifugal and gravitational forces inside a classifier chamber, separating the feed flour into a fine and a coarse fraction (Assatory *et al.*, 2019). Air classification is thus based on a size and density difference between starch granules and protein bodies. In electrostatic separation, an electric field is applied to separate the feed material based on differences in dielectric properties. This technique is mostly used to separate protein-rich particles from fibre-rich particles (Assatory *et al.*, 2019).

Dry fractionation leads to protein-rich fractions that still contain carbohydrates. The nutritional implications of incorporating carbohydrates into meat analogues remain debatable. On one hand, the inclusion of carbohydrates in the form of starch can increase blood sugar levels after a meal, which is generally regarded as an unhealthy outcome (Anderson *et al.*, 2009). On the other hand, inclusion of carbohydrates, especially the dietary fibres, can contribute to more balanced diets and reduced caloric consumption for consumers with a non-vegetarian diet (Svihus & Hervik, 2016).

The functionality of dry fractionated proteins is different compared to that of protein isolates. Dry fractionated proteins can be preferred in case the other components enhance the functionality of the protein-rich ingredient. Besides composition, also the state of the protein will depend on the fractionation process applied. During wet fractionation, specifically during the drying step to remove water at the end of the process, the proteins are exposed to high temperatures, which can compromise their native protein structure (Schutyser & van der Goot, 2011). In dry fractionation no drying is necessary, completely avoiding the denaturation of the proteins.

1.3 Improving the functionality of meat analogue ingredients

To overcome the possible functionality limitations of protein-rich fractions, several strategies exist to modify the properties of these fractions to better fit certain applications. One strategy to tune the properties of plant proteins is to employ heat treatment or toasting. For example, dry heating of faba bean protein fractionated through milling and air classification at temperatures from 75 to 175 °C resulted in higher water holding capacity and less soluble protein (Bühler, Dekkers, Bruins, & Goot, 2020). In this way, dry heating of the faba bean protein-rich fraction resulted in comparable properties to commercial soy protein concentrate recovered through wet fractionation.

Another route is to modify the proteins through enzymatic treatment. Previously, it was already shown that enzymes like transglutaminase can be employed to crosslink different plant proteins, such as soy, yellow pea, and Bambara groundnut (Djoullah, Djemaoune, Husson, & Saurel, 2015; Djoullah, Husson, & Saurel, 2018; Liu *et al.*, 2021; Ruzengwe, Amonsou, & Kudanga, 2020; Sun & Arntfield, 2011). The reactivity of such enzymes depends on protein structure, and is thus intertwined with fractionation pathways.

The introduction of dry fractionated proteins into meat analogues may potentially alter the texture of those products compared to the traditional protein isolates used

in meat analogues. But even outside of dry fractionated proteins, it is crucial to gain a deeper understanding of meat analogue texture to enhance their overall quality and organoleptic experience. To address this, we have to delve further into the comprehensive characterization of material textures.

1.4 Texture characterization of meat analogues

Texture in meat analogues started to become important from the 1950s onwards, when technological innovation sky-rocketed. The creation of texture and the analysis of the obtained texture has been studied intensively ever since. An internal structure that mimics the structure animal meat is considered as a key success factor for those products (Michel, Hartmann, & Siegrist, 2021). The development of meat analogues with animal meat-like texture, however, highly requires the detailed characterization of texture.

Characterization of the texture of meat analogues can be done by sensory methods as well as instrumental methods (Schreuders, Schlangen, Kyriakopoulou, Boom, & van der Goot, 2021). Sensory methods are expensive, time-consuming, and often qualitative. Therefore, instrumental methods are regularly used for more objective information on the internal texture of meat analogues. These instrumental methods can be divided into mechanical, spectral, and imaging techniques (Schreuders *et al.*, 2021).

Imaging techniques are primarily used to characterize macro- and microstructure of meat analogues. On a macroscale, the current practice is to rely on visual examinations of the fibrous structures of meat analogues by folding it manually to expose the inner structure. While presenting images of the internal structures serves as a straightforward and efficient method to compare fibrousness of meat analogues, it is a subjective analysis. Thus, a quantitative method for visual structure characterization of meat analogues at the macroscale is lacking. With regards to microstructure, microscopy methods (such as scanning electron microscopy, confocal laser scanning microscopy, and atomic force microscopy) have been employed to characterize fibrous regions in meat analogues (Schreuders *et al.*, 2021).

Mechanical techniques, such as tensile tests, compression tests, and Warner Bratzler tests, have been primarily used to characterize the macroscopic properties of meat and to analyse meat analogues also. Specifically tensile testing has been used frequently to describe anisotropy in high temperature shear cell products (Dekkers *et al.*, 2016; Schreuders *et al.*, 2019; Taghian Dinani, Charles Carrillo, Boom, & van der Goot, 2023; Taghian Dinani, van der Harst, Boom, & van der Goot, 2023). In the case of meat, the ratio between tensile parameters along the parallel and perpendicular directions to

the fibre orientation offers insight into the anisotropy of the structure (Barbut, 2015). This explains why soy protein isolate-pectin blends were previously shown to exhibit anisotropy indices higher than 1 (Dekkers *et al.*, 2016). However, previous research showed that mechanical anisotropy does not always agree with visual observations of the products (Schreuders *et al.*, 2019).

Spectroscopy techniques can offer insight into the local composition, intermolecular interactions, and anisotropy of meat analogues (Schreuders *et al.*, 2021). Fourier Transform Infrared, Near-Infrared, Mid-Infrared, Nuclear Magnetic Resonance, and Raman spectroscopy have been previously used to quantify composition and secondary protein conformation in meat and meat analogues. Fluorescence polarization and light reflectance are indirect spectroscopy techniques that have the capability to assess the visual fibrousness of meat analogues (Ranasinghesagara, Hsieh, Huff, & Yao, 2009; Ranasinghesagara, Hsieh, & Yao, 2005, 2006). The specific alignments of fibres lead to distinct patterns of light reflectance and fluorescence polarization.

Most of these techniques focus on a single length scale and do not capture the texture of meat analogues across the full spectrum or in an objective manner. There is still a need for a clear characterization method for the internal structure and/or texture of meat analogues.

1.5 Aim and outline of this thesis

The aim of this thesis was to investigate the potential of dry fractionation as a route to produce protein-rich ingredients for meat analogue product applications (Figure 1.2). The thesis aim can be divided into three objectives, which are:

1. To investigate dry fractionated ingredients from mung bean, yellow pea, and cowpea for meat analogue applications;
2. To investigate the potential of enzymatic crosslinking to enhance functional properties of mung bean and yellow pea protein;
3. To quantify textural and mechanical properties of fibrous products.

To do so, protein-rich fractions are produced through dry fractionation and further modified by enzyme treatment. Additionally, visual and mechanical characterization of meat analogues is performed.

In **Chapter 2**, dry fractionation of mung bean, yellow pea, and cowpea is investigated as a route to produce protein-rich fractions. The composition and functional properties of the different crops are compared. We know from literature that protein-rich

fractions exhibit a different functionality compared to protein isolates, which explains the further research towards tuning the properties of the fractions for application into meat analogues. Therefore, in **Chapter 3**, we study the effect of transglutaminase crosslinking on mechanical and rheological properties of protein isolate model systems. As enzyme kinetics are highly dependent on protein structure, we investigate and propose crosslinking mechanisms of transglutaminase in relation to the protein fractionation pathway applied in **Chapter 4**.

Chapter 5 describes how the visual internal structure of meat analogues can be quantified through computer vision. In **Chapter 6**, a novel and optimized tensile testing method is proposed to unravel mechanical differences in fibrous structures of meat analogues. **Chapter 7** gives a critical discussion and future outlook, additionally we speculate on what exactly is ‘fibrous’ in terms of meat analogues.

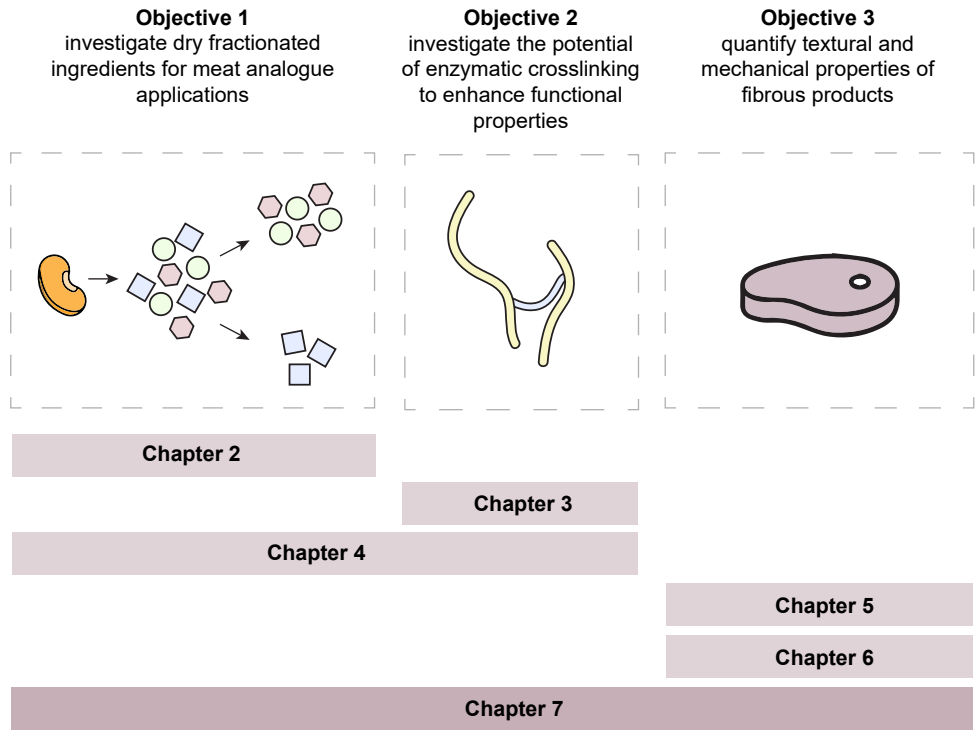


FIGURE 1.2 Schematic illustration of the outline of the thesis.



2

Chapter 2

Dry fractionation to produce functional fractions from mung bean, yellow pea, and cowpea flour

This chapter has been based on the publication: Schlangen, M., Taghian Dinani, S., Schutyser, M.A.I., van der Goot, A.J. (2022) Dry fractionation to produce functional fractions from mung bean, yellow pea, and cowpea flour. *Innovative Food Science & Emerging Technologies*, 78, 103018.

Abstract

Dry fractionation of mung bean, yellow pea, and cowpea was performed to investigate the compositions and functional properties of the obtained fractions. Dry fractionation consisted of milling and subsequent air classification using three air classifier wheel speeds. Water holding capacity, gelation, and rheological properties of all fractions were studied. Separation between protein and starch granules was successfully performed by air classifying, as visualized with scanning electron microscopy images. Protein contents in fine fractions ranged from 42% to 58% (w/dw), which was dependent on classifier wheel speed and material source. The correlation between water holding capacity and protein content was dependent on material source. Gelation of fine fractions occurred at lower concentrations than flours and coarse fractions. Fine fractions of all materials formed gels with higher elastic modulus (G') than the flour and coarse fractions, while the flour and coarse fractions formed more solid-like gels (lower $\tan \delta$).

2.1 Introduction

The shift in the consumption of animal-based products to plant-based products requires the creation of high quality plant-based food products including meat analogues and dairy alternatives. These plant-based food products are most often produced from soy, because of its favourable functional properties (Day & Swanson, 2013; Schreuders *et al.*, 2019). Recently, the potential of yellow pea was shown as an alternative to soy as a major component of plant-based products (Osen, Toelstede, Wild, Eisner, & Schweiggert-Weisz, 2014; Schreuders *et al.*, 2019; Vogelsang-O'Dwyer, Zannini, & Arendt, 2021). The interest in yellow pea originates from the fact that it is less connected to genetically modified organism questions, less allergenic, high in nutritional value, highly available, and is cultivated in moderate climates compared to soy (Lam, Can Karaca, Tyler, & Nickerson, 2018). Yellow pea is used in different types of plant-based products commercially, such as dairy alternatives and meat analogues. Next to yellow pea, mung bean also gained interest as a source for proteinaceous ingredients. Mung bean is mainly used in Asia for its high starch content and quality, but recently mung beans are considered more sustainable and inexpensive to cultivate in comparison to soy (Brishti *et al.*, 2017). Mung bean protein isolate is suggested to be applicable in multiple plant-based products such as egg replacers and meat analogues (Brishti *et al.*, 2021; US 2017 / 0238590 A1, 2017). Cowpea is one of the most important legumes in African countries and also a nutritious and strategic candidate for incorporation into food products (Asif, Rooney, Ali, & Riaz, 2013; Carneiro da Silva *et al.*, 2019; Kebede & Bekeko, 2020; Kethireddipalli, Hung, McWatters, & Philips, 2002; Prinyawiwatkul, McWatters, Beuchat, & Phillips, 1996). Cowpea is nowadays used as the main high-protein ingredient to produce the deep-fried paste called Akara (McWatters, 1983; Mofoluke, Olusegun, Adeoye, Ramota, & Toyin, 2013). In this study, mung bean, yellow pea, and cowpea are compared on their functional properties.

Protein ingredients from legumes, which are currently used in plant-based food products, are classified as protein isolates. Protein isolates are produced by wet fractionation, mainly with extraction under alkaline or acidic conditions, iso-electric precipitation, and spray drying (Boukid, Rosell, Rosene, Bover-Cid, & Castellari, 2021). While this method often yields isolates with high protein contents, the process requires large amounts of water and energy (Schutyser & van der Goot, 2011). Additionally, wet fractionation alters the protein functionality due to the processing conditions used, such as high temperature during drying and large shifts in pH (Vogelsang-O'Dwyer *et al.*, 2021; Zhu, Tang, Cheng, Li, & Tong, 2021). Dry fractionation, as an alternative to wet fractionation, produces protein-rich fractions through milling and subsequent air classification of legumes. Milling fragments the cotyledon cells of legumes, thereby

liberating the starch granules from the surrounding matrix that contains smaller protein bodies and fibres (Möller, van der Padt, & van der Goot, 2021). Subsequently, air classification is used to separate the protein particles from the starch granules based on their density. Previous research showed that dry fractionation of mung bean, yellow pea, and cowpea can yield a protein content (dry based) of up to 55.6 w/dw%, 62.3 w/dw%, and 51.3 w/dw% respectively, but did not analyse the functionality of the resulting ingredients (Pelgrom, Boom, & Schutyser, 2015; Tyler, Youngs, & Sosulski, 1981; Zhu, Wang, Cheng, Li, & Tong, 2020).

Dry-enriched pulse protein ingredients have a different functionality than protein isolates due to their composition and processing history (Schutyser & van der Goot, 2011; Vogelsang-O'Dwyer *et al.*, 2021; Zhu *et al.*, 2021). While there is relatively a lot of knowledge on the process of dry fractionation and the resulting composition of the materials, their functional properties are mostly unexplored. Previously, Funke, Boom, & Weiss (2022) showed that there were no noteworthy differences in emulsification behaviour in different fractions with similar protein content produced from lentil. However, they found that rheological properties of the formed emulsions were dependent on the protein content of the fractions. (Funke *et al.*, 2022). Also for other food products, such as meat analogues, it is important to understand the functional properties of protein-rich fractions (Kyriakopoulou, Dekkers, & van der Goot, 2019). Therefore, the next step is to focus on the composition – functionality relationship of fractions produced by dry fractionation.

In the present study, we first report on the particle size, morphological and compositional changes of mung bean, yellow pea, and cowpea throughout the dry fractionation process. We then aim to study the differences and similarities in functional and rheological properties of dry fractionated ingredients from mung bean, yellow pea, and cowpea. The research question to be answered in this paper is “How are composition and functionality related in fractions of mung bean, yellow pea, and cowpea produced by dry fractionation”. We hypothesize that dry fractionation of mung bean, yellow pea, and cowpea can yield protein-rich fractions with interesting functional properties for future application in plant-based food products.

2.2 Materials & methods

2.2.1 Materials

Dehulled mung beans (*Vigna radiata*) and dehulled yellow peas (*Pisum sativum L.*) were obtained from Vladex (Middelharnis, the Netherlands). Whole cowpeas (*Vigna unguiculata*) were obtained from African Food Products (Unidex B.V. Hillegom, the Netherlands). Flour from mung bean, yellow pea, and cowpea had an average dry matter content of 91.5 wt%, 90.8 wt%, and 90.3 wt%, respectively.

2.2.2 Milling & air classification

The method for milling and air classification was adopted from Möller *et al.* (2021) & Pelgrom, Vissers, Boom, & Schutyser (2013). Specifically, for flour preparation, the legumes were pre-milled into grits with a pin mill (LV 15M, Condux-Werk, Wolfgang bei Hanau, Germany). Then, the grits were milled into flour with a ZPS50 impact mill (Hosokawa-Alpine, Augsburg, Germany). The ZPS50 mill speed was 8000 rpm and the classifier wheel speed of the mill was 4000 rpm. During milling, the air flow was 52 m³/h and the feed rate was ~500 g/h. The minimum batch size used was 900 g.

The legume flours were separated into fine (protein-rich) and coarse (starch-rich) fractions by air classification with an ATP50 classifier (Hosokawa-Alpine, Augsburg, Germany). In this step, the air flow was fixed at 47 m³/h and the feed rate was set at ~0.25 kg/h. Moreover, three classifier wheel speeds of 8000, 10000, and 12000 rpm were applied for the production of fine and coarse fractions from mung bean, yellow pea, and cowpea with varying compositions. The loss in overall dry matter content during air classification was 20, 14, and 10% for mung bean, 27, 13, and 43% for yellow pea and 14, 13, and 25% for cowpea at classifier wheel speeds of 8000, 10000, and 12000, respectively.

2.2.3 Compositional analyses of flour, fine fractions, and coarse fractions

The dry matter content of the flour, fine fraction, and coarse fraction was determined by drying around 1 gram of sample overnight in an oven (Binder GmbH, Tuttlingen, Germany) at 105 °C.

The protein content of the flour, fine fraction, and coarse fraction was measured using a Rapid N Exceed Dumas (Elementar, Langenselbold, Germany) in duplicate. Moreover, the nitrogen conversion factors of mung bean, yellow pea, and cowpea flour

and fine fractions were determined based on their amino acid composition patterns (Table 2.1). These amino acid patterns were determined by a validated method based on ISO-13903:2005. In this method, samples were oxidized with performic acid to stabilize cysteine and methionine, before overnight hydrolysis in 6 mol/L hydrochloric acid. Subsequently, the samples were separated by anion-exchange chromatography and detected after post-column derivatization with ninhydrin by an L-8900 amino acid analyser (Hitachi, Tokyo, Japan). Norvaline served as an internal standard for quantification. Tryptophane was determined by a validated method based on ISO-13904:2005. With 5-methyltryptophane as an internal standard, samples were hydrolysed in a saturated barium hydroxide solution under nitrogen in an autoclave. Tryptophane and the internal standard were determined by reversed-phase HPLC with fluorescence detection. The nitrogen conversion factors were calculated by dividing the combined weight of all amino acid residues by the combined nitrogen content of all amino acid residues. Table 2.1 shows the nitrogen conversion factors used for mung bean, yellow pea, and cowpea ingredients which were 5.7, 5.5, and 5.7, respectively.

The starch content of the flour, fine fraction, and coarse fraction was analysed with the Megazyme Starch Assay Kit (Megazyme International Ireland Ltd, Bray, Ireland).

Dimensionless protein and starch contents were calculated by Eq. 2.1 for an increase and Eq. 2.2 for a decrease:

$$\hat{c} = \frac{c - c_{flour}}{100 - c_{flour}} \quad (\text{Eq. 2.1})$$

$$\hat{c} = -\frac{c - c_{flour}}{0 - c_{flour}} \quad (\text{Eq. 2.2})$$

where \hat{c} is the dimensionless protein or starch content, c is the concentration of protein or starch in the fraction, c_{flour} is the concentration of protein or starch in the initial flour.

2.2.4 Particle size analysis

The particle size distribution of mung bean, yellow pea, and cowpea flour and fractions was determined with a Mastersizer 3000 (Malvern Instrument Ltd., Worcestershire, UK) equipped with a dry dispersion unit (Aero S, UK). A dispersion pressure of 4 bar was applied and the volume-weighted particle size distribution was estimated using laser diffraction (Mie theory). The particle size distribution of each sample was measured 5 times and was expressed as D [4,3], also known as volume moment mean.

2.2.5 Scanning electron microscopy

The mung bean, yellow pea, and cowpea flour and fractions were visualized using a scanning electron microscope with secondary electron detection (JCM-7000 NeoScope, JEOL Ltd., Tokyo, Japan). Powder samples were sputter-coated with a gold layer. Next, the coated samples were placed into the microscope chamber for observation. The acceleration voltage was set at 10.0 kV and the magnification used was between 450x and 750x.

2.2.6 Water holding capacity (WHC)

A high water holding capacity of an ingredient is often desirable in food applications. Water holding capacity of all flours and fractions was determined following the method described by Geerts, Dekkers, van der Padt, & van der Goot (2018). For all flours and fractions, a 2% (w/v) dispersion in demineralised water was agitated overnight in a centrifuge tube at ambient temperature. The dispersion was then centrifuged (Syrvall Lynx 4000, Thermo Scientific, Waltham, United States) at 10,000 rpm and 25 °C for 30 min to separate the pellet and the supernatant. The pellets were weighed and subsequently dried overnight at 105 °C to measure the dry matter content. The water holding capacity was determined according to Eq. 2.3. All the measurements were performed in triplicate.

$$\text{WHC} \left(\frac{\text{g water}}{\text{g dry sample}} \right) = \left(\frac{M_{\text{wet pellet}} - M_{\text{dry pellet}}}{M_{\text{dry sample}}} \right) \quad (\text{Eq. 2.3})$$

where M is the weight of the pellets or samples.

2.2.7 Least gelation concentration (LGC)

A low gelation concentration of an ingredient can be beneficial from both an economic and sustainability point of view. Therefore, the least gelation concentration (LGC) of the flour and fractions was measured based on a method by Adebawale & Lawal (2003). Dispersions of 2 w/w% to 20 w/w% were made with demineralized water in 15 mL tubes. The dispersions were heated in a water bath (TW8, Julabo GmbH, Seelbach, Germany) at a temperature of 90 °C for 1 hour, rapidly cooled in a bath of cold water and further cooled in a fridge at 4 °C for 2 hours. The LGC was determined as the concentration when the sample from the inverted tube did not slip or fall. All the measurements were performed in triplicate.

TABLE 2.1 Amino acid compositions and nitrogen conversion factors of flour and fine fraction from mung bean, yellow pea, and cowpea. In this table, data is shown as the mean \pm standard deviation. Moreover, in each row, means with different lower case letters indicate significant differences, where * indicates a significant difference of $p < 0.05$, ** indicates a significant difference of $p < 0.01$ and *** indicates a significant difference of $p < 0.001$. AA: amino acid.

Amino acids		Mung bean (mg AA/g protein) Flour	Yellow pea (mg AA/g protein) Flour
Hydrophilic	Arginine ***	65.54 \pm 0.28 ^c	83.62 \pm 0.29 ^a
	Asparagine & Aspartic acid*	108.91 \pm 0.00 ^a	107.04 \pm 0.29 ^{ab}
	Glutamine & Glutamic acid **	165.93 \pm 0.56 ^a	161.42 \pm 0.58 ^{ab}
	Histidine ***	24.75 \pm 0.28 ^d	20.96 \pm 0.00 ^f
	Lysine ***	67.72 \pm 0.56 ^b	70.67 \pm 0.00 ^a
	Serine ***	49.31 \pm 0.28 ^c	46.23 \pm 0.29 ^d
	Threonine ***	32.08 \pm 0.00 ^d	35.13 \pm 0.29 ^b
	Tyrosine ***	29.90 \pm 0.28 ^d	33.69 \pm 0.00 ^a
	SUM*	544.14 \pm 1.12 ^{bc}	558.82 \pm 1.74 ^a
Hydrophobic	Alanine **	40.59 \pm 0.28 ^a	40.47 \pm 0.29 ^a
	Cysteine ***	6.14 \pm 0.28 ^c	12.33 \pm 0.00 ^a
	Glycine ***	33.86 \pm 0.28 ^d	40.28 \pm 0.00 ^a
	Isoleucine **	41.58 \pm 0.00 ^a	40.88 \pm 0.29 ^a
	Leucine ***	74.85 \pm 0.00 ^{ab}	69.65 \pm 0.29 ^c
	Methionine ***	11.68 \pm 0.28 ^b	7.40 \pm 0.00 ^d
	Phenylalanine ***	57.03 \pm 0.00 ^b	47.05 \pm 0.29 ^c
	Proline **	39.40 \pm 0.28 ^{ab}	38.42 \pm 0.29 ^c
	Tryptophan ***	9.50 \pm 0.00 ^c	8.63 \pm 0.00 ^d
	Valine ***	49.11 \pm 0.00 ^a	44.17 \pm 0.29 ^d
	SUM***	363.75 \pm 0.84 ^a	349.26 \pm 1.74 ^b
Ratio hydrophobic : hydrophilic***		0.67:1 ^a	0.63:1 ^c
Nitrogen conversion factor***		5.70 \pm 0.00 ^a	5.54 \pm 0.00 ^c

Cowpea (mg AA/g protein)	Mung bean (mg AA/g protein)	Yellow pea (mg AA/g protein)	Cowpea (mg AA/g protein)
Flour	Fine fraction	Fine fraction	Fine fraction
64.20±0.31 ^c	67.83±0.79 ^b	83.77±0.63 ^a	68.10±1.40 ^b
103.85±0.00 ^c	107.14±0.70 ^{ab}	103.25±0.12 ^c	105.34±2.62 ^{bc}
160.16±0.31 ^b	162.31±0.71 ^{ab}	151.56±0.00 ^c	161.59±4.45 ^{ab}
26.73±0.00 ^c	27.64±0.29 ^b	21.92±0.06 ^e	29.56±0.65 ^a
63.32±0.31 ^c	64.01±0.67 ^c	66.64±0.16 ^b	62.69±1.34 ^c
47.11±0.31 ^d	52.36±0.07 ^a	46.88±0.31 ^d	50.88±0.88 ^b
35.71±0.31 ^{ab}	31.58±0.05 ^d	34.26±0.10 ^c	36.38±0.54 ^a
31.11±0.00 ^c	30.36±0.65 ^{cd}	32.46±0.38 ^b	32.37±0.47 ^b
532.18±0.93 ^c	543.22±0.22 ^{bc}	540.74±1.70 ^{bc}	546.92±12.35 ^{ab}
39.88±0.00 ^{ab}	39.32±0.00 ^b	38.50±0.03 ^c	39.73±0.59 ^b
9.20±0.62 ^b	6.27±0.05 ^c	11.81±0.04 ^a	9.04±0.06 ^b
35.93±0.00 ^c	34.10±0.24 ^d	38.35±0.17 ^b	35.41±0.35 ^c
39.66±0.31 ^b	39.99±0.16 ^b	38.60±0.10 ^c	39.79±0.73 ^b
70.99±0.00 ^c	76.08±0.38 ^a	68.00±0.12 ^d	73.91±1.45 ^b
11.39±0.00 ^b	11.73±0.05 ^b	7.89±0.05 ^c	13.20±0.17 ^a
52.14±0.00 ^d	59.80±1.20 ^a	46.19±0.13 ^c	55.20±1.21 ^c
36.81±0.00 ^d	40.01±0.22 ^a	38.06±0.12 ^c	38.60±0.69 ^{bc}
9.86±0.31 ^{ab}	9.76±0.03 ^{bc}	8.39±0.10 ^d	10.13±0.01 ^a
46.01±0.00 ^c	47.85±0.14 ^b	41.51±0.11 ^e	45.97±0.72 ^c
351.87±1.24 ^b	364.90±2.31 ^a	337.30±0.96 ^c	361.00±5.97 ^a
0.66:1 ^b	0.67:1 ^a	0.62:1 ^c	0.66:1 ^b
5.68±0.00 ^c	5.68±0.00 ^b	5.52±0.00 ^f	5.67±0.00 ^d

2.2.8 Rheological properties

The rheological properties of the dry fractionated materials were studied according to a method previously described by Kornet *et al.* (2021). The flour and fractions were dissolved in demineralised water at a concentration of 15 wt% and agitated with a magnetic stirrer at room temperature for 1 hour until all material was dissolved. The rheological properties of samples were measured with a MCR301 rheometer (Anton Paar, Graz, Austria) combined with a CC-17 concentric cylinder geometry. Two small angle oscillatory shear (SAOS) measurements were performed: a temperature sweep and a frequency sweep. A temperature sweep was performed by increasing the temperature from 20 to 95 °C at a rate of 3 °C/min. Subsequently, the samples were kept at 95 °C for 10 minutes and cooled back to 20 °C at a rate of 3 °C/min. Next, the formed gels were subjected to a frequency sweep from 0.01 to 10 Hz (at a strain of 1%). The storage modulus (G') and loss modulus (G'') were recorded during both measurements. The individual G' values reported in this study correspond to the last data point of the temperature sweep. The loss factor ($\tan \delta$) was calculated according to Eq. 2.4.

$$\tan \delta = \frac{G'}{G''} \quad (\text{Eq. 2.4})$$

Straight after the SAOS measurements, the analysis was continued with a large amplitude oscillatory shear (LAOS) measurement. A strain sweep from 0.1-1000% in 80 logarithmic steps (at a frequency of 1 Hz) was performed while recording the G' and G'' . The end of the linear viscoelastic regime (LVE) was expressed as the critical strain (γ_c). The crossover strain ($\gamma_{G'=G''}$) was determined as the point where G' and G'' overlap. Rheological measurements were performed in triplicate.

2.2.9 Statistical analysis

In this study, significant differences between measured values were determined by ANOVA analysis using a Duncan post hoc test ($p \leq 0.05$) in SPSS software (version 25). It is worth mentioning that all measurements were performed at least in triplicate unless stated otherwise. Then, the mean values and standard deviations (as a measure of error) were calculated and reported.

2.3 Results & discussion

2.3.1 Milling of starch-containing legumes

During milling, the cotyledons of legumes are broken up into starch granules and protein particles. Figure 2.1 shows the scanning electron microscopy (SEM) images of mung bean, yellow pea, and cowpea flours obtained after milling. In this figure, the starch granules from mung bean, yellow pea, and cowpea can be recognized as elongated, round particles and are shown by the S letter in these SEM images. The smaller, asymmetrical particles are most probably protein and fibre particles (indicated as P/F in Figure 2.1). Larger clusters of combined starch granules and protein and/or fibre particles are visible as cellular material and are shown by CM letters in the SEM images. Previous research by Möller *et al.* (2021) showed similar results for milling of yellow pea and identified the small round particles adhering to the surface of the starch granules as protein bodies. In mung bean flour, the smaller protein and/or fibre particles seem to be more associated with the starch granules than for yellow pea and cowpea flour. SEM images of previous research by Zhu *et al.* (2020) also showed a strong association of protein/fibre particles to starch granules in mung bean flour. It is possible, therefore, that separation of protein and starch through air classification is harder for mung bean than for yellow pea and cowpea. The use of a higher milling speed can lead to a change in the degree of association between protein particles and starch granules. However, at increasingly high milling speeds, the starch granules can be damaged, hindering again size-based separation by air classification (Zhu *et al.*, 2020).

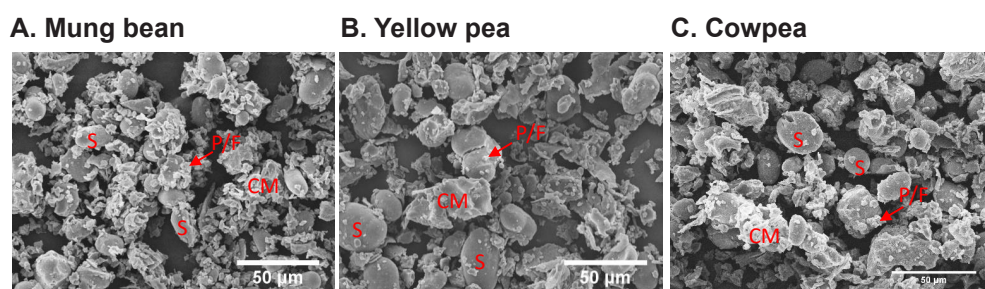


FIGURE 2.1 Scanning electron microscopic pictures of mung bean (A), yellow pea (B), and cowpea flour (C) milled at 4000 rpm. S: starch granule. CM: cellular material. P/F: protein and/or fibre particles. Scale bars always represent 50 μm .

2.3.2 Air classification of legume flours

After milling of mung bean, yellow pea, and cowpea into flours, the materials were air classified at three different classifier wheel speeds: 8000, 10000, and 12000 rpm. SEM images in Figure 2.2 show that all air classifier wheel speeds yield a good separation into a fine fraction (protein-rich) and a coarse fraction (starch-rich) for all tested materials. Small and irregularly shaped protein particles are visible in all fine fractions, while the coarse fractions mostly contain oval-formed starch granules. Furthermore, relatively fewer impurities are observed in the mung bean coarse fractions than in the yellow pea and cowpea coarse fractions (Figure 2.2). Perhaps, mechanical characteristics during milling lead to relatively more non-starch particles that have a similar size as starch granules in the yellow pea and cowpea coarse fractions. For all materials, the fine fraction at 8000 rpm shows some small starch granules, which become fewer when the classifier wheel speed is further increased. This implies that upon increasing the classifier wheel speed, the fine, protein-rich fraction is further enriched and the protein content increases. In fact, increasing the classifier wheel speed decreases the size of the particles that are selected to pass the classifier wheel. Theoretically, this implies that smaller particles, such as protein, can pass the classifier wheel, while larger particles, such as starch granules, cannot pass. The air classification process can be characterised by a cut point, which is the diameter of the particle that has an equal chance to end up either in the fine or the coarse fraction (Pelgrom *et al.*, 2013).

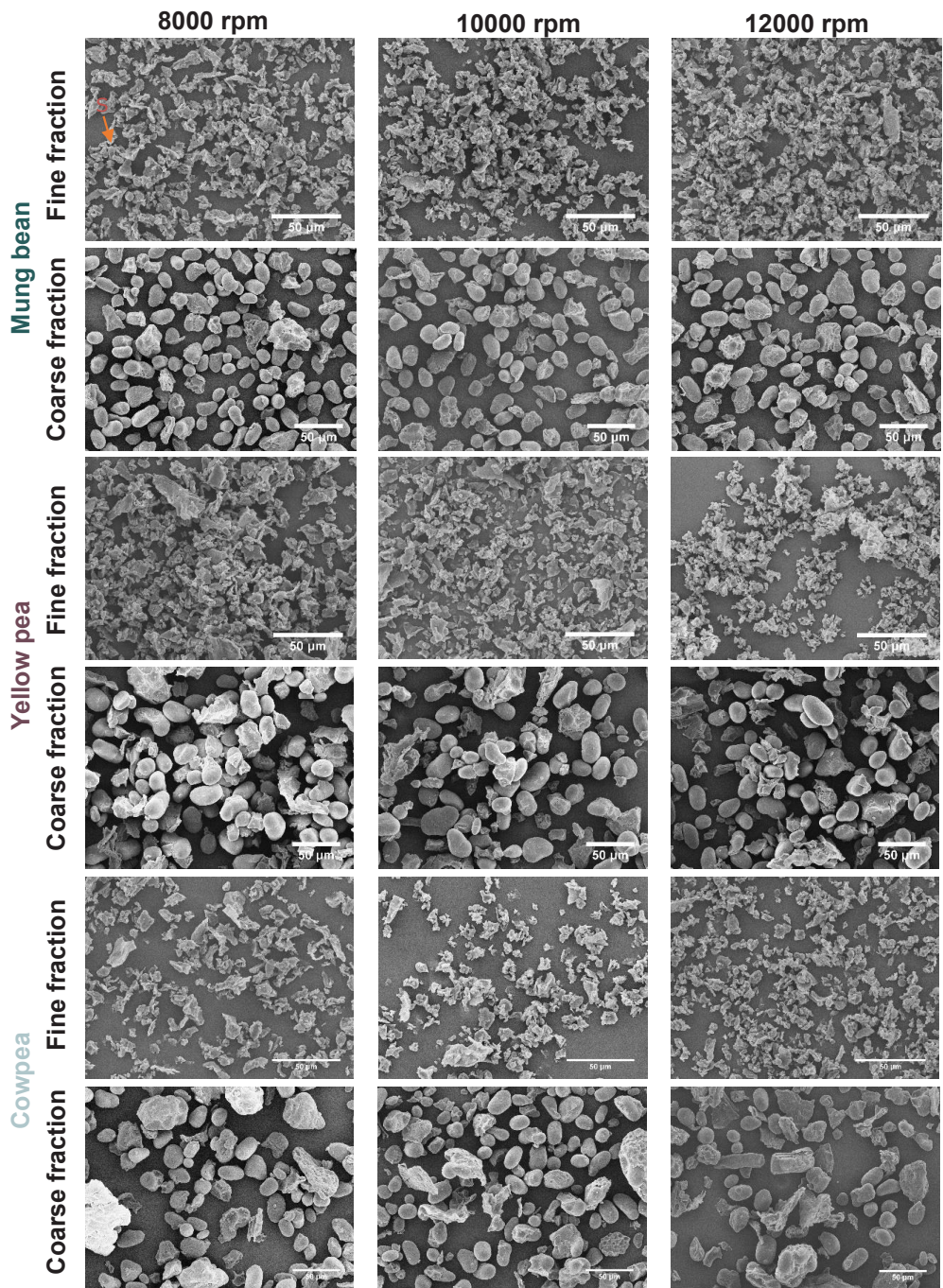


FIGURE 2.2 Scanning Electron Microscope (SEM) images of fine fractions and coarse fractions produced at air classifier wheel speeds of 8000, 10000, and 12000 rpm for mung bean, yellow pea, and cowpea. Magnifications ranging between 450x and 750x, scale bars always represent 50 µm.

This result is complemented by the particle size distribution as measured with the Mastersizer (Figure 2.3). Figure 2.3 shows that upon increasing the classifier wheel speed, the $D[4,3]$ of the fine fraction decreases significantly for all materials. Similar results were also reported by Pelgrom *et al.* (2013) for the average particle size of air classified yellow pea at increasing classifier wheel speeds. Interestingly, the $D[4,3]$ of the flour is highly dependent on raw material, with cowpea showing a significantly higher $D[4,3]$ than mung bean and yellow pea. This suggests that cowpea flour has larger particles on average than mung bean and yellow pea flour. The SEM images of cowpea flour (Figure 2.1C) and cowpea coarse fractions (Figure 2.2) do not contain larger particles than those of mung bean and yellow pea.

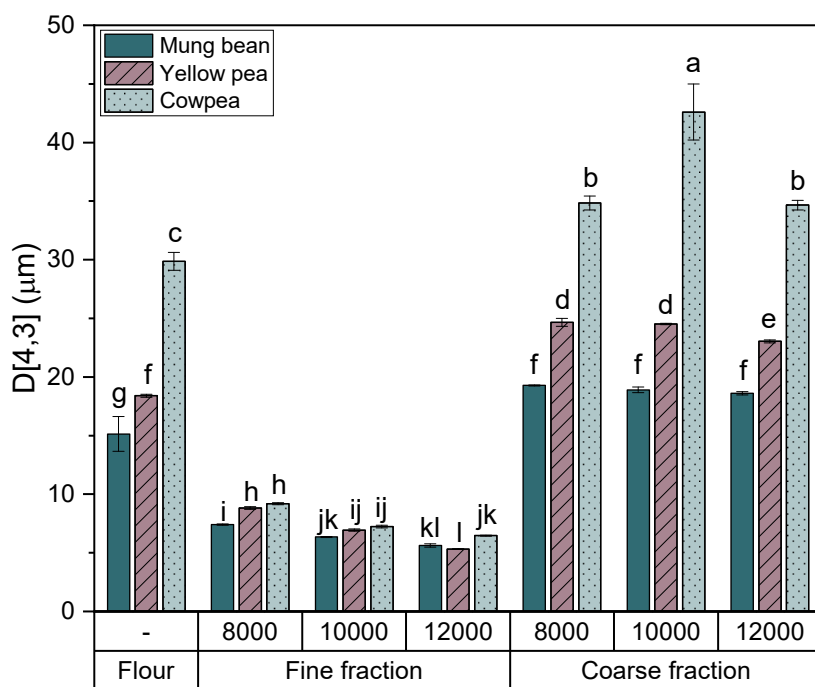


FIGURE 2.3 $D[4,3]$ of flour, fine fraction, and coarse fraction of mung bean, yellow pea and cowpea. Fine and coarse fractions were produced at air classifier wheel speeds of 8000, 10000, and 12000 rpm. Error bars represent standard deviation based on 5 measurements. In this figure, means with different letters represent significant differences ($p \leq 0.001$).

2.3.3 Composition of flour, fine fraction, and coarse fraction

The protein content of mung bean, yellow pea, and cowpea flour significantly increased upon dry fractionation into fine fractions and significantly decreased upon dry fractionation into coarse fractions (Figure 2.4A). The protein content of the fine fractions of mung bean, yellow pea, and cowpea was dependent on the air classifier wheel speed, with a higher speed increasing their protein content. The differences were significant between 8000, 10000, and 12000 rpm for yellow pea and cowpea, while the difference was not significant between 10000 and 12000 for mung bean ($p>0.05$). Pelgrom *et al.* (2013) reported similar results about dry fractionation of yellow pea and they attributed these results to fewer particles passing the classifier wheel at higher speeds.

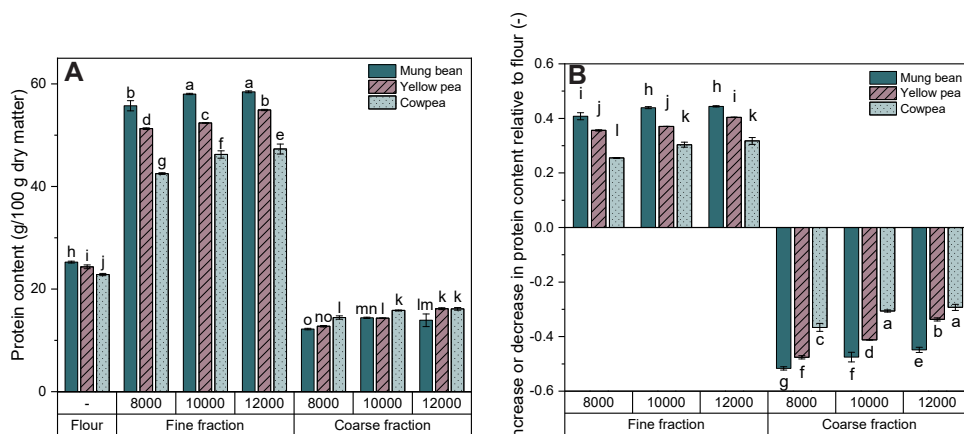


FIGURE 2.4 A) Protein content of the flour, fine, and coarse fractions of mung bean, yellow pea, and cowpea at various air classifier wheel speeds. B) Protein content of fine fraction and coarse fraction of mung bean, yellow pea, and cowpea at various air classifier speeds expressed as a dimensionless number: fine fraction is reported as an increase, while coarse fraction is reported as a decrease. Different letters represent significant differences ($p\leq 0.001$).

Figure 2.4 also shows that mung bean had the highest protein content in the flour and the fine fractions, whereas cowpea had the lowest protein content in the flour and the fine fractions. Therefore, the initial differences in protein content between the flour of the different materials are reflected in the protein content of the fine fractions (Figure 2.4A). A dimensionless protein content was calculated according to Eq. 2.1 and Eq. 2.2 and reported in Figure 2.4B. Reporting the protein content as a dimensionless value helps us to understand the effect of the composition of the raw material on the potential of dry fractionation. The maximum protein content of protein bodies was previously reported to be between 70 and 80% for legumes, indicating that a value

of 1 cannot be reached in practice (Plant & Moore, 1983; Tombs, 1967). Figure 2.4B shows significant differences between almost all fractions, indicating that the increase or decrease in protein content differs between material sources. This proves that there is more than solely the raw material composition that determines the final composition of the fractions after air classification. As the starch granule morphologies of mung bean, yellow pea, and cowpea were found to be similar in SEM images, different starch morphologies could not be used to explain the difference in protein content either (Figure 2.2). Previous research by Möller *et al.* (2021) showed that protein particles were still associated with starch granules after milling of yellow pea. The attachment or detachment of protein particles to starch granules could influence the separation ability in air classification. Mung bean, yellow pea, and cowpea probably have different associations between protein particles and starch granules, which might affect the final composition of the fractions after air classification.

Now diving deeper into the proteins themselves, the amino acid compositions of the flours and fine fractions were analysed (Table 2.1). Here, the fine fractions have a different amino acid composition than the flours. Therefore, it becomes clear that dry fractionation changes the amino acid composition. However, the differences are subtle, to a level where they do not significantly affect the ratio of hydrophilic and hydrophobic amino acids for example. Differences between mung bean, yellow pea, and cowpea in the ratio of hydrophilic and hydrophobic amino acids are of importance to mention. Yellow pea had a lower ratio of hydrophobic:hydrophilic amino acid compared to mung bean and cowpea, which could change the functional properties, such as water holding capacity and gelation.

Next to the protein content, the starch content of the dry fractionated materials was measured (Figure 2.5A). Air classification of all three materials led to significant depletion of starch in the fine fraction and a significant enrichment of starch in the coarse fraction. Initial differences in starch content between materials in the flour were reflected in the fine fraction, and to a lesser extent in the coarse fraction. The starch content of cowpea is significantly higher than the starch content of mung bean and yellow pea in the flour, fine fraction, and coarse fraction. As starch granules are larger than protein particles, this result also explains the higher D[4,3] values for cowpea in comparison to the other raw materials (Figure 2.3). Figure 2.5A furthermore suggests the presence of starch granules in the cowpea fine fractions at all speeds. SEM images did not show additional (whole) starch granules in the cowpea fine fractions in comparison to the mung bean and yellow pea fine fractions. This suggests the presence of broken starch granules in the cowpea fine fraction. Broken starch granules in the initial flour make separation by air classification harder, as previously reported by (Zhu *et al.*, 2020). Figure 2.5B shows that, similar to protein content, starch content of the fine and coarse fraction is dependent on more than solely flour composition. The high starch content

in cowpea fractions could not be related to the fact that cowpeas were whole, whereas mung bean and yellow pea were dehulled. Previous research by (Saldanha do Carmo *et al.*, 2020) showed that dehulling had no significant impact on protein-enrichment and functional properties, but did increase the starch-enrichment in coarse fractions. The starch-enrichment in the coarse fractions of cowpea in this study was not related to dehulling, as the cowpeas were whole.

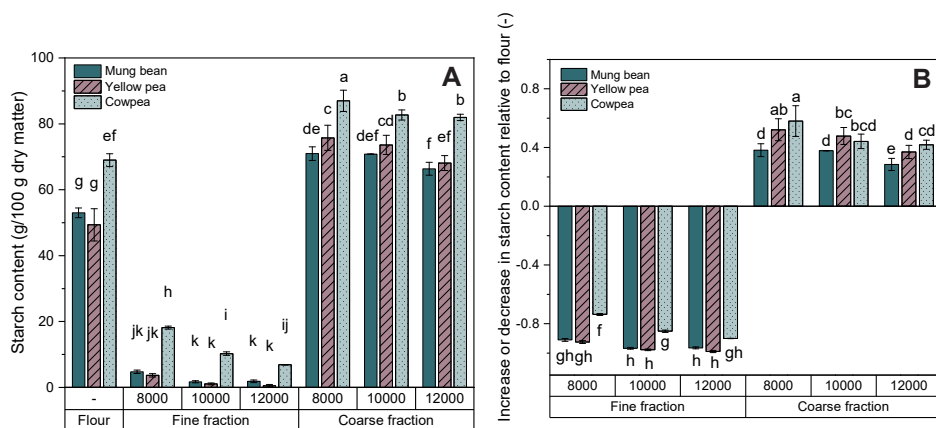


FIGURE 2.5 A) Starch content of the flour, fine fraction, and, coarse fraction of mung bean, yellow pea, and cowpea at various air classifier wheel speeds. B) Starch content of fine fraction and coarse fraction of mung bean, yellow pea, and cowpea at various air classifier speeds expressed as a dimensionless number: fine fraction is reported as a decrease, while coarse fraction is reported as an increase. Different letters represent significant differences ($p \leq 0.001$).

Furthermore, it is noticeable that the protein content in both the fine and the coarse fraction increases upon increasing the air classifier wheel speed, whereas the opposite is true for the coarse fraction. Pelgrom *et al.* (2013) also observed this trend and attributed it to the fact that fewer particles pass the classifier wheel into the fine fraction, and thus, more protein particles end up in the coarse fraction. Therefore, the overall protein content in the coarse fraction increases, which consequently leads to a decrease in overall starch content.

As the protein content increases upon increasing classifier wheel speed, the protein yield is known to decrease (Pelgrom *et al.*, 2013; Xing *et al.*, 2020). The theoretical protein yield in the fine fraction decreases from 0.66 to 0.62 to 0.59 g/g for mung bean air classified at 8000, 10000, and 12000 rpm, respectively. For yellow pea (0.63, 0.56, 0.47 g/g) and cowpea (0.55, 0.46, 0.44 g/g), lower protein yields of the fine fraction were found when increasing the air classifier wheel speed from 8000 to 10000 to 12000 rpm, respectively. A balance between protein content and protein yield is important for future application of dry fractionation in industry, as well as for environmental reasons. Figure 2.4A shows that the protein contents of the mung bean fine fractions produced

at 10000 and 12000 rpm are similar and there is not a significant difference ($p>0.05$) between them. Because of this, combined with the decreasing yield, we chose to continue with the fine and coarse fractions produced at an air classifier wheel speed of 10000 rpm for all materials.

2.3.4 Functional properties of fine and coarse fractions

The functionality of the flours, fine fractions, and coarse fractions of all materials was evaluated based on their water holding capacity (WHC) and least gelation concentration (LGC). Figure 2.6 shows that WHC depends on the material as well as the type of fraction. The fine fractions produced from mung bean, yellow pea, and cowpea had a higher WHC (2.14 ± 0.13 , 1.53 ± 0.05 and 2.06 ± 0.04 g/g, respectively) in comparison to literature values reported for faba bean concentrate and pea fine fractions (1.25 and 0.97 g/g, respectively) (Bühler *et al.*, 2020; Saldanha do Carmo *et al.*, 2020).

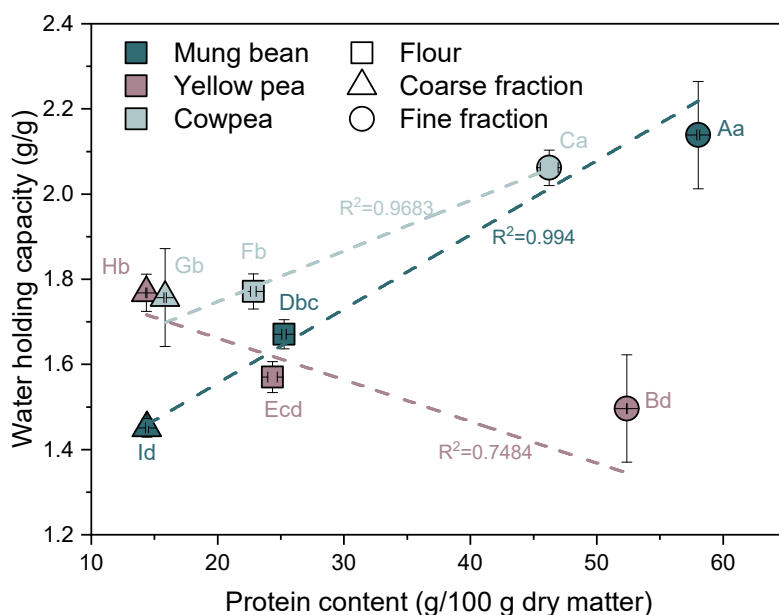


FIGURE 2.6 Water holding capacity (g/g) in relation to protein content (g/100 g dry matter) for flour (square), fine fraction (circle) and coarse fraction (triangle) of mung bean, yellow pea, and cowpea. Capital letters indicate significant differences in protein content ($p \leq 0.001$), small letters indicate significant differences in water holding capacity ($p \leq 0.001$).

For mung bean and cowpea, the WHC of the flour and fractions increased with increasing protein content, showing positive linear correlations of 0.9940 and 0.9683, respectively. This result suggests that protein might be the dominant component that binds water in mung bean and cowpea. Contradictory, yellow pea flour and

fractions decreased in WHC with increasing protein content, with a negative linear correlation of 0.7484. Saldanha do Carmo *et al.* (2020) also reported that WHC of the coarse fraction from yellow pea and faba bean is richer than that of the fine fraction. The WHC results of this study show that at least for mung bean and cowpea, starch does not play a large role in water holding. This was expected because native starch granules are considered hard particles with limited water absorption ability (BeMiller & Whistler, 2009). The observation that the mung bean and cowpea fine fraction have a higher WHC than the yellow pea fine fraction may be accounted for by their difference in the number of hydrophobic amino acids (Table 2.1). The yellow pea fine fraction has a significantly lower amount of hydrophobic amino acids compared to the fine fractions from mung bean and cowpea (Table 2.1). However, other factors, like amongst others conformation of proteins, could also play a role (Ahmed, Al-Ruwaih, Mulla, & Rahman, 2018; Keivaninahr, Gadkari, Zoroufchi Benis, Tulbek, & Ghosh, 2021; Paredes-Lopez, Ordórica-Falomir, & Olivarez-Vazquez, 1991; Zayas, 1997). Previous research by (Saldanha do Carmo *et al.*, 2020) showed that WHC of coarse fractions from peas and faba beans slightly improved when whole instead of dehulled materials were used. They attributed this difference due to a higher fibre content in the whole materials. As cowpeas were whole instead of dehulled, an increased WHC of the coarse fraction is expected.

Similar to WHC, LGC was dependent on both the material as well as the type of fraction (Figure 2.7). A lower LGC is equivalent to less material (in %) necessary to form a gel and this could thus be advantageous from a sustainability as well as cost point of view. Figure 2.7 shows that mung bean has the lowest LGC for the flour, fine fraction, and coarse fraction.

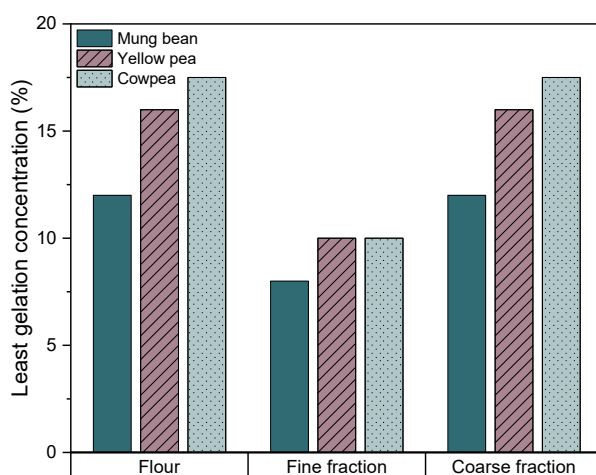


FIGURE 2.7 Least gelation concentration (%) of mung bean, yellow pea, and cowpea, flour, fine fraction and coarse fraction. Standard deviation is 0 for all samples.

Brishti *et al.* (2017) previously also showed superiority of LGC of mung bean protein isolate over soy protein isolate. The flour of each material has an identical LGC to the coarse fraction of that corresponding material. Furthermore, Figure 2.7 clearly shows that the fine fraction has a lower LGC in comparison to the flour and the coarse fraction. Given the higher protein content in the fine fraction, it can be hypothesized that protein is superior in gel formation in comparison to other components such as starch. Previous research by Chinma, Ariahu, & Abu (2013) showed that a combination of protein and starch led to a lower LGC than starch alone. They suggested that the composition, as well as the interaction between the components, influenced the gelling properties.

2.3.5 Gelation behaviour

The gelation behaviour of the flour, fine fraction, and coarse fraction of all materials was studied during and after thermal treatment using rheology. Figure 2.8 shows an abrupt increase in the G' and G'' of the flour and coarse fractions around 70 °C and the fine fractions at around a range of 75-95 °C. The steep increase in G' and G'' observed in the flour and the coarse fraction of all materials is expected to emerge from water absorption and swelling of the starch granules, as the flour and coarse fraction are high in starch. Similar conclusions were reported by (Kornet *et al.*, 2021). Onset gelatinization temperature of legume starches is on average between 58 and 72 °C (Hoover, Li, Hynes, & Senanayake, 1997; Huang *et al.*, 2007; Ratnayake, Hoover, & Warkentin, 2002; Singh, Nakaura, Inouchi, & Nishinari, 2008).

The increase in G' and G'' observed in the fine fraction is most likely caused by protein denaturation, since protein is the major constituent in the fine fractions. This is supported by previous studies on the denaturation temperature of mung bean globulins and pea globulins and the transition temperature of cowpea flour that all fall within the range of 78 – 83 °C (Henshaw, Mcwatters, Akingbala, & Chinnan, 2003; Messian, Sok, Assifaoui, & Saurel, 2013; Tang & Sun, 2010). Table 2.2 shows that the final G' values of the fine fraction of mung bean, yellow pea, and cowpea after thermal treatment (12248 ± 1138 , 3988 ± 547 , and 9729 ± 1419 Pa, respectively) are found to be significantly higher than the G' values of pea protein concentrate produced by aqueous fractionation ($G'=1174 \pm 185$ Pa) (Kornet *et al.*, 2021). This shows the rich functionality of protein-rich fractions produced by dry fractionation in comparison to more traditional methods of fractionation such as aqueous fractionation. The G' values of the fine fractions of mung bean, yellow pea, and cowpea are significantly higher than the flour and coarse fractions. This is in line with previous research by Aguilera & Rojas (1996) who found that gels containing higher levels of protein developed a higher G' than gels containing higher levels of starch. Even though the composition of the fine fractions

from mung bean, yellow pea, and cowpea is relatively similar, the G' values after thermal treatment differ greatly. This implies that gelation behaviour is not only related to the composition of the material, but also to protein characteristics, amongst others amino acid composition (Table 2.1) (Paredes-Lopez *et al.*, 1991; Zayas, 1997). Proteins that contain more hydrophobic amino acids, for example, tend to establish a stronger gel network (Zayas, 1997). This might suggest that the materials with a higher G' value after thermal treatment, such as the mung bean fine fraction, fit applications where a strong gel network is preferred, such as meat analogues or gelled dairy alternatives (Kyriakopoulou, Keppler, van der Goot, & Boom, 2021). Materials with a lower G' value after thermal treatment, such as the yellow pea fine fraction, might be more suitable for applications where gel network formation is less important, such as plant-based milks (Kyriakopoulou *et al.*, 2021).

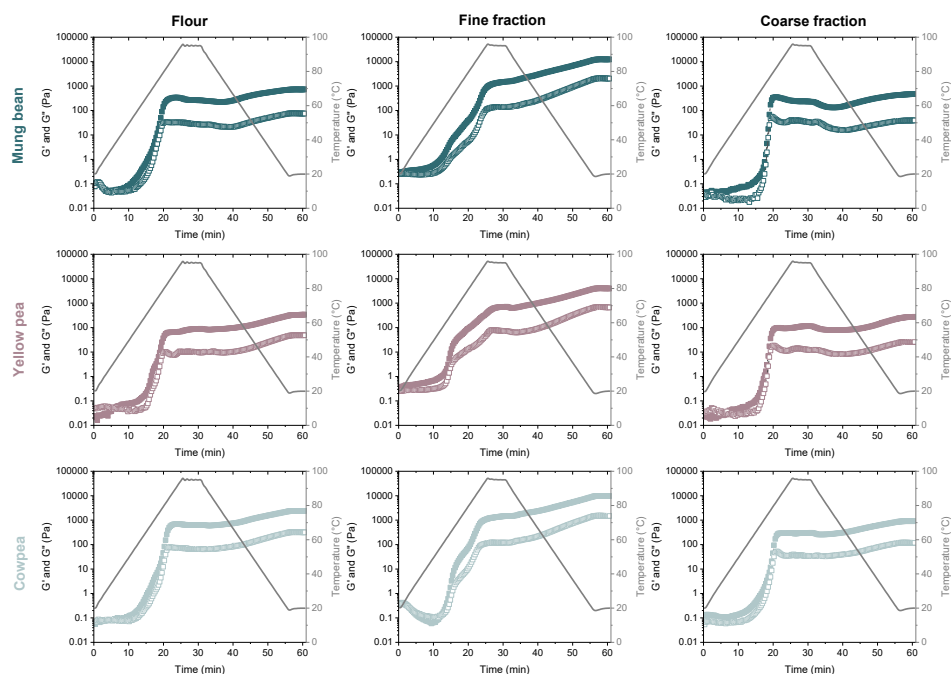


FIGURE 2.8 Temperature sweeps (20–95 °C, $f = 1$ Hz, $\gamma = 1\%$) of mung bean, yellow pea, and cowpea flour, fine fraction and coarse fractions at 15 w/w% dispersions. G' : dark colours, G'' : light colours. Temperature: solid grey line.

TABLE 2.2 Average storage modulus (G'), loss factors ($\tan \delta$), critical strains (γ_c) and crossover strains ($\gamma_{G'=G''}$) of the gelled flour, fine fraction and coarse fractions from mung bean, yellow pea, and cowpea. The storage modulus and loss factor correspond with the values of the last data point from the temperature sweeps and the critical and crossover strains are determined from the strain sweeps. Different letters represent significant differences within rows ($p \leq 0.001$).

Rheological parameters	Mung bean			Yellow pea	
	Flour	Fine fraction	Coarse fraction	Flour	Fine fraction
G' (Pa)	727 ± 292^e	12248 ± 1138^a	467 ± 243^e	338 ± 24^e	3988 ± 547^c
$\tan \delta$	0.10 ± 0.01^e	0.17 ± 0.00^a	0.08 ± 0.00^c	0.14 ± 0.01^b	0.17 ± 0.00^a
γ_c (%)	3.65 ± 0.85^{bcd}	3.16 ± 0.00^{cd}	7.87 ± 1.84^a	4.87 ± 1.84^{bc}	2.15 ± 0.00^d
$\gamma_{G'=G''}$ (%)	215 ± 0^{bcd}	215 ± 0^{bcd}	332 ± 126^{bc}	248 ± 58^{bcd}	192 ± 39^{cd}

After thermal treatment, the flour, fine fraction, and coarse fraction from mung bean, yellow pea, and cowpea display solid-like behaviour, as it was found that $G' > G''$. The ratio between G' and G'' , also called the loss factor $\tan \delta$, indicates the strength of the solid. As previously described by (Steffe, 1992), $\tan \delta < 1$ indicates a material that is a solid, where a strong solid is considered when $\tan \delta \ll 1$. As the $\tan \delta$ values of the flour and coarse fractions are smaller than the $\tan \delta$ value of the fine fraction, we can say that the flour and coarse fractions form more solid-like gels than the fine fractions for mung bean, yellow pea, and cowpea (Table 2.2).

Differences between material sources are also visible (Figure 2.8 and Table 2.2). The fine fraction of mung bean has a significantly higher G' value than those of yellow pea and cowpea. This might be related to the protein content of mung bean which is also significantly higher in comparison to yellow pea and cowpea (Figure 2.4). This explanation does not hold for the G' difference between the fine fraction of yellow pea and cowpea, where cowpea has a significantly higher G' value than yellow pea even though its protein content is significantly lower (Figure 2.4). Therefore, protein characteristics, such as degree of hydrophobicity, could play a role. The ratio of hydrophobic:hydrophilic amino acids is lower for the yellow pea fine fraction than for the cowpea fine fraction for example (Table 2.1). During heating, proteins denature and hydrophobic patches are exposed, which on its turn improves the gel network structure formation and G' values (Lamsal, Jung, & Johnson, 2007; Malik & Saini, 2017; Zayas, 1997).

After thermal treatment, the linear viscoelastic regime (LVR) was studied by a strain sweep at constant frequency and constant temperature (Figure 2.9). Within the LVR, G' was always higher than G'' , indicating solid-like behaviour. The end of the linear

Coarse fraction	Cowpea		
	Flour	Fine fraction	Coarse fraction
277 ± 95^c	2386 ± 865^d	9729 ± 1419^b	901 ± 204^e
0.10 ± 0.03^c	0.13 ± 0.01^b	0.15 ± 0.00^{ab}	0.13 ± 0.00^b
5.36 ± 1.25^b	3.16 ± 0.00^{cd}	2.15 ± 0.00^d	2.82 ± 0.58^d
316 ± 0^{bc}	365 ± 85^{ab}	100 ± 0^d	487 ± 184^a

viscoelastic regime was defined as the strain at the first data point that deviated 5% or more from the linear part, or γ_c . After the critical strain, the material becomes progressively more fluid-like, disrupting the initial structured network. A longer LVR, and, therefore, a higher critical strain (γ_c), indicates a network that is better able to withstand deformation. Overall, the fine fraction of each source had a shorter LVR than the flour and the coarse fraction (Table 2.2). Thus, starch-rich materials form a network that is better able to withstand deformation in comparison to protein-rich materials. The mung bean coarse fraction had the longest LVR with a critical strain value of 7.87%.

Figure 2.9 shows that the G' and G'' in the linear part of the fine fractions in the strain sweeps were around one magnitude higher than the G' and G'' in the linear part of the flour and coarse fractions for mung bean, yellow pea, and cowpea. Furthermore, all fractions from all materials showed a crossover point from solid-like behaviour to liquid-like behaviour during the strain sweep, also expressed as $\gamma_{G'=G''}$ (Figure 2.9, Table 2.2). Coarse fractions showed crossover points at higher strain levels in comparison to the flours and fine fractions (Table 2.2). One could interpret this as the flour and fine fractions starting to flow at smaller deformations in comparison to the coarse fractions.

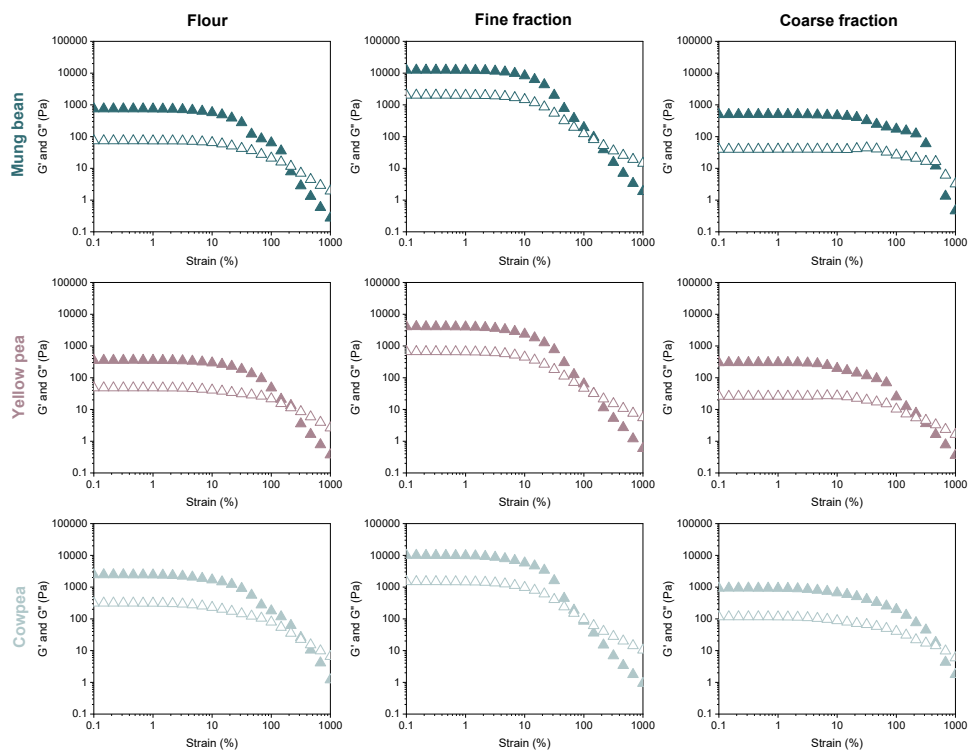


FIGURE 2.9 Strain sweeps ($20\text{ }^{\circ}\text{C}$, $f = 1\text{ Hz}$) of mung bean (green), yellow pea (pink), and cowpea (blue) of flour, fine fraction and coarse fraction. G' : dark colours/closed symbols, G'' : light colours/open symbols.

2.4 Conclusion

Fine (protein-rich) fractions and coarse (starch-rich) fractions were produced by air classification from mung bean, yellow pea, and cowpea flours. Air classifier wheel speed could be used to tailor the composition of the fine and coarse fractions. Mung bean yielded fine fractions with significantly higher protein contents than yellow pea and cowpea. Water holding capacity correlated positively with protein content for mung bean and cowpea, whereas it correlated negatively with protein content for yellow pea. As the composition of the material sources is more or less comparable, this result suggests that the difference might be related to protein characteristics. The fine fractions of each source formed gels with the highest G' value after thermal treatment, whereas the flour and coarse fractions formed more solid-like gels that were able to withstand larger deformations ($<\tan \delta$ and $>\text{critical strain}$). To conclude, differences in functionality between flours, fine fractions, and coarse fractions are most likely related to differences in composition. Functional differences between fine fractions from mung bean, yellow pea, and cowpea can be explained by differences in protein characteristics rather than protein content. Dry fractionation of mung bean, yellow pea, and cowpea was shown to be a successful method to obtain protein-rich ingredients with functional properties that match those necessary for incorporation in plant-based food products.

3

Chapter 3

Mechanical and rheological effects of transglutaminase treatment on dense plant protein blends

This chapter has been published as Schlangen, M., Ribberink, M.A., Taghian Dinani, S., Sagis, L.M.C., van der Goot, A.J. (2023) Mechanical and rheological effects of transglutaminase treatment on dense plant protein blends. Food Hydrocolloids. 136, part A, 108261.

Abstract

Pea protein isolate (PPI) and mung bean protein isolate (MBPI) are rising alternatives for soy protein isolate in producing meat analogues. Transforming these isolates into full products is challenging due to their differences in functional properties compared with soy. Here, we report on the use of transglutaminase to improve the mechanical and rheological properties of dense MBPI and PPI dispersions. Gels from PPI and MBPI (40 wt.% dry matter) were produced with 0, 0.1, 0.3, 0.5, and 0.7 wt.% transglutaminase and incubation temperatures of 30, 40, 50, and 60 °C. Their mechanical and rheological properties were determined by tensile and closed cavity rheometer tests. The degree of crosslinking was determined by the OPA assay. Transglutaminase significantly increased fracture stress and strain of PPI gels, and to a lesser extent those of MBPI gels. The amount of free amino groups confirmed that this increase in PPI was due to formation of additional crosslinks. Amplitude sweeps identified that the rheological properties of PPI gels and MBPI gels were affected by the addition of transglutaminase, but in an opposite manner. Stress relaxation experiments showed that transglutaminase increased the elasticity of PPI gels and formed mainly small aggregates in MBPI gels. This work showed that the fibrous structure diminished when >0.1 wt.% transglutaminase was added to PPI / MBPI - wheat gluten blends. To conclude, transglutaminase can be used to create intermolecular crosslinks in PPI gels, creating a full network, while mostly intramolecular crosslinks are formed in MBPI gels, leading to a cluster structure.

3.1 Introduction

Plant-based meat analogues that aim to mimic whole cut meats need to have a fibrous texture to meet consumers' demands. Such texture is achieved by using plant proteins with good gel properties combined with a structuring method, such as extrusion or shear cell technology. Soy protein and wheat gluten are well-known protein ingredients for the production of meat analogues due to their favourable gelation properties and their ability to form fibres (Schreuders *et al.*, 2019). Recently, other plant proteins, such as mung bean protein and yellow pea protein, have been shown to be promising alternatives to soy. Pea protein is less allergenic, high in nutritional value, and cultivated in moderate climates (Lam, Paulsen, & Corredig, 2008). Mung beans are considered more sustainable and inexpensive to cultivate in comparison to soy (Brishti *et al.*, 2017). However, mung bean and pea have less optimal gelling properties to produce meat analogues than soy (Bildstein, Lohmann, Hennigs, Krause, & Hilz, 2008; Brishti *et al.*, 2021).

To improve the gelling properties, transglutaminase can be used. Transglutaminase catalyses inter- and/or intra- molecular $\epsilon(\gamma\text{-glutamyl})\text{-lysine}$ crosslinking between glutamine and lysine residues. The crosslinking forms high molecular weight proteins that can modify functional properties such as viscosity, gelation, solubility, and water holding capacity (Gharst, Clare, Davis, & Sanders, 2007). Several studies have proven that transglutaminase can increase gelation of different plant proteins, such as soy, pea, and Bambara groundnut protein (Forghani, Eskandari, Aminlari, & Shekarforoush, 2017; Ruzengwe, Amonsou, & Kudanga, 2020; Schäfer, Zacherl, Engel, Neidhart, & Carle, 2007; Shand, Ya, Pietrasik, & Wanasundara, 2008; Sun & Arntfield, 2011), thereby affecting the techno-functional properties of these protein isolate gels (Moreno *et al.*, 2020). However, an extensive exploration is missing of the mechanical and rheological properties of transglutaminase treated dense plant protein gels. Additionally, the effect of transglutaminase on mung bean protein has not been reported at all.

Other than gelling properties, the use of transglutaminase is also described as a route to improve fibrousness of extruded plant protein by crosslinking and affecting the speed of structure formation. Zhang *et al.* (2021) showed that increasing the concentration of transglutaminase (0 – 0.2 wt.%, dry basis ratio) improved the orientation of fibre formation as well as the tensile properties of high moisture extruded peanut protein. Excessive addition of transglutaminase (>0.3 wt.%, dry basis ratio), however, negatively influenced the protein rearrangement and fibrous structure (Zhang *et al.*, 2021). It has to be noted that structure formation in high moisture extrusion cooking is different from structure formation in the high temperature shear cell (Cornet *et al.*, 2022). The effect of transglutaminase on fibrousness and structure of meat analogues produced in

the high temperature shear cell has not been investigated before.

This study explores the effect of transglutaminase treatment on mechanical and rheological properties and fibrousness of gelled and sheared dense plant protein gels. Fibrous structures were formed with the shear cell. We hypothesize that an increasing concentration of transglutaminase improves the mechanical and rheological properties of pea protein isolate gels and mung bean protein isolate gels. Furthermore, based on the study of Zhang *et al.* (2021), we predict that fibrousness will increase at low transglutaminase concentrations, and decrease at higher transglutaminase concentrations.

3.2 Materials & Methods

3.2.1 Materials

Pea protein isolate (PPI) (NUTRALYS® F85M) and vital wheat gluten (WG) (VITENS® CWS) were obtained from Roquette Frères S.A. (St. Louis, Missouri, USA). Mung bean protein isolate (MBPI) (UNIMUNG M70) was obtained from Barentz (Hoofddorp, the Netherlands). The protein contents of PPI, MBPI, and WG, as measured with Dumas, were 74.5 wt.% (N x 5.4), 68.9 wt.% (N x 5.7), and 75.2 wt.% (N x 5.6) on a dry basis, respectively. PPI, MBPI, and WG had an average dry matter content of 92.6 wt.%, 94.3 wt.%, and 92.6 wt.%, respectively. The suppliers reported maximum fat contents of 9 wt.% and 6 wt.% and maximum ash contents of 4 wt.% and 7 wt.% for PPI and MBPI, respectively. The amino acid compositions of PPI and MBPI are reported in Table 3.1, where glutamine and lysine are highlighted because these amino acids are required to allow the crosslinking reaction of transglutaminase. Transglutaminase (ACTIVA wm) was obtained from Ajinomoto Co. (Ajinomoto, Tokyo, Japan). The composition of the enzyme preparation is 1% transglutaminase (activity of 100 U/g) and 99% maltodextrin. We use the term transglutaminase in this study to refer to the enzyme preparation that includes both transglutaminase and maltodextrin. O-Phthalaldehyde, 2-Mercaptoethanol, sodium dodecyl sulphate, and L-lysine were obtained from Sigma-Aldrich (Zwijndrecht, the Netherlands).

TABLE 3.1 Amino acid composition of PPI and MBPI.

Amino acids	PPI (mg AA/g protein)	MBPI (mg AA/g protein)
Alanine	43.7	42.5
Arginine	90.1	72.8
Asparagine + Aspartic acid	116.9	122.4
Cysteine	9.9	3.9
Glutamine + Glutamic acid	183.1	181.3
Glycine	40.8	35.8
Histidine	21.1	24.6
Isoleucine	49.3	48.4
Leucine	83.1	88.1
Lysine	73.2	70.3
Methionine	9.9	12.3
Phenylalanine	54.9	68.4
Proline	40.8	44.1

Amino acids	PPI (mg AA/g protein)	MBPI (mg AA/g protein)
Serine	49.3	55.3
Threonine	36.6	31.4
Tryptophan	9.9	8.6
Tyrosine	33.8	33.1
Valine	53.5	56.9

3.2.2 Preparation of pea protein isolate and mung bean protein isolate dispersions

Transglutaminase (TGase) at enzyme concentrations of 0, 0.1, 0.3, 0.5, and 0.7 wt.% (of the total weight) was dissolved in demi water. Protein isolate (pea protein isolate or mung bean protein isolate) was added to obtain an overall dry matter content of 40 wt.%. The dispersion was mixed with a spatula. The effect of TGase on fibrousness was studied with a second set of dispersions, where protein isolates were blended with wheat gluten (WG) simultaneously in a 1:1 ratio to the final dry matter content of 40%. Both sets of dispersions were incubated for 30 minutes in the high temperature shear cell (HTSC) to allow crosslinking by TGase at 30, 40, 50, or 60 °C. After incubation, the temperature in the HTSC, with the sample inside, was further heated to 120 °C within 5 minutes.

3.2.3 Gelation and shearing of protein dispersions

The dispersions described in section 3.2.2 were further processed into gels and sheared gels in the HTSC (Grabowska *et al.*, 2016). Both gels and sheared gels received a heat treatment. The protein dispersions were heated in the pre-heated HTSC at 120 °C and at a shear rate of 0 s⁻¹ (for gels) or at a shear rate of 39 s⁻¹ (for sheared gels) (controlled by a Haake PolyLab QC drive, Germany) for 15 min. Next, the HTSC was cooled down to 25 °C in 5 min. The final products were transferred to sealed plastic bags to prevent moisture loss.

3.2.4 Determination of the amount of free amino groups

The degree of crosslinking of gels and sheared samples was determined as a reduction in the amount of free amino groups. This amount was determined by a modified O-Phthalaldehyde (OPA) assay (Goodno, Swaisgood, & Catignani, 1981; Schäfer *et al.*, 2007). The OPA reagent was prepared by diluting 80 mg OPA (dissolved in 2 mL 96% ethanol), 50 mL sodium tetraborate buffer solution (0.1 M, pH 9.5), 50 mL 20% sodium dodecyl sulphate (SDS) and 0.2 mL of 2-mercaptoethanol to 100 mL with MilliQ. The

OPA reagent was stored in a glass bottle wrapped in aluminium foil until use.

Gelled and sheared samples were freeze-dried using an Epsilon 2-6D LSCplus freeze dryer (Martin Christ GmbH, Osterode am Harz, Germany). The lyophilized samples were diluted to a concentration of 10 mg sample in one mL phosphate buffer (0.1 M, pH 8) including 2 w/v% SDS reagent. Proteins were hydrolyzed during a 1-hour incubation step, followed by centrifugation at 4000 x g for 10 min (Sorvall Legend XFR, Thermo Scientific, Massachusetts, United States). After centrifugation, 50 µL of the supernatant was added to 2 mL of OPA reagent and vortexed. After two min of incubation at room temperature, the absorbance of the mixture was measured at 340 nm with a spectrophotometer (Hach DR6000 UV/VIS, Colorado, United States) against a blank of phosphate buffer with OPA reagent. A calibration curve was made with L-lysine standards of 0, 0.2, 0.4, 0.8, 1.6, 3.2, 4.8, and 6 mM, where 6 mM corresponded to 3.0×10^{-8} moles of free NH_2 groups. Based on the calibration curve, the contents of free amino groups were expressed as moles of lysine- NH_2 and the moles of free amino groups were calculated. Duplicates were made and the absorbance of each solution was measured three times.

3.2.5 Amplitude sweeps

Amplitude sweeps were performed at elevated temperature with a closed cavity rheometer (CCR) (RPA elite, TA instruments, New Castle, Delaware, USA). The samples were prepared by mixing the ingredients in ratios as previously described in section 3.2.2 and incubating the material for 30 minutes at 50 °C in a water bath. Next, the samples were placed between two plastic films in the CCR cavity that was sealed to allow a pressure up to 4.5 bar. The amplitude sweep consisted of two steps. First, the sample was heated at 120 °C for 2 minutes without shear treatment. Second, amplitude sweeps were performed at a constant frequency of 1 Hz and a temperature of 120 °C. The linear viscoelastic regime (LVR) was calculated for all curves and was defined as the maximum strain before a 5% G' deviation from linear. The G' and G'' values corresponding to the maximum strain before a 5% G' deviation were recorded. The crossover point was determined as the first measured strain value after . The loss factor, $\tan\delta$, was calculated by dividing the G'' value at the last point within the LVR over the G' value at the last point within the LVR. To study the transition behaviour from the LVR to the crossover point, the flow transition index was calculated with Eq 3.1.

$$\text{Flow transition index} = \frac{\text{strain at crossover point}}{\text{strain at the end of LVR}} \quad (\text{Eq. 3.1})$$

3.2.6 Stress relaxation tests

Stress relaxation tests were used to investigate the rheological properties of the materials. The stress relaxation tests were performed with a closed cavity rheometer (CCR) (RPA elite, TA instruments, New Castle, Delaware, USA) in two steps. In the first step, the material was heated at 120 °C and deformed at 0.98% strain and 1 Hz for 1 min and cooled to 30 °C afterward. In the second step, a pre-step strain of 0.1% was applied for 15 s, after which a step strain of 80% was maintained for 105 s. The stress exerted by the material was recorded during the second step. Stress relaxation curves were fitted with a multi-mode standard solid model, which in terms of spring-dashpot models consists of three Maxwell elements ($k=3$) and a single spring in parallel (Eq 3.2). The model is described with the following equation:

$$\sigma(t) = \sum_{k=1}^3 \gamma_0 G_k e^{-t/\lambda_k} + \gamma_0 G_{\infty} \quad (\text{Eq. 3.2})$$

where $\sigma(t)$ is the stress at time (t), γ_0 is the step-strain, G_k and λ_k are the spring coefficient and relaxation time of the k^{th} Maxwell mode, and $\gamma_0 G_{\infty}$ is the residual elasticity (Marques & Creus, 2012). The relaxation time is defined as $\lambda_k = \eta_k / G_k$, where η_k is the viscosity of the dashpot of the k^{th} mode. A viscosity-weighted average relaxation time ($\bar{\lambda}$) was calculated from the λ_k of the 3 elements (Eq 3.3):

$$\bar{\lambda} = \frac{\sum \lambda_k \eta_k}{\sum \eta_k} = \frac{\sum \lambda_k^2 G_k}{\sum \lambda_k G_k} \quad (\text{Eq. 3.3})$$

3.2.7 Tensile strength analysis

Tensile strength of the gelled and sheared HTSC products was analysed using a Texture Analyser (TA.XTPlusC, Stable Micro Systems, Surrey, United Kingdom) equipped with a 5 kg load cell (Schreuders *et al.* 2019). Specimens were cut from the gelled and sheared products in parallel and perpendicular directions to the shear direction with a dog-bone-shaped mould (Figure 3.1). The dimensions (thickness and width) of the cut specimens were measured and accounted for when determining tensile strength. The ends of the specimens were placed into the tensile grips with a gap width of 15.5 mm.

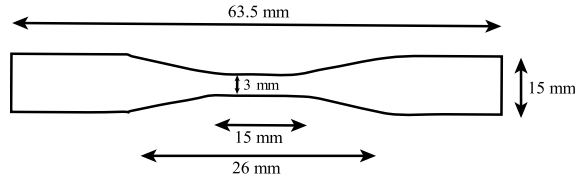


FIGURE 3.1 Illustration of the dog-bone-shaped mould used for tensile strength analysis and its dimensions.

A uni-axial tensile test was performed at room temperature with a displacement rate of 1 mm/s. The force required to keep this displacement rate was recorded by Exponent Connect software (Stable Micro Systems, Surrey, United Kingdom). The true stress (σ [Pa]) and strain (ϵ [-]) were defined as:

$$\epsilon_h(t) = \ln \frac{h(t)}{h_0} \quad (\text{Eq. 3.4})$$

$$A(t) = \frac{h_0}{h(t)} \cdot A_0 \quad (\text{Eq. 3.5})$$

$$\sigma(t) = \frac{F(t)}{A(t)} \quad (\text{Eq. 3.6})$$

where h_0 is defined as the gap width (15.5 mm), $h(t)$ is defined as the length at time t , $A(t)$ is defined as the cross-sectional area A of the specimen at time t , A_0 is the initial cross-sectional area of the specimen calculated by multiplying the thickness and width of the specimen and $F(t)$ is the force per unit of area $A(t)$. Here, we assume that the specimen's volume did not change during measurement (i.e. that the material's Poisson ratio is equal to 0.5). The fracture point was defined as the point following a dramatic decrease in stress in the stress-strain curve. The Young's Modulus was calculated from the slope of the stress-strain curve of the first 1.5 mm of displacement. The transition point from elastic to plastic behaviour was defined as the last data point in the linear regime of the stress-strain curve and was calculated with a 2% offset line. The transition stress and transition strain were determined for each specimen. The anisotropic index was calculated by dividing the fracture stress in the parallel direction by the fracture stress in the perpendicular direction. The anisotropic index was only calculated for sheared samples. Three specimens parallel and three specimens perpendicular to the shear direction were analysed for each HTSC sample. The average of the three specimens of each HTSC sample was calculated, after which an overall average and standard deviation were determined from the three sample averages.

3.2.8 Statistical analysis

All measurements were performed in triplicate unless stated otherwise. The mean values and standard deviations were calculated and used as a measure of error. Significant differences of the measured values were determined by ANOVA analysis followed by a Duncan post hoc test. Significance was defined as $p < 0.05$.

3.3 Results

3.3.1 Free amino groups

Transglutaminase (TGase) catalyses the reaction between lysine ϵ -amino group residues and γ -carboxamide amino group residues to covalently crosslink the amino acids. Because the amino groups are involved in the crosslinking reaction, a decrease in the number of free amino groups confirms the activity of TGase (Huang *et al.*, 2010; Ruzengwe *et al.*, 2020). An OPA assay was used to quantify a possible decrease of the free amino groups of gelled PPI and gelled MBPI with different TGase concentrations (0, 0.1, 0.3, 0.5, and 0.7 wt.%) and different incubation temperatures (30, 40, 50, and 60 °C) (Figure 3.2).

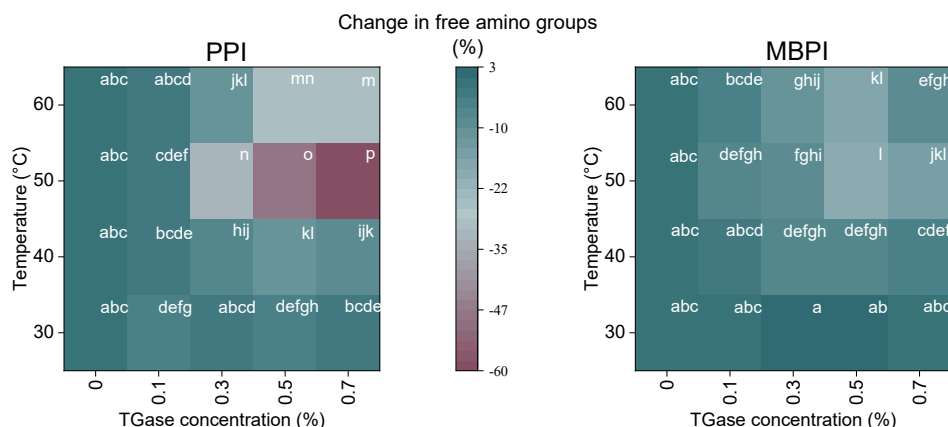


FIGURE 3.2 Change in free amino groups in gelled PPI and gelled MBPI at different TGase concentrations (0–0.7 wt.%) and different incubation temperatures (30, 40, 50, and 60 °C). The values of 0 wt.% TGase were subtracted from all other values within each row. Different letters indicate significant differences ($p < 0.05$).

The number of free amino groups at 0 wt.% TGase was subtracted from all other values at each incubation temperature to calculate the change in free amino groups. This presents us with the changes in free amino groups induced by TGase for each incubation temperature. Non-normalized data can be found in the Supplementary Material. From Figure 3.2, it became clear that TGase had a more pronounced effect on PPI than MBPI. Further, the number of free amino groups in PPI gels and MBPI gels were affected by both incubation temperature and TGase concentration. More TGase led to a decrease in the number of free amino groups, indicating additional crosslinking by TGase. With higher incubation temperature, the number of free amino groups also decreased. The most noticeable decrease in the number of free amino groups was

observed when the TGase concentration increased in the range of 0 to 0.7 wt.% at an incubation temperature of 50 °C for PPI gels and MBPI gels (Figure 3.2). This result may be explained by the optimal activity of TGase at this temperature (Gaspar & De Góes-Favoni, 2015). The use of an incubation temperature of 50 °C for MBPI gels led to a decrease in free amino groups up to 0.5 wt.% TGase, while for PPI gels a decrease in free amino groups up to 0.7 wt.% TGase was found (Figure 3.2). A concentration of more than 0.5 wt.% TGase in MBPI gels did not give additional crosslinking, which effect was previously reported by Ruzengwe *et al.* (2020). The decrease with 0 – 0.7 wt.% TGase addition in PPI gels is almost 4 times larger than in MBPI gels at 50 °C (Figure 3.2), suggesting more crosslinking in PPI.

The free amino groups of gelled PPI-WG and gelled MBPI-WG were studied as well (Figure 3.3). These gelled samples were incubated at 50 °C with different TGase concentrations (0-0.7 wt.%). A significant decrease in the number of free amino groups was found when TGase was added to PPI-WG and MBPI-WG gels (Figure 3.3). MBPI-WG gels decreased similarly in free amino groups upon addition of 0.5 wt.% TGase (-236 ± 37 nanomoles / g sample) (Figure 3.3) as gels composed of solely MBPI (-243 ± 25 nanomoles / g sample) (Figure 3.2).

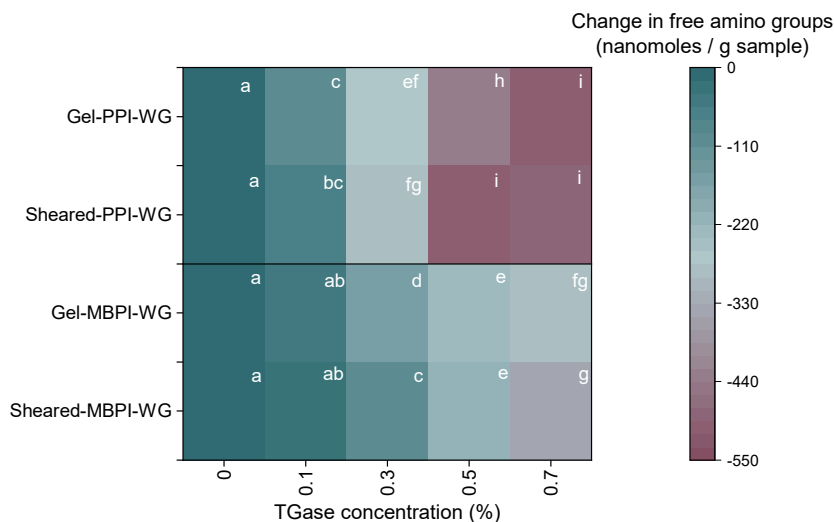


FIGURE 3.3 Change in free amino groups in gelled PPI-WG and MBPI-WG and sheared PPI-WG and MBPI-WG at different TGase concentrations (0-0.7 wt.%) at an incubation temperature of 50 °C. The values of 0 wt.% TGase were subtracted from all other values within each row. Different letters indicate significant differences ($p < 0.05$).

Theoretically, if we assume that WG does not react with TGase, we would expect only half the decrease (-122 nanomoles / g sample) in free amino groups upon addition of WG (because MBPI is present in half the amount in MBPI-WG blends). As this is not

the case, we conclude that WG in MBPI-WG gels also participates in the crosslinking reaction initiated by TGase. WG contains small amounts of lysine and is rich in glutamine, which are both substrates for TGase (Žilić, 2013). PPI-WG gels decrease -435 ± 2 nanomoles / g sample upon the addition of 0.5 wt.% TGase (Figure 3.3), whereas PPI gels decrease -998 ± 20 nanomoles / g sample (Figure 3.2). Theoretically, the decrease in free amino groups in PPI-WG gels would be -499 nanomoles / g sample, and this value is quite close to the value measured in this study. Therefore, we have to consider the fact that TGase influences crosslinking of both MBPI and WG in MBPI-WG gels, whereas the presence of WG seems to affect the crosslinking of PPI negatively. Additionally, significant differences in free amino groups were visible between gelled and sheared samples in PPI-WG with 0.5 wt.% TGase. This suggests that during shearing, additional crosslinks were formed. Most likely, these crosslinks are not due to TGase, as enzymes are deactivated at high temperatures such as 120 °C. It is more likely that the decrease in free amino groups might be caused by the additional mixing effect of shearing. By mixing, more opportunities might be created for proteins to meet and crosslink.

3.3.2 Shear rheology: amplitude sweeps

Amplitude sweeps were performed to determine G' , G'' , the linear viscoelastic regime (LVR), the flow transition index, and the crossover point ($G' = G''$) for PPI and MBPI doughs with no (0 wt.%), small amounts (0.1 wt.%) and large amounts (0.5 wt.%) of TGase. In the LVR, all samples indicated solid-like and elastic behaviour as $G' > G''$ (Figure 3.4). Furthermore, all samples show a crossover point from solid-like behaviour to liquid-like behaviour at increasing strain values. Without TGase (0 wt.%), MBPI gels have a longer LVR and a higher G' modulus than PPI gels (Table 3.2). Those measurements show that MBPI is a stronger material than PPI. Upon increasing the TGase concentration, the LVR of both PPI gels and MBPI gels changed. In PPI gels, the LVR increased from 7.36% to 9.96%, and to 13.54% with increasing the TGase concentration from 0 to 0.1 to 0.5 wt.%, respectively. Herz *et al.* (2021) & Moreno *et al.* (2020) also previously showed the extension of the LVR of PPI and SPI gels upon TGase addition. In contrast, the LVR of MBPI gels became shorter with increasing TGase concentration from 13.55% to 9.97% and to 7.36% strain for 0, 0.1, and 0.5 wt.% TGase, respectively. A shorter LVR generally corresponds to a material that is less able to withstand deformation, which could be expected when additional crosslinks are formed. Both PPI and MBPI gels show an increase in G' values at increasing TGase concentrations (Table 3.2). This trend was also seen in previous research by Sun & Arntfield (2011) who added TGase to salt-extracted PPI.

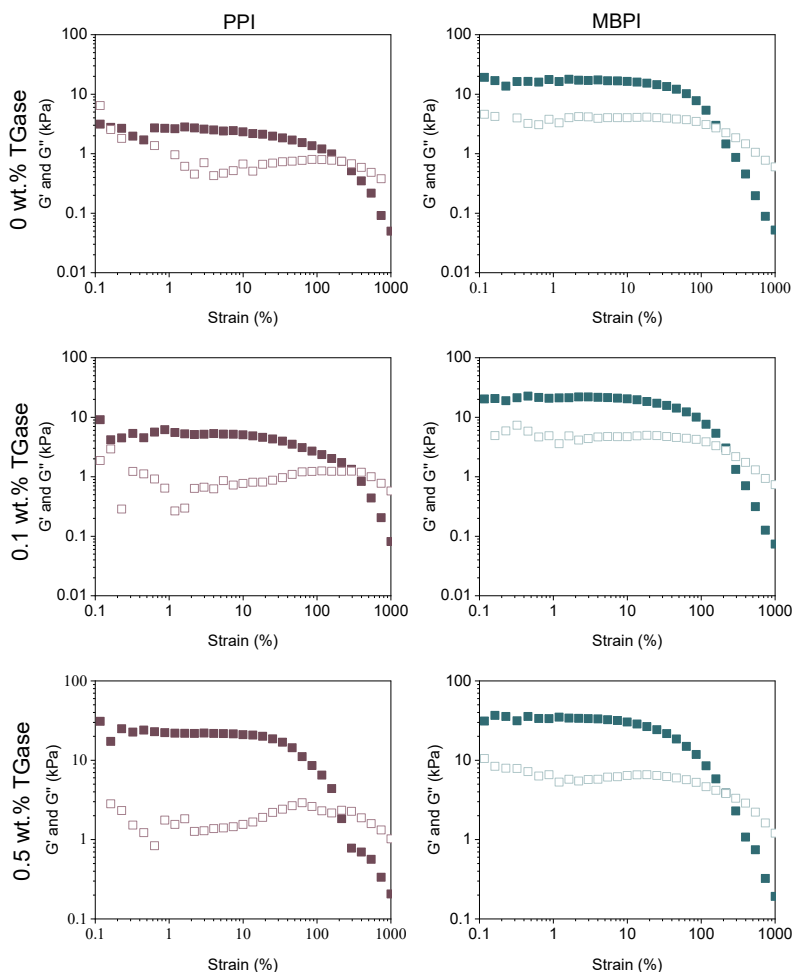


FIGURE 3.4 Storage (G' , square) and loss modulus (G'' , triangle) of PPI (pink) and MBPI (green) with different TGase concentrations (0, 0.1, 0.5 wt.%) as a function of strain amplitude at a frequency of 1 Hz at 120 °C.

The loss factor ($\tan\delta$) provides information about the elastic nature of the material and was calculated within the LVR for all samples (Table 3.2). The loss factor of PPI gels decreased with increasing TGase concentration, indicating a shift to more elastic behaviour. This supports previous research that also showed a decrease in loss factor upon the addition of TGase to Bambara groundnut protein isolate and soy protein isolate gels (Herz *et al.*, 2021; Ruzengwe *et al.*, 2020). The loss factor of MBPI gels also decreased with increasing TGase concentration, but to a lesser extent than in case of PPI gels.

The crossover point of MBPI gels was found at higher strains upon the addition of TGase

from 0 to 0.1 wt.% and remained stable at a higher TGase concentration. In PPI gels, the crossover point at 0.1 wt.% TGase is at a higher strain than for TGase concentrations of 0 and 0.5 wt.%. As the crossover point in PPI and MBPI remains relatively stable upon addition of TGase, a change in LVR also leads to a change in flow transition index. The flow transition index was calculated to evaluate the behaviour from the LVR to the crossover point, which can also be described as the breaking behaviour of the structure. A lower value of the flow transition index means more brittle behaviour (Anton Paar, 2022; Corker, Ng, Poole, & García-Tuñón, 2019). Here, we found that the flow transition index for PPI gels decreased for increasing TGase concentration, whereas the opposite effect was found for MBPI gels. Thus, in the flow transition, PPI gels became more brittle, while MBPI gels became more ductile upon TGase addition.

TABLE 3.2 Linear viscoelastic regime (LVR), crossover point ($G'=G''$), and flow transition index as calculated from the amplitude sweeps. The strain (%) and flow transition index do not contain standard deviations, as these were discrete data. All replications performed showed similar results for the strain (%) and flow transition index though.

Material	TGase (wt.%)	LVR			Crossover point	Flow transition index
		Strain (%)	G' (kPa)	$\tan\delta$	Strain (%)	
PPI	0	7.36	2.32 ± 0.28	0.29 ± 0.02	158.29	21.50
	0.1	9.96	4.85 ± 0.65	0.17 ± 0.01	215.23	21.60
	0.5	13.54	20.01 ± 1.58	0.09 ± 0.00	158.22	11.68
MBPI	0	13.55	15.29 ± 0.68	0.27 ± 0.02	116.58	8.60
	0.1	9.97	19.60 ± 0.51	0.25 ± 0.01	158.52	15.89
	0.5	7.36	30.34 ± 0.59	0.21 ± 0.00	158.56	21.54

3.3.3 Shear rheology: stress relaxation

Stress relaxation tests were performed to understand the influence of TGase on the elasticity and relaxation behaviour of the materials. Wittek, Zeiler, Karbstein, & Emin (2020) previously suggested that the maximum shear stress can be interpreted as a measure of elasticity. Elasticity, here, refers to the elastic part of the viscoelastic behaviour of PPI and MBPI. MBPI gels had a higher maximum stress than PPI gels and were, therefore, more elastic (Figure 3.5A). In PPI gels and MBPI gels, the addition of 0.5 wt.% TGase increased the maximum stress, and thus the elasticity. Shand *et al.* (2008) previously showed enhanced elasticity of PPI gels that were treated with TGase as well. In a stress relaxation test, a viscoelastic material shows a gradual decrease in stress, whereas an ideal viscous material relaxes instantly, and an ideal elastic material does not relax at all (Wittek *et al.*, 2020). Figure 3.5A shows that both MBPI and PPI gels show a monotonic decrease with time, which indicates viscoelastic behaviour.

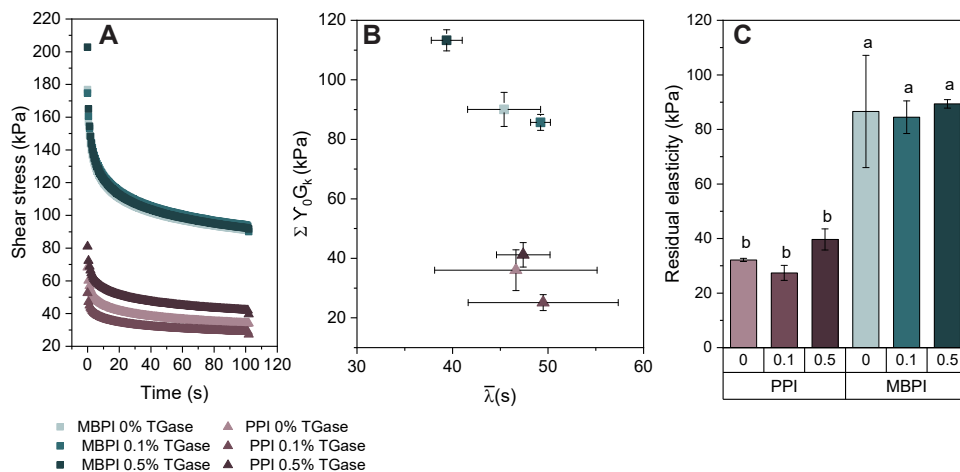


FIGURE 3.5 A) Stress relaxation curves of MBPI gels and PPI gels at 80% strain, heated to 120 °C and cooled back to 30 °C, with different concentrations of TGase (0, 0.1, 0.5 wt.%). B) Parameter plot of multi-mode standard solid model fit to curves of A). C) Residual elasticity of multi-mode standard solid model curves.

To further study the relaxation behaviour of the PPI and MBPI gels, the stress relaxation curves of Figure 3.5A were fitted with a multi-mode standard solid model with 3 parallel Maxwell elements (Eq. 3.2). The fitting parameter $\gamma_0 G_k$ was summed and a viscosity-weighted average of the relaxation time ($\bar{\lambda}$) was calculated (Eq. 3.3) and plotted in Figure 3.5B. The full fit data of the 3 separate model elements can be found in the Supplementary Material (Table S3.1). For MBPI gels, a TGase concentration of 0.5 wt.% resulted in a significant increase in the intensity of the stress coefficient ($\gamma_0 G_k$) in comparison to 0 and 0.1 wt.% (Figure 3.5B). Furthermore, at a TGase concentration of 0.5 wt.%, the relaxation behaviour of MBPI gels shifted towards shorter relaxation times. PPI gels, on the other hand, showed a decreased intensity at 0.1 wt.% TGase compared to 0 and 0.5 wt.% TGase (Figure 3.5B). No differences in average relaxation times were found for PPI gels upon increasing TGase concentration.

The constant ($\gamma_0 G_\infty$) in the multi-model standard solid model (Eq. 3.2) is defined as the residual elasticity which is left after relaxation (Salimi, Abbassi-Sourki, Karrabi, & Reza Ghoreishy, 2021). MBPI gels have a higher residual elasticity than PPI gels (Figure 3.5C). Additionally, both MBPI and PPI gels show a slight dip in residual elasticity at 0.1 wt.% TGase compared to 0 and 0.5 wt.% TGase, although not necessarily significant.

3.3.4 Macrostructure

The morphologies of gelled and sheared samples were analysed by manually deforming these samples and visually inspecting the gel structure and/or fibres (Figure 3.6).

Overall, MBPI gels were stiffer and crumblier compared to the more compact, elastic and uniform structure of PPI gels. This observation is further supported by a higher Young's Modulus for MBPI gels compared to PPI gels (Supplementary Material: Figure S3.3). PPI gels did not break upon manual deformation when more than 0.1 wt.% TGase was added, whereas gels did break into two parts when no TGase was added (Figure 3.6). Therefore, the macrostructure of PPI gels became more stretchable upon the addition of TGase. A similar observation was made when determining the critical strain of the LVR (Figure 3.4). The visual macrostructure of MBPI gels was hardly affected by any TGase addition. As TGase affected the physical properties of MBPI gels (Figure 3.4), but not the macrostructure, we suggest that the microstructure is what TGase changes in MBPI gels.

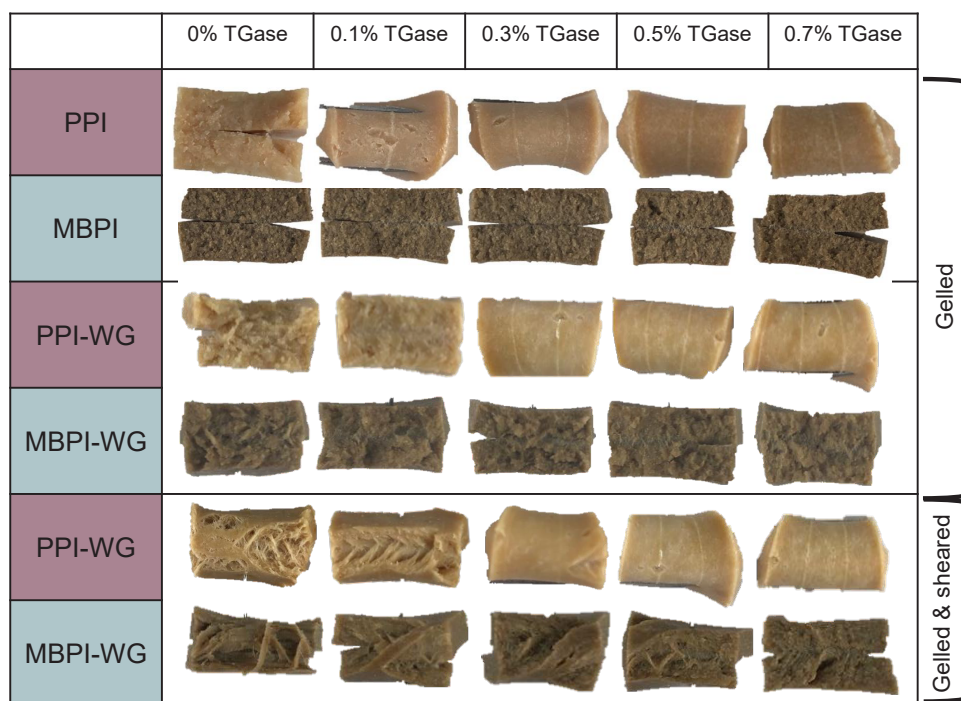


FIGURE 3.6 Visual observation of gelled and sheared (39 s⁻¹) samples of pea protein isolate (PPI), mung bean protein isolate (MBPI), PPI-wheat gluten (WG) blends and MBPI-WG blends with different concentrations of TGase (0.0-0.7%) incubated at 50 °C. Samples were deformed manually in the direction of the shear flow.

The addition of WG to PPI made the gel structure stickier and less uniform compared to the gel without WG (Figure 3.6). Beyond 0.3 wt.% TGase, the PPI-WG blend gel did not break, suggesting that TGase increased the stretchability of the gel. Similar to MBPI gels, MBPI-WG gel structures were not affected by TGase. For the formation of fibrous structures, blends of PPI-WG and MBPI-WG were sheared at 120 °C in the shear cell (Figure 3.6). The fibrous structure of PPI-WG without TGase was in line with

the previous observation by Schreuders *et al.* (2019). The fibrous structure of PPI-WG became less apparent when more TGase was added, which was previously also observed by Zhang *et al.* (2021) in the extrusion of peanut protein with TGase. Additionally, beyond 0.3 wt.% TGase, the structure became more deformable and did not break upon manual deformation. The fibres formed in MBPI-WG structures became thicker, crumblier, and easier to break compared to PPI-WG. The fibrous MBPI-WG structure also diminished upon increasing amounts of TGase.

3.3.5 Mechanical properties in extension

TGase concentration and incubation temperature were expected to also influence the mechanical properties in extension of the gels and sheared gels. To test this, the shear cell samples were subjected to a tensile test, parallel and perpendicular to the direction of the shear flow. For gels, only results in the parallel direction are shown, because the results found in the perpendicular direction were similar. The tensile stress was measured as a function of tensile strain, and from these curves the fracture stress, fracture strain, Young's Modulus, transition point stress and transition point strain were determined for all gelled samples and visualized in heatmaps (Figure 3.7).

Fracture stress increased significantly for PPI gels with increasing incubation temperature and TGase concentration, supporting previous findings by Shand *et al.* (2008) (Figure 3.7). A maximum value for the fracture stress was found after incubation at 50 °C and 60 °C using 0.5 wt.% TGase. Previous research on soy protein gels also found major changes in textural parameters upon addition of TGase (Herz *et al.*, 2021; Herz, Schäfer, Terjung, Gibis, & Weiss, 2021; Liu *et al.*, 2021). In contrast, the effect of TGase on fracture stress of MBPI gels was limited under all process conditions tested. The fracture strain of PPI gels and MBPI gels was affected in a similar way as fracture stress (Figure 3.7): higher values were obtained for the fracture strain of PPI gels treated at 50 °C and 60 °C using 0.5 wt.% TGase. The fracture stress and strain reached an optimum at 0.5 wt.% TGase in both PPI and MBPI gels at 50 °C and 60 °C. At higher concentrations of TGase (0.7 wt.%), the fracture stress and strain slightly decreased in both PPI and MBPI gels at temperatures of 50 °C and 60 °C. Furthermore, the Young's Moduli of MBPI gels were significantly larger than the Young's Modulus of PPI gels (Supplementary Material). These results indicate that the MBPI gels are stiffer than PPI gels. The Young's Modulus of PPI gels did not change upon addition of TGase, whereas in MBPI gels a decrease in Young's Modulus was observed. As the Young's Modulus and LVR of MBPI gels became smaller upon addition of TGase, while the macrostructure was not affected, we suggest that TGase changes the microstructure of MBPI gels (Figure 3.4 & Figure 3.6).

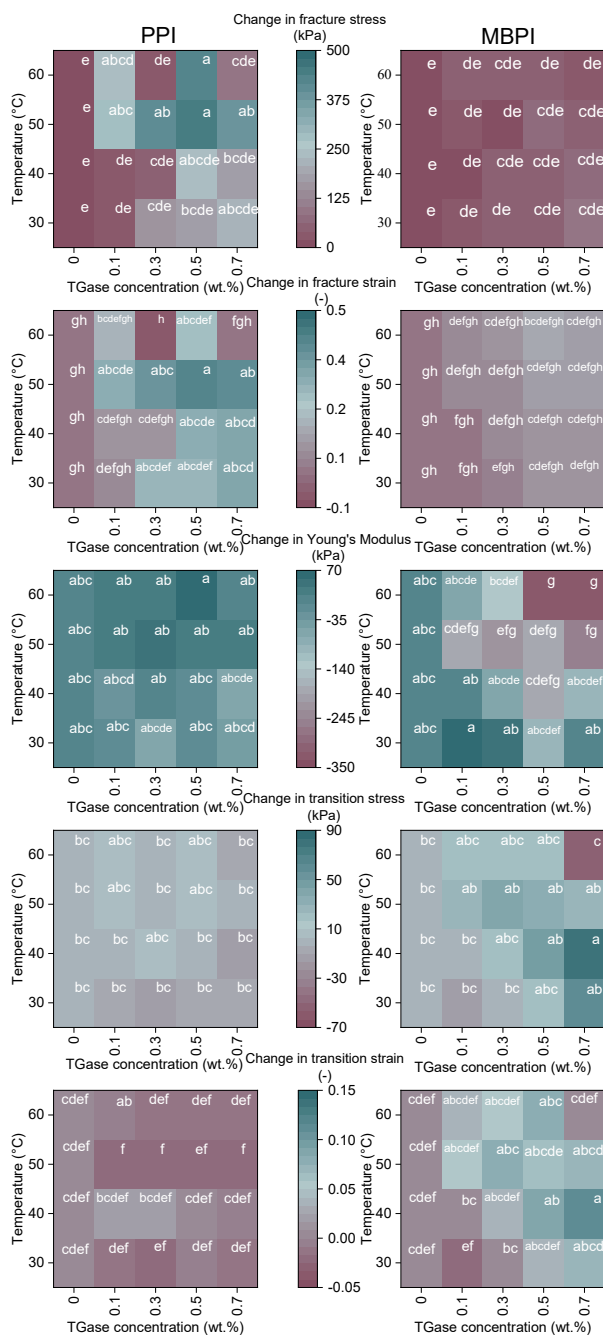


FIGURE 3.7 Change in fracture stress, fracture strain, Young's Modulus, transition stress and transition strain for PPI and MBPI gels at different temperatures and TGase concentrations. The values of 0 wt.% TGase were subtracted from all other values within each row. Non-normalized data can be found in the Supplementary Material. Different letters within one heatmap indicate significant differences ($p < 0.05$).

The transition point is defined as the last linear point on the stress-strain curve. The transition point represents the transition from linear viscoelastic behaviour to plastic (non-linear) behaviour. TGase concentration and incubation temperature did not have a large effect on the transition stress of PPI gels, whereas the transition stress of MBPI gels increased with 80 kPa from 0 wt.% TGase to 0.7 wt.% TGase at 40 °C (Figure 3.7). Furthermore, significant effects were seen on the transition strain of MBPI (Figure 3.7). Especially at 40 °C, there was a clear increase in transition strain at higher TGase concentration in MBPI gels. This suggests that the elastic portion of the tensile curves became longer, and thus suggests that the stretchability of the material increased. Increased stretchability could be a result of crosslinking. Thus, we can conclude that TGase changed PPI gels at large deformation tensile properties, while MBPI gels were changed at small deformation tensile properties.

From the previous results, it was concluded to continue with an incubation temperature of 50 °C. To create a fibrous, meat-like structure, wheat gluten (WG) was added to the PPI and MBPI and the blends were gelled and sheared and the fracture stress was analysed (Figure 3.8). The fracture stress of gelled PPI-WG (84.02 ± 25.73 kPa) and gelled MBPI-WG (169.28 ± 30.16 kPa) (Figure 3.8) was lower than gels from solely PPI (163.21 ± 14.21 kPa) or MBPI (257.50 ± 27.13 kPa) without TGase (Supplementary Material: Figure S3.3).

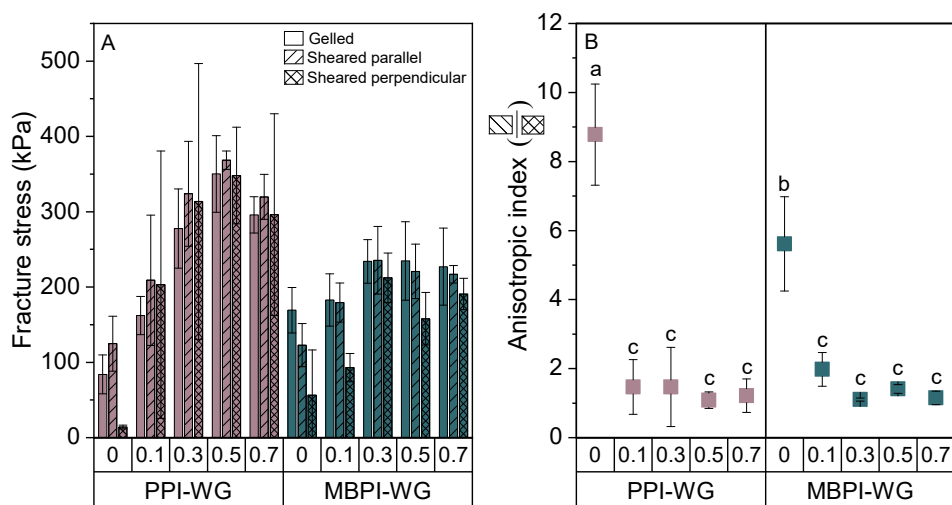


FIGURE 3.8 A) Fracture stress of gelled, parallel direction sheared, and perpendicular direction sheared blends of PPI-WG (pink) and MBPI-WG (green) at different TGase concentrations and incubated at 50 °C. B) Anisotropic index of PPI-WG (pink) and MBPI-WG (green) samples at different TGase concentrations and incubated at 50 °C.




TGase increased the fracture stress of gelled PPI-WG samples from 0 wt.% up to 0.5 wt.% (84.02 ± 25.73 kPa to 350 ± 50.88 kPa), and to a lesser extent increased the fracture stress of gelled MBPI-WG samples (169.28 ± 0.16 kPa to 234.72 ± 52.18 kPa) (Figure 3.8A). The fracture stress of sheared MBPI-WG and sheared PPI-WG increased in both the parallel and perpendicular directions to the shear flow up to an addition of 0.3 and 0.5 wt.% TGase. The difference between parallel and perpendicular samples at 0 wt.% TGase suggests an anisotropic material. The anisotropic index of PPI-WG at 0 wt.% TGase is much higher than previous results obtained by (Schreuders *et al.*, 2019), which may be because no salt was added and samples were incubated in this study. The fracture stresses in the parallel and perpendicular samples became more or less similar upon increasing TGase concentration for both MBPI-WG and PPI-WG. This corresponded to a decrease in the anisotropic index, which is observed from 0 to 0.1 wt.% TGase (Figure 3.8B), and supports the decrease in fibrousness in the macrostructure analysis (Figure 3.6).

3.4 Discussion

When combining all results, it can be concluded that transglutaminase (TGase) affected pea protein isolate (PPI) in a different way than it affected mung bean protein isolate (MBPI) gels (Figure 3.9).

TGase was shown effective to change behaviour of PPI gels in the large deformation regime (macrostructure, non-linear part tensile test), while the behaviour of MBPI gels was mostly affected in the small deformation regime (stress relaxation, linear part tensile test). At 0 wt.% TGase, PPI gels had more free amino groups compared to MBPI (Supplementary Material: Figure S3.1). This result suggests better accessibility of the amino acid groups in the case of PPI, because the amino acid compositions of PPI and MBPI indicate around equal presence of glutamine and lysine (Table 3.1). Therefore, TGase should be able to crosslink amino acids in both PPI and MBPI. However, the structure and conformation of the proteins play a decisive role. Previous research on non-gluten proteins also showed that the effect of TGase was indeed influenced by the nature of the proteins used (Tomić, Torbica, & Belović, 2020).

TGase affected the amplitude sweeps of both PPI and MBPI gels. The longer LVR with increasing TGase concentration in PPI gels was probably due to a larger density of crosslinks formed, making the material more ductile (Schreuders *et al.*, 2021). The higher ductility with increased TGase concentration was also visible in the macrostructure of the PPI gels as a more stretchable gel structure (Figure 3.6). The LVR of MBPI gels becomes shorter with increasing TGase concentration, suggesting a change to a more brittle material.

	<div></div> <div>Free amino acid groups</div>	<div></div> <div>Strain sweep</div>				<div></div> <div>Stress relaxation</div>	
		G' (LVR)	Strain (LVR)	$\text{Tan}\delta$ (LVR)	FTI	λ_k	Residual elasticity
PPI	<div><div>-</div><div>-</div><div>-</div></div>	<div><div>+</div></div>	<div><div>+</div></div>	<div><div>-</div></div>	<div><div>-</div></div>	<div><div></div></div>	<div><div></div></div>
MBPI	<div><div>-</div></div>	<div><div>+</div></div>	<div><div>-</div></div>	<div><div>-</div></div>	<div><div>+</div></div>	<div><div>-</div></div>	<div><div></div></div>

FTI: flow transition index, YM: Youngs Modulus, λ_k : average relaxation time

 Increases with increasing TGase concentration  Decreases with increasing TGase concentration




 No effect

FIGURE 3.9 Overview of effects of TGase on free amino groups, strain sweep, stress relaxation, macrostructure and tensile tests for PPI and MBPI gels.

The increased G' values at higher TGase concentrations suggested that both PPI gels and MBPI gels are forming stronger networks by the addition of TGase (Sun & Arntfield, 2011). At the same time, PPI and MBPI gels showed a lower loss factor, meaning that gels were formed with more elastic nature. This permitted a substantial elongation of the product under increasing strain before the structure was distorted. The increased elasticity at higher TGase concentration was also confirmed by the increased maximum stress in stress relaxation tests. Furthermore, the increased elasticity was visible in the macrostructure of PPI gels (Figure 3.6). TGase addition led to a lower value for the flow transition index in PPI gels, which indicates that PPI gels transitioned from a weak network to a stiff and elastic material upon the addition of TGase. This effect was explained as a closer packing of the gel network by Corker, Ng, Poole, & García-Tuñón (2019) and Dabbaghi *et al.* (2021). On the other hand, MBPI gels transition gradually to flow, as the flow transition index increased with addition of TGase. This behaviour is characteristic of a gradual stretch or disentanglement of the polymer network (Dabbaghi *et al.*, 2021). The increase in stress coefficient combined with a shift towards smaller relaxation times for MBPI gels might suggest that TGase produced smaller aggregates instead of creating a more crosslinked network in MBPI. Here the connection can also be drawn to the limited effect of TGase on tensile parameters for MBPI gels. Tensile tests are large deformation tests and focus on the whole network

 Macrostructure	 Tensile test			
	Stress (fracture)	Strain (fracture)	YM	Transition point
+	+	+	○	○
○	○	○	-	+

of the material instead of smaller aggregates. This again confirmed that TGase mostly forms smaller aggregates in MBPI instead of the whole sample. Due to the formation of small, more compact aggregates, the effective volume fraction in MBPI gels decreased, decreasing the LVR as well (Figure 3.4). In PPI gels, effects were visible mostly at larger deformation, suggesting more intermolecular crosslinking of TGase. Intermolecular crosslinking created a strong PPI gel network, increasing the elasticity and therefore elongating the LVR (Figure 3.4). We, therefore, hypothesize that differences between the effect of TGase on PPI and MBPI arise from differences in location and accessibility of glutamine and lysine amino acid groups. In PPI, glutaminase and lysine groups are well accessible for TGase, enabling the formation of a complete network with intermolecular TGase-induced covalent bonds (Figure 3.10). This strengthens the overall gel network, especially visible in large deformation tests. Upon deformation, the covalent TGase bonds keep the gel network intact, until a maximum force is applied which finally breaks the bonds (Figure 3.10). In MBPI, there was only a minor change in free amino groups (OPA), so some crosslinks were formed. However, we believe that in MBPI mostly intramolecular covalent bonds were formed, which could be caused by the location and poor accessibility of glutamine and lysine groups (Figure 3.10). It can be expected that intramolecular crosslinks created more compact gel aggregates. Then, upon deformation, the hydrophobic interactions are the limiting factor

and will break first, enabling the protein chains to move away from each other and partly start to stretch (Figure 3.10). So although addition of TGase may lead to partial covalent crosslinking in MBPI, physical crosslinks (hydrogen bonds) will probably still dominate the rheological behaviour rather than covalent crosslinking. Therefore, some properties (such as tensile tests and macrostructure) did not change for MBPI, even at high enzyme concentrations.

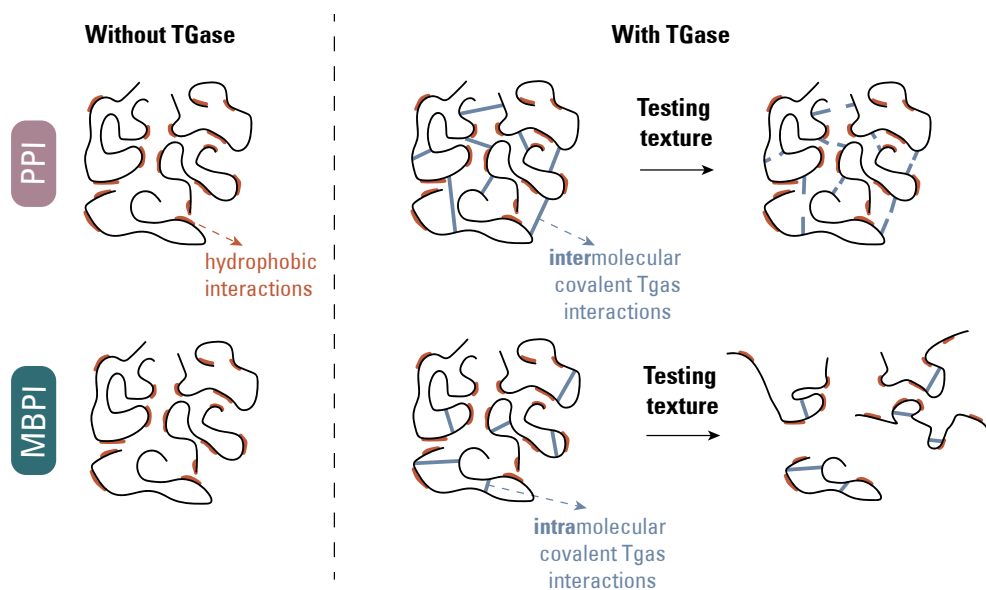


FIGURE 3.10 Hypothesized network formation of PPI and MBPI gels with transglutaminase and hypothesized structure breakdown upon texture testing such as tensile tests, stress relaxation tests and amplitude sweeps.

The amount of TGase also played an important role in the structure formation of PPI and MBPI. At low TGase concentrations (0.1 wt.%), mainly intra-aggregate crosslinks could be formed. This could mean that the protein aggregates become more compact. With more compact aggregates, there will be a higher mobility in the system causing a lower residual elasticity in both PPI and MBPI gels. By adding more transglutaminase (0.5 wt.%), TGase can also form aggregate-aggregate crosslinks, increasing the residual elasticity again. On the other hand, very high amounts of TGase (> 0.5 wt.%) decreased fracture stress and strain in PPI and MBPI gels. Possibly, excessive crosslinking of glutamine and lysine inhibited a uniform development of the protein network and the improvement of gel breaking strength (Guo *et al.*, 2013; Jong & Koppelman, 2002). Previous research on the addition of TGase to Bambara groundnut protein isolate also revealed a significant reduction in rheological properties upon higher TGase additions (Ruzengwe *et al.*, 2020).

Upon the addition of wheat gluten (WG), we encountered changes in behaviour. In PPI-WG and MBPI-WG sheared gels, the fibrous structure as well as the mechanical anisotropy reduced at higher TGase concentrations. This result can be explained by the fact that TGase is able to form a heteropolymer gel between different types of proteins at high substrate concentrations (Gaspar & De Góes-Favoni, 2015; Motoki & Kumazawa, 2000). In this case, TGase could form crosslinks between amino groups of WG and PPI or MBPI. The two-phase separated system then changes to a single phase, preventing fibre formation. The reduction in visual fibrous structure is also confirmed on a mechanical level by the fracture stress in parallel and perpendicular directions that become more or less equal upon addition of TGase. This indicates a decrease in mechanical anisotropy. To conclude, in sheared PPI-WG and MBPI-WG samples, the application of transglutaminase does not seem beneficial at first glance. However, when using small amounts, we can use TGase application as a method to tailor the fibrous structure to fit certain meat analogue product groups.

3.5 Supplementary material

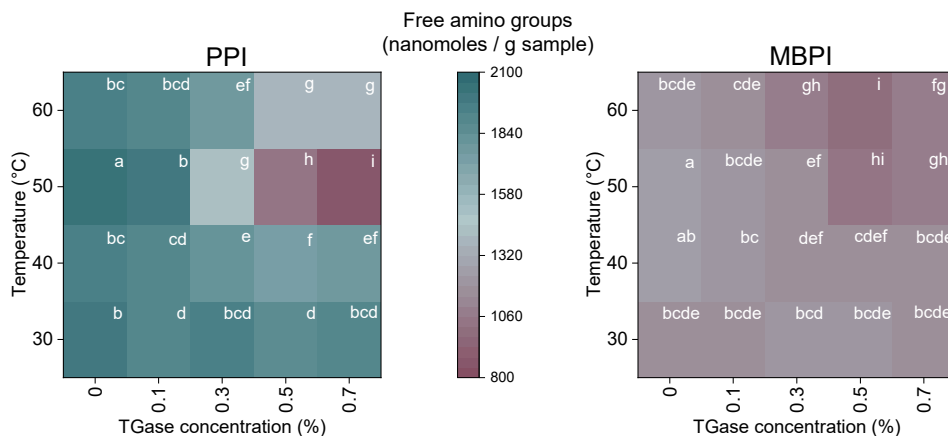


FIGURE S3.1 Amount of free amino acid groups (non-normalized) of PPI and MBPI gels with varying TGase concentration (0-0.7 wt.%) and incubation temperature (30-60 °C). Different letters within one heatmap indicate significant differences ($p < 0.05$).

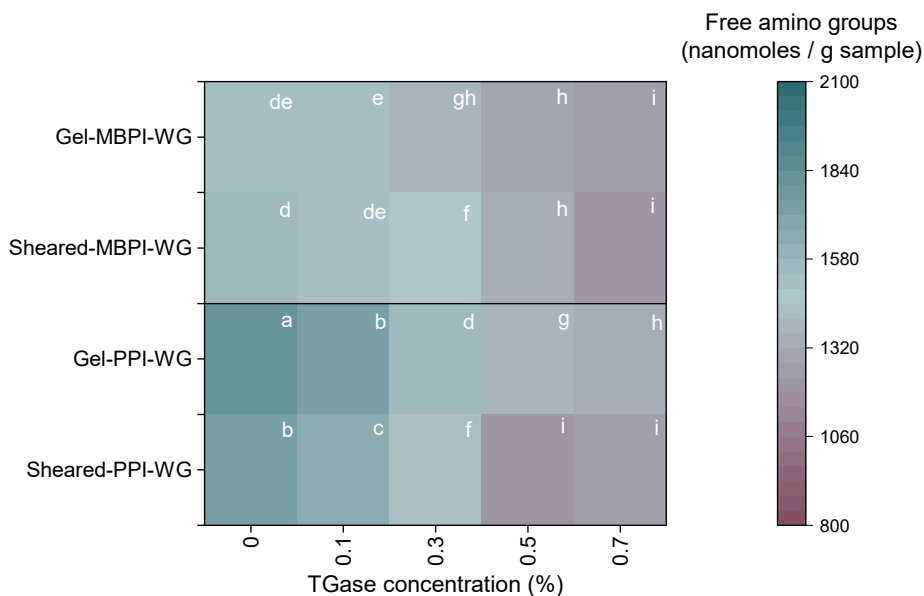


FIGURE S3.2 Amount of free amino acid groups (non-normalized) of gelled and sheared, PPI-WG and MBPI-WG at different TGase concentrations (0-0.7 wt.%) and an incubation temperature of 50 °C. Different letters indicate significant differences ($p < 0.05$).

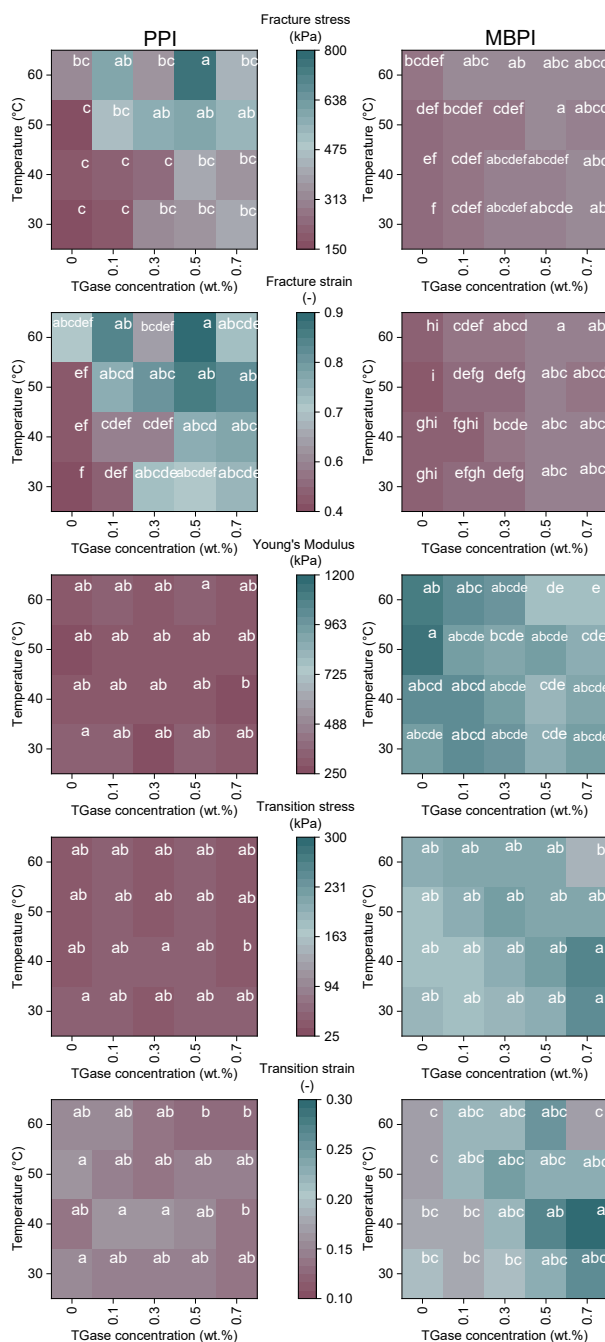


FIGURE S3.3 Non-normalized fracture stress, fracture strain, Young's Modulus, transition stress and transition strain of PPI and MBPI gels with varying TGase concentration (0-0.7 wt.%) and incubation temperature (30-60 °C). Differences letters within one heatmap indicate significant differences ($p < 0.05$).

TABLE S3.1 Full 3 element fit data of stress relaxation experiments.

	$\gamma_o G1$	$\gamma_o G2$	$\gamma_o G3$	λ_1	λ_2	λ_3	$\gamma_o G_\infty$
PPI 0 wt.% TGase	10734±4931	11745±1169	13566±1001	0.8±0.3	5.8±1.2	51.2±9.7	32129±573
PPI 0.1 wt.% TGase	7583±1878	7689±452	9860±981	0.9±0.4	6.3±1.7	54.1±8.7	27396±2770
PPI 0.5 wt.% TGase	12035±4261	12668±789	16483±1336	0.8±0.3	6.1±0.9	51.6±2.9	39671±3880
MBPI 0 wt.% TGase	27907±5700	28066±2998	34078±7139	0.8±0.3	6.1±1.1	49.9±4.1	86562±20569
MBPI 0.1 wt.% TGase	22912±729	27124±700	35664±1301	1.0±0.0	6.8±0.2	53.9±1.1	84482±5943
MBPI 0.5 wt.% TGase	46834±3207	30696±4544	35735±2136	1.2±0.0	3.2±0.1	43.1±1.5	89355±1555

4

Chapter 4

How fractionation procedure of mung bean protein affects transglutaminase crosslinking

This chapter has been published as Schlangen, M., Raak, N., Taghian Dinani, S., Corredig, M., van der Goot, A.J. (2023) How fractionation procedure of mung bean protein affects transglutaminase crosslinking. Food Hydrocolloids. 145, 109067.

Abstract

Transglutaminase is often used to improve functional properties of plant proteins. Here, we report on the effects of the fractionation procedure on transglutaminase susceptibility of mung bean proteins at three length scales: molecular, colloidal, and bulk. Dispersions of 4 wt.% mung bean protein fractions were treated with transglutaminase. The four fractions were obtained through (1) dry fractionation (fine fraction); (2) dry fractionation with additional heating; (3) lab-scale wet fractionation; and (4) a commercial protein isolate. Analysis of rheological properties (at 9.5 wt.% dry matter) revealed that transglutaminase crosslinking formed tougher materials when using the fine fraction, the heated fine fraction, and the wet fractionated isolate, while the rheological properties of the protein isolate were hardly changed. Proteins in all fractions were crosslinked by transglutaminase at molecular scale, as confirmed by an increase in large molecular weight bands in gel electrophoresis, but the extent of crosslinking depended on the fraction used. The molecular changes also resulted in altered physical chemical properties for some fractions, as revealed by protein dispersibility, confocal laser scanning microscopy, and particle size distribution. At the colloidal scale, transglutaminase crosslinking led to an increased particle size in the fine fraction and heated fine fraction, while particle sizes of the wet fractionated isolate and commercial protein isolate were mostly unaffected. The differences between the fractions were explained by three mechanistic crosslinking routes. To conclude, protein fractionation procedure greatly affected susceptibility to transglutaminase.

4.1 Introduction

In the past decade, plant proteins have become an important ingredient in foods, amongst other with the aim to replace meat and dairy products. Especially soy and yellow pea protein are used in plant-based foods, because of their favourable functional properties (Kyriakopoulou, Dekkers, & van der Goot, 2019; Vatansever, Tulbek, & Riaz, 2020). Another legume that is gaining attention as a potential food ingredient is mung bean (*Vigna radiata*). Mung beans are inexpensive to cultivate in comparison to soy and are drought resistant (Brishti *et al.*, 2021). Mung beans contain a high amount of protein (± 25 g protein / 100 g dry matter) that is rich in essential amino acids (Du *et al.*, 2018; Mubarak, 2005; Yi-Shen, Shuai, & Fitzgerald, 2018). So far, the starch fraction of mung bean has been widely studied, while mung bean protein is still underexplored. Protein extracted from mung bean showed great potential to form structures in food, and in particular, in meat analogue applications (Brishti *et al.*, 2021, 2017; Schlangen, Dinani, Schutyser, & van der Goot, 2022). However, mung bean protein, when combined with wheat gluten, generally gives weaker structures upon heating compared with soy protein when combined with wheat gluten, suggesting that more protein interactions occur in the soy based material compared with mung bean (Schlangen *et al.*, 2023; Schreuders *et al.*, 2019). The introduction of additional protein crosslinks in mung bean, for example through, heating, chemical treatment, or enzymatic treatment, could be a route to obtain higher viscosity and stronger gels, which enhances its potential as a value added ingredient in plant-based meat and dairy alternatives (Buchert *et al.*, 2010; Singh, 1991).

Transglutaminase (TGase) is an enzyme that is widely studied for crosslinking different plant proteins, such as soy, pea, and Bambara groundnut protein (Djoullah, Djemaoune, Husson, & Saurel, 2015; Liu *et al.*, 2021; Mattice & Marangoni, 2021; Nivala, Nordlund, Kruus, & Ercili-Cura, 2021; Ruzengwe, Amonsou, & Kudanga, 2020; Shand, Ya, Pietrasik, & Wanasundara, 2008; Sun & Arntfield, 2011; Zhang *et al.*, 2021). TGase catalyses intra- and inter-molecular crosslinking reactions between lysine (acyl acceptor) ϵ -amino groups and glutamine (acyl donor) γ -carboxamide groups and, thus, forms covalent bonds (Gaspar & De Góes-Favoni, 2015). The crosslinking of proteins by TGase can lead to high molecular weight proteins that can give stronger gels and increased water holding capacity (Gaspar & De Góes-Favoni, 2015; Shand *et al.*, 2008). Recently, it was shown that TGase improved the mechanical and rheological properties of gels produced from pea protein isolate, while gels from mung bean protein isolate were relatively unaffected (Schlangen *et al.*, 2023). Then, it was hypothesized that the lysine and glutamine amino groups in mung bean protein isolate were less available or accessible for TGase to crosslink.

The availability of amino groups is partly determined by the structure of the protein, which in turn is dependent on the protein fractionation procedure. Conventional wet fractionation, based on alkaline extraction and isoelectric precipitation, yields ingredients with a protein purity of 80 wt.% at least (Assatory, Vitelli, Rajabzadeh, & Legge, 2019; Rivera, Siliveru, & Li, 2022), but at the cost of protein structural changes and, thus, often a loss of native protein characteristics (Schutyser, Pelgrom, van der Goot, & Boom, 2015). An alternative to wet fractionation is dry fractionation. With dry fractionation, plant proteins are enriched in a fine fraction obtained via milling and air classification (Pelgrom, Boom, & Schutyser, 2015; Schlangen *et al.*, 2022). An advantage of dry fractionation is that the protein native structure is preserved. The fraction enriched in proteins after dry fractionation often has a different technological and nutritional functionality compared with that of the commercial protein isolate counterparts (Opazo-Navarrete, Schutyser, Boom, & Janssen, 2018; Vogelsang-O'Dwyer *et al.*, 2020). This is because of the mild process conditions used during dry fractionation and the fact that the fractions obtained contain many other components next to protein. Therefore, the susceptibility of proteins to TGase is expected to be different depending on processing routes used to make the protein-rich fractions and molecular architecture, with a lower susceptibility in more aggregated protein structures. Indeed, the accessibility of TGase is determined by the steric availability of the lysine and glutamine residues.

Pelgrom, Boom, & Schutyser (2015) and Schutyser, Pelgrom, van der Goot, & Boom (2015) showed that TGase can be used to crosslink mildly fractionated pea proteins and found that this resulted in a stronger heat-induced gel compared with un-crosslinked pea proteins. However, to date, there are no other studies that report on the use of TGase to crosslink plant proteins in fine fractions obtained through dry fractionation. Furthermore, there are no prior studies on the effect of fractionation procedure on the susceptibility of proteins to TGase crosslinking activity. The current work aims to fill the above research gaps.

Thus, the aim of this study was to investigate the effect of mung bean protein fractionation procedures on the susceptibility of those proteins to TGase crosslinking. A fine fraction, a heated fine fraction, a pH precipitated wet fraction, and a commercial protein isolate were compared on their susceptibility to TGase crosslinking activity. We hypothesize that the dispersibility of the protein will affect the susceptibility to TGase. Susceptibility to TGase was studied at three different length scales: (1) molecular scale (gel electrophoresis), (2) colloidal scale (particle size, protein dispersibility, and microstructure), and (3) bulk scale (rheology). Here, colloidal scale refers to the nanometre to micrometre range and thus referring to protein present in particles that are solvated, but not in solution.

4.2 Materials & Methods

4.2.1 Materials

Dehulled mung beans (*Vigna radiata*) were obtained from Vladex (Middelharnis, the Netherlands). The average dry matter content was assumed to be the same as for flour from dehulled mung beans and was 91.5 wt.%. Mung bean protein isolate (UNIMUNG M70) was obtained from Barentz (Hoofddorp, the Netherlands). The protein content and dry matter content of the protein isolate were 68.9 wt.% (N x 5.7) on dry basis and 94.3 wt.%, respectively. The supplier of the protein isolate reported a maximum fat content of 6 wt.%.

Transglutaminase (ACTIVA wm) was obtained from Ajinomoto Co. (Ajinomoto, Tokyo, Japan). The composition of the enzyme preparation is 1% transglutaminase and 99% maltodextrin, and the activity was reported by the suppliers as 100 U/g. We use the term transglutaminase (TGase) in this study to refer to the enzyme preparation that includes both transglutaminase and maltodextrin. N-Ethylmaleimide (NEM) and sodium chloride were obtained from Sigma-Aldrich (Missouri, USA).

4.2.2 Preparation of the fractions

Four different mung bean protein fractions were used in this study. An overview of their fractionation pathways is visualized in Figure 4.1. Milling and air classification parameters used were based on previous research results (Schlangen *et al.*, 2022). For preparation of the fine fraction, the legumes were first pre-milled into grits with a pin mill (LV 15 M, Condux-Werk, Wolfgang bei Hanau, Germany). Next, the grits were milled into a flour with a ZPS50 impact mill (Hosokawa-Alpine, Augsburg, Germany). The ZPS50 mill speed used was 8000 rpm, the classifier wheel speed was set to 4000 rpm, the air flow was 52 m³/h, and the feed rate was ~500 g/h. A batch size of 3 kg mung beans was used. The obtained flour was separated into a fine (protein-rich) and coarse (starch-rich) fraction by air classification with a ATP50 classifier (Hosokawa-Alpine, Augsburg, Germany). Here, a classifier wheel speed of 10,000 rpm, an air flow of 47 m³/h, and a feed rate of ~250 g/h were used. The heated fine fraction was prepared by mixing the fine fraction (either 9.5 wt.% dry matter for rheology, or 4 wt.% protein for other experiments) with MilliQ water on a vortex for 1 min, followed by heating this dispersion at 90 °C for 30 min. Subsequently, the dispersion was rapidly cooled with cold tap water.

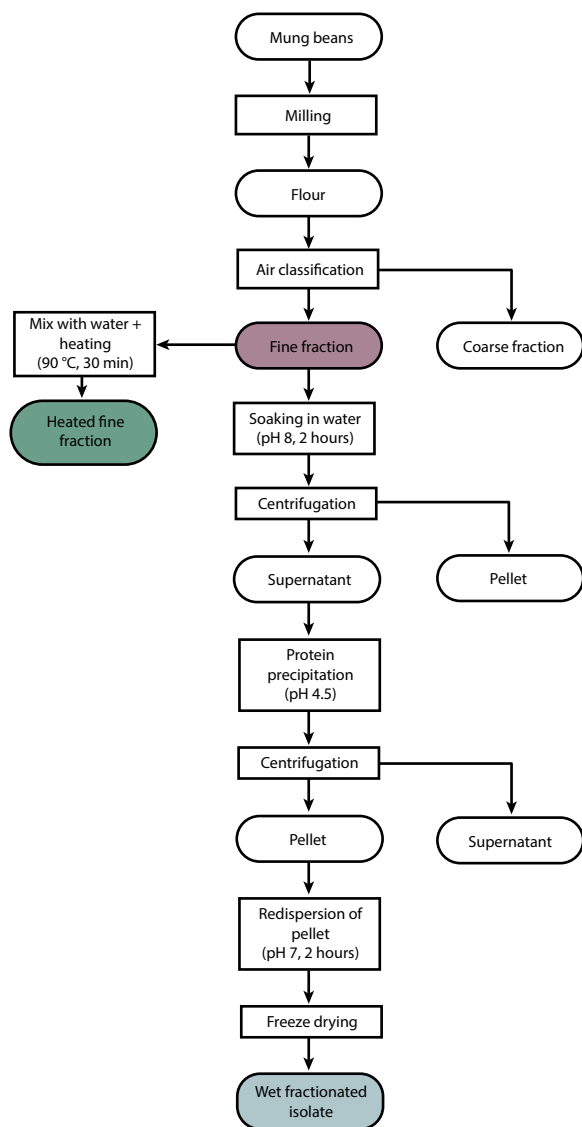


FIGURE 4.1 Fractionation scheme of fine fraction, heated fine fraction, and wet fractionated isolate prepared from mung beans.

The wet fractionation process was based on an extraction process developed by Kornet *et al.* (2021). The fine fraction was dispersed under mild agitation in demineralized water and the pH was adjusted to 8 with a solution of 1.7 M NaOH. After 2 h, the dispersion was centrifuged at 10,000 x g for 30 min. The supernatant was taken for further purification by adjusting the pH to 4.5 with a solution of 1 M HCl. Then the dispersion was centrifuged again at 10,000 x g for 30 min. The obtained pellet was

separated from the supernatant and redispersed at pH 7. The resulting dispersion was agitated for at least 2 h. The dispersion was frozen and lyophilized with a Christ Alpha 1-2-LD freeze dryer (Salm en Kipp, Breukelen, the Netherlands) at -48 °C and 0.75-0.92 mbar. The wet fractionated isolate was used in dry powder form for all analyses. The fine fraction, heated fine fraction, and wet fractionated isolate were compared with a commercial protein isolate. The fractionation procedure of the commercial protein isolate is unknown.

Protein contents of the fractions were determined using a Rapid N Exceed Dumas (Elementar, Langensfeld, Germany) in duplicate. Based on previous research, a nitrogen conversion factor of 5.7 was used for mung bean protein (Schlangen *et al.*, 2022). The dry matter content of the fractions was determined by drying around 1 g of sample overnight in an oven (Binder GmbH, Tuttlingen, Germany) at 105 °C. The ash content of the fractions was determined by drying around 500 mg of sample in a Nabertherm ash oven (Nabertherm GmbH, Lilienthal, Germany) at 500 °C for 3 h. An overview of the compositions of the fractions is shown in Table 4.1.

TABLE 4.1 Composition of mung bean fractions and pH of mung bean fractions dispersed in MilliQ at 9.5 wt.% dry matter.

	Dry matter content (g/100 g)	Ash content (g/100 g dry matter)	Protein content (g/100 g dry matter)	pH of dispersions (-)
Fine fraction	92.71 ± 0.05	7.06 ± 0.05	58.00 ± 0.23	6.05
Heated fine fraction	92.71 ± 0.05	7.06 ± 0.05	58.00 ± 0.23	5.89
Wet fractionated isolate	96.88 ± 0.25	4.72 ± 0.01	82.62 ± 4.73	6.75
Protein isolate	94.20 ± 0.12	3.68 ± 0.00	69.34 ± 0.11	6.87

4.2.3 Rheological properties of the dispersions

The rheological properties of the samples with and without TGase were analysed by small angle oscillatory shear (SAOS) measurements and a strain sweep. The fractions were dissolved in demineralised water at a concentration of 9.5 wt.% dry matter with 0 U/g protein (without) or 7.6 U/g protein (with) TGase. The samples were mixed vigorously with a vortex. The rheological properties of the samples were measured with a MCR301 rheometer (Anton Paar, Graz, Austria) combined with a CC-17 concentric cylinder geometry. Two SAOS measurements were performed: a temperature sweep and a frequency sweep. The temperature sweep was performed by subjecting the samples to an incubation step of 50 °C for 30 min (based on optimal conditions found in previous research by Schlangen *et al.* (2023) and controlled by a water bath) at a frequency of 1 Hz and a strain amplitude of 1%. Subsequently, the samples were cooled down to 20 °C at a rate of 3 °C/min and kept at 20 °C for 5 min to equilibrate. Next, the

incubated samples were subjected to a frequency sweep from 0.01 to 10 Hz (at a strain of 1%). Straight after the SAOS measurements, a strain sweep was performed. The strain was varied from 0.1-1000% in a logarithmic manner (6 points per decade, at a frequency of 1 Hz). The storage modulus (G') and loss modulus (G'') were recorded during all measurements. The end of the linear viscoelastic regime (LVR) was calculated for all curves and was defined as the maximum strain before a 5% G' deviation from linear. The strain at the end of the LVR in the strain sweeps was expressed as the critical strain (γ_c). The critical strain and corresponding stress values were plotted in a texture map, as previously described by Schreuders *et al.* (2021). Rheological measurements were performed in triplicate, except for the wet fractionated isolate with and without TGase, which was analysed in duplicate, due to limited availability of material.

4.2.4 Crosslinking of diluted dispersions with transglutaminase

To study the susceptibility of the proteins to TGase under diluted conditions, the fractions were dissolved in MilliQ at 4 wt.% protein with a NaCl concentration of 0.005 M. The diluted dispersions were treated with 0 or 7.6 U/g protein TGase and mixed vigorously with a vortex. The samples were then incubated at 50 °C for 30 min in a ThermoMixer F2.0 (Eppendorf, Hamburg, Germany). The enzyme concentration and incubation conditions were based on conditions used previously (Schlangen *et al.*, 2023). Subsequently, 8 mM N-ethylmaleimide (NEM) was added to all samples to stop the enzymatic reaction.

Another set of samples was produced to study the effect of TGase on solely the protein fraction in the supernatants obtained after centrifugation. Here, the fractions were dissolved in MilliQ at 4 wt.% protein (NaCl concentration of 0.005 M) and centrifuged at 5,000 x g at 21 °C for 10 min. Next, the supernatant was treated with TGase as described before. Subsequently, 8 mM N-ethylmaleimide (NEM) was added to all samples to stop the enzymatic reaction. We refer to this set of samples with post-centrifugation treatment.

4.2.5 Gel electrophoresis

Gel electrophoresis under reducing conditions was performed to obtain insights on the crosslinking of different protein subunits, using an Invitrogen™ system according to manufacturer's instructions (ThermoFisher Scientific, Waltham, MA, USA). The TGase treated dispersions were centrifuged (5,000 x g, 21 °C, 10 min), and the supernatants were analysed to investigate effects on the proteins induced by TGase. We refer to these samples as pre-centrifugation treatment. Additionally, the post-centrifugation treated samples were analysed as explained in section 4.2.4. The pre- and post-centrifugation treated samples, before and after TGase crosslinking, were first diluted to 2 mg protein/

mL with MilliQ. Subsequently, 13 μ L of the sample was mixed with 5 μ L of NuPAGETM LDS sample buffer and 2 μ L NuPAGETM reducing agent. The mixtures were heated at 95 °C for 5 min in a thermoshaker (IKA-Werke GmbH, Staufen, Germany) and rapidly cooled in an ice bath afterwards. Aliquots of 7 μ L were injected into a NuPAGETM precast gradient gel (4-12% polyacrylamide). The first and last well of the gel were injected with 10 μ L of Precision Plus ProteinTM Marker (Bio Rad Laboratories). The gel was run at 200 V for 35 min using an XCell SureLockTM Mini-Cell filled with NuPAGETM MES SDS running buffer. The gel was stained with SimplyBlueTM SafeStain solution for 4.5 h, rinsed in MilliQ overnight and subsequently digitalised with a ChemiDoc XRS (Bio Rad Laboratories, Inc., Hercules, CA, USA).

4.2.6 Protein dispersibility

The protein dispersibilities of the dispersed fraction from section 4.2.4 with and without TGase were analysed. The term protein dispersibility is used instead of solubility, because it is possible that part of the protein is present in the supernatant as colloidal aggregates rather than fully dissolved. The dispersions were centrifuged at 5,000 \times g at 21 °C for 10 min. The protein contents of the dispersions and the supernatants were analysed using Dumas (Dumatherm, Gerhardt GmbH & Co. KG, Königswinter, Germany) with a protein conversion factor of 5.7. The protein dispersibility was calculated using Eq. 4.1.

$$\text{Protein dispersibility} = \frac{\text{Protein content in supernatant}}{\text{Protein added}} \times 100\% \quad (\text{Eq. 4.1})$$

4.2.7 Microstructure characterization

The microstructures of the dispersions without and with TGase were characterized using confocal laser scanning microscopy (CLSM) (Nikon C2, Nikon Instrument Inc., Tokyo, Japan). Rhodamine B (Sigma Aldrich, St. Louis, MO) was dissolved in MilliQ until a final concentration of 1 mg/mL. Approximately 60 μ L of each dispersion and 5 μ L of the Rhodamine B staining solution were loaded onto glass slides and mixed with a pipette tip. The stained samples were analysed using CLSM with a 20x objective and 60x objective (data not shown). A laser line of 561 nm was used for excitation to induce fluorescence emission. Images were made using two samples taken from two separate dispersions. Representative images are shown.

4.2.8 Particle size analysis

The particle size distributions of the dispersions (pre-centrifugation) with and without TGase were measured using static light scattering with a Mastersizer 2000 (Malvern Instruments Ltd., UK). A volume-based mode was used because of the multi-component nature of the protein fractions. The particle size distribution of the post-centrifugation treated samples with and without TGase was measured using dynamic light scattering with a Zetasizer Lab (Malvern Panalytical Ltd., Malvern, UK). The post-centrifugation treated samples were diluted to 1:8 (v/v) in MilliQ before analysis. The measurements of the diluted samples were carried out at 25 °C after 120 s equilibration time. A refractive index of 1.45 was used for the measurements with the Mastersizer as well as the Zetasizer. Particle size analyses were performed in triplicate.

4.2.9 Statistical analysis

All measurements were performed in duplicate unless stated otherwise. The mean values and standard errors were calculated and used as a measure of error. Significant differences of the measured dispersibility values were analysed by ANOVA with a post hoc Duncan test. Significant differences of the measured rheological properties were determined by an independent t-test. Equality of variances was analysed with Levene's test, unequal variances were assumed when $p > 0.05$. Significance was defined as $p < 0.05$.

4.3 Results & Discussion

4.3.1 Effect of crosslinking at bulk scale

Bulk changes were studied with rheology at a standardized dry matter content of 9.5 wt.%. The compositions of all fractions are presented in Table 4.1, which shows that the fine fractions contain most non-proteinaceous components. The development of the elastic modulus (G') with time is shown in Figure 4.2, where the dispersions were incubated for 30 min at 50 °C with and without TGase. A frequency sweep was performed after incubation showing that $G' > G''$ over the entire frequency range for all samples, indicating solid-like behaviour (Supplementary Material: Figure S4.1).

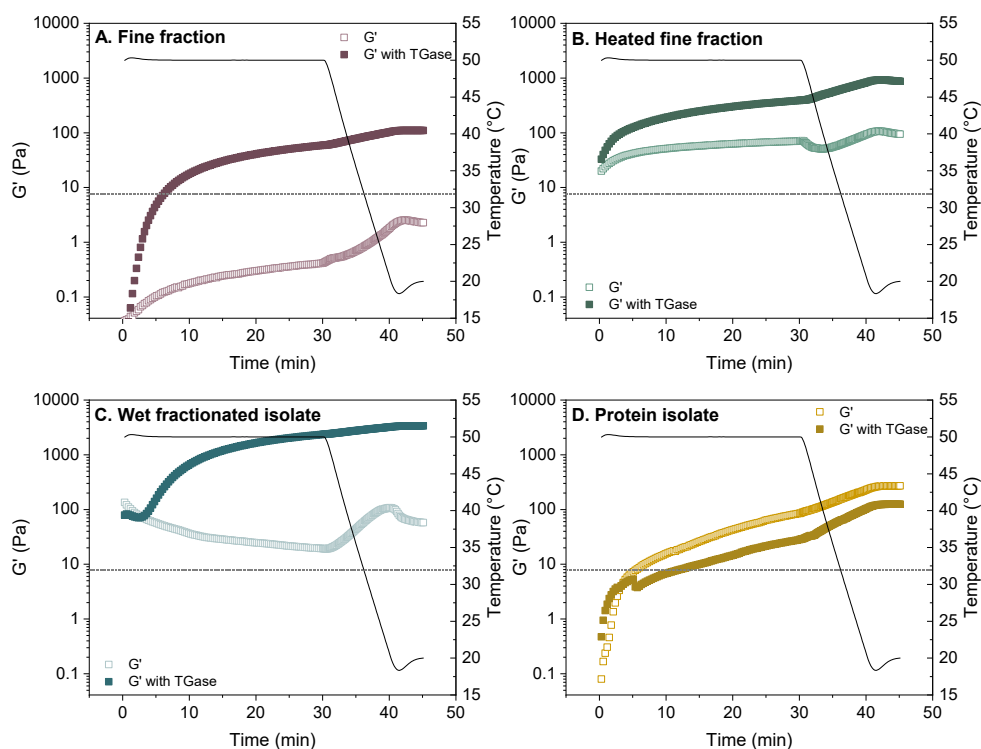


FIGURE 4.2 Representative temperature sweep of A: fine fraction, B: heated fine fraction, C: wet fractionated isolate, and D: protein isolate without (light, open symbols) and with (dark, closed symbols) TGase. Black lines indicate incubation temperature profile. Horizontal dashed line indicates minimum torque limit, which was taken as a factor 10 higher than reported by the supplier.

During incubation, there were clear differences in the rheological properties of the samples depending on the composition and fractionation procedure of the fractions.

Without TGase, we observed an increase in G' over time in the fine fraction, heated fine fraction, and protein isolate (Figure 4.2A, B, D). Thus, heating at 50 °C alone changed the rheological properties in these fractions. We believe that the increase in G' was due to hydration and solvent inclusion of the protein aggregates at 50 °C and consequently the increase in particle-particle interactions. Comparing the G' profiles of the fine fraction and heated fine fraction without TGase, we noted that the heated fine fraction had higher G' values overall (Figure 4.2A, B). This suggests that the heated fine fraction forms a network-like structure at the start of the measurement already, which can be explained by the additional heating step in the fractionation procedure. The wet fractionated isolate without TGase showed a decrease in G' during the heating period, and an increase in G' started upon cooling. The decrease in G' during the heating period may be due to a temperature-dependent decrease in viscosity. A decrease in viscosity normally occurs in materials, including gels, in case no additional interactions or crosslinks are created upon heating. The wet fractionated isolate had a relatively high G' value (~ 100 Pa) at the start of the measurement, and might therefore already be in a certain gelled state. It is important to note that the fine fraction and heated fine fraction are multi-component ingredients, as they still contain other components, such as fibre. Fibre could increase G' during incubation by holding water, but it might also interfere with protein network formation.

The application of TGase resulted in distinct rheological effects amongst the various fractions. TGase crosslinking increased the G' of the fine fraction, heated fine fraction, and wet fractionated isolate (Figure 4.2A, B, C), indicating a stiffening of the materials. On the other hand, TGase crosslinking decreased the G' of the protein isolate (Figure 4.2D), indicating a softer material. In the fine fraction, we believe that TGase crosslinking within individual protein particles resulted in an enhanced G' value. The same explanation may hold for the heated fine fraction. However, here the effect is smaller, because an initial network may already have been formed due to the processing applied to make this fraction. The highest G' values with TGase were found for the wet fractionated isolate (Figure 4.2C). The decreased G' in the protein isolate with TGase does not necessarily indicate a reduced susceptibility to TGase, as there is still a difference with the moduli without TGase. The limited effects of TGase on the protein isolate aligns with previous studies by Shand *et al.* (2008) and Pelgrom, Boom, & Schutyser (2015). They also demonstrated a limited effect of TGase on rheological properties in commercial pea protein isolate compared with native pea protein. The results were explained by considering partial or complete denaturation of the proteins in the isolate, which led to a decrease in solubility.

The texture map depicts the properties of all fractions without and with TGase (Figure 4.3). The addition of TGase to the fine fraction, heated fine fraction, and wet fractionated isolate led to an increase in the critical strain and the corresponding stress

values, and thus resulted in tougher materials compared with those without TGase. The strongest and most stretchable material was obtained by addition of TGase to the wet fractionated isolate. Previous research by Shand *et al.* (2008) also showed that addition of TGase to pea protein isolate and soy protein isolate led to tougher materials. The addition of TGase to mung bean protein isolate in this study induced a more subtle change towards higher critical strain values. The small effect of TGase on rheological properties of the protein isolate is therefore considered to be a result of the fractionation procedure.

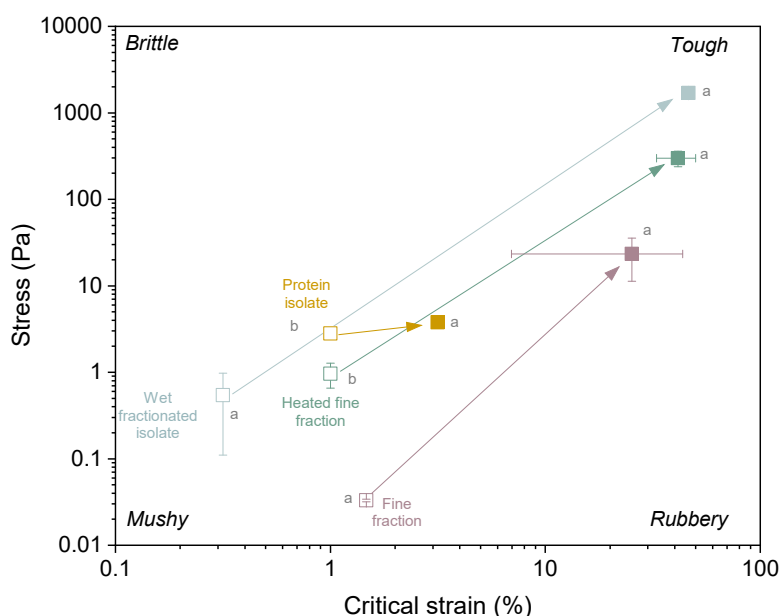


FIGURE 4.3 Texture map at the end of the linear viscoelastic regime for fine fraction, heated fine fraction, wet fractionated isolate, and protein isolate without (open symbols) and with (closed symbols) TGase. Different letters indicate significant differences ($p < 0.05$) in stress between TGase treatment and the control within each fraction. Significance for critical strain (%) could not be determined, because at least one group had a variance of zero. Arrows indicate the changes in behaviour when TGase is added and are solely provided to guide the eye.

One effect of the fractionation procedure is that it can alter the amino acid availability. However, we previously reported that mung bean protein isolate has a higher level of lysine and glutamine (70.3 mg lysine/g protein and 181.3 mg glutamine including glutamic acid/g protein) (Schlangen *et al.*, 2023), compared with the mung bean fine fraction (64.0 mg lysine/g protein and 162.3 mg glutamine (including glutamic acid)/g protein) (Schlangen *et al.*, 2022). It can thus be concluded that the differences in rheological properties between TGase treated fine fractions and protein isolates cannot be explained by amino acid availability.

4.3.2 Effect of crosslinking on molecular length scale

The formation of crosslinked protein molecules through addition of TGase was studied using SDS-PAGE (Figure 4.4). Here, we analysed both the entire dispersion (pre-centrifugation) as well as only the supernatant fractions after centrifugation (post-centrifugation) to gain a better understanding of the difference of TGase treatment between all proteins compared to solely soluble proteins. The suspensions without TGase were also studied under non-reducing conditions to obtain insight on their natural molecular aggregation states.

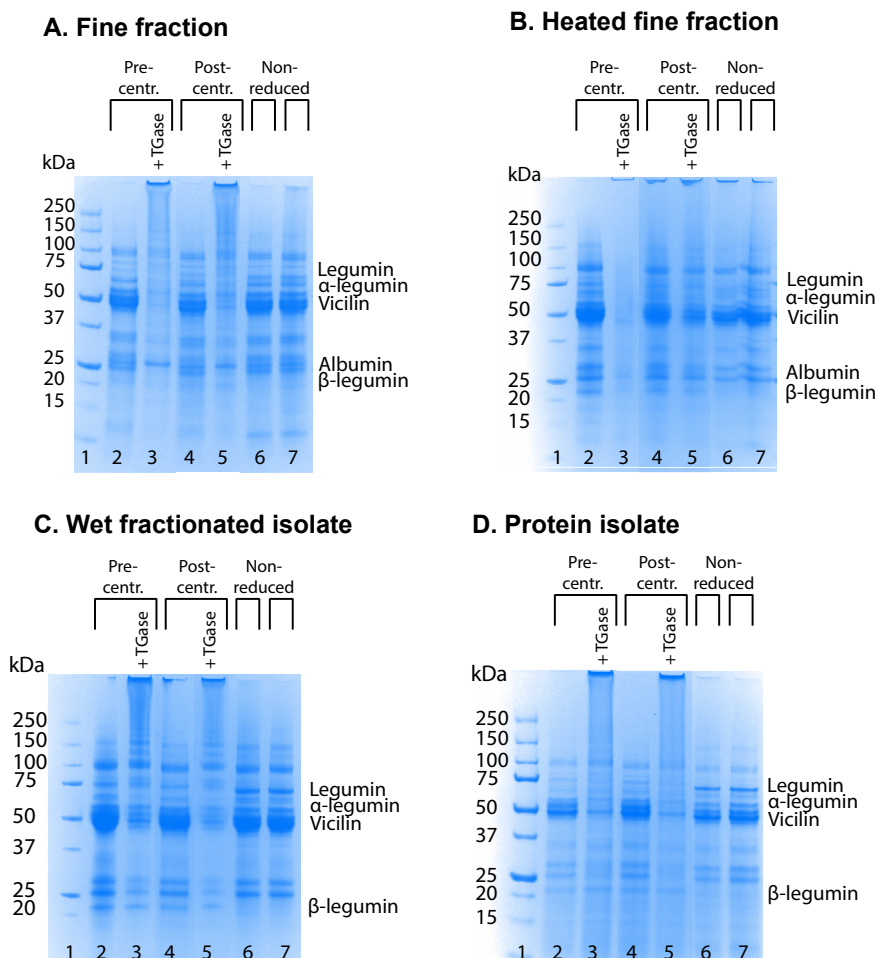


FIGURE 4.4 SDS-PAGE of the pre-(lane 2-3) and post-centrifugation (lane 4-5) treated fractions of A) fine fraction, B) heated fine fraction, C) wet fractionated isolate, D) protein isolate without and with TGase under reducing conditions. Non-reduced represents the pre- (lane 6) and post-centrifugation treated (lane 7) fractions without TGase in non-reducing conditions.

Clear differences were visible in molecular composition between the different fractions without TGase (Figure 4.4) (Brishti *et al.*, 2021; Rahma, Dudek, Mothes, Görnitz, & Schwenke, 2000; Zhong & Xiong, 2020). Here, the band patterns of the pre-centrifugation treatment (full dispersion) without TGase (lane 2) and the treatment without TGase on the corresponding supernatant (post-centrifugation) (lane 4) were similar, as anticipated, given that both fractions have a similar history. The fine fraction, heated fine fraction, and wet fractionated isolate had a high intensity band at 50 kDa, indicating presence of vicilin (lane 2 in Figure 4.4A, B, C). Furthermore, the fine fraction and heated fine fraction contained albumin, indicated by the bands at ~ 26 kDa (lane 2 in Figure 4.4A, B). Theoretically, the soluble albumins should have been removed in the fractionation process of the wet fractionated isolate and protein isolate, and should thus not be present in those fractions. The band patterns of the fine fraction, heated fine fraction, and wet fractionated isolate without TGase were relatively similar, but there was a clear difference compared with the composition of the protein isolate. The protein isolate consisted of mainly vicilin and α -legumin, as indicated by the clear bands at ~ 50 kDa and ~ 60 kDa (lane 2 in Figure 4.4D). The differences in molecular composition between the protein isolate and the other fractions can be related to the isolation and precipitation of the protein isolate (Figure S4.2).

Crosslinking with TGase led to clear changes in the electrophoretic migration in all pre- and post-centrifugation treated samples (Figure 4.4). All samples had crosslinked proteins, which shows that TGase was able to crosslink all fractions. With TGase addition, the band intensities of the low molecular weight polypeptides decreased and new high molecular weight bands appeared, indicating crosslinking of proteins. This is in accordance with previous research on Bambara groundnut protein isolate, faba bean protein, and pea globulins, for which it was also described that addition of TGase led to the disappearance of most low molecular weight polypeptide bands (Djoullah *et al.*, 2015; Nivala, Mäkinen, Kruus, Nordlund, & Ercili-Cura, 2017; Ruzengwe *et al.*, 2020). Most samples with TGase also showed a high intensity band retained at the bottom of the well. These bands indicate the presence of insoluble, high molecular weight compounds, induced by TGase, that are not able to migrate through the gel (for example lane 3 in Figure 4.4A). As the SDS-PAGE profiles of the pre-centrifugation and post-centrifugation treatments were relatively similar, it may be suggested that crosslinking is predominantly taking place between soluble protein subunits (Figure 5).

Some protein subunits were found to be more susceptible to TGase crosslinking than others. More specifically, all low molecular weight bands in the fine fraction decreased in intensity upon addition of TGase except for the band at ~ 26 kDa (lane 2-5 in Figure 4.4A). This result confirmed previous reports that the major albumin subunit at ~ 26 kDa is less available or less accessible for TGase to crosslink (Djoullah *et al.* 2015). This effect

was less evident for the heated fine fraction, suggesting that heating increased the availability of this subunit for TGase crosslinking, by for example facilitating exposure of its amino acid residues (Figure 4.4B). Earlier reports showed an increased reaction yield for pea albumin in denatured state due to improved accessibility to the lysine and glutamine groups (Djoullah, Husson, & Saurel, 2018). Thus, it could be concluded that the heated fine fraction had a higher total amount of proteins available for TGase crosslinking compared to the fine fraction. In the wet fractionated isolate, TGase addition mostly reduced the intensity of the band at ~ 50 kDa (Figure 4.4C), suggesting that crosslinking mostly occurred to the vicilin-like storage protein (Rahma *et al.*, 2000). Vicilin was also prone to TGase crosslinking in the fine fraction (Figure 4.4A lane 2 versus 3). Previously, Nivala *et al.* (2017) showed that vicilin was highly prone to TGase crosslinking in faba bean protein. They argued that vicilin is more soluble than legumin, which explained their increased availability for TGase crosslinking (Nivala *et al.*, 2017). It is also worth noting that the less reactive albumins are lost in the wet fractionated isolate, due to the extraction process (Kornet *et al.*, 2021). Therefore, the total amount of reactive protein subunits in the wet fractionated isolate may be higher than in the fine fraction and heated fine fraction.

SDS-PAGE analyses proved that TGase crosslinking occurred at molecular length scale in all protein fractions independent of fractionation procedure applied. However, SDS-PAGE is a qualitative measurement and only measures the soluble protein fraction. Therefore, protein dispersibility, microstructure, and particle size analyses were performed at the colloidal length scale to better understand the different effects of TGase on the change in rheological properties of mung bean protein.

4.3.3 Protein dispersibility changes upon TGase addition

The next step to explain the effects above is to analyse the dispersibility of the protein fractions. It can be expected that dispersible protein has a higher susceptibility to TGase than protein that is not dispersible. Here, we use the term protein dispersibility rather than protein solubility, as the mung bean proteins may form colloiddally stable aggregates that remain suspended after low speed centrifugation.

There were clear differences in protein dispersibility values between the different fractions before TGase treatment (Figure 4.5). The protein isolate had the lowest dispersibility, while the wet fractionated isolate had the overall highest dispersibility. The latter is presumably due to the removal of water-insoluble compounds during protein extraction in the wet fractionated isolate. However, the prevention of agglomeration during freeze drying instead of spray drying may also explain the high dispersibility of the wet fractionated isolate. The greater availability of dispersible protein in the wet fractionated isolate may have resulted in a large increase in the G' upon TGase addition

as shown in section 4.3.1. Further, it might be that crosslinking the low quantity of dispersible protein present in the protein isolate was not enough to induce a change in G' and form a strong gel (Figure 4.2). Heating of the fine fraction increased its protein dispersibility compared to the non-heated fine fraction. This was probably due to the loosening of the native structures with temperature leading to increased hydration. Aggregation is less likely to have taken place in the heated fine fraction, because this would have led to a decrease in protein dispersibility. These results demonstrated that fractionation procedure changes protein dispersibility due to changes in colloidal interactions. Based on this information, it is thus plausible that denaturation and aggregation during the protein isolation process had reduced the protein dispersibility, thereby limiting the accessibility of the protein isolate reactive groups to TGase.

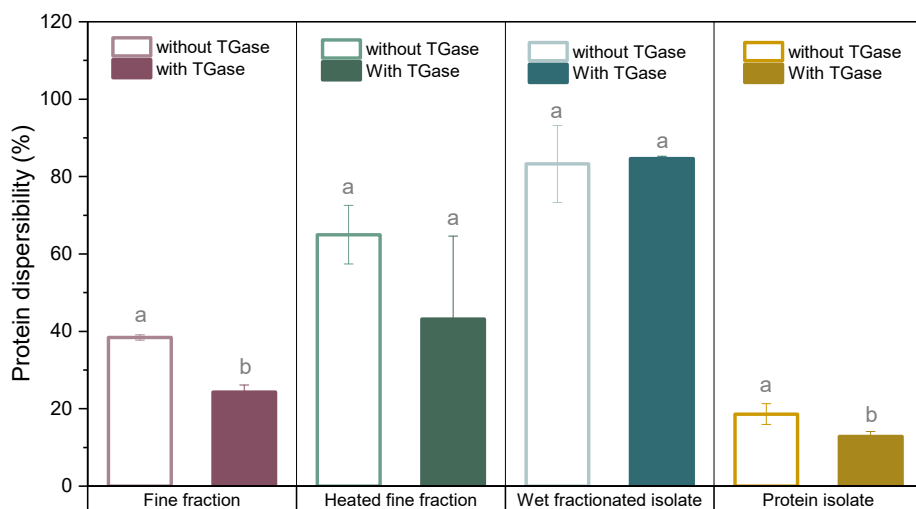


FIGURE 4.5 Protein dispersibility at 4 wt.% protein, without (0 U/g protein) and with (7.6 U/g protein) TGase of fine fraction, heated fine fraction, wet fractionated isolate, and protein isolate. Different letters indicate significant differences between treatments of the same fraction ($p < 0.05$).

To determine the possible changes with addition of TGase, we studied the amount of protein that was dispersible after the TGase treatment as well (Figure 4.5). Clear differences in protein dispersibility were observed when TGase was added to the protein fractions. We found that even though TGase crosslinking led to changes in molecular sizes (Figure 4.4), it did not always change the dispersibility of the samples (Figure 4.5). The addition of TGase decreased the protein dispersibility of the fine fraction, heated fine fraction (though not significant), and the protein isolate, probably due to covalent TGase crosslinking. This aligns with the results of the gel electrophoresis, where TGase crosslinking resulted in an increase in molecular weight of the protein subunits (Figure 4.4). Previous research also showed a decrease in protein solubility of

faba bean protein upon TGase treatment (Nivala *et al.*, 2017). Contradictory, the protein dispersibility of the wet fractionated isolate was not affected by TGase addition. Thus, the crosslinked proteins of the wet fractionated isolate remained dispersible according to this measurement.

4.3.4 Microstructure changes upon TGase addition

Confocal laser scanning microscopy (CLSM) was used to determine possible changes in the microstructure of the protein aggregates without and with TGase. Without TGase, we observed clear differences in microstructure between the different protein fractions (Figure 4.6). The fine fraction and heated fine fraction had similar irregularly shaped particles, while the particles present in the wet fractionated isolate were slightly larger (Figure 4.6A, B, C). The microstructure of the protein isolate revealed distinct wrinkled surface particles at all conditions tested, which is typical for spray dried proteins (Brishti *et al.*, 2020; Lan, Xu, Ohm, Chen, & Rao, 2019) (Figure 4.6D). To further understand protein-enzyme interactions, dispersions were prepared with 1 M NaCl, treated with or without TGase and their microstructure was studied with CLSM. The high concentration of NaCl can change protein dispersibility of the fractions, possibly exposing different amino acid groups and thus changing protein-enzyme interactions. Without TGase, the addition of NaCl to the fine fraction and the heated fine fraction decreased the size of the visible structures compared to the microstructure without NaCl (Figure 4.6A,B). Thus, salt limited the swelling of the particles. The microstructures of the wet fractionated isolate and protein isolate before TGase treatment remained unchanged upon an increase in NaCl concentration (Figure 4.6). We conclude that those particles were denser and did not have the ability to swell and adsorb water.

Treatment with TGase did not change the microstructure of all dispersions. The addition of TGase in the fine fraction and heated fine fraction induced aggregation, as visualized by larger particles, as well as larger voids in the CLSM images (Figure 4.6A, B). This is in agreement with the increase in G' (Figure 4.2A, B) and the decrease in protein dispersibility (Figure 4.5) upon addition of TGase to those fractions. No clear differences were evident between dispersions with and without TGase for the wet fractionated isolate and the protein isolate (Figure 4.6C, D). Previously, Nivala *et al.* (2021) also showed that addition of TGase to faba bean protein gels did not change the microstructure. They suggested that inter-molecular covalent crosslinks formed by TGase reinforced the particle structures without causing massive rearrangements in spatial distribution (Nivala *et al.*, 2021). TGase crosslinks mostly soluble proteins, whereas mostly proteins captured in insoluble particles are visible as bright parts in the CLSM picture. This could explain the lack of discernible differences in the microstructure upon the addition of TGase to the wet fractionated isolate and protein isolate. At 1 M

NaCl, only the microstructure of the fine fraction was affected by TGase treatment, (Figure 4.6A). The microstructures of the heated fine fraction, wet fractionated isolate, and protein isolate at 1 M NaCl remained unchanged upon TGase treatment (Figure 4.6B,C,D). Due to changes in colloidal state at high NaCl concentration, it seems that the proteins don't swell and become less accessible for TGase.

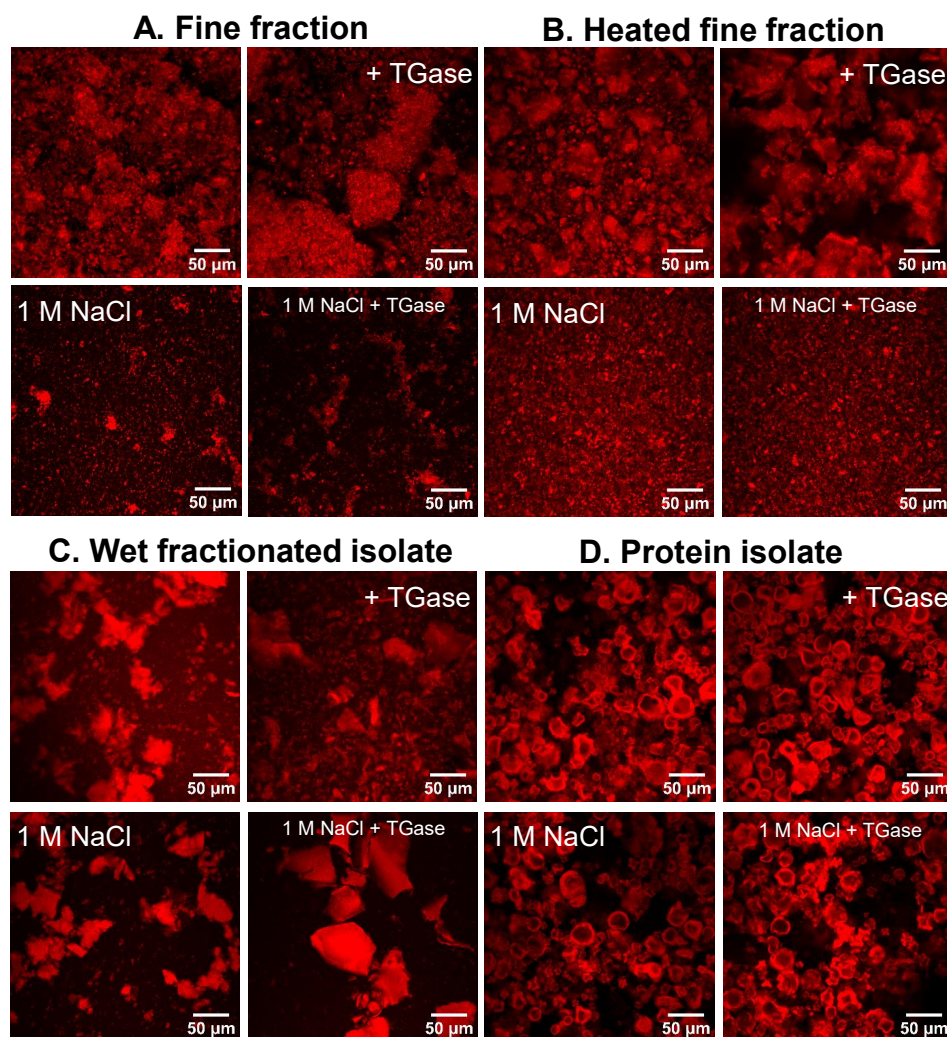


FIGURE 4.6 The microstructure of dispersions of A) fine fraction, B) heated fine fraction, C) wet fractionated isolate, and D) protein isolate at low (0.005 M) NaCl concentration and high (1 M) NaCl concentration without TGase and with TGase. Protein is stained in red with Rhodamine B. Magnification 20x, scale bar represents 50 μm .

4.3.5 Changes in particle size distribution upon TGase addition

To better determine potential enzyme-induced aggregation of protein particles, the dispersions before and after TGase crosslinking were tested for changes in their particle size distribution. Particle size distributions of the full dispersions with and without TGase are shown in Figure 4.7.

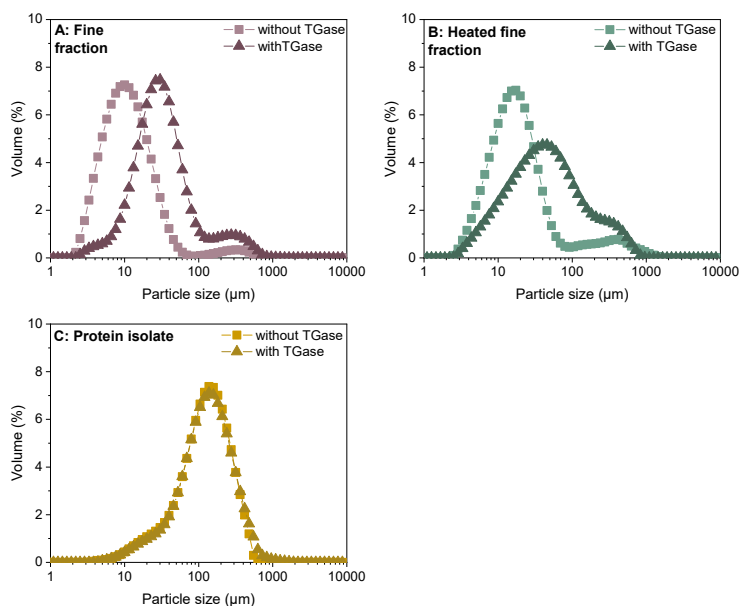


FIGURE 4.7 Representative particle size distributions of dispersions of A) fine fraction, B) heated fine fraction, and C) protein isolate, without TGase (squares) and with TGase (triangles). Results for the wet fractionated isolate are missing, as these could not be measured due to their small particle size (<2μm) and low obscuration levels.

Without TGase, the protein isolate contained larger size particles than the fine fraction and heated fine fraction, further supporting the differences in microstructure (Figure 4.6). A profound effect of TGase addition on particle size distribution was observed: the particle size distribution of the fine fraction and heated fine fraction shifted to larger particle sizes (Figure 4.7A & B). This suggests that TGase is either forming inter-aggregate crosslinks, or it is making individual particles more prone to aggregation. These results are in agreement with the decrease in protein dispersibility, the observed change in microstructure and the increase in protein subunit size as described previously (Figure 4.6). The particle size distribution of the protein isolate was unaffected by TGase addition. This implies that no changes in size occurred at the colloidal scale in the protein isolate, suggesting that these particles are mostly inert. It is important to acknowledge that crosslinking of protein subunits was observed at the molecular scale in the protein isolate (Figure 4.4). Consequently, even though crosslinking may

have occurred in the limited number of dispersible particles present in the protein isolate, they would not have grown to a size that would have been detectable by the Mastersizer. This can be partly a result from the fact that the Mastersizer analysis favours the detection of larger particles.

As previously suggested, the limited effect of TGase in the protein isolate could be due to its relatively low dispersibility (Figure 4.5). To test this hypothesis, the post-centrifugation treated samples (obtained as a supernatant by centrifugation) were treated with TGase and their particle size distribution were analysed by dynamic light scattering (Figure 4.8).

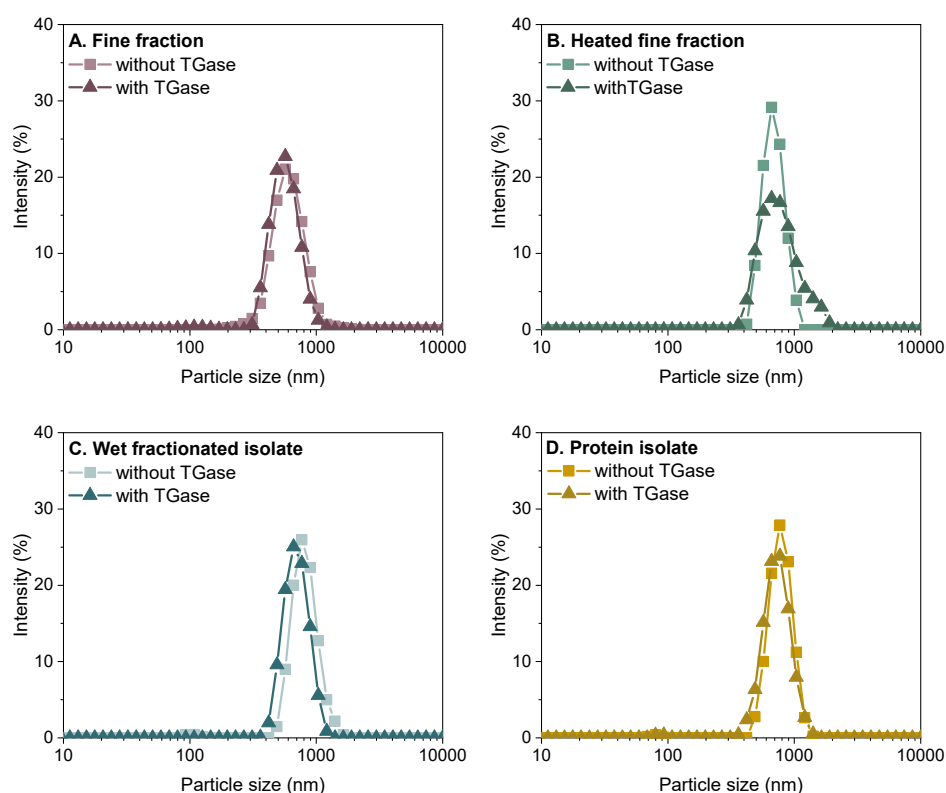


FIGURE 4.8 Particle size distributions of the post-centrifugation treated fractions of A) fine fraction, B) heated fine fraction, C) wet fractionated isolate, and D) protein isolate, without TGase (squares & light colour) and with TGase (triangles & dark colour).

Here, without TGase, the post-centrifugation treated fine fraction had a slightly smaller particle size than the other post-centrifugation treated fractions. TGase crosslinking affected the various post-centrifugation treated fractions differently. The particle size distribution of the post-centrifugation treated fine fraction and protein isolate did not

change upon addition of TGase (Figure 4.8A, D). The reason for this could be that the soluble proteins are diluted and dispersible, lowering the chance of particle-particle crosslinking. On the other hand, the post-centrifugation treated proteins of the heated fine fraction were susceptible to TGase treatment (Figure 4.8B). By addition of TGase, the main peak in the particle size distribution broadened towards larger particle sizes in the post-centrifugation treated heated fine fraction. Here, TGase might induce inter-aggregate crosslinking between soluble proteins, increasing the overall particle size. Previous research showed that the particle size of TGase treated proteins will increase when inter-aggregate crosslinks are formed, while it may decrease when intra-aggregate crosslinks are formed (Djoullah, Krechiche, Husson, & Saurel, 2016). Therefore, the slight decrease in particle size in the post-centrifugation treated wet fractionated isolate by TGase addition is of interest (Figure 4.8C). When combined with the results of the protein dispersibility and microstructure, this observation may imply that the majority of crosslinks formed in the soluble wet fractionated isolate are intra-aggregate crosslinks.

4.3.6 Proposed crosslinking mechanism

The protein isolate has a higher number of glutamine and lysine groups relative to the fine fraction, as previously reported (Schlangen *et al.*, 2022, 2023). Therefore, this cannot account for the limited TGase crosslinking observed in the protein isolate as compared with the fine fraction. To explain the susceptibility of proteins to TGase, we hypothesize that the mung bean protein is present in three states, each having a different susceptibility to TGase (Figure 4.9). The first state is a dense inert particle that does not swell in contact with water. This could be the result of intensive heat treatment and lack of hydration when mixing the powder in water (for example in the case of the protein isolate). The second state is related to dispersed colloidal particles that have absorbed water, leading to swollen particles. The third state is that of the proteins that are soluble. Protein in dense inert particles are hypothesized not to react with TGase (mechanism 1). Protein present in swollen particles can react with TGase, and their crosslinking may lead to an increase in the density of the particles (Flory & Rehner, 1943) and/or potentially crosslinking of particles (mechanism 2). Soluble protein can most easily react with TGase, forming protein aggregates that might remain in solution or form particles (mechanism 3). The specific mechanism(s) of crosslinking depend on the fractionation procedure of the fractions and their composition. Approximately 80% of the protein isolate is not dispersible and particles appeared dense (Figure 4.5 & 4.6), implying that protein is mostly present as the dense inert particles that hardly react as explained by mechanism 1. However, the roughly 20% of dispersible protein in the protein isolate will be crosslinked by TGase through mechanism 3, explaining the increase in molecular size (Figure 4.4D). Furthermore, the subtle decrease in

rheological properties may be due to densifying of the 20% dispersible protein, which then contributes less to the overall network upon crosslinking by TGase (Figure 4.2D). The wet fractionated isolate is highly dispersible (Figure 4.5), suggesting that mechanism 3 is primarily responsible for TGase crosslinking. The fine fraction and heated fine fraction contain both dispersible and non-dispersible protein (Figure 4.5). TGase crosslinking of the dispersible protein mainly follows mechanism 3. For the non-dispersible protein, we hypothesize that the proteins will be present in swollen particles after hydration that allow for the possibility for TGase to crosslink proteins inside the particles. The possibility that TGase would also crosslink the swollen particles with each other cannot be excluded, which would explain the increase in particle size upon TGase addition in the fine fraction and heated fine fraction (Figure 4.7). The hypothesis of swollen particles is supported by the effect of salt addition. Salt reduced the swelling of particles as shown in section 4.3.4, confirming that without salt, water and thus also the TGase can penetrate the particles.

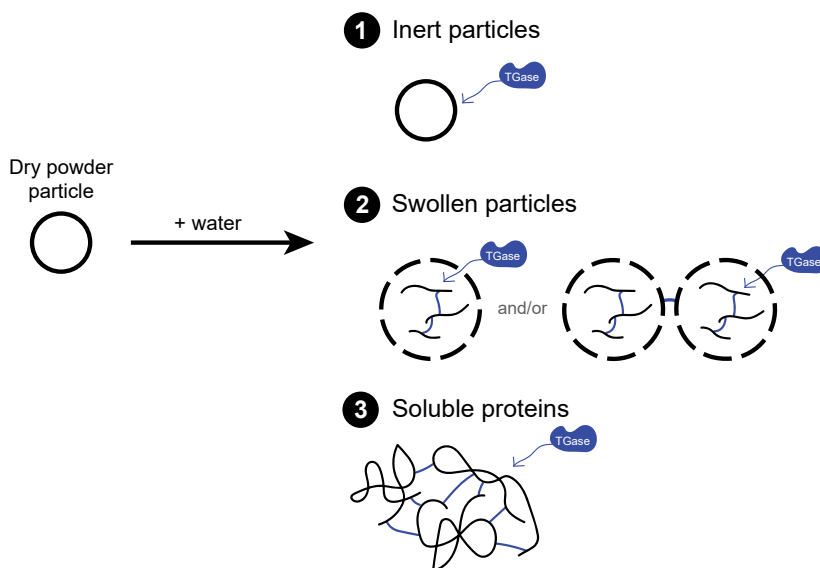


FIGURE 4.9 Schematic illustration of proposed mechanisms of TGase crosslinking.

4.4 Conclusions

This study describes the effects of mung bean protein fractionation on susceptibility to crosslinking by TGase and the consequences for its products at three different length scales. We showed that TGase crosslinking was independent of fractionation procedure at the molecular scale, but was greatly dependent on fractionation procedure at colloidal and bulk scale. To explain the different crosslinking effects of TGase on the various mung bean protein fractions, we hypothesized that mung bean protein can be present in different states. The first state is a dense protein particle, which does not swell upon hydration and is rather inert. The second state is a swollen particles in which TGase can diffuse, leading to both intra- and interparticle crosslinks. The last state is that of soluble proteins. These proteins can be readily crosslinked leading to still soluble aggregates or swollen particles. We concluded that proteins in the commercial protein isolate are mostly present as dense protein particles, which explains the limited effect on the rheological properties, despite some detected molecular crosslinks of the small soluble protein fractions present in this isolate. The fine fraction and heated fine fraction possess mostly swollen particles, which explains observed changes on all length scales. The relatively high dispersibility and high amount of highly TGase reactive globulins increased susceptibility to TGase in the wet fractionated isolate, explaining the large effect on the rheological properties, but limited effect on colloidal scale. We can conclude that changes in microstructure and protein dispersibility, as a result of fractionation procedure, affect susceptibility of the proteins to TGase.

4.5 Supplementary material

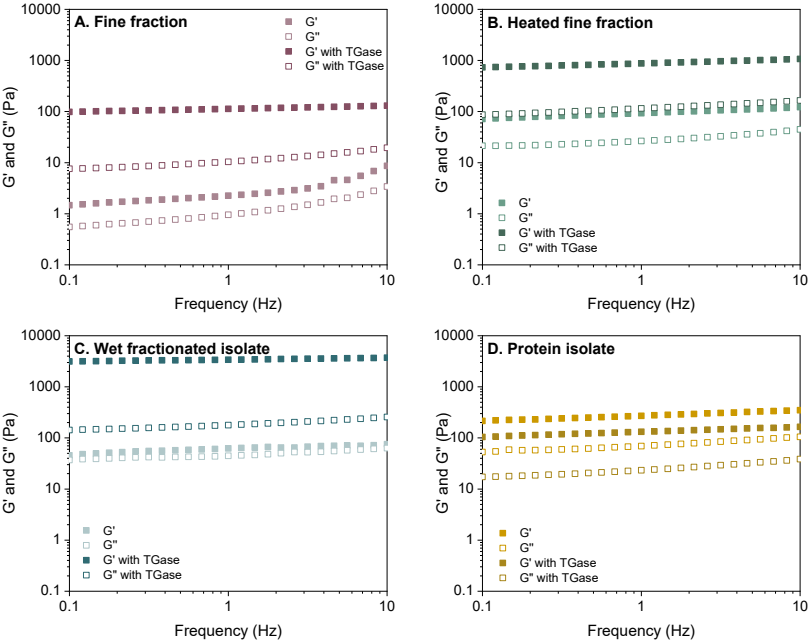


FIGURE S4.1 Representative frequency sweeps of A) fine fraction, B) heated fine fraction, C) wet fractionated isolate, and D) protein isolate. Data is shown as G' and G'' without (○) U/g protein) and with (●) 7.6 U/g protein) TGase.

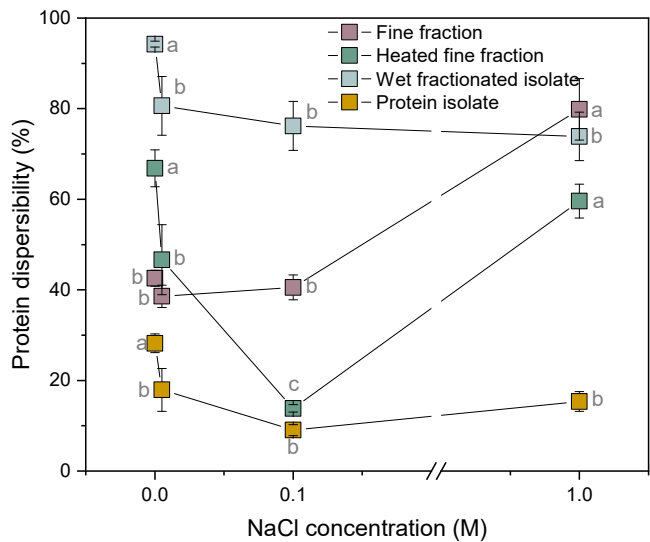


FIGURE S4.2 Protein dispersibility at 4 wt.% protein of the fine fraction, heated fine fraction, wet fractionated isolate, and protein isolate as affected by NaCl concentration (0, 0.005, 0.1, and 1 M). NaCl concentration is defined as the concentration of NaCl that the fractions were dispersed in. Lines are solely added to guide the eye. Different letters indicate significant differences between different NaCl concentrations within one fraction ($p < 0.05$).

5

Chapter 5

Quantitative characterizations of visual fibrousness in meat analogues using automated image analysis

This chapter has been published as Ma, Y., Schlangen, M., Potappel, J., Zhang, L., van der Goot, A.J. (2023) Quantitative characterizations of visual fibrousness in meat analogues using automated image analysis. *Journal of Texture Studies*. Accepted for publication.

Yizhou Ma and Miek Schlangen should be considered joint first authors

Abstract

A desirable quality of plant-based meat analogues is to resemble the fibrous structure of cooked muscle meat. While texture analysis can characterize fibrous structures mechanically, assessment of visual fibrous structures remains subjective. Quantitative assessment of visual fibrous structures of meat analogues relies on expert knowledge, is resource-intensive, and time-consuming. In this study, a novel image-based method (Fiberlyzer) is developed to provide automated, quantitative, and standardized assessment of visual fibrousness of meat analogues. The Fiberlyzer method segments fibrous regions from 2D images and extracts fibre shape features to characterize the fibrous structure of meat analogues made from mung bean, soy, and pea protein. The computed fibre scores (the ratio between fibre length and width) demonstrate a strong correlation with expert panel evaluations, particularly on a per-formulation basis ($R^2 = 0.93$). Additionally, the Fiberlyzer method generates fibre shape features including fibre score, fibre area, and the number of fibre branches, facilitating comparisons of structural similarity between meat analogue samples and cooked chicken meat as a benchmark. With a simple measurement setup and user-friendly interface, the Fiberlyzer method can become a standard tool integrated into formulation development, quality control, and production routines of plant-based meat analogue. This method offers rapid, cheap, and standardized quantification of visual fibrousness, minimizing the need for expert knowledge in the process of quality control.

5.1 Introduction

Sustainability, health, and animal welfare concerns have motivated consumers to replace their dietary protein sources from animals to plants, boosting the demand for plant-based meat analogues (McClements & Grossmann, 2022). As alternatives, meat analogues have the highest success rate when they deliver a sensory experience similar to the experience of consuming meat (Michel, Hartmann, & Siegrist, 2021). Texture, in particular a fibrous structure, is one of the most defining quality attributes of meat analogues for consumer acceptability (Elzerman, Hoek, van Boekel, & Luning, 2011). A fibrous and muscle meat-like texture can be produced through thermomechanical processing of plant proteins by, for example, high moisture extrusion (HME) cooking, low moisture extrusion (LME) cooking, or high temperature shear cell (HTSC) technology (Dekkers, Boom, & van der Goot, 2018; Grabowska, Tekidou, Boom, & Goot, 2014; Kyriakopoulou, Dekkers, & van der Goot, 2019; McClements & Grossmann, 2022; Webb, Dogan, & Li, 2023). In recent years, LME, HME cooking and HTSC technology have produced meat analogues with a range of different structures containing various plant protein compositions (Kyriakopoulou *et al.*, 2019; McClements & Grossmann, 2022; Webb *et al.*, 2023).

To better compare between samples, fibrous structures of meat analogues are often characterized by mechanical, spectral, and imaging techniques (McClements, Weiss, Kinchla, Nolden, & Grossmann, 2021; Schreuders, Schlangen, Kyriakopoulou, Boom, & van der Goot, 2021). Mechanical anisotropy, measured through tensile testing, is generally used to describe fibrous structures of HTSC products, but does not always agree with visual observations of macrostructure (Barbut, 2015; Schreuders, Schlangen, Bodnár, *et al.*, 2021). Only weak correlations were found between consumer visual assessment of fibrous structures and mechanical attributes in meat analogues (Godschalk-Broers, Sala, & Scholten, 2022). Thus, it remains uncertain whether fibrous structures of meat analogues can be fully characterized by mechanical anisotropy. Hence, relying solely on the mechanical anisotropy of meat analogues may not be sufficient to assess their textural quality. Spectral techniques, such as fluorescence polarization and light reflectance, can also indirectly characterize visual fibrousness of meat analogues. The fibre orientations (i.e. anisotropic structures) create unique light reflectance and fluorescence polarization patterns, which can be used to measure fibrous structures of meat analogues (Ranasinghesagara, Hsieh, Huff, & Yao, 2009; Ranasinghesagara, Hsieh, & Yao, 2006). However, such spectral methods require special instrumentations and algorithm development, which complicates the general use of this visual fibrousness characterization process. In practice, many studies relied on manual inspections of the fibrous structures of meat analogues (Dekkers, Nikiforidis,

& van der Goot, 2016; Grabowska *et al.*, 2014, 2016; Jia, Curubeto, Rodríguez-alonso, Keppler, & van der Goot, 2021; Krintiras, Göbel, van der Goot, & Stefanidis, 2015; Osen, Toelstede, Wild, Eisner, & Schweiggert-Weisz, 2014; Schreuders *et al.*, 2019). While reporting images of inner structures is a simple and effective way to compare the visual fibrousness of meat analogues, it limits the results to subjective and qualitative interpretations. A robust and quantitative measurement of visual fibrousness of meat analogues can provide objective characterization of fibre formation across different formulations and processing parameters, making subjective human evaluations less important. Furthermore, with an automated and quantitative measurement of fibrousness, it can monitor the production of meat analogues and provide feedback for structuring improvement.

A promising technique for developing such a method is computer vision (CV). CV is a collection of algorithms that allow digital interpretation of visual information from images and videos. CV has been widely used in agri-food applications, such as in meat analogue colour analysis, 3D food printing performance, and meat quality evaluation (Fan *et al.*, 2013; Ma, Potappel, Chauhan, *et al.*, 2023; Taheri-Garavand, Fatahi, Omid, & Makino, 2019). Furthermore, one study applied a CV algorithm, called Hough transformation, to calculate a fibre index for a set ($n=9$) of meat analogues produced through HME cooking (Ranasinghesagara, Hsieh, & Yao, 2005). The study found that fibre index calculated from image analysis correlated well with a non-invasive fluorescence polarization method. However, as Hough transformation only detects straight lines on an image, the method developed by Ranasinghesagara *et al.* (2005) may have limitations when detecting inner structures with curved or bended fibres as for example found in HTSC samples. Other CV techniques such as shape analysis have been applied to provide comprehensive morphological characterizations of barley kernels and wheat grains (Sharma, Kumar, & Alam, 2021; Zapotoczny, Zielinska, & Nita, 2008). These morphological analysis methods can potentially be adopted to measure the visual fibrousness of meat analogues. Furthermore, while the conventional evaluations by human experts can only provide a single value to assess fibrousness, a CV-based method has the potential to offer visual similarity assessment, for example using real meat, because it can characterize multiple morphological features of the fibrous structures. A first step in the development of this tool is the validation of the quantitative measure of fibrous structure with a CV-based method and to place it into context with human evaluations, which can then establish practical significance of an automated method (Ma, Potappel, Schutyser, Boom, & Zhang, 2023). Eventually, such tool could replace time- and resource-consuming human evaluations for the quality control of meat analogues.

This study aims to develop an automated visual assessment method called “Fiberlyzer” based on CV to quantify fibrousness of meat analogues. Specifically, the Fiberlyzer

method utilizes image segmentation followed by shape analysis to calculate a robust fibre score to serve as an alternative to human evaluation. The computed fibre score is then validated by expert fibre scores collected from a survey. Additionally, the method generates a unique texture fingerprint for each image, allowing precise comparison between texture of meat and meat analogues.

5.2 Materials & Methods

5.2.1 Materials

Soy protein isolate (SPI) (Supro 500E), pea protein isolate (PPI) (NUTRALYS® F85M), and mung bean protein isolate (MBPI) (UNIMUNG M70) were obtained from Solae (Dupont, St. Louis, MO, USA), Roquette Freres S.A. (St. Louis, Missouri, USA), and Barentz (Hoofddorp, NL), respectively. SPI, PPI, and MBPI were composed of 81.7 wt.% (N x 5.7), 74.5 wt.% (N x 5.4), and 68.9 wt.% (N x 5.7) protein on a dry weight basis using a rapid N exceed® analyzer (Elementar, Langenselbold, Germany). SPI, PPI, and MBPI had a dry matter content of 91.2 wt.%, 92.4 wt.%, and 97.3 wt.%, respectively. Cooked chicken breast (Scharrel Kipfilet, Albert Heijn, the Netherlands), tofu (Biologische tofu naturel, Albert Heijn, the Netherlands), and vegan chicken (De Vegetarische Slager Kipstuckjes, Unilever, the Netherlands) were purchased at a local supermarket (Albert Heijn, the Netherlands).

5.2.2 Sample preparation

To obtain meat analogue samples with a variety of textures, plant proteins were structured using the high temperature shear cell (HTSC) technology (Wageningen University & Research, the Netherlands). First, protein doughs were prepared by manually mixing various amounts of demineralized water with SPI, PPI, or MBPI to achieve final dry matter concentrations of 35, 40, or 45 wt.% (Table 5.1). In addition, blended protein doughs were made by combining SPI and PPI or SPI and MBPI in a 50:50 ratio (Table 5.1). Formulations made from MBPI and SPI with 45 wt.% dry matter are missing, as these could not be structured into meat analogues in preliminary experiments due to poor protein hydration. In total, 13 formulations were prepared for subsequent shear cell structuring.

TABLE 5.1 Overview of the dry matter composition of the doughs prepared from mung bean protein isolate (MBPI), pea protein isolate (PPI), soy protein isolate (SPI), and combinations of SPI-MBPI and SPI-PPI.

Protein ingredient(s)	MBPI (wt.%)	PPI (wt.%)	SPI (wt.%)	Total dry matter (wt.%)
MBPI	35	-	-	35
	40	-	-	40
PPI	-	35	-	35
	-	40	-	40
	-	45	-	45
SPI	-	-	35	35
	-	-	40	40
SPI-MBPI	17.5	-	17.5	35
	20	-	20	40
	22.5	-	22.5	45
SPI-PPI	-	17.5	17.5	35
	-	20	20	40
	-	22.5	22.5	45

The protein doughs were covered with parafilm and left to hydrate at room temperature (20 °C) for 30 min. The doughs were then loaded into a pre-heated HTSC to structure them into meat analogues. During the HTSC process, the materials were sheared at a rate of 39 s⁻¹, 120 °C for 15 min (controlled by a Haake PolyLab QC drive, Germany). Subsequently, the samples were cooled at 0 s⁻¹ for 5 min, using an external oil bath with a temperature of 25 °C. The cooled sample was removed from the HTSC, tempered to room temperature, sealed in an air-tight bag, and stored in the freezer (-18 °C) until further analysis. Freezing can positively impact the fibrous appearance and has previously been applied to texturize animal and fish proteins and soy protein gels (Chantanuson, Nagamine, Kobayashi, & Nakagawa, 2022; Dekkers *et al.*, 2018).

5.2.3 Image acquisition and pre-processing

The frozen HTSC sample was first thawed to 20 °C, and 3 squares of approximately 3 × 3 cm were randomly cut out and manually folded open in the direction parallel to the shear flow to expose the inner structure. The folded sample was held in place by a clamp and imaged in a light-controlled photo booth with a digital camera (A6000, SONY, Japan) equipped with a 100 mm macro lens (Tokina, Tokyo, Japan). The camera was placed approximately 20 cm from the folded sample. Figure 5.1A and 5.1B provide an example image of the inner structure of the HTSC sample. After obtaining the raw images, a region of interest was manually selected by cropping out the background to allow assessment of the inner structure of the HTSC samples (Figure 5.1C). For samples

that were completely fractured (i.e. Figure 5.1B), region of interest was only focussed on half of the sample to avoid fracture edges (Figure 5.1D).



FIGURE 5.1 Example images of samples produced for this study. A: an image of a folded sample made of soy protein isolate (35%). B: an image of a folded sample made of mung bean protein isolate (35%). C: the cropped image of soy protein isolate sample shown in A. D: the cropped image of mung bean protein isolate sample shown in B.

5.2.4 Expert visual assessment of fibrous structures

Quantitative visual assessment was performed through an online survey designed in Qualtrics (Washington, USA). Twenty-six experts with prior experience in evaluating macrostructures of HTSC meat analogues were recruited for this study. The survey consisted of 13 images of HTSC meat analogues, three images of commercial samples (cooked chicken breast, tofu, and vegan chicken), and two mirrored images as quality control samples. The two mirrored images were included to check whether the experts rated products with identical fibrousness similarly. All images were acquired and pre-processed as described in section 5.2.3.

Experts were instructed to evaluate fibrousness of the samples on a visual analogue slider ranging from 0 to 100. The slider contained 5 labels (not fibrous, somewhat fibrous, fibrous, very fibrous, and extremely fibrous) at the 0, 25, 50, 75, and 100 positions. Furthermore, images of a non-fibrous and an extremely fibrous HTSC sample served as references and were presented to the experts at the beginning of each survey question. For every HTSC and commercial sample, 1 out of 5 images was randomly selected and presented to an expert. With 26 experts, this resulted in at least 5 evaluations per image. The median of the 5 scores was calculated and used as a measure for expert visual fibrousness. All experts were presented the same mirrored images to evaluate the consistency in fibrousness evaluations.

5.2.5 Fiberlyzer: automated visual assessment of fibrous structures

Fiberlyzer, a Python-based image analysis method, was developed to automate the visual assessment of fibrous structures of the HTSC meat analogue samples. The automated visual assessment pipeline consisted of image collection, segmentation,

and shape analysis (Figure 5.2). The image collection and pre-processing step was introduced in section 5.2.3, and the details of segmentation and shape analysis steps are introduced in the following sections.

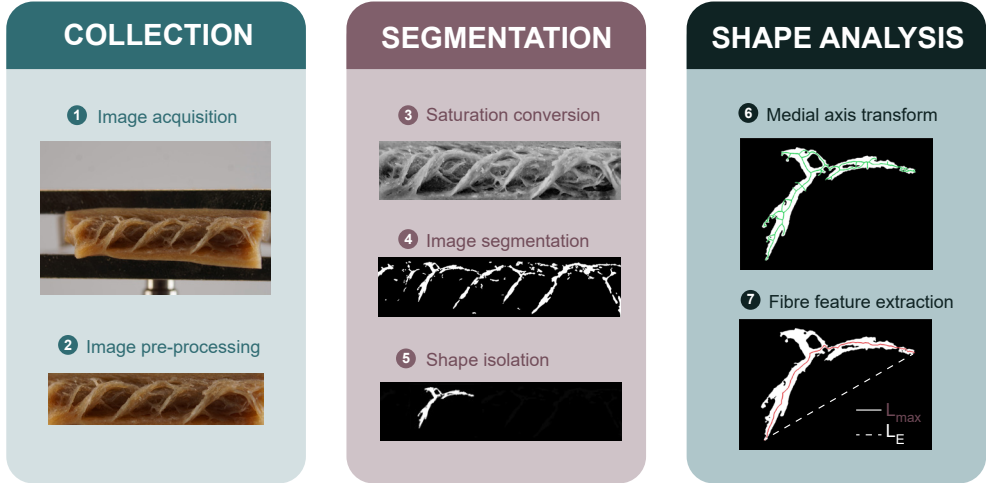


FIGURE 5.2 Fiberlyzer workflow consisting of collection, segmentation, and shape analysis. L_{max} indicates longest skeleton path. L_E indicates Euclidian distance between start and end points of the longest path.

5.2.5.1 Segmentation of fibrous regions

To automatically identify the fibrous regions of an inner structure, a segmentation method is required. The saturation values of colour images have shown correlations to 3D shape perceptions in the human visual system (Marlow, Gegenfurtner, & Anderson, 2022). Therefore, a saturation-based technique was used to identify and segment potentially fibrous regions on the pre-processed image. The images were first converted into the HSV colour space, and a threshold level was set to create a binary image. The binary image was smoothed using the Gaussian pyramid construction and median blur with a filter size of 7×7 pixels. Connected component analysis was then performed to identify and locate the individual fibrous regions using a connectivity of 4. A minimal area of a connected component was defined as a fraction of the total image size and used to filter unwanted noise from the prior binarization step.

5.2.5.2 Fibre shape analysis

Each isolated region was then analysed separately to obtain various shape features. For each region, image skeletonization was used to identify a set of curves that pass through the centre of connected regions known as the “skeleton”. The longest path (L_{max}) was found by iteratively looping through all unique pairs of branches of the skeleton.

Meanwhile, the Euclidean distance (L_E) between the start and end points of the longest path was calculated, and a curvature factor was then determined by taking the ratio between L_{\max} and L_E . Only regions with a curvature factor of less than 1.2 were further analysed to avoid over-curved skeletons. The shortest distance from each pixel on a skeleton to the edge of the shape was then calculated for each isolated skeleton. These distances were averaged to obtain the width of the potential fibrous region. Image skeletonization was then performed on all isolated regions to obtain the length, width, area, and number of branches of the individual region. A fibre score, F , was calculated for each region with equation 5.1.

$$F = \frac{\text{longest skeleton path length}}{\text{average path width}} \quad (\text{Eq. 5.1})$$

The average fibre score, \bar{F} , was calculated among all isolated regions of one image and served as the main shape feature to quantify fibrousness of the meat analogue sample. To obtain the best segmentation parameters, a grid search was performed using a range of minimal area (from 0.005% to 0.05%) and saturation threshold (from 80 to 95 %) to calculate \bar{F} of each image.

5.2.6 Visual fibre similarity analysis

While the computed fibre score from Fiberlyzer gives a quantitative fibrousness assessment at the image level, additional fibre similarity analysis was carried out to measure how closely the fibrous structure from HTSC samples resembles cooked chicken breast. The obtained fibre shape features of HTSC samples were compared with those obtained from a reference image of cooked chicken breast. Distributions of fibre score, area, and number of branches were overlayed with those from the reference image, respectively. The overlapped area of the two distributions, $f(x)$ for meat analogue samples and $g(x)$ for the reference sample, was estimated by calculating the coefficient of overlapping (Δ) using a method developed by Ridout & Linkie (2009) (Eq. 5.2).

$$\Delta(f, g) = \int \min \{f(x), g(x)\} dx \quad (\text{Eq. 5.2})$$

where x represents the individual shape feature of fibre score, fibre area, or number of fibre branches.

The $\Delta(f, g)$ of each shape feature was then averaged to obtain a collective similarity score between a given HTSC sample and the reference chicken breast.

5.2.7 Data analysis and software availability

Pearson's correlation tests were conducted using the R programming language. The Fiberlyzer method was developed in-house using the OpenCV, NumPy, Pandas, and Matplotlib libraries in the Python programming language. The software including a graphical user interface, raw scripts, and raw images used for the software development are open source and can be accessed through: <https://git.wur.nl/yizhou.ma/fiberlyzer3>.

5.3 Results & Discussion

In the following sections, the expert assessment of visual fibrousness is first introduced to understand structural differences among the high temperature shear cell (HTSC) samples produced in this study. We then highlight the shape feature measurements from the Fiberlyzer method. The aggregated measurement from the Fiberlyzer method was correlated with the expert assessment as a validation. A visual fibre similarity analysis between a reference cooked chicken image and HTSC sample images was also performed to select formulations with the highest potential to mimic chicken. Lastly, we discuss the limitations and future applications of the Fiberlyzer method.

5.3.1 Expert assessment of visual fibrousness

Visual fibrousness of meat analogues and commercial products (tofu, vegan chicken, and chicken) were assessed in a survey of 26 meat analogue experts. Quality control samples (mirrored images of a HTSC sample) were included in the survey to check the consistency of the fibre scoring among the experts. No significant difference ($p > 0.05$) in fibre score was found between the two quality control images ($\mu_{\text{mirrored image}} = 43.1$, $\mu_{\text{non-mirrored image}} = 42.8$), showing that the experts were consistent when assigning fibre scores. However, the expert fibre scores of the quality control samples had a large variation with a range between 0 to 85 (Figure S5.1). The large scoring variation is likely due to that the experts were untrained to specifically rate fibrousness of HTSC samples, so the fibre scores were not primed toward a certain range or calibrated with standards. Nevertheless, the expert survey revealed differences in fibrousness among the surveyed samples (Figure 5.3). MBPI 35 and 40 wt.% were found to exhibit no visual fibrousness, with median fibre scores of 0. The fibrousness assessment agrees with previous findings, where pure MBPI-based meat analogues were described as ‘gel-like’ and displayed no fibre formation (Samard & Ryu, 2019; Schlangen, Ribberink, Taghian, Sagis, & van der Goot, 2023). For PPI samples, at 35 and 40 wt.% , very minimal fibrousness was found from the expert survey. In previous studies, PPI was often blended with other ingredients, such as wheat gluten and pectin, to assist structure elongation and form anisotropy (Schreuders *et al.*, 2019; Schreuders, Schlangen, Bodnár, *et al.*, 2021). However, PPI alone has been texturized into a fibrous structure at high dry matter content (45 wt.%) using HME cooking before (Osen *et al.*, 2014). This finding from Osen *et al.*, (2014) agrees with the fibre scores rated by the experts in this study, showing the potential of producing fibrous structures of PPI at high dry matter content (45 wt.%).

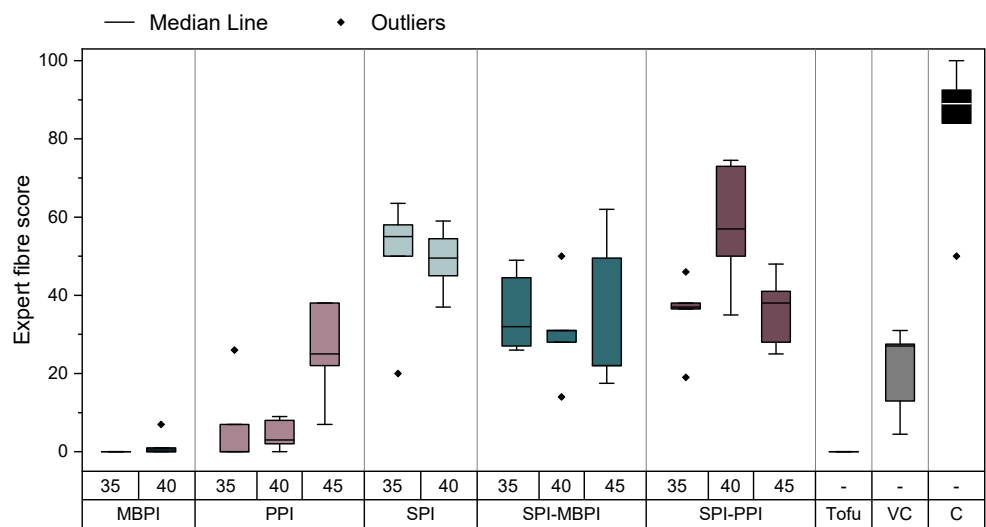


FIGURE 5.3 Expert fibre scores of high temperature shear cell samples with various dry matter contents (35, 40, and 45 wt.%). SPI: soy protein isolate; PPI: pea protein isolate; MBPI: mung bean protein isolate. VC: vegan chicken. C: chicken.

SPI samples and SPI-PPI blends both showed higher fibre scores compared to the other HTSC samples (Figure 5.3). Typically, wheat gluten or pectin is added to SPI to induce fibre formation in shear structuring, as SPI alone was previously shown not to form a fibrous structure (Dekkers *et al.*, 2016). However, freezing may have assisted fibre formation in this study. It is also worth mentioning that the blend of two non-gluten proteins (SPI-MBPI and SPI-PPI) could be structured into fibrous products, which was only reported from a previous HME cooking study (Wittek, Karbstein, & Emin, 2021). Overall, the variations in expert fibre scores show that inner structures of HTSC samples exhibit differences. The wide range of expert fibre scores can therefore be used as references for the subsequent validation of the Fiberlyzer method.

5.3.2 Fibre shape features in meat analogues

The image-based Fiberlyzer method can provide measurements of fibre shape features including the fibre score, fibre area, and number of fibre branches. For example, Figure 5.4 highlights distributions of shape features of four images acquired in this study. Figure 5.4A shows the variation in computed fibre score among cooked chicken, MBPI with 35 wt.% dry matter, SPI-PPI with 35 wt.% dry matter, and tofu images. The chicken image had a bimodal distribution of the computed fibre score with peaks centres around 5 and 17.

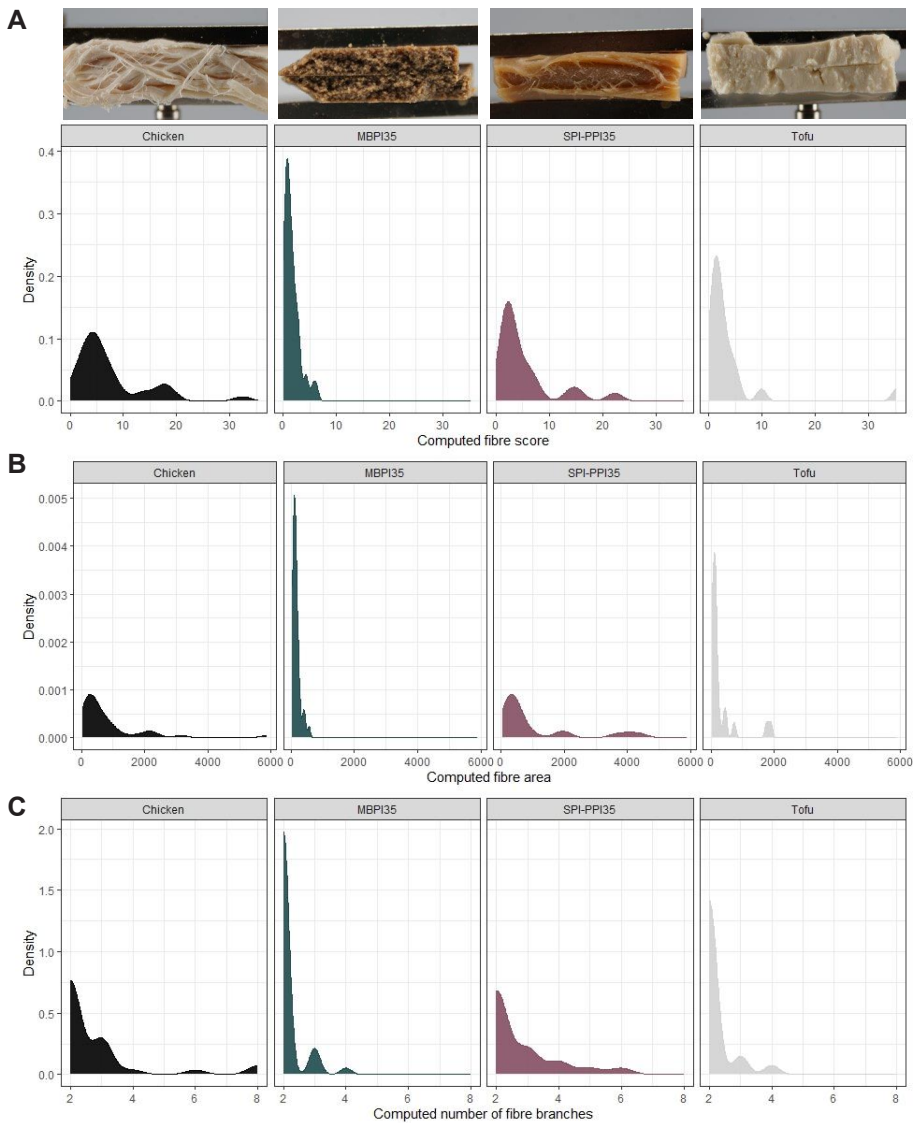


FIGURE 5.4 Example measurements of fibre shape features of chicken, mung bean protein isolate (35 wt.%) (MBPI35), a blend of soy protein isolate and pea protein isolate (35 wt.%) (SPI-PPI35), and tofu. A: distributions of computed fibre score. B: distributions of computed fibre area. C: distribution of number of fibre branches.

Such a broad range of fibre scores agreed with the hierarchical fibre presence of cooked chicken (Figure 5.4A) as meat muscle fibres occur at different length scales (van der Sman & van der Goot, 2023). MBPI with 35 wt.% dry matter had a narrow distribution with a low fibre score peak around 3. The narrow distribution of the fibre score

corresponded well with the image of the sample, of which the MBPI 35 wt.% dry matter sample appeared to be crumbly and grainy. On the other hand, the computed fibre score distribution of SPI-PPI with 35 wt.% dry matter was bimodal with a broad distribution of scores, similar to chicken. The fibrousness of the SPI-PPI 35 wt.% dry matter was also scored closer to chicken in the expert evaluation (Figure 5.3). The similarity in fibre score distribution between chicken and SPI-PPI 35 wt.% dry matter may explain the higher expert fibre score that SPI-PPI 35 wt.% dry matter received (Figure 5.3). The computed fibre score may therefore be an indication of the expert fibre scores collected from the survey.

However, the tofu image also yielded a computed fibre score distribution that was relatively similar to the HTSC samples (Figure 5.4A). Nonetheless, the computed fibre distribution of tofu disagreed with the expert panel results in Figure 5.3, where all experts gave a fibre score of 0 for the tofu image. Tofu may carry a different fractal appearance from HTSC samples upon folding, because of its relatively isotropic structure. Also, the surface moisture on tofu may have interfered with the fibre segmentation algorithm developed in this study. The unexpected high fibre score indicated that tofu was an outlier in visual fibrousness assessment using Fiberlyzer and was therefore discarded for subsequent analysis.

For the area distributions (Figure 5.4B), MBPI with 35 wt.% dry matter showed a sharp distribution centred around a lower value compared to the broad distribution of chicken. The lower fibre area may correspond to the crumbly and granular texture observed in the image. The small granules were segmented and identified by the Fiberlyzer as small fibre areas. By comparing the area distributions, SPI-PPI with 35 wt.% dry matter had a similar fibre area range as the chicken image, indicating the potential similarity in visual fibrousness. Figure 5.4C illustrates distributions of number of fibre branches identified in the samples. Again, the SPI-PPI sample with 35 wt.% dry matter appeared to have a more similar distribution to chicken than the MBPI with 35 wt.% dry matter. The distinct fibre shape features of different samples showed the potential of using the Fiberlyzer method to characterize fibrous structures of HTSC samples.

5.3.3 Validation of computed fibre scores

Although fibre shape feature distributions can characterize the fibrous structures of HTSC samples, further analysis is needed to directly compare the computed fibre shape features to the expert fibre scores. The fibre shape features were averaged per image to produce aggregated representations of fibre score, fibre area, and the number of fibre branches. Because segmentation parameters during image analysis can impact the shape feature calculation, a grid search was performed to identify the best combination of segmentation parameters. The correlation of determination (R^2) was used as the

parameter selection criterion when determining the segmentation parameters of threshold percentile and minimal fibre area. During preliminary experiments, we only found significant correlations between the averaged computed fibre score and the expert fibre score, so the subsequent validation focused on evaluating computed fibre score as an automated measurement to replace expert visual assessment.

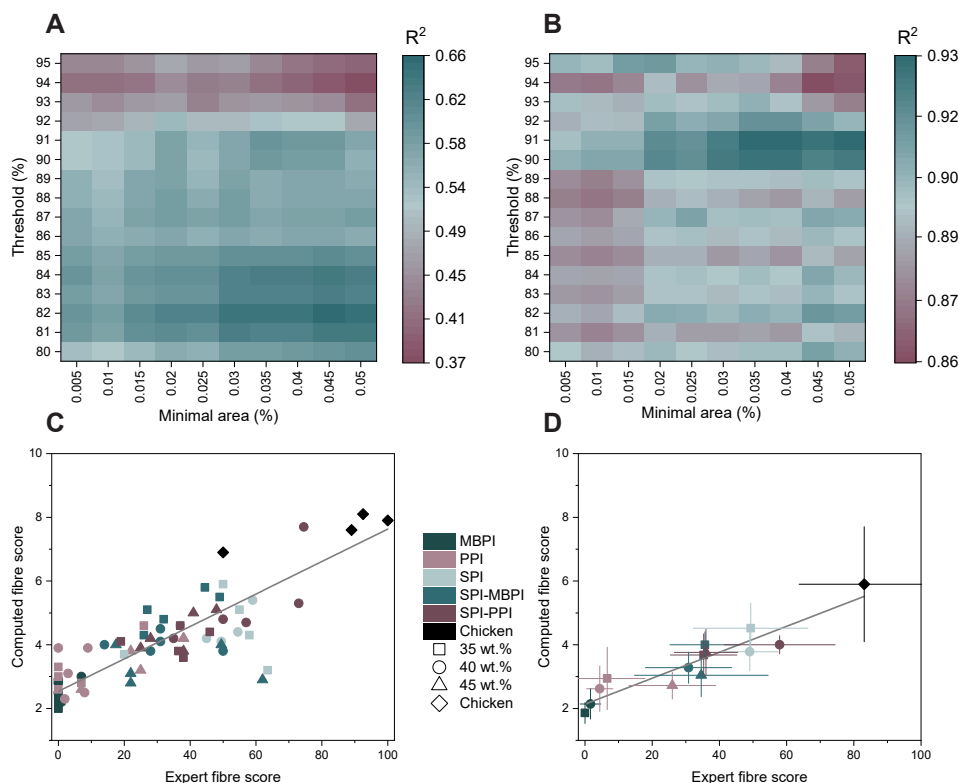


FIGURE 5.5 Parameter correlation on A) per image basis and B) per formulation basis, and corresponding scatter plots of expert fibre score vs. computed fibre score with C) threshold percentile of 82% and minimal area of 0.045 %, and D) threshold percentile of 91 % and minimal area of 0.04%.

The correlation between the computed fibre score and expert fibre score was influenced by both the threshold percentile and the minimal area (Figure 5.5A). A high threshold percentile reduced the R^2 value, likely due to the exclusion of fibrous regions during the saturation-based segmentation step. Conversely, a low threshold percentile led to an overestimation of fibrous regions, including non-fibrous areas (i.e. noise) falsely identified as region of interests. When the minimal area was set below 0.03%, a decrease in correlation was observed, probably due to the inclusion of relatively small regions (i.e. noise) that are non-fibrous in nature but that were used in the calculation of the computed fibre score. The combination of an 82% threshold percentile and a

0.045% minimal area yielded the highest R^2 value and were thus selected as the best segmentation parameters on a per-image basis. These parameters were used to plot the computed fibre score against the expert fibre score, resulting in a R^2 of 0.66 on a per image basis (Figure 5.5C). This moderate correlation suggests that the Fiberlyzer method can partially replace the expert evaluation of visual fibrousness. The computed fibre scores effectively differentiated between the non-fibrous images (MBPI) and highly fibrous images (chicken). However, comparing the other samples remains inconclusive due to the variations in fibrous structure from image to image.

To account for the image-to-image variations, Figure 5.5B and D present a formulation-based comparison by averaging the scores of 5 images of the same formulation. Here, a higher threshold percentile (91%) and a lower minimal area (0.040 %) improved the R^2 to 0.93. From Figure 5.3 it already became evident that there were considerable variations in the expert fibre scores. Figure 5.5D reveals large variations in computed fibre score as well. The variations in computed fibre score can be attributed to the inhomogeneous fibre distribution within the meat analogues, which may be a desired property of the product. However, the variations could also be explained by variations in selecting of samples and/or imaging technique. The large inner structure variations were also reported in other studies based on x-ray tomographic characterizations (Nieuwland, Heijnis, van der Goot, & Hamoen, 2023). Similar to the expert survey results, chicken images scored higher than the meat analogue images, despite variations in computed fibre scores. Overall, the averaged result on a formulation basis improved the correlation ($R^2 = 0.93$), suggesting that the Fiberlyzer is a practical method to replace expert fibre assessment digitally.

5.3.4 Image-based similarity analysis

While the computed fibre score provides automated and direct quantification of fibrous structures, it is also important to understand how closely the HTSC samples can mimic the visual appearance of meat products. To quantify the similarity found in the three fibre shape features (fibre score, fibre area, or number of fibre branches), a similarity analysis method (Eq. 5.2) was implemented by considering the distribution overlapping between a HTSC sample image and a reference chicken image (Figure S5.2). Figure 5.6A shows the similarity analysis based on overlapping of averaged shape feature distributions. Four other chicken images were used as benchmarks to establish a threshold similarity score. In Figure 5.6A, the chicken similarity scores ranged from 0.64 to 1, indicating that a “chicken-like” sample should have a similarity score of at least 0.64. Among each formulation, a large variation was found again, due to the structural heterogeneity of the HTSC samples as discussed in section 5.3.2. Although with variations, MBPI samples were found to be the most dissimilar to the

chicken reference image (Figure 5.6A). Samples made from other formulations had no clear distinctions when comparing all three shape features to determine similarity. Several samples had a similarity score exceeding the threshold as indicated by the dash line, which suggests resemblance to the reference cooked chicken image according to the Fiberlyzer method. However, similarity score computed based on the average parameters may not provide the required resolution to differentiate fibrous structures among HTSC samples.

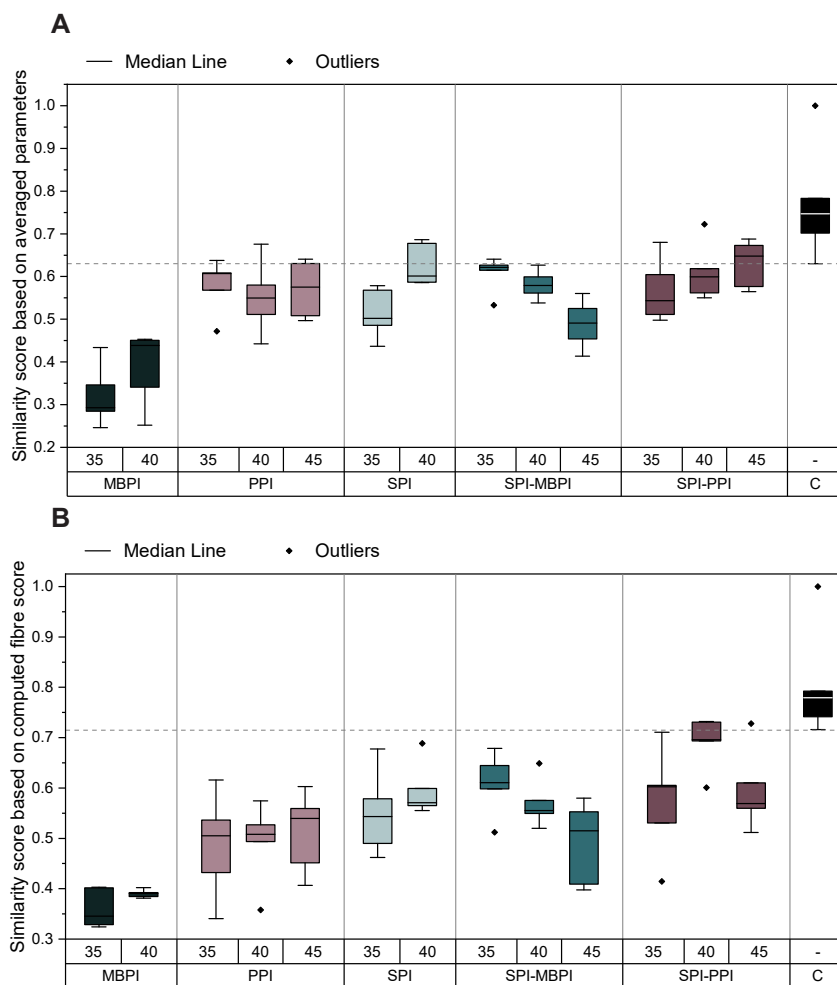


FIGURE 5.6 Visual similarity analysis between high temperature shear cell samples and cooked chicken based on averaged shape features (A) and computed fibre score (B). SPI: soy protein isolate; PPI: pea protein isolate; MBPI: mung bean protein isolate. C: cooked chicken. Samples were produced at dry matter contents of 35, 40, and/or 45 wt.%. Dashed line indicates similarity threshold to cooked chicken.

With no clear distinction in fibre similarity based on three shape features, Figure 5.6B evaluates fibre similarity using the fibre scores alone. A new similarity threshold (0.72) was determined based on the reference chicken images. A large range of similarity (0.35 to 0.6) was found in the PPI samples, indicating large structural variations in terms of fibrous structures. Structural variation may be desired as it suggests heterogeneity. However, in practice, too large of a structural variation may not be desirable because it impacts perceived spatial uniformity (McClements & Grossmann, 2022). The SPI and SPI-MBPI samples had a similar trend to PPI samples, which agrees with the similar range of expert fibre scores received by these samples. A unique sample among the similarity analysis was SPI-PPI with 40 wt.% dry matter with a median similarity score of 0.70, very close to the similarity threshold found earlier (0.72). Therefore, from a formulation selection perspective, SPI-PPI with 40 wt.% dry matter may have the most potential of visually mimicking the cooked chicken appearance.

5.4 General discussions

The Fiberlyzer method has demonstrated its potential as an alternative and automated method to assess fibrousness in HTSC samples. However, there are some limitations that the image-based Fiberlyzer method carries. First, as shown in Figure 5.4A, tofu was misidentified to have fibrous structures due to false fibre segmentations. Therefore, suitable samples for the Fiberlyzer method should be limited to meat analogues that are free of surface moisture to minimize interference of light reflection. In addition, a parameter search demonstrated in section 5.3.3 may be necessary to identify the best image processing parameters because the Fiberlyzer method relies on a saturation-based segmentation method. Changes of lighting conditions and imaging devices may further impact the segmentation parameters, so calibrations may be needed when implementing the method with a new imaging setup. Lastly, the Fiberlyzer method requires to fold the HTSC sample to expose the inner structure. The folding leads to fracturing of the HTSC sample, making it impossible to assess fibrous structure non-destructively for in-situ measurements.

Despite the mentioned limitations, the Fiberlyzer method can serve as a digital method to replace the conventional expert inspection of visual fibrousness of meat analogues in most of the cases. In addition to the immediate application in the assessment of visual fibrousness, the Fiberlyzer method may empower potential future applications. One potential future application lies in the optimization of formulations and processing conditions for meat analogues. The method can be used to precisely pinpoint differences between the meat products and the analogues. The use of the method can lead to valuable insights on the effect of different ingredients, dry matter contents,

temperature, shear rate, and other processing conditions on the visual texture of the products. This information can then be used to optimize and tailor the texture of meat analogues to fit consumer wishes. Additionally, with Fiberlyzer being a rapid method for quantification of visual fibrousness, it could serve as a valuable tool for quality control in meat analogue production industry. For example, deviations and inconsistencies in products are easily detected with the Fiberlyzer method.

Furthermore, the unique fingerprint of visual texture provided by the Fiberlyzer method holds potential to be used in meat analogue research and development. By conducting comparative analyses between meat and meat analogues, a deeper understanding of the differences in textural properties can be achieved. This knowledge can then help to further develop meat analogues that exhibit a closer resemblance to the texture and visual appearance of animal meat. The similarity score in this study was calculated based on cooked chicken as a reference. In the course of time, alternative reference products can be used, such as fish, pork, or beef to allow a broader similarity assessment across meat types.

In the future, the Fiberlyzer method has the potential to bridge the gap between visual fibrousness and mechanical texture properties of meat analogues. Previous studies showed that mechanical anisotropy was not always linked to a visually fibrous macrostructure (Schreuders, Schlangen, Bodnár, *et al.*, 2021). By connecting the computed fibre scores with mechanical analyses, such as tensile testing, the relation between mechanical anisotropy and visual fibrousness can be further understood. Such a clear understanding of fibrous structures helps to develop meat analogues that can best appeal to consumers.

5.5 Conclusions

This study developed and validated an automated visual assessment method (Fiberlyzer) to quantitatively characterize fibrous structures in meat analogues based on image analysis. Fibre shape features were successfully segmented and measured in terms of fibre score (ratio between length and width), fibre area, and number of fibre branches. Among the fibre shape features, fibre score was found to be correlated to expert assessments of fibrousness both at the image ($R^2 = 0.66$) and formulation levels ($R^2 = 0.93$). A similarity analysis was performed to identify the most similar HTSC samples to a reference cooked chicken image, offering a new criterium of selecting visually-mimicking samples for meat analogue applications. The Fiberlyzer method is open-source and simple to be implemented into the current product development routine of meat analogues. Such a digital tool can further contribute to formulation development in the production of meat analogues and enhance the current understanding of visual and textural fibrous structures in meat analogues.

5.6 Supplementary material

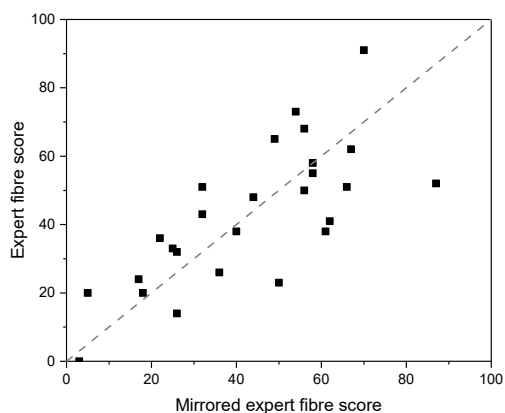


FIGURE S5.1 Expert fibre scores of the quality control sample (mirrored vs. original).

5



FIGURE S5.2 Reference cooked chicken image used for the similarity analysis.

6

Chapter 6

Advanced tensile testing as a new tool to quantify properties of food

This chapter has been published as Schlangen, M., Schlangen, E., van der Goot, A.J. (2023) Advanced tensile testing as a new tool to quantify properties of food. Current Research in Food Science. 7, 100577.

Abstract

Mechanical properties of food products are regularly analysed by tensile tests. The aim of this study was to demonstrate the potential of using advanced tensile testing techniques to better understand the mechanical properties of anisotropic food products, such as meat analogues and certain dairy products. The effects of various tensile testing parameters, including tensile gauge length and deformation rate, on the interpretation of mechanical properties of meat analogues was studied. Additionally, digital image correlation, an image analysis technique, was used for true distance recording and analysis of fracturing behaviour of the products. An isotropic product was prepared from solely soy protein isolate, and an anisotropic product was prepared from soy protein isolate and pectin using the shear cell technology. The tensile properties of the products were studied with four different moulds with varying gauge lengths of 17.5, 15, 11.5, and 8.5 mm, and at three deformation rates of 46.2, 23.1, and 11.6 mm/min. A smaller gauge length and slower deformation rate improved visualization and interpretation of the multi-stage descending branch in force – distance curves of anisotropic products. Additionally, tensile parameters, specifically toughness, proved to be more accurate at small gauge length and slow deformation rate, because overestimation due to rapid crack propagation was prevented. True distance data obtained with digital image correlation further improved the interpretation of the fracturing behaviour of the products. Inhomogeneous strain distribution in anisotropic products was shown with digital image correlation, in contrast to the homogeneous strain distribution observed in isotropic products. Furthermore, the Poisson's ratio, obtained through digital image correlation, explained inherent differences in structure and plasticity between isotropic and anisotropic meat analogues. This study shows the importance of careful selection of testing parameters and techniques. Moreover, it advises the use of digital image correlation for better measurement of fracture mechanics and strain distribution.

6.1 Introduction

Preparation and consumption of foods normally involve large deformations. The mechanical and fracturing behaviour of foods becomes complex at large deformations, but at the same time important to understand in product development (Lu & Abbott, 2004). The mechanical and fracturing behaviour can be studied using various mechanical tests, such as compression tests, Warner Bratzler tests, and tensile tests (Schreuders, Schlangen, Kyriakopoulou, Boom, & van der Goot, 2021). Among the different methods, tensile tests are commonly used to characterize anisotropic structures of food products, such as certain dairy products and meat analogues (Ak, Bogenrief, Gunasekaran, & Olson, 1993; Ak & Gunasekaran, 1997; Dekkers, Nikiforidis, & van der Goot, 2016).

A tensile test is a mechanical analysis to study the resistance of a material against tearing. In a tensile test, a material is placed between two grips and extended in a uni-axial direction at a fixed strain rate. When a force is applied to a food product, it will fracture at the weakest points, which are often located at the interfaces between dispersed and continuous phases. Comprehending the fracture behaviour of food products can provide insights into their multi-phase structure, which makes it possible to tailor the fracture characteristics as desired. Previously, it has been shown that tensile testing is regularly used to evaluate the texture of meat and meat analogue structures as well as dairy products, such as mozzarella (Ak & Gunasekaran, 1997; Schreuders, Schlangen, Kyriakopoulou, *et al.*, 2021). Currently, most studies on food that use tensile tests report a few tensile parameters: fracture stress, fracture strain, and Young's Modulus (Chen, Zhang, Zhang, Kaplan, & Wang, 2022; McClements, Weiss, Kinchla, Nolden, & Grossmann, 2021; Pietsch, Werner, Karbstein, & Emin, 2019; Schreuders *et al.*, 2019). Here, the fracture stress is defined as the maximum stress before a rapid decrease in stress, the fracture strain is defined as the strain at the fracture stress, and the Young's Modulus is defined as the slope of the elastic part of the stress-strain curve. However, the potential of tensile tests for food products is not yet fully utilized. There is little to no effort in literature on finding the exact tensile testing parameters to use and how to obtain any additional tensile parameters such as Poisson's ratio and local strain.

We, therefore, analysed how the method is applied to non-food materials following material science rules. It has been established in related disciplines that the rate of tensile testing and the tensile gauge length can have a significant impact on test outcomes (Ak & Gunasekaran, 1997; Bate, Ridley, & Sotoudeh, 2008; Hertsberg, 1996). The force – strain results of a tensile test always consist of two contributions: (1) the crack opening and (2) the elastic deformation over the total gauge length (Figure 6.1) (Hordijk, 1991). While the crack opening remains constant, the elastic

deformation changes when the gauge length is altered. When the gauge length is too long, the elastic contribution is large and will lead to unstable/undetailed fracture. An accurate measurement of fracture energies and analysis of the force-deformation curve requires a stable displacement-controlled experiment. Certain materials, such as meat analogues, are characterized by relatively high crack velocities and often exhibit brittle behaviour. To mitigate this issue, it is essential to minimize the elastic energy in the specimen. One possible approach is to reduce the size of the specimen (van Mier, 1997). Thus, a proper selection of the testing rate and gauge length will allow greater insights from the resulting data. These insights can, then, be employed to gain a comprehensive understanding of how to enhance meat analogue structures.

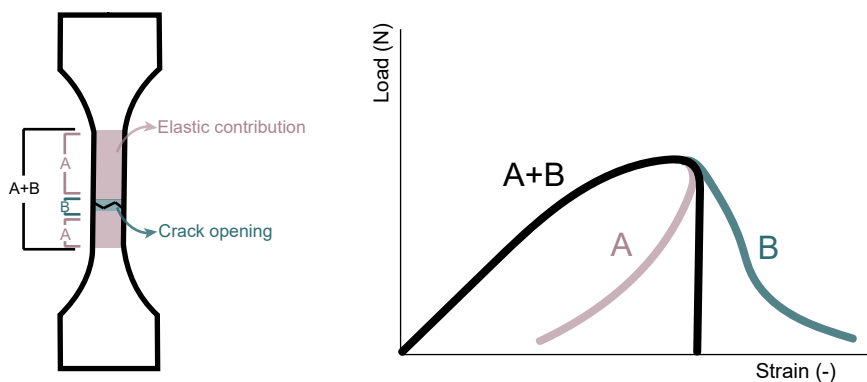


FIGURE 6.1 Schematic illustration of the two contributions to the force – strain results: elastic contribution and crack opening.

Furthermore, conventional tensile testing uses linear variable differential transformers (LVDT's) to precisely measure the deformation of (part of) the samples. However, the application of LVDT's on soft samples is complex, and often unprecise. A virtual extensometer via, for example, digital image correlation (DIC) is an alternative for LVDT's. Previously, it was proven that DIC correlated excellently with LVDT measurements in human tendons (Luyckx *et al.*, 2014). However, the application of DIC for food materials is unexplored, except for one study on surimi gels (Park, Park, & Yoon, 2023).

Therefore, the objective of this study is to show how testing conditions impact tensile testing results and to demonstrate the potential of DIC to facilitate better interpretation of mechanical properties of food products. Those findings will be presented as both raw and processed tensile data. It is important to mention that anisotropic structures of food products can be evaluated at different length scales. This study focusses on macroscopic properties of food products, but we acknowledge that structural properties over multiple length scales are important. Here, the extensive mechanical properties of

two distinct structures were studied: a homogeneous, isotropic product composed of soy protein isolate, and a heterogeneous, anisotropic product composed of soy protein isolate and pectin. The latter product has to be described as a water-in-water emulsion of pectin in soy protein isolate, and can be readily transformed into an anisotropic and often fibrous product through shear structuring. However, the chosen materials in this study are solely model products to demonstrate the potential of advanced tensile testing to get better insights in the mechanical properties of isotropic and anisotropic food products.

6.2 Materials & methods

6.2.1 Materials

Soy protein isolate (SPI) (Supro 500E IP) was obtained from Solae (DuPont, St. Louis, MO, USA). SPI had a protein content of 81.7 ± 1.1 % based on dry weight ($N \times 5.7$ as measured by Dumas). The dry matter content of SPI was 93.7 ± 0.2 %. Pectin from citrus peel (SLBQ6929V) (high methylated, 92.2 wt.% dry matter) was obtained from Sigma-Aldrich (Zwijndrecht, the Netherlands). White paint and black spray paint were obtained from Flexa (AkzoNobel, Sassenheim, the Netherlands) and OK (European Aerosols, Wolvega, the Netherlands), respectively.

6.2.2 Preparation of SPI and SPI-pectin blends

Two biopolymer mixtures (SPI and SPI-pectin) were prepared with a constant dry matter content of 44 wt.%. Previous research found that SPI alone forms an isotropic structure, while SPI combined with pectin forms an anisotropic structure (Dekkers *et al.*, 2016). The addition of pectin was thus specifically chosen for its positive impact on the texture. The SPI blend comprised of 44 wt.% SPI (dry based) and 56 wt.% demi water. The SPI/pectin blend comprised of 41.8 wt.% SPI (dry based), 2.2 wt.% pectin (dry based) and 56 wt.% demi water. First, the SPI was mixed with the demi water with a spatula and left to hydrate for 30 min. Then, in the case of the SPI-pectin blend, pectin was added to the hydrated sample and mixed thoroughly.

6.2.3 Shear-induced structuring with the high temperature shear cell

The prepared blends were structured into products with the high temperature shear cell (HTSC). The method for shear-induced structuring with the HTSC was based on previous research by Dekkers, Nikiforidis, & van der Goot (2016). SPI and SPI-pectin blends were placed into the pre-heated HTSC and not sheared at 0 s^{-1} for SPI and sheared at 39 s^{-1} for SPI/pectin for 15 min at 140°C . Subsequently, the HTSC was cooled down to 25°C within 5 min, after which the samples were taken out and placed in plastic bags to prevent moisture loss. The samples were frozen at -18°C before further analysis. HTSC samples were prepared in triplicate. The macrostructures of the isotropic SPI and anisotropic SPI-Pectin products are shown in Figure 6.2.

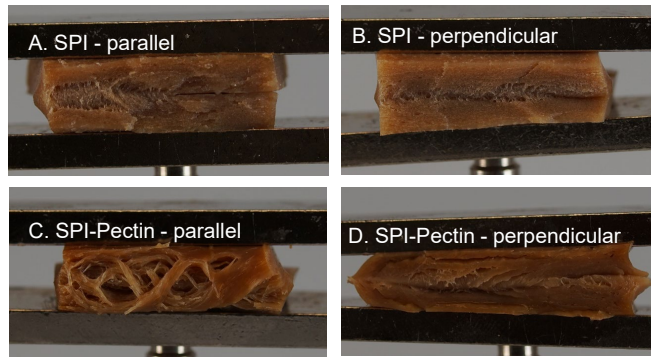


FIGURE 6.2 Representative macrostructures of meat analogues with A. SPI in parallel direction to shear flow, B. SPI in perpendicular direction to shear flow, C. SPI-Pectin in parallel direction to shear flow, and D. SPI-Pectin in perpendicular direction to shear flow. Samples are approximately 1.5 cm in width.

6.2.4 Tensile strength analysis

Tensile strength analysis of the HTSC products was performed using a Texture Analyser (TA.XTPlusC, Stable Micro Systems, Surrey, United Kingdom) equipped with a 5 kg load cell. An incision was made in the HTSC product so that it could lay flat. Specimens were cut from the HTSC products in parallel and perpendicular direction to the shear flow with dog-bone-shaped moulds (Figure 6.3B, C). The dog-bone-shape was specifically chosen to direct the stress to the middle of the specimen for controlled fracture. These moulds were 3D printed in four different sizes (Table 6.1) (Figure 6.3A) to study the effect of the gauge length on tensile parameter extraction. Moulds were designed and printed with the intention of incorporating a sharp diagonal edge, thereby ensuring optimal cutting performance (Figure 6.3A). Specimens were given a dog-bone shape to ensure that crack propagation and eventually fracturing occurred in the measurement zone. The thickness and width of the cut specimen varied (due to the shape of the cone-in-cone HTSC) and were, thus, measured and accounted for in calculation of stress and strain. The ends of the specimens were placed into the sandpaper-coated tensile grips with a gap width of 20, 23.3, 26 or 30.5 mm dependent on gauge length (Table 6.1).

TABLE 6.1 Gauge length and gap width of 3D printed tensile moulds, and corresponding deformation rate.

	Gauge length (mm)	Gap width (mm)	Deformation rate (mm/min)
Mould 1	17.5	30.5	70.4
Mould 2	15.0	26.0	60.0
Mould 3	11.5	23.3	53.8
Mould 4	8.5	20.0	46.2, 24.1, and 11.5

Before implementing the tensile test, the frontal surface of the specimens was painted with a thin layer of white acrylic paint. Afterwards, black spray paint was used to create randomly distributed black dots on the white specimen for employing digital image correlation (DIC). A uni-axial tensile test was performed at room temperature with a deformation rate of 46.2, 53.8, 60 or 70.4 mm/min dependent on gauge length (Table 6.1). The smallest mould (8.5 mm gauge length) was also analysed at 24.1 and 11.5 mm/min. The force and displacement were recorded by the Exponent Connect Software (Stable Micro Systems, Surrey, United Kingdom). The true stress σ (Pa) was calculated with equation 6.1:

$$\sigma(t) = \frac{F(t)}{A(t)} [\text{Pa}] \quad (\text{Eq. 6.1})$$

where $F(t)$ is the force per unit of area $A(t)$. Here, we assume that the specimen's volume did not change during measurement, i.e. that the material's Poisson ratio (transverse strain / axial strain) is equal to 0.5. The area $A(t)$ is a dynamic value and is calculated with equation 6.2:

$$A(t) = \frac{h_0}{h(t)} \times A_0 [\text{m}^2] \quad (\text{Eq. 6.2})$$

where h_0 is the initial gauge length (m) at $t = 0$, $h(t)$ is the gauge length at time t , $A(t)$ is the cross-sectional area A (m^2) of the tensile bar at time t , and A_0 is the initial cross-sectional of the specimen calculated by multiplying the thickness and width of the specimen.

The true strain ε (-) was calculated with equation 6.3:

$$\varepsilon_h(t) = \ln \frac{h(t)}{h_0} \quad (\text{Eq. 6.3})$$

The fracture point was defined as the point following a sharp decrease in stress in the stress-strain curve. The Young's Modulus, or stiffness, was defined as the slope of the linear part of the stress-strain curve. The toughness was defined as the area under the stress-strain curve. The anisotropy indices were calculated with equation 6.4.

$$\text{Anisotropy index} = \frac{\text{Tensile parameter parallel to shear direction}}{\text{Tensile parameter perpendicular to shear direction}} \quad (\text{Eq. 6.4})$$

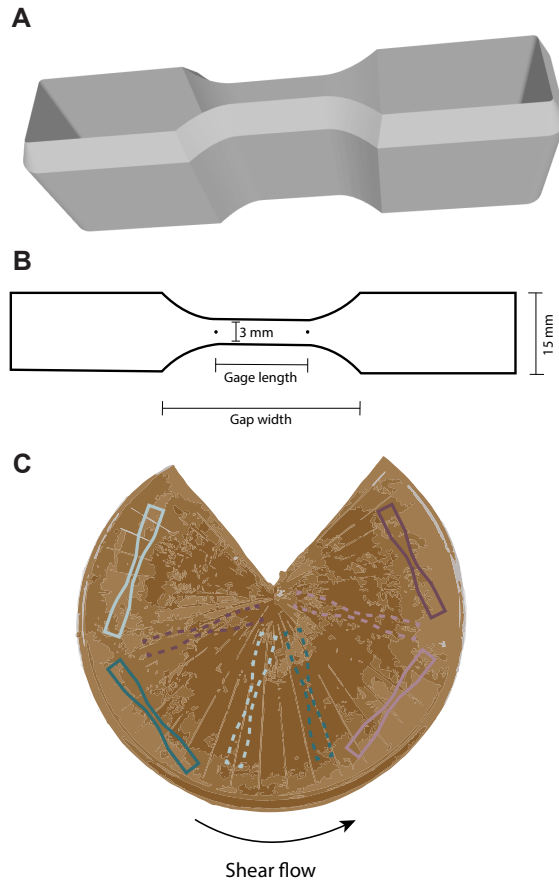


FIGURE 6.3 Visual representation of A. 3D model of tensile mould, B. tensile mould dimensions, C. position of specimen cut from meat analogue with full lines parallel to shear flow direction and dotted lines perpendicular to shear flow direction. Gauge lengths were 8.5 mm, 11.5 mm, 15 mm, 17.5 mm.

6.2.5 Digital Image Correlation

Digital Image Correlation (DIC) was utilized during tensile testing to obtain true deformation values and to further understand the fracture mechanics of the specimen. Prior to tensile testing, the frontal surface of the specimen was painted white (Wolkenwit Kleurtester, Flexa, AkzoNobel Decorative Coatings BC, Sassenheim, the Netherlands) and randomly distributed black dots were applied with black spray paint (OK Spsitlak Mat, European Aerosol s, Wolvega, the Netherlands) (Figure 6.4A). This pattern is necessary to enhance the contrast for DIC analysis. A Sony 4K FDR-AX53 equipped with a Zeiss 2.0/4.4-88 mm lens was utilized to acquire a video at 25 fps during the test process. The open source Ncorr2 and Ncorr_Post software were employed for DIC

analysis (Blaber, Adair, & Antoniou, 2015; Nežerka, Antoš, Sajdlová, & Tesárek, 2016). All frames of the video were loaded into the Ncorr2 software and analysed. The region of interest was specified manually and the software formed a virtual grid with subsets. The deformation of each subset, a set of pixels, was monitored based on the reference image. The reference image was the image taken before deformation was applied. The subset position of the reference image was described as $P(x,y)$, while the position of the deformed image is described as $P'(x',y')$. Monitoring of all subset movements occurred through correlation. Subsequently, the DIC results were loaded into Ncorr_Post to obtain displacement data. Here, a virtual extensometer was utilized to measure the displacement between two distinct sets of points on the reference image. The first two points were selected as the limits of the gauge section, while the second two points were selected in the vicinity of the crack area with a distance of 3 mm (Figure 6.4B). The true distance data for each analysed frame was synchronized with the corresponding time and force measurements recorded by the texture analyser. Due to the high computational intensity of DIC analysis, only one specimen per condition was analysed.

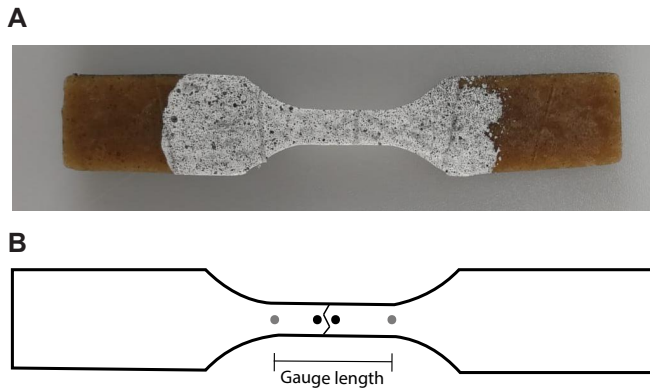


FIGURE 6.4 A) Example of painted specimen for tensile testing and DIC analysis and B) example of virtual extensometer points with grey points indicating the gauge length and black points indicating the area around the crack. The vertical lines in A) are an intrinsic property of the HTSC product due to grooves on the surface of the cones to prevent slip. These lines did not affect the measurements as far as the authors are aware.

6.3 Results & discussion

6.3.1 Effect of gauge length

The effect of gauge length was evaluated by interpreting the force-distance curves of isotropic and anisotropic products measured parallel to the shearing direction (Figure 6.5). Here, the results are presented as individual curves rather than averages. The variation between the individual curves can be seen as a measure for heterogeneity in structure, which is a result of the anisotropy of the product. Gauge length affected the outcomes of the measurements of anisotropic products more than isotropic products. In isotropic specimen, we observed that force increased with distance until a fracture point, which was evidenced by a rapid decrease in force (Figure 6.5A).

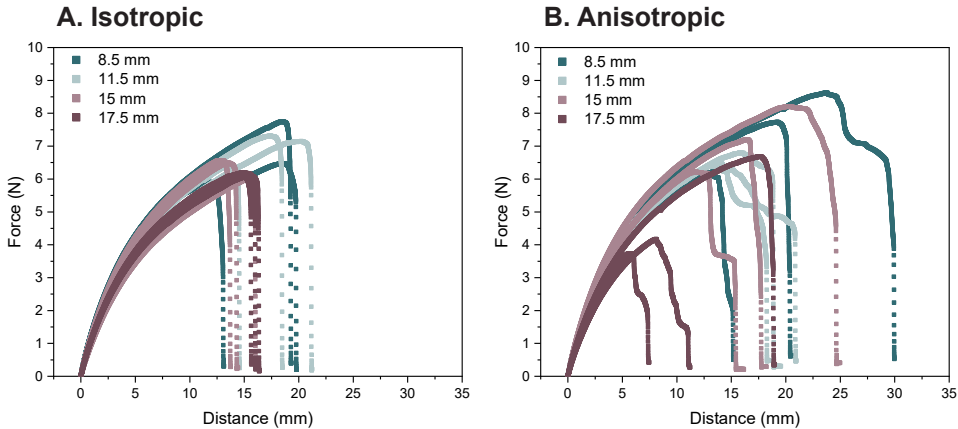


FIGURE 6.5 Force-distance curves of A: Isotropic and B: Anisotropic products with varying gauge lengths measured parallel to the shearing direction. Measurements were performed in triplicate and individual curves are shown.

In general, homogeneous materials tend to behave more brittle (van Mier, 1997). This agrees with the results of our isotropic product consisting of SPI, which is considered as a relatively homogeneous material. The curve shapes between different gauge lengths were similar in the isotropic specimen (Figure 6.5A). Furthermore, variance between triplicates was small for the 15 mm and 17.5 mm gauge length, while it was slightly larger for the 11.5 and 8.5 mm gauge lengths. The 8.5 and 11.5 mm gauge lengths also reached a larger distance and higher force at fracture (Figure 6.5A). While this was unexpected, we believe that this may be due to the extension outside the gauge section of the specimen. The contribution of the extension outside of the gauge section was larger in short specimen compared to large specimen. Additionally, there is the chance

that specimen with longer gauge sections contain more defects or inhomogeneities than the specimen with shorter gauge lengths (Liu, Shen, Yang, Zheng, & Zhang, 2017). Therefore, the longer specimen were more likely to suffer from fracture earlier in the tensile test procedure. In anisotropic specimen, the variance between triplicates was rather large, indicative of a heterogeneous material (Figure 6.5B). The tensile curve shape of anisotropic specimen was also dependent on gauge length. For a gauge length of 15 mm, we observed that the force increased with distance, and rapidly decreased after the fracture point. For smaller gauge lengths (11.5 and 8.5 mm), the material fractured in multiple stages. The fracturing process is then considered to be a zone of discontinuous microcracking ahead of a continuous macrocrack (van Mier, 1997). A long fracture process was expected for the anisotropic products, where inhomogeneities lead to both weaker and stronger areas in the sample. In tensile testing, the nucleation of microcracks is the first phase of the fracture process (Figure 6.6).

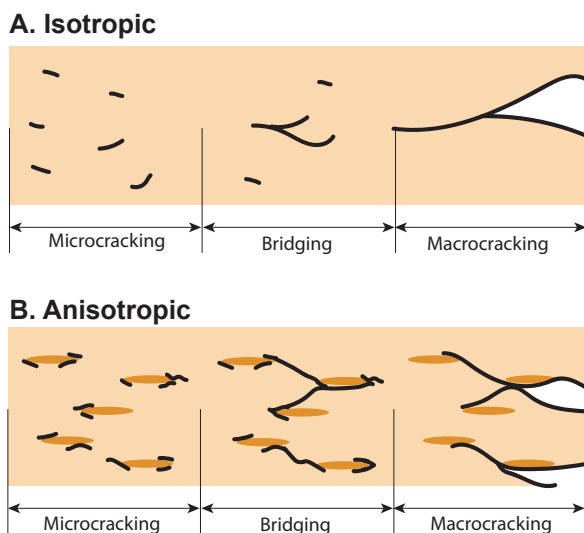


FIGURE 6.6 Mechanisms of fracturing in A) homogeneous isotropic products and B) heterogeneous anisotropic products. Black lines indicate cracks.

Then, bridging of these microcracks occurs, which causes automatic propagation to a macrocrack (Figure 6.6A). In isotropic products, the propagation into a macrocrack proceeds quickly, as evidenced by the rapid decrease in stress at the fracture point (Figure 6.5A). However, the bridging of microcracks can be inhibited by the presence of a dispersed phase, such as pectin. The dispersed phase can delay the onset of macrocracking or fracturing (Figure 6.6B). This phenomenon is reflected in the distinctive shape of the descending branch observed in the force-distance curve of the anisotropic specimen, which exhibited a prolonged decline compared to the isotropic specimen (Figure 6.5B). The contribution of the elastic deformation was smaller

for shorter gauge lengths. Thus, the use of shorter gauge lengths provided a better approximation of the true fracturing behaviour of the products compared to longer gauge lengths (van Mier, 1997).

It is important to take two considerations into account when deciding on the gauge length. First, the gauge length must be larger than the defects inside the material that will control the fracture (Luyten, Van Vliet, & Walstra, 1992). Defects of approximately 750 μm were found in previous research on anisotropic meat analogues (Dekkers *et al.*, 2016). Thus, this sets a lower limit of gauge length. Second, the gauge length must be small enough to get continuously increasing deformation (van Mier, 1997). Here, gauge lengths of 8.5 mm were chosen for continuation of further experiments based on the considerations described above.

6.3.2 Effect of texture analyser deformation rate

The effect of three different deformation rates (46.2, 23.1, and 11.55 mm/min) was evaluated by interpreting the force – distance curves in isotropic and anisotropic products with a gauge length of 8.5 mm (Figure 6.7).

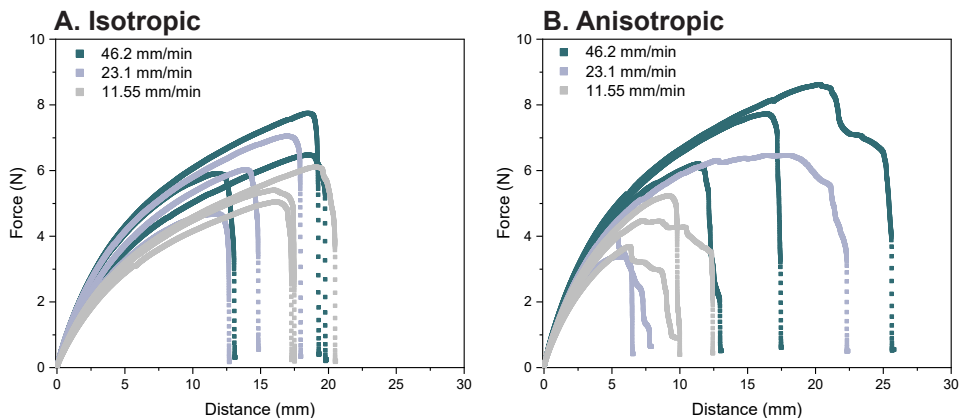


FIGURE 6.7 Force-deformation curves of A: Isotropic and B: Anisotropic products with gauge length 8.5 mm at varying deformation rate. Measurements were performed in triplicate and individual curves are shown.

Here, we observed that deformation rate had a different effect on the isotropic products than on the anisotropic products. In isotropic specimen, decreasing the deformation rate led to a more defined and rounded off fracture point (Figure 6.7A). In anisotropic specimen, decreasing the deformation rate led to a shorter fracture distance (Figure 6.7B). Furthermore, the fracture propagation was slower at 11.55 mm/min, as evidenced by a more defined fracture zone. Propagation of microcracks into macrocracks probably proceeded slower at a lower deformation rate, which is

beneficial for understanding the fracture properties (Figure 6.6). The energy storage and dissipation mechanisms in viscoelastic materials are reliant on their relaxation times. Consequently, the measurements of the material properties are impacted by the rate of deformation (Ferry, 1980). This was for example evident in the isotropic specimen where a deformation rate of 11.55 mm/min induced a degree of relaxation in the product, as evidenced by a more concave curve shape (Figure 6.7A). This was not observed at the higher deformation rate of 46.2 mm/min (Figure 6.7A). Lower deformation rates provided more time for dissipating mechanisms to transpire, which led to lower stiffness. This relationship between deformation and material properties has been previously observed by Ak, Bogenrief, Gunasekaran, & Olson (1993), Schab, Tiedemann, Rohm, & Zahn (2022), and Sliwinski, Kolster, & van Vliet (2004) in tensile testing of mozzarella cheeses, caramel, and wheat dough, where lower deformation rates resulted in decreased fracture stresses.

The observations described above suggest that the fracture process is composed of multiple stages. This indicates the heterogeneity of the product, which leads to weaker areas that fracture initially, and relatively stronger areas that fracture later. We can thus argue that increased anisotropy or heterogeneity of the product leads to a more extended descending branch. In the anisotropic specimen it was also clear that deformation rate did not change the linear part of the curve, but only affected the non-linear and fracture zone of the curve (Figure 6.7B). Specifically for anisotropic specimen, a slower deformation rate was, thus, beneficial for interpreting the tensile test results. Therefore, a gauge length of 8.5 mm and a deformation rate of 11.55 mm/min were used in the following results.

6.3.3 Tensile parameters

Various tensile parameters exist that can be extracted from the stress – strain curves. Here, we will describe fracture stress, fracture strain, Young's Modulus, and toughness for an isotropic product and an anisotropic product (Figure 6.8). There were clear differences in tensile parameters between the isotropic and anisotropic product. We found that anisotropic specimen had a lower fracture stress, fracture strain, and toughness compared to the more homogeneous, isotropic specimen (Figure 6.8A, B, D). However, anisotropic specimen did have a higher Young's Modulus than isotropic specimen (Figure 6.8C). Thus, anisotropic specimen were weaker, yet stiffer, through the addition of a dispersed pectin phase to SPI to make the product anisotropic. Products with a high toughness, such as the isotropic specimen in this study, are considered to be ductile materials, while products with a low toughness, such as the anisotropic specimen in this study, are considered to be more brittle (Hertsberg, 1996; Schab *et al.*, 2022).

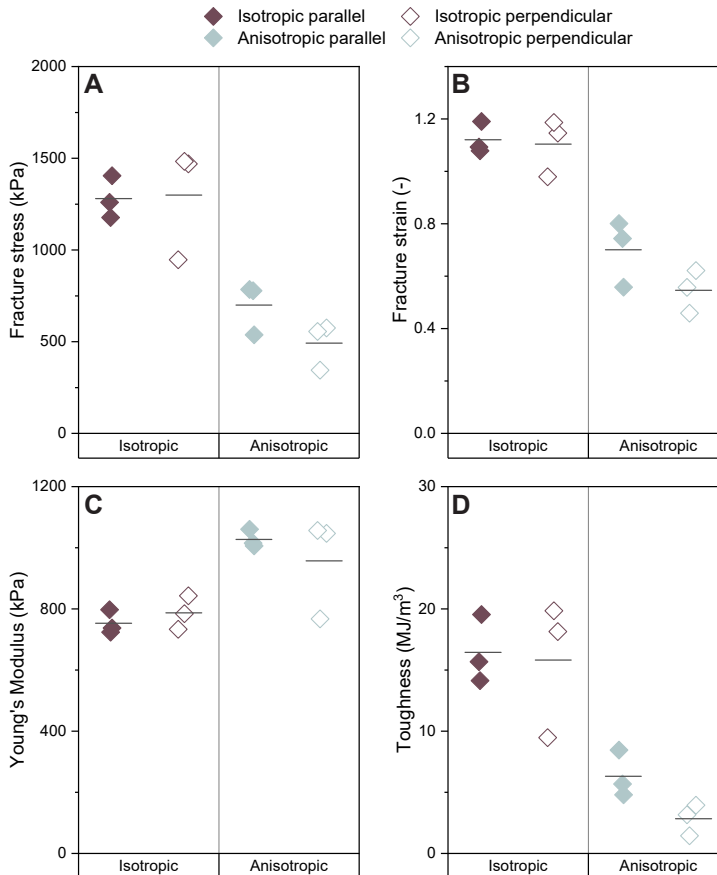


FIGURE 6.8 A) Fracture stress, B) Fracture strain, C) Young's Modulus, D) Toughness of an isotropic and an anisotropic product analysed with a gauge length of 8.5 mm and a deformation rate of 11.55 mm/min. Specimen were analysed in the direction parallel (closed symbols) and perpendicular (open symbols) to the shear flow. Tests were performed in triplicate and individual data points are shown. Horizontal line indicates mean value.

However, the toughness results of the isotropic products have to be interpreted with caution. The absolute values of the toughness are probably overestimated in the case of (especially) the isotropic product, due to the static, continuous deformation rate (Figure 6.9). If available, it would be better to use dynamic strain control in tensile testing to overcome this issue. In dynamic strain control, the controlling factor in tensile testing is the strain rather than the displacement, resulting in enhanced stability of the crack propagation (van Mier & van Vliet, 2002).

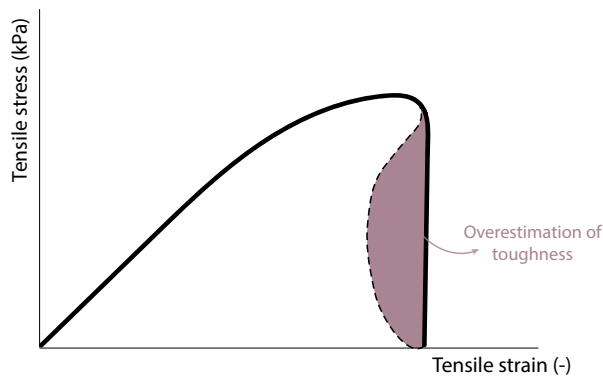


FIGURE 6.9 Schematic illustration of overestimation of the toughness in case of isotropic products.

The anisotropy index of the fracture stress is often found to correlate with fibrousness in case of soy-based products (Dekkers *et al.*, 2016; Schreuders *et al.*, 2019; Schreuders, Schlangen, Bodnár, *et al.*, 2021). Here, we observed that the anisotropy index of the fracture stress, Young's Modulus, and toughness of isotropic products was approximately 1 (Figure 6.10). This was as expected, because the isotropic products had not been sheared. Indeed, the fracture stress anisotropy index of the anisotropic products was higher than 1, confirming the anisotropic nature of the products (Figure 6.10).

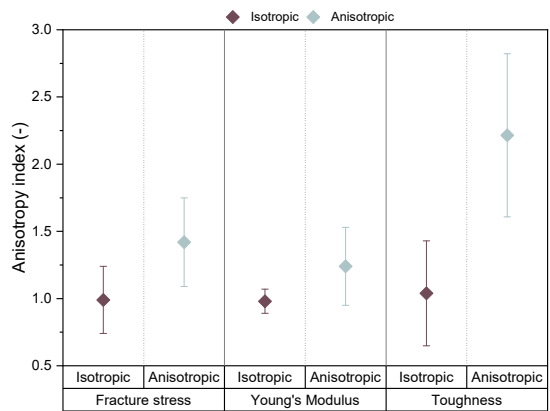


FIGURE 6.10 Anisotropy index of fracture stress, Young's Modulus, and toughness of isotropic and anisotropic products analysed with a gauge length of 8.5 mm and a deformation rate of 11.55 mm/min. Specimen analysed in the direction parallel to shear flow were divided by specimen analysed perpendicular to shear flow. Tests were performed in triplicate and mean values including standard deviation are shown.

Previous research by Dekkers *et al.* (2016) also showed an anisotropy index higher than 1 upon addition of pectin to SPI and attributed this to weakening of the structure due to the orientation of the dispersed pectin phase in the perpendicular direction. They

suggested that the dispersed phase either forms weak areas in the composite, or the adhesion between the dispersed and the continuous phase is weak. We introduce the anisotropy index of the Young's Modulus and toughness as new tensile parameters for meat analogue analysis. The Young's Modulus anisotropy index of the anisotropic products was only slightly higher than 1. This was expected, because large deformation properties, such as fracture stress, are much more affected by weak areas in the sample, such as pectin, than small deformation properties (van Vliet, 1996). The occurrence of anisotropy in the linear region of the Young's Modulus is, therefore, unlikely. A previous study, however, did show the importance of a high anisotropy index (~ 7.3) of the Young's Modulus in cooked chicken (Schreuders *et al.*, 2019). Quantifying anisotropy in the linear regime of the stress-strain curve is therefore still an important parameter to describe similarities and differences between meat and meat analogues. At low strains, the stress-strain curves for both parallel and perpendicular specimen show similar behaviour because primary deformation is taking place in the continuous phase gel network. However, as the strain exceeds the linear region, the perpendicular specimen exhibited lower strain values at fracture (Figure 6.8). This was likely due to the presence of relatively weak dispersed-continuous phase interfaces in this direction, as previously described by Dekkers *et al.* (2016). Conversely, the fracture of the anisotropic specimen in the parallel direction probably occurred within the continuous phase, since there were fewer weak interfaces in this direction. Fibrousness would thus be better detected by fracture parameters rather than Young's Modulus. A fracture parameter is, amongst others, the toughness. The toughness anisotropy index of anisotropic specimen was higher than 2, further confirming the anisotropic nature of these products (Figure 6.10). This is striking because the absolute toughness in the parallel direction of the anisotropic specimen was rather low (Figure 6.8D). These results suggest that the anisotropy index of toughness may be a more effective metric for distinguishing variations in properties between isotropic and anisotropic products compared to the anisotropy index of fracture stress and Young's Modulus. This would become even more evident once the overestimation of the toughness of the isotropic product would be reduced.

6.3.4 Poisson's ratio and true distance recording with DIC

In mechanical analysis studies that involve tensile testing, the deformation rate recorded by the texture analyser is generally used. However, in most cases, this leads to overestimations of certain tensile parameters. Furthermore, the deformation of the tensile grips and load cell contribute to the recorded distance, and are thus influencing the results. Therefore, we studied the difference between using the distance recorded by the texture analyser and the true distance from digital image correlation (DIC) (Figure 6.11). Here, the distance recorded by the texture analyser takes into account

the complete gap section between the tensile grips, while the distance recorded by DIC is determined over specified virtual extensometer points in the image, being the gauge section and the area around the crack (3 mm) (Figure 6.4B). For both isotropic and anisotropic specimen, we observed differences in distance recorded by the texture analyser compared to DIC (Figure 6.11A & B).

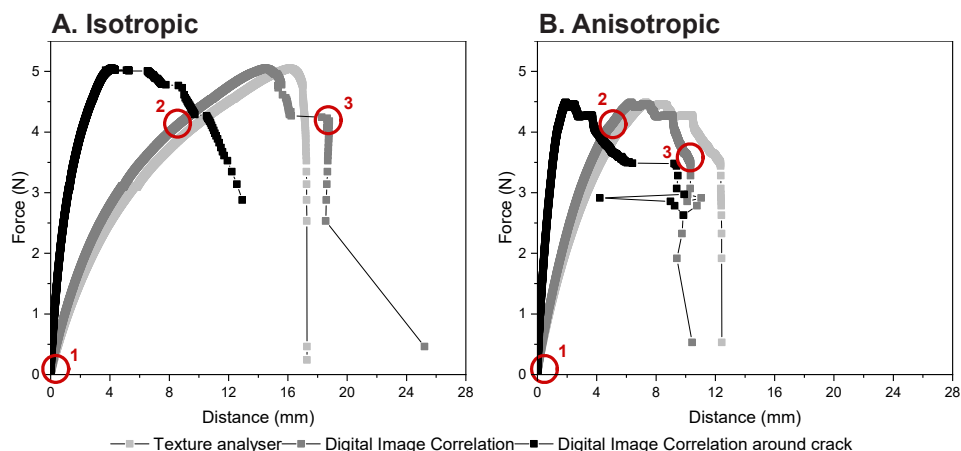


FIGURE 6.11 Force – distance curves recorded by texture analyser (light colour), digital image correlation of the gauge length (medium colour), and digital image correlation around the crack (dark colour) for A. Isotropic and B. Anisotropic products. A gauge length of 8.5 mm was used for all specimen. Circles with numbers correspond to DIC images in Figure 6.14, with 1: start, 2: halfway, and 3: crack.

The force-distance curves obtained from the texture analyser and DIC were expected to be similar in terms of the overall trend of the graph, as both methods measure the same physical quantities. However, there may be differences in the details of the curves. The linear part of the force – distance curve was similar comparing the texture analyser and DIC of the gauge section (Figure 6.11A & B). From the point where the curve starts to deviate from linearity, the displacement was slower in DIC compared to the texture analyser. This may be explained by slippage between the specimen and the tensile grips, which is not recorded in DIC (Zhou, Liu, Shao, & Wang, 2013). However, the placement of the virtual extensometer points greatly affected the force – distance curve. When the virtual extensometer was placed around the crack area (Figure 6.4B), we observed a much steeper curve compared to the texture analyser and the DIC of the gauge section in both isotropic and anisotropic products (Figure 6.11A & B). This was due to the smaller distance when the virtual extensometer is placed around the crack area. Other than that, the ascending branch was relatively unaffected by using DIC. However, the descending branch of the force-distance curve recorded with DIC around the crack exhibited a more gradual decrease compared to both DIC over the gauge length and the texture analyser (Figure 6.11A & B). DIC can measure displacement at many points

along the surface of the material, providing a higher resolution of the displacement field. Independent of the product (isotropic versus anisotropic), distance recording with DIC enabled us to identify fracture properties that were otherwise not visible.

In calculations of the tensile stress and strain, a constant volume (Poisson's ratio of 0.5) is often assumed (van Vliet, 2013). However, a dynamic Poisson's ratio during tensile testing can be calculated based on DIC-results. The Poisson's ratio offers a consistent means to compare the structural capabilities of actual materials, irrespective of their homogeneity (Greaves, Greer, Lakes, & Rouxel, 2011). The Poisson's ratio of both isotropic and anisotropic specimen decreased upon uni-axial extension in both the parallel and perpendicular direction to shear (Figure 12). This behaviour agrees with the nature of inelastic polymer materials (Zhou *et al.*, 2013). The decrease in Poisson's ratio was greater in anisotropic specimen (from 0.43 to 0.11) than in isotropic specimen (from 0.18 to 0.05).

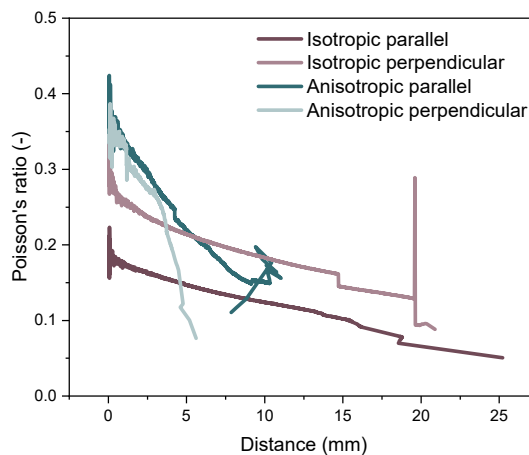


FIGURE 6.12 Dynamic Poisson's ratio over distance during tensile testing for isotropic and anisotropic products parallel (dark) and perpendicular (light) to the shear direction.

Overall, at small deformation, anisotropic specimen had a higher Poisson's ratio than isotropic specimen, indicating that anisotropic samples were relatively elastic. The higher Poisson's ratio of the anisotropic specimen may be attributed to greater porosity in these samples (Jahanbakhshian, Hamdami, & Shahedi, 2018). As the void spaces increase, there is a corresponding increase in the axial strain compared to the lateral strain. Previous research also showed that air bubbles in meat analogues produced from calcium caseinate played a crucial role in fibrousness (Wang, Tian, Boom, & van der Goot, 2019). Upon larger deformation, the Poisson's ratio of anisotropic specimen quickly decreased to values below that of isotropic specimen. This agrees with previous research on rheological properties of isotropic and anisotropic products made from

soy, where anisotropic products exhibited a more plastic behaviour compared to a more elastic behaviour in isotropic products (Schreuders *et al.*, 2021). Furthermore, the Poisson's ratio of both isotropic and anisotropic specimen was dependent on measurement direction (Figure 6.12). Even though isotropic products were not sheared, the Poisson's ratio in the perpendicular direction was higher than in parallel direction, suggesting probably less breakdown in this direction. In anisotropic specimen, after an initial period of overlap, the Poisson's ratio decreased faster in the perpendicular direction than in the parallel direction. It is worth noting that the Poisson's ratio was determined over the entire gauge length and width of the tensile specimen, including the crack area. The strain in the tensile direction (y) thus includes both elongation of the material and crack opening. The strain in the other direction (x) only includes elongation of the material.

Figure 6.12 showed that the assumption of a Poisson's ratio of 0.5 does not hold true for the materials in this study. Thus, the dynamic Poisson's ratio was implemented in calculations of the stress-strain curves as shown in Figure 6.13. The contribution of the dynamic Poisson's ratio was accounted for in the calculation of the stress by the cross-sectional area ($A(t)$) with equation 6.5:

$$A(t) = width_{DIC}(t) \times \left(\frac{width_{DIC}(t)}{width_0} \times thickness_0 \right) \quad (\text{Eq. 6.3})$$

where $A(t)$ is the cross-sectional area dependent on time, $width_{DIC}(t)$ is the width over time recorded by DIC, $width_0$ is the width at $t = 0$, and $thickness_0$ is the thickness at $t = 0$. Here, we made the assumption that the thickness of the tensile specimen decreased with the same fraction as the width of the specimen. The use of two camera viewpoints would enable direct measurement of the decrease in thickness and, hence, an even more precise determination of the cross-sectional area.

The use of a dynamic Poisson's ratio instead of a static Poisson's ratio (of 0.5) led to a decreased value for the stress in both the isotropic and the anisotropic products (Figure 6.13A, B). Moreover, it became clear that in the anisotropic specimen mostly the non-linear part of the graph decreased with a dynamic Poisson's ratio. On the other hand, in the isotropic specimen, stress reduced from the curve's onset when using the dynamic Poisson's ratio. Similar to the force-distance curves (Figure 6.11), the placement of the virtual extensometer around the crack area influenced the stress-strain curves as well (Figure 6.13). Both the isotropic and anisotropic specimen showed a steeper increase in stress when analysing only the area around the crack. Furthermore, both products also showed a slower descending branch of the curve, facilitating the interpretation of fracturing behaviour.

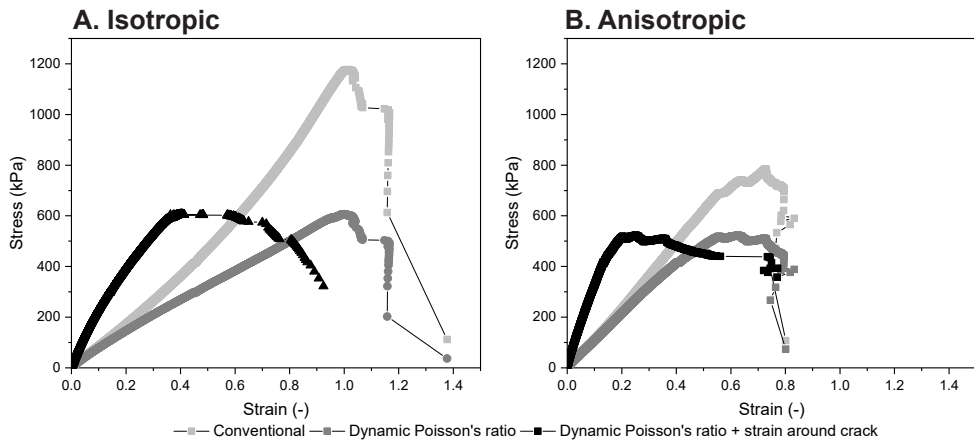


FIGURE 6.13 Stress-strain curves of A) isotropic and B) anisotropic products parallel to the direction of shear calculated the conventional way (assumption Poisson's ratio 0.5), with a dynamic Poisson's ratio, and with a dynamic Poisson's ratio and strain calculated around the crack area.

More specifically, the anisotropic specimen clearly showed a lag phase between maximum stress and fracture, where the stress only decreased slightly (Figure 6.13B). The stress in the isotropic specimen, on the other hand, decreased gradually after the maximum stress had been reached (Figure 6.13A). The placement of the virtual extensometer around the gauge section of the specimen provided a more representative measurement of the overall deformation behaviour of the material. On the other hand, the virtual extensometer placed around the crack provided information about the local deformation and can be useful to understand fracture mechanisms.

6.3.5 The use of DIC analysis to obtain information on fracturing behaviour

The starting, halfway and cracking DIC images of a isotropic and anisotropic specimen are shown in Figure 6.14. Regions in blue indicate areas that experienced less deformation, while regions in red indicate areas that experienced more deformation and are, thus, likely areas for fracture to occur. The starting and halfway images of the isotropic and anisotropic specimen were relatively similar, while there were clear differences in the cracking images (Figure 6.14). This suggests that differences between isotropic and anisotropic food products mainly occurred in the large deformation area. This observation aligns with the similarity in Young's Modulus and differences in large deformation tensile parameters as previously described (Figure 6.8). The crack images revealed that the isotropic specimen had a homogeneous strain distribution, while the anisotropic specimen had a heterogeneous strain distribution.

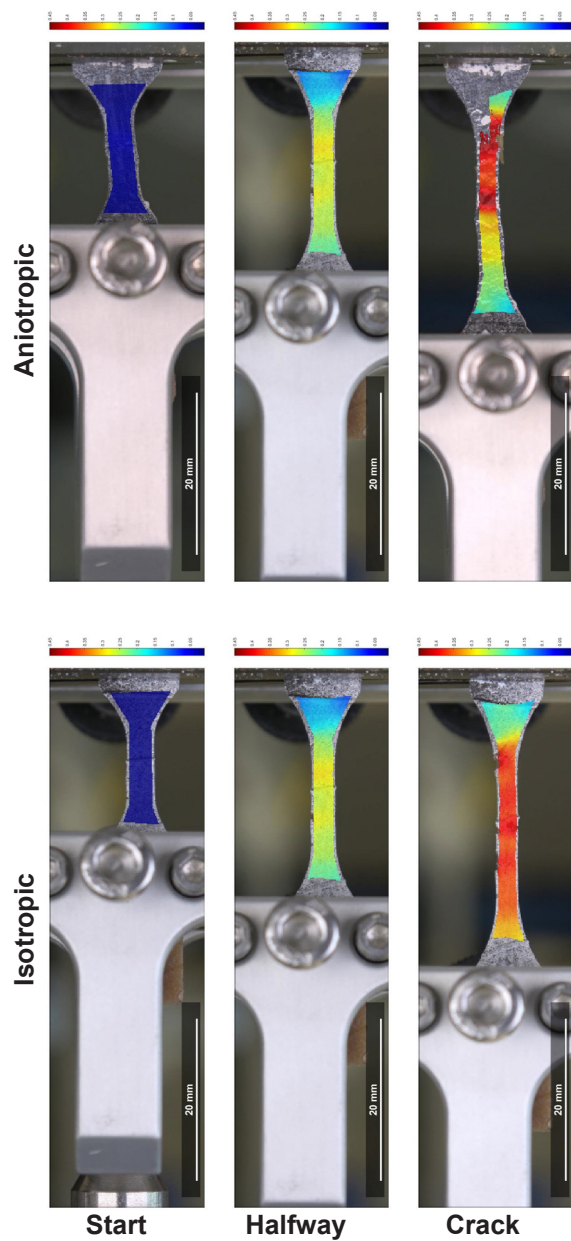


FIGURE 6.14 DIC images of start, halfway and just before cracking of tensile test analysis of an isotropic and anisotropic products parallel to the shear flow direction. Images were taken based on the distances defined in Figure 6.8. Axis bounds are set between 0.01 and 0.45 strain. Scale bar depicts 20 mm.

The anisotropic specimen showed highly localized strain, depicting weaker areas in the sample that are more prone to cracking. This can be explained by the large

plastic deformation of the anisotropic specimen (Godara, Raabe, Bergmann, Putz, & Müller, 2009), as also observed in section 6.3.4. When a specific region within the anisotropic specimen undergoes plastic flow, it serves as a focal point for maximal energy absorption or accumulation of damage, thereby safeguarding other regions from experiencing substantial damage (Godara *et al.*, 2009). The plastic contribution is due to the addition of a dispersed phase in the anisotropic specimen, while the isotropic specimen was considered a more homogenous matrix consisting of a single continuous phase (Dekkers *et al.*, 2016). The interfaces between the continuous and dispersed phase in the anisotropic products are relatively weak areas that are more prone to cracking. Previous research found that addition of egg white or whey protein to surimi gels led to higher local strain concentrations in tensile tests (Park *et al.*, 2023). They suggested that an increase in particle-particle interactions decreased the water-particle interactions, thereby decreasing the elasticity of the samples.

DIC is computationally intensive, especially when working with large deformations. This is because DIC requires the analysis of large amounts of image data and is, therefore, time consuming. Currently, the use of DIC for large numbers of samples is not feasible, as it would take an unreasonable amount of time and computational resources to process all data. Therefore, DIC is typically used for a limited number of samples. Despite these limitations, DIC turns out to be a valuable tool for characterizing the mechanical properties of food materials, such as anisotropic meat analogues.

6.4 Conclusions

In this study, the effects of tensile gauge length, deformation rate, and digital image correlation on the interpretation of mechanical properties of food products were analysed. We showed that a smaller gauge length and a lower deformation rate led to better visibility of the multi-stage fracture zone, especially for anisotropic products. Toughness was an important parameter to characterize mechanical properties of food, as it showed profound differences between homogeneous, isotropic products and heterogeneous, anisotropic products. Furthermore, the true distance data obtained from DIC was found to be more accurate than the distance data obtained from the texture analyser. The placement of the virtual extensometer points around the crack area further increased the accuracy and interpretability of the results in DIC. The use of DIC allowed for a better differentiation between the isotropic and anisotropic food products from a strain distribution perspective. By continuously monitoring the strain in the gauge section of the sample during testing, DIC could be used to maintain a constant strain in the gauge section of the specimen. Overall, this study highlights the importance of careful selection of testing parameters and techniques in evaluating mechanical properties of meat analogues. Therefore, we recommend to use short tensile gauge lengths and DIC for a dynamic Poisson's ratio and true distance recording in tensile testing of anisotropic foods. The placement of a virtual extensometer around the crack area is advised for obtaining information on fracture mechanics. Furthermore, a stable fracturing process and a better measurement of the descending branch can be obtained by controlling the deformation around the crack, as measured by a virtual extensometer. Last, we advise to examine various tensile deformation rates and to demonstrate the differences that emerge. It is important to emphasize that we are not claiming advanced tensile testing only is sufficient to draw conclusions about the fibrous nature of food products. Therefore, future work could involve systematically varying the ratio of pectin to soy protein isolate and coupling this to microstructure characterization to study the relationship between structural attributes and mechanical properties.

7

Chapter 7

General discussion

Current meat analogues are often produced from highly refined protein ingredients, such as protein isolates from soy, wheat, and pea. These protein isolates are well characterized and possess desirable functional properties, such as gelation, that allow their use in meat analogues. Consequently, research in the field of meat analogues has been primarily conducted using these protein isolates. However, there is growing recognition that the use of protein isolates in meat analogues is not always necessary or desired. This explains why less-refined protein fractions, for example produced via dry fractionation, are being explored. Yet, the transition from protein isolates to less-refined protein fractions is not trivial, as the relationships between the properties of these fractions and the resulting properties of the final meat analogues are not fully understood. The latter is further hindered by the lack of suitable analytical methods to quantify the properties of meat analogues. Mostly, macroscopic characteristics, such as visual fibrousness, are analysed subjectively. Mechanical properties, analysed using tensile testing, do present a quantitative measure of the macroscopic characteristics of meat analogues. However, tensile testing is often not used to its full potential.

The aim of this thesis was to investigate the potential of dry fractionation as a route to produce protein-rich ingredients for meat analogue product applications. This aim was divided into three objectives, which were: 1) to investigate dry fractionated ingredients for meat analogue applications, 2) to investigate the potential of enzyme crosslinking to enhance functional properties, and 3) to quantify textural and mechanical properties of fibrous products. We particularly focussed on mung bean, which is an alternative to soy and pea, as a protein source for meat analogues. This chapter first provides an overview of the main findings of this thesis before delving into a discussion on next generation ingredients for meat analogues and the techniques used for characterizing their texture. In addition, the concept of “fibrousness” is addressed. The chapter concludes with a discussion on science and applications of meat analogues of the future.

7.1 Main findings and conclusions

Ideally, ingredients for meat analogues are produced in a sustainable manner, which is characterised by minimal use of water, chemicals, and energy. Therefore, dry fractionation is often considered a potentially attractive route. The possibilities of dry fractionation to produce functional ingredients from plants was explored in **Chapter 2**. Although conventionally (yellow) pea is often used for dry fractionation, in this chapter we described the use of mung bean and cowpea as crops to be processed by dry fractionation as well.

Chapter 2 further describes the gelation and water holding capacity of the obtained

ingredients from dry fractionation. The fine fractions, obtained through dry fractionation, had higher water holding capacities and higher moduli upon gelation than the flour and coarse fractions. It was found that the fine fractions extracted from mung beans were highly functional with respect to water holding capacity, gelation concentration, and gel properties. Those properties makes mung bean an interesting candidate for inclusion in meat analogues. Nonetheless, initial experiments revealed that the gels formed with these ingredients lacked the necessary strength and cohesion to form a meat analogue with the shear cell technology. Additionally, no fibrous structures were identified.

Therefore, we explored transglutaminase crosslinking of commercial mung bean and pea protein isolates to improve their gel strength in **Chapter 3**. Transglutaminase improved tensile strength and extended the linear viscoelastic regime of pea protein isolate gels. Further, transglutaminase changed the behaviour of pea protein isolate in the large deformation regime (macrostructure, non-linear part tensile test), while the behaviour of mung bean protein isolate was mostly affected in the small deformation regime (stress relaxation, linear part tensile test). Overall, the effect of transglutaminase on mung bean protein isolate was much smaller than its effect on pea protein isolate. Further it was found that incubation of commercial protein isolates with transglutaminase (> 0.1 wt.%) negatively influenced the fibrousness of the resulting products, most likely due to formation of a heteropolymer gel network.

To better understand the limited effect of transglutaminase on mung bean protein isolate we studied how the fractionation route affects the ability of transglutaminase to crosslink mung bean protein as shown in **Chapter 4**. Molecular transglutaminase crosslinking occurred in mung bean protein irrespective of the fractionation procedure. However, the effects of crosslinking at larger length scales depended on the protein dispersibility of the fraction. The fine fraction, containing mostly swollen particles, was most susceptible to transglutaminase crosslinking.

Meat analogue textures are often analysed using qualitative visual observations, making comparison of different samples challenging. In **Chapter 5**, an image analysis method to quantify fibrousness in meat analogues was presented. Three fibre shape features, fibre score (ratio between length and width), fibre area, and number of fibre branches, were successfully segmented and obtained from meat analogue images. We found that the fibre score positively correlated to expert assessments of fibrousness on an image level ($R^2 = 0.66$) and on a formulation level ($R^2 = 0.93$).

Chapter 6 described that conventional tensile testing can be extended with digital image correlation. This method can be used to show differences in strain distribution and dynamic Poisson's ratio of isotropic and anisotropic products. The anisotropic product was found to exhibit heterogeneous, multi-stage fracture patterns, while the

isotropic product exhibited homogeneous fracture patterns. We also demonstrated that tensile gauge length and deformation rate are crucial in interpretation of tensile test data.

7.2 Dry fractionation as a route to create ingredients for meat analogues

Of all dry fractions produced in **Chapter 2**, the mung bean fine fraction was found to carry the highest potential for incorporation into meat analogues. However, processing a mung bean fine fraction into a meat analogue using the shear cell technology did not result in visual fibrous macrostructures (Figure 7.1A). While commercial protein isolates from mung bean were not very susceptible to transglutaminase (**Chapter 3 & 4**), the mung bean fine fraction was (**Chapter 4**). Therefore, under optimized conditions, we combined the mung bean fine fraction with transglutaminase and processed this blend into meat analogues in the shear cell. Notably, this combination yielded a visible fibrous structure (Figure 7.1B). We hypothesize that protein blends require a certain magnitude of continuous phase viscosity and local elasticity to facilitate dispersed phase elongation and to prevent the elongated phases from reverting back to a spherical shape. This is combined with the fact that the fine fraction consists of multiple components, which explains why a fibrous product could be obtained. We assume that the protein, fibre, and other minor components in the fine fraction form multiple phases within the hydrated dough. Thus dry fractionated ingredients can be tuned towards application in meat analogues. Dry fractionation is, therefore, a highly promising choice to produce protein-rich ingredients for application into meat analogues.

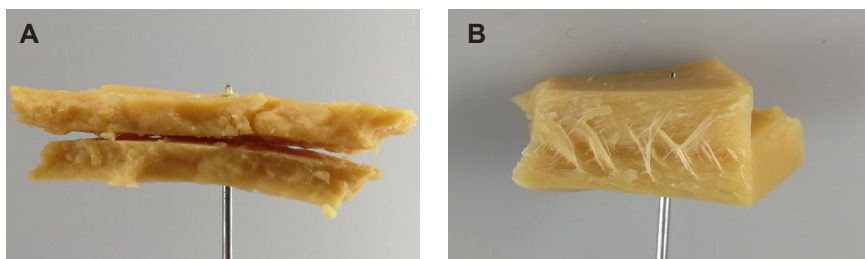


FIGURE 7.1 A) mung bean fine fraction (40 wt.%), B) mung bean fine fraction (39.5 wt.%) + transglutaminase (0.5 wt.%).

However, examining the efficiency of protein extraction processes is also important when considering dry fractionated ingredients for meat analogues. Therefore, we take a closer look at the protein yield of dry fractionated ingredients compared to conventional

protein isolates. The theoretical protein yield of the mung bean fine fraction produced at an air classification wheel speed of 10,000 rpm was approximately 0.62 g/g, but in practical terms, the yield was closer to around 0.45 g/g. This indicates that a significant amount of material always ends up in other fractions than the protein-rich fine fraction. The loss occurs due to fouling (Pelgrom, Vissers, Boom, & Schutyser, 2013), but also due to the fact that a considerable amount of protein ends up in the coarse fraction (protein content of ~13 wt.%). It has to be mentioned that the loss due to fouling will not be as relevant in a continuous industrial process. Previously, it was reported that the protein yield of soy protein isolate from soy flour by conventional isoelectric point precipitation ranged between 0.3 - 0.6 g/g (De Moura, Campbell, De Almeida, Glatz, & Johnson, 2011; Tamayo Tenorio, Kyriakopoulou, Suarez-Garcia, van den Berg, & van der Goot, 2018). The protein yield of mung bean protein isolate produced with isoelectric point precipitation was approximately 0.6 g/g (De Moura *et al.*, 2011). Despite dry fractionation presenting a sustainable alternative to wet fractionation when considering water, energy, and chemical use, it may not necessarily improve resource efficiency. The coarse fraction, often considered as the rest stream of dry fractionation, is a non-pure starch fraction. To valorise this fraction, its purity should either be enhanced through further processing, or alternative applications should be found. In the case of mung bean, the starch holds significant value in Asia, particularly to produce glass noodles. Production of glass noodles could therefore be a potential application for the non-pure coarse fraction. Other applications include incorporation in plant-based cheeses, which often contain starch, or incorporation into bakery products.

7.3 Textural characterization of meat analogues and future options

Texture is one of the most important food quality parameters and includes the properties that can be seen and felt. The quantification of the texture, specifically the heterogeneous texture of meat analogues, is a challenging task, as it encompasses both visual and mechanical aspects. We elaborate on three texture characterization methods for meat analogues in the next sections.

7.3.1 Quantifying visual fibrousness

Visual fibrousness can be successfully quantified by the Fiberlyzer, which is an image analysis tool (**Chapter 5**). Even though the designed tool was rather robust, there are some limitations still. The application of this method to meat analogues produced using methods other than shear cell technology or using different lighting conditions for imaging will require calibrations for each product and preparation procedure.

Additionally, sample preparation for imaging should be standardized to further improve the method. For shear cell samples, the Fiberlyzer method requires an image of the inner structure of the sample. This involves folding the sample parallel to the direction of the shear flow, which ultimately leads to fracture. The act of folding the sample is a human action that potentially introduces a level of bias or subjectivity into the method. In the future, it would be beneficial to standardize the folding process by using a specifically designed device for this purpose.

Furthermore, a comparison of the tool to other methods of quantifying visual fibrousness is recommended. For instance, previous studies on fibrous products produced through extrusion have successfully quantified the visual fibrousness using an optical fibre method based on the continuous time random walk theory (Ranasinghesagara, Hsieh, & Yao, 2006; Snel, Bellwald, van der Goot, & Beyrer, 2022). It would be interesting to investigate whether these methods result in similar trends in visual fibrousness or whether perhaps they capture different textural aspects.

7.3.2 Digital image correlation

Digital image correlation (DIC) was used to obtain information on crack propagation, localized strain differences, true distance data, and dynamic Poisson's ratio's (**Chapter 6**). However, we have only touched the surface of what is possible with DIC. The next step is to link the local strain data to local structure details. This has previously been shown by linking porosity of alloy die castings measured using X-Ray Tomography (XRT) to ductility of the material analysed by tensile testing coupled with DIC (Zhang *et al.*, 2020). It may even be possible to perform 3D-DIC combined with XRT by embedding fiducial markers in the product. In-situ tensile testing using scanning electron microscopy (SEM) was successfully performed in the past to relate structural breakdown of aluminium alloy to mechanical failure (Xia *et al.*, 2022). In-situ tensile testing using SEM can possibly be further extended by DIC to obtain local strain information. In the case of meat analogues, cryo-SEM or environmental-SEM would be preferred to avoid structural changes in the product due to drying and fixation. Alternatively, the fracture surface of the tensile test specimen could be examined with microscopy and scattering methods to obtain both structural and compositional insights into the areas of the sample that exhibit mechanical weakness.

Furthermore, we can turn to non-food applications of DIC and apply DIC in a similar manner to food. In fibre-reinforced epoxy, DIC has been applied to accurately show that strains in the structural fibres were smaller than strains in the matrix upon compression (Canal, González, Molina-Aldareguía, Segurado, & Llorca, 2012). It would be interesting to capture the strain differences in the dispersed and continuous phase in meat analogue products in a similar manner. In meat analogues, the interface between

the dispersed and continuous phases is often considered to be key in fibrous structure formation (Dekkers, Nikiforidis, & van der Goot, 2016; van der Sman & van der Goot, 2023). Due to the smoothing nature of DIC, it is hard to capture the strain gradients at the interfaces (Canal *et al.*, 2012). However, by decreasing the DIC subset size, it is possible to capture strain variations at interfaces in greater detail. For example, DIC was used to measure elastic and bonding properties of the interface transition zone in cement-based materials, as demonstrated by Gu, Kim, Kim, Seo, & Kim (2023) and Lee *et al.* (2013). Possibly, a similar approach can be interesting for meat analogues as well to gain a deeper understanding of the interface between the continuous and dispersed phase.

7.3.3 Compression tests and multi point indentation

Compression tests are another mechanical testing method to characterize texture properties. In the context of meat analogues, compression tests have been primarily conducted on specimens created through extrusion cooking and on comminuted meat analogue products, like burgers and nuggets (Schreuders, Schlangen, Kyriakopoulou, Boom, & van der Goot, 2021). Compression tests have not been used on meat analogues produced with the shear cell, because the samples are too thin (~2-4 mm). Compression testing of those samples requires the use of a smaller probe and to conduct compression tests to a smaller depth.

On the macro-mesoscale, we can use multi-point indentation to gain insights on the spatial mechanical properties of meat analogues. Previous work already demonstrated the ability of multi-point indentation to capture and quantify spatial mechanical heterogeneity of meat analogues and animal meat (Boots *et al.*, 2021). We measured the spatial heterogeneity in elastic modulus by performing multi-point indentation on meat analogues created from different ingredients (Figure 7.2). Meat analogues created from pea protein isolate alone and wheat gluten alone showed variations in elastic modulus across the sample (Figure 7.2A,C). These variations can be attributed to the inclusion of air pockets within the samples, which results in decreased resistance when this part of the product is subjected to indentation.

When combining ingredients, such as pea protein isolate with wheat gluten, we know from literature that a fibrous texture is achieved (Schreuders *et al.*, 2019). In terms of mechanical properties, we observe horizontally oriented bands in the product with a relatively low elastic modulus (Figure 7.2B). This suggests that the elastic modulus varies directionally, aligned with the shear flow direction during processing in the shear cell (Figure 7.2B). The mechanical heterogeneity in the blend likely stems from the fact that pea protein isolate and wheat gluten possess different phase properties (Schreuders *et al.*, 2020). However, the directionality of the mechanical variations is

thought to be a consequence of the processing method applied.

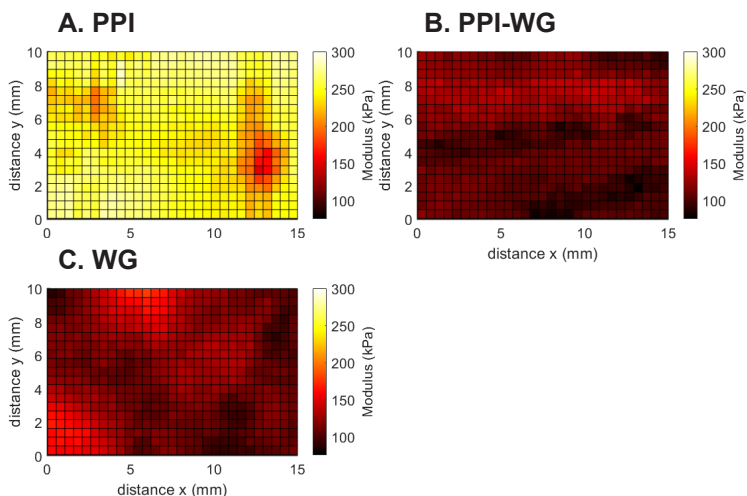


FIGURE 7.2 Multi-point indentation elasticity maps for different ratios of PPI-WG. A. PPI 40 wt.%, B. PPI-WG 20-20 wt.%, and C. WG 40 wt.%. For all samples the shear direction is from left to right.

Multi-point indentation serves as a valuable technique to quantify mechanical heterogeneity at the macro/meso length scale. This technique holds more potential than currently used. For example, by varying the probe size it may be possible to investigate even smaller length scales. Furthermore, while the focus so far has been on elastic modulus as the primary mechanical parameter, the transition point from elastic to plastic behaviour can be quantified as well. The mechanical indentation test itself can also be modified to conduct a stress relaxation or creep test, for example.

7.4 Connecting visual fibrousness to mechanical anisotropy

Visual fibrousness and mechanical anisotropy represent two distinct aspects of the concept of texture. Visual fibrousness relates to the appearance of structures, including fibres. Mechanical anisotropy relates to the physical properties and behaviour of fibrous materials, like the tensile strength of a composite material. These differences demonstrate that the term fibrousness contains multiple aspects.

Mechanical anisotropy is often used to describe fibrous structures of HTSC products, but does not always agree with macrostructure observations. For example, only weak correlations were found between consumer visual assessment of fibrous structures and

mechanical attributes in plant based hamburgers (Godschalk-Broers, Sala, & Scholten, 2022). Thus, it remains uncertain whether fibrous structures of meat analogues can be characterized by mechanical anisotropy alone. To further study and understand the relationship between visual fibrousness and mechanical anisotropy, we subjected the samples from **Chapter 5** to a tensile test and evaluated their mechanical properties. The obtained mechanical properties were then compared to the computed fibre score. The computed fibre scores showed a significant correlation with fracture stress ($R>0.65$) and fracture strain ($R>0.73$) measured both parallel and perpendicular to the shear flow direction (Figure 7.3).

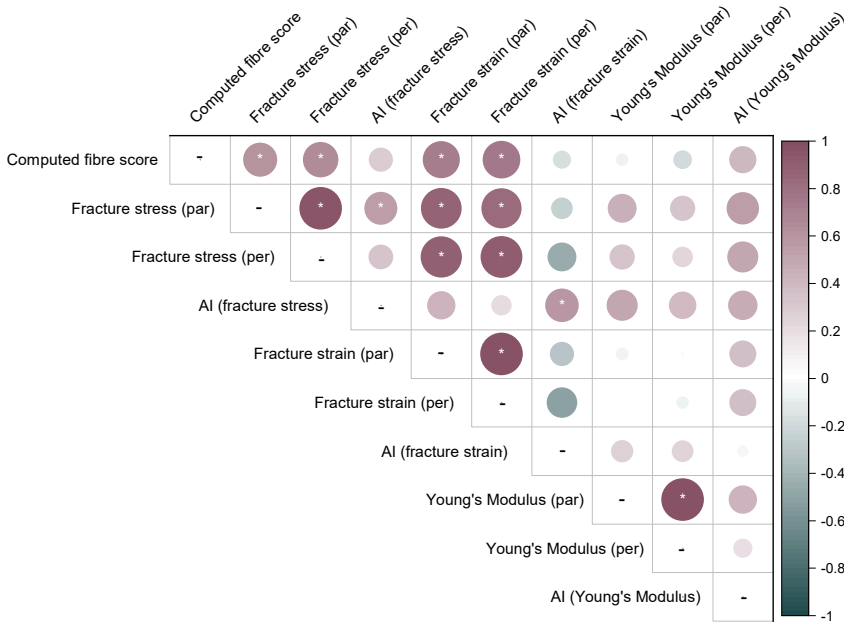


FIGURE 7.3 Pearson correlations of mechanical properties and computed fibre scores. Par: parallel to shear direction. Per: perpendicular to shear direction. AI: anisotropy index. *: significant result ($p<0.05$).

Furthermore, it becomes clear that parallel and perpendicular mechanical properties are highly correlated with each other and that anisotropy indices do not correlate with computed fibre score (Figure 7.3.). Figure 7.4 visualizes the positive correlation between the fracture strain in the perpendicular direction and the computed fibre score. It must be noted that the resulting mechanical data as well as the computed fibre scores exhibit relatively high standard deviations and that this is most likely due to the inherent heterogeneity of the meat analogues. In general, a higher fracture strain in the perpendicular direction resulted in a more visually fibrous inner structure of the HTSC sample. Samples from MBPI, for example, had low fracture strains and low computed

fibre scores. This matches our findings from **Chapter 3** where we found MBPI-based meat analogues to be relatively crumbly and gel-like with low fracture strains.

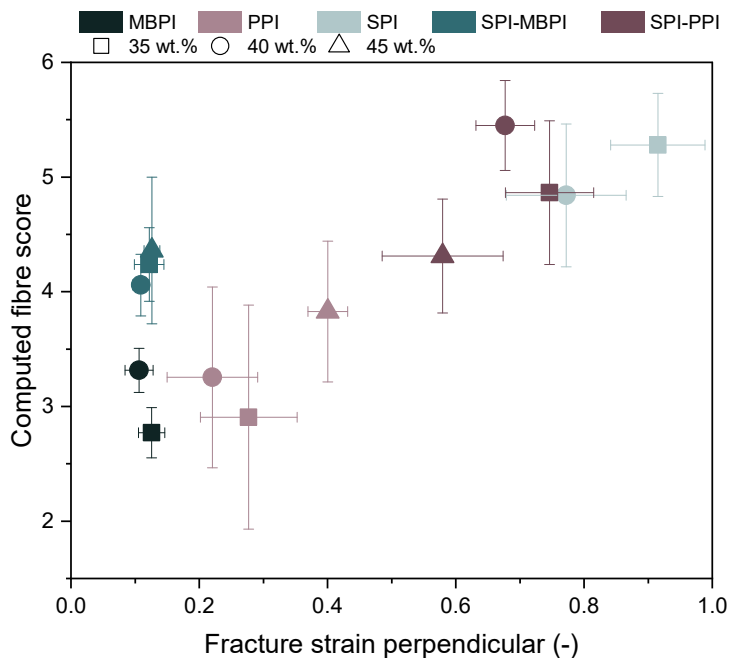


FIGURE 7.4 Computed fibre score versus fracture strain in the perpendicular direction to shear flow. MBPI: mung bean protein isolate. PPI: pea protein isolate. SPI: soy protein isolate. 35, 40, and 45 wt.% indicate dry matter contents.

The SPI-MBPI samples appeared as outliers in Figure 7.4. It could be that the mechanical properties of the SPI-MBPI samples tend to behave more as the MBPI only samples, so having a low fracture strain. The visual fibrous structure of the SPI-MBPI samples tends to behave more like the SPI only samples, with a higher computer fibre score. Nevertheless, for most samples the correlation between perpendicular fracture strain and computed fibre score seems relevant.

The ratio between tensile strength in parallel and perpendicular direction to the shear flow is the anisotropic index (Figure 7.5). SPI-PPI 45 wt.% exhibited the highest mechanical anisotropy, while this sample had an average computed fibre score (4.31). Remarkably, SPI-PPI at 35 wt.% did not exhibit mechanical anisotropy, whereas it did have a relatively high computed fibre score (5.45). The relatively low dry matter content may have resulted in a gel network with low connectivity. Elongated phases may have formed, but due to the low connectivity of the network, the orientation of the phases was not possible, resulting in no mechanical anisotropy. MBPI 40 wt.% exhibited negative anisotropy, meaning that the material was stronger in the direction

perpendicular to the shear flow. Here, it could be possible that the gel network is partly disrupted in the parallel direction during shear structuring, decreasing the tensile strength in this direction. The MBPI 40 wt.% sample may therefore be too intensively processed. To verify this, a series of lower shear rates can be applied to the MBPI 40 wt.% blend in the future. Furthermore, some samples with a positive mechanical anisotropy, such as PPI 35 wt.% and 40 wt.%, were accompanied by a low computed fibre score, suggesting that mechanical anisotropy and computed fibre score are not always correlated. This indicates that a visually fibrous structure may not always have a high mechanical anisotropy at fracture as characterized by the tensile test. This was previously also reported for meat analogues with pea protein isolate combined with wheat gluten (Schreuders *et al.*, 2019).

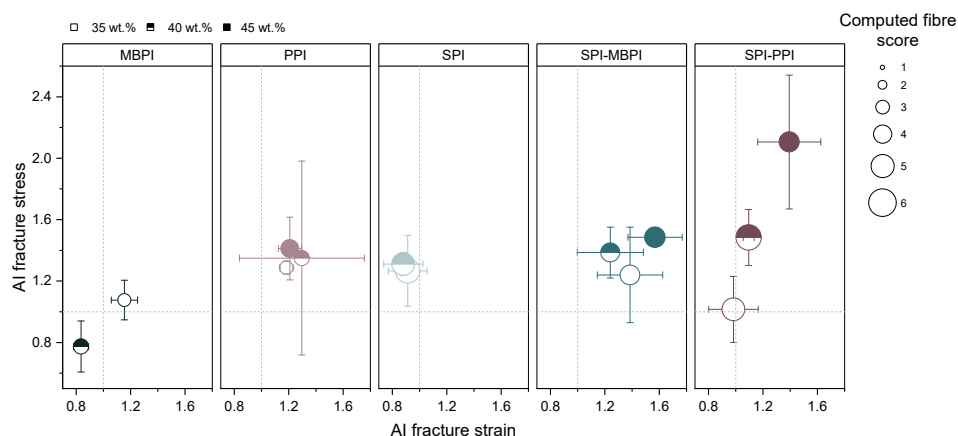


FIGURE 7.5 Anisotropy index map and computed fibre score of HTSC samples. MBPI: mung bean protein isolate. PPI: pea protein isolate. SPI: soy protein isolate. 35, 40, and 45 wt.% indicate dry matter contents.

Upon further visualization of the mechanical properties, it was found that even though anisotropy index of the Young's Modulus is not correlated with the computed fibre score, it may have been impacted by extreme outliers of the SPI-PPI samples (Figure 7.6). In general, an increase of anisotropy index of the Young's Modulus leads to higher visual fibrousness. In previous studies, mechanical anisotropy was often characterized at the fracture point, but Figure 7.6 suggests that differences in elasticity at low strain from the parallel and perpendicular directions possibly also indicate visual fibrousness. Previously, cooked chicken was characterized with a high anisotropy index of the Young's Modulus (~ 7.3) (Schreuders *et al.*, 2019). Therefore, anisotropy of the Young's Modulus values may be an interesting future design criterion when striving to mimic animal meat.

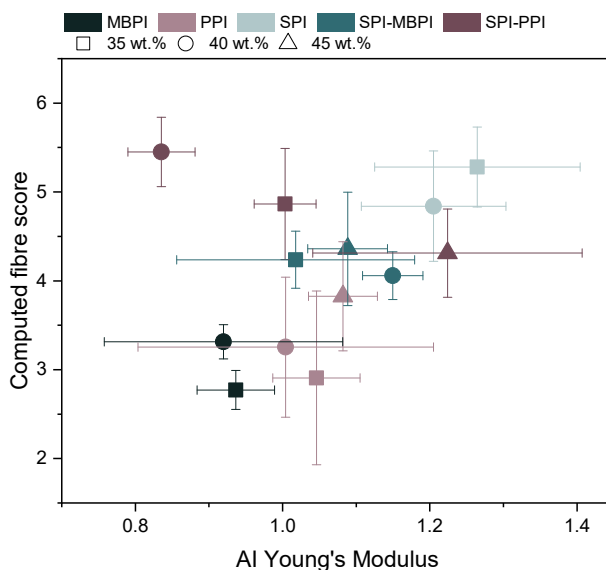


FIGURE 7.6 Computed fibre score versus anisotropy index of Young's Modulus. MBPI: mung bean protein isolate. PPI: pea protein isolate. SPI: soy protein isolate. 35, 40, and 45 wt.% indicate dry matter contents.

From these results we can conclude that visual fibrousness and mechanical anisotropy are related in some cases. The high correlation between fracture strain and computed fibre score and Young's Modulus and computed fibre score suggest that visual fibrousness is dependent on elastic properties and deformability of the product.

7.5 Use of knowledge from adjacent science fields

We start this section by further exploring the meaning of the word fibrousness. The Meriam-Webster definition of fibrous is “containing, consisting of, or resembling fibres”, “capable of being separated into fibres”, and “tough, sinewy”. This definition implies that fibrousness encompasses various aspects. The fact that fibrous means “capable of being separated into fibres” suggests the presence of interfaces between individual fibres in a product. The definition of fibrous being “tough, sinewy” in case of food products implies that the product has certain sensory properties. It has to be mentioned that tough has a mechanical definition as well, being the integral of the stress-strain curve.

In an extensive literature search (conducted on 04-10-2023) through Scopus, we found that depending on the exact term, the term “fibrous” is used across different disciplines (Figure 7.7). The term “fibrous” is predominantly used in medicine, material science,

and physics & astronomy (Figure 7.7A). In the context of medicine, the term “fibrous” is used to describe various tissues within the human body. In material science, “fibrous” typically relates to the composition of materials with a fibrous or filament-like structure, such as composite materials reinforced with structural fibres. This implies that the material contains separate phases being the matrix and the structural fibres. Agricultural and bioscience studies generally describe products being “fibrous” at larger length scales compared to other science fields like material science and engineering.

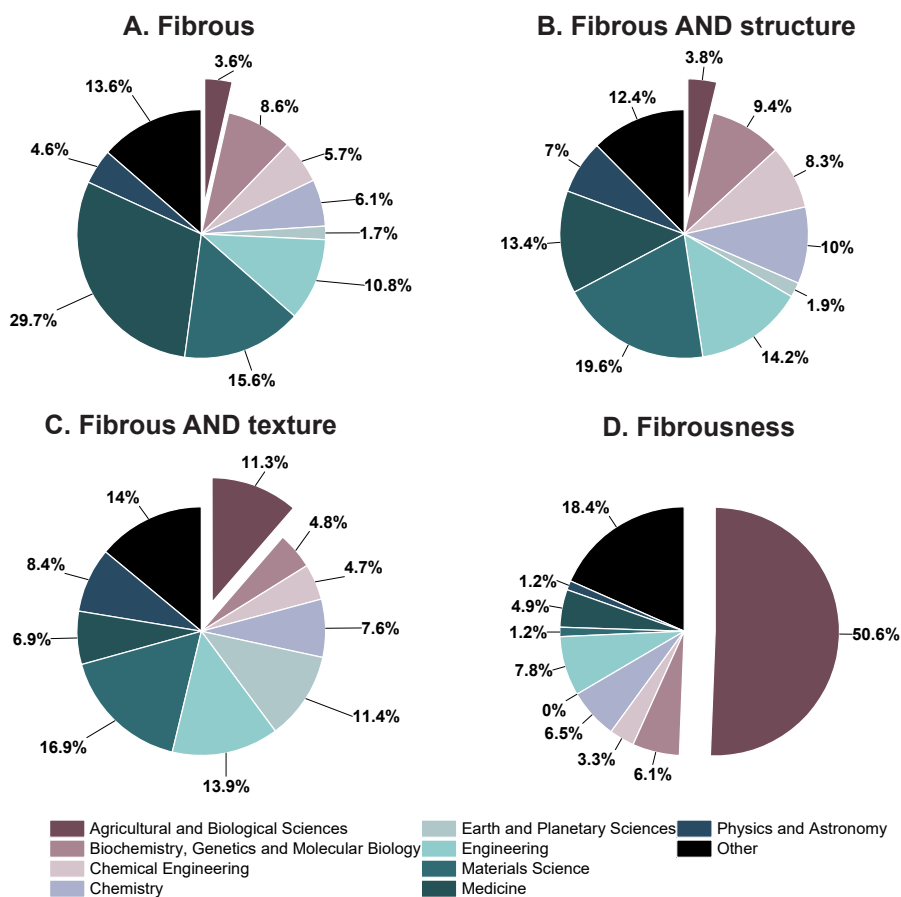


FIGURE 7.7 Literature search results for terms A) Fibrous, B) Fibrous AND structure, C) Fibrous AND texture, and D) Fibrousness across disciplines.

The inclusion of a second search term “structure” leads to an increased number of papers in the material science and engineering fields (Figure 7.7B). This is probably due to the fact that these fields often involve studying structures of materials across various length scales, such as molecular and crystalline structures. In material science, fibre orientation and composition can be tuned to obtain products with desired mechanical

properties. For instance, in composite materials, a fibrous structure can enhance strength and durability. In engineering fields, like in civil engineering, the fibrous nature of reinforced concrete provides tensile strength, toughness, and flexibility, ensuring the stability of structures. The use of the term “texture” instead of “structure”, leads to a significant increase of number of papers from agricultural and biosciences (Figure 7.7C). Here, texture is often associated with the physical properties of products, such as the mechanical strength upon deformation of food or plants. The term “fibrousness” is predominantly used in agricultural and biosciences (Figure 7.7D). In food science, fibrousness plays a crucial role in the development of meat analogues. Food scientists purposely engineer the fibrous structure of meat analogues to mimic the mouthfeel and appearance of animal meat. In essence, fibrousness is a multidimensional quality that encompasses both structural texture and mechanical properties.

Fibrousness in case of meat analogues is a term that is related to structural properties across various length scales. On a nanoscale, protein aggregates can align in a shear flow direction (van der Sman & van der Goot, 2023). While protein alignment results in anisotropy on a nanoscale, it is unclear yet whether this is perceivable for humans while consuming these products. So it may very well be that the anisotropy at nanoscale does not necessarily contribute to fibrousness as a sensory property. On a microscale, fibrousness in meat, and potentially meat analogues, involves the presence of interfaces and the arrangement of individual fibres within the matrix. It has long been established that the formation of fibrous structures in meat analogues requires phase separation and elongation of the dispersed phase (Dekkers, Boom, & van der Goot, 2018; Tolstoguzov, 2006; van der Sman & van der Goot, 2023). The presence of separate phases inherently implies the presence of interfaces in the material, aligning with the definition of “fibrous” as “capable of being separated into fibres”. However, the ability to separate these individual phases into fibres may be on a too small length scale for human taste perception, particularly in the case of shear cell and extrusion technology. The question therefore remains whether one should pursue structure formation of meat analogues at a micro- to nanoscale. Other technologies, such as 3D printing, can generate structures that are capable of being separated into fibres at larger length scales (such as macro). On a macroscale, fibrousness is mostly related to the overall texture of the product, which includes both visual and mechanical elements, as described in Section 7.1.4. In addition, these individual length scales may be interconnected. A change in structure on a small length scale is likely to result in a corresponding change in properties on larger length scales. Thus, future research should focus on finding the relationship between fibrousness at these length scales.

Other science fields can teach us valuable insights on the role of fibrousness and anisotropy. We take concrete and metal science as an example. From concrete science, we know that structural fibres with defined properties included as a dispersed phase

improve the elasticity and toughness of the composite material. The contribution of structural fibres to concrete delays propagation of microcracks into a macrocrack, which explains the increased toughness of the composite material (Alimrani & Balazs, 2023; H. Lee, Choi, & Kim, 2023). Inspired by this principle, we can deliberately blend ingredients to engineer meat analogues towards specific mechanical properties, such as increased toughness. To increase toughness, the structural fibres or dispersed phase should have lower Young's Modulus, but higher fracture stress and strain compared to the continuous phase. In meat analogues based on soy protein isolate, the dispersed phase (acting as the structural fibres here) therefore requires a Young's Modulus lower than 800 kPa, but a fracture stress and strain higher than 1300 kPa and 1.1, respectively (Schlangen, Schlangen, & van der Goot, 2023). Upon tension, the relatively weaker continuous phase will fracture first, after which the relatively stronger dispersed phase will take over the residual stress. The microcracks occurring in the continuous phase upon tension present themselves as a visual fibrous structure, a desired product property in meat analogues.

To increase the elasticity of a meat analogue, we can also turn to concrete science for inspiration. A product needs a dispersed phase with a higher Young's Modulus than the continuous phase (matrix) to increase the elasticity (Alimrani & Balazs, 2023). In the case of meat analogues produced from a matrix of soy protein isolate, this implies a dispersed phase ingredient with Young's moduli higher than approximately 800 kPa (Schlangen *et al.*, 2023). It will be a challenge to find such ingredient.

From metal science, we learn that loaded wires lengthen, generating a normal force, upon twisting. This is called the Poynting effect and is also described as the normal stress response of a material under shear, or $N_D = G_N \gamma^2$ (Poynting, 1909). The coefficient in the quadratic stress relation, G_N , is called the Poynting modulus (Ghorbani *et al.*, 2021). Recently, it was shown that fibre orientation influences on Poynting modulus in meat and meat analogues (Giménez-Ribes, Oostendorp, van der Goot, van der Linden, & Habibi, 2024). Meat exhibited great differences in Poynting modulus when measured in direction parallel compared to perpendicular to fibre orientation (Giménez-Ribes *et al.*, 2024). In the case of meat analogues, this difference was less pronounced. To bridge this gap and to make meat analogues more closely resemble real meat, valuable insights can be drawn from adjacent fields. In polymer gels, for instance, porosity greatly determines the Poynting effect (De Cagny *et al.*, 2016). Furthermore, research in soft tissues has revealed that fibre orientation also affects the Poynting modulus (Horgan & Murphy, 2017). A recent study also showed that fibres oriented at 45, -45, and 90 ° had a higher (absolute) Poynting effect than those oriented at 0 ° (Araújo & Nunes, 2020).

7.6 Shaping meat analogues of the future

Meat analogue technology has come a long way since Protose in the 1890s, but there are still many possibilities to improve today's meat analogues. The question is thus how we will shape the meat analogues of the future? Here, we propose three research areas that could contribute to the innovations in meat analogues: (1) ingredient requirements, (2) protein quality, and (3) data-driven solutions.

7.6.1 Hypothesis on ingredient requirements for structure formation

As shown in Section 7.1.2, a mung bean fine fraction crosslinked with transglutaminase could be shear structured into a fibrous product, whereas a mung bean fine fraction alone could not. We hypothesize that the mung bean fine fraction alone lacks the necessary continuous phase viscosity and local elasticity to facilitate dispersed phase elongation. It becomes therefore evident that there are ingredient requirements for the formation of fibrous structures for meat analogues. The addition of transglutaminase increases protein-protein interactions, which in case of mung bean probably provided the necessary viscosity and local elasticity of the continuous phase to allow creation of a fibrous structure.

Fibres are in principle interfaces that break up through an external force. This implies that at least two phases, a continuous and a dispersed phase, were present in the product. We previously hypothesized that the dispersed phase then deforms into elongated droplets upon shearing, resulting in an increased interface. The key question is how to achieve droplet elongation and how to maintain the droplet shape after elongation. We propose that elongation of the droplets relies on the viscosity of the phases. Furthermore, we propose that a certain magnitude of local elasticity of the continuous phase is required to prevent the elongated phase from reverting into a spherical shape.

To further explore the viscosity requirements for structure formation, we employ the concept of the Grace curve (Grace, 1982). The Grace curve describes how droplet deformation correlates to viscosity ratio between the dispersed phase and the continuous phase. It is an empirical fit of the critical capillary number needed to induce droplet break up as a function of viscosity ratio (Grace, 1982). The capillary number is defined as the ratio of viscous stresses to interfacial stress following Eq. 7.1:

$$Ca = \frac{\mu_c \dot{\gamma} R}{\sigma} \quad (\text{Eq. 7.1})$$

where Ca is the capillary number, μ_c is the viscosity of the continuous phase, $\dot{\gamma}$ is the shear rate, R is the droplet radius, and σ is the interfacial tension.

Within a viscosity ratio range of 0.1 and 1, the critical Ca is lower, meaning that droplet breakup occurs at lower shear rates in case of simple shear flow. As interpreted by Schreuders (2021), optimal deformation is then achieved when the viscosity ratio of the dispersed phase and continuous phases are well-matched. When the material is on the Grace curve threshold, the dispersed phase droplets undergo more substantial deformation during shear structuring, which is thought to be related to larger interfaces and thus enhanced fibrousness. It is plausible that the addition of transglutaminase to the mung bean fine fraction increases the viscosity of the protein-rich, continuous phase. As a result, the material moves towards a smaller viscosity ratio and higher Ca , approaching the Grace curve threshold (Figure 7.8). This explains why a fibrous structure was obtained for the transglutaminase crosslinked mung bean fine fraction, while it was not for the mung bean fine fraction alone. Furthermore, the increased viscosity of the continuous phase due to transglutaminase crosslinking increases the numerator in the Ca equation, implying that a lower shear rate is required for elongation of the dispersed phase. This can be further verified by treating the mung bean fine fraction with different concentrations of transglutaminase to directly influence the number of crosslinks and thus the viscosity of the continuous phase.

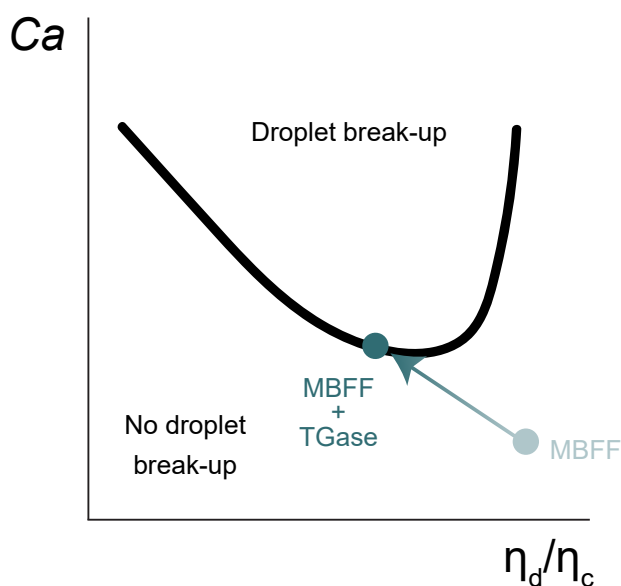


FIGURE 7.8 Schematic illustration of grace curve including possible positions of the mung bean fine fraction (MBFF) without and with transglutaminase (TGase). η_d : viscosity of dispersed phase. η_c : viscosity of continuous phase. Ca : capillary number.

The Ca equation also contains the interfacial tension. In case of a high interfacial tension, there is a strong tendency to minimize surface area, causing droplets to adopt a spherical shape. In the case of lower interfacial tension, higher shear stresses are required for droplet deformation and break-up. A high interfacial tension, thus, resists droplet deformation, while a low interfacial tension allows for more deformation and possibly elongation of the phases.

The local elasticity of the different phases present in meat analogue structures also affects the deformation of droplets during thermomechanical processing. Elasticity influences droplet deformation during both shearing and relaxation. A high elasticity ratio (dispersed/continuous phase) is reported to both reduce deformation (Lerdwijitjarud, Sirivat, & Larson, 2002; Mighri, Carreau, & Ajji, 1998) or enhance deformation (Mukherjee & Sarkar, 2009; Yu, Bousmina, Zhou, & Tucker, 2004) during shearing. These contradicting effects illustrate the complex behaviour of viscoelastic blends under flow. Upon and after shearing, interfacial tensions induce relaxation in deformed droplets. Schreuders *et al.* (2021) argued that a higher elasticity of the continuous phase can more effectively promote deformation and suppress the relaxation of the elongated dispersed phase back to a spherical shape. The relationship between matrix elasticity and deformation of a dispersed phase was also previously shown in non-food polylactide/polyamide blend extrudates, where a highly elastic matrix promoted deformation and extension of nodules into fibrils (Yousfi *et al.*, 2018). In **Chapter 4**, we showed that transglutaminase improved the elasticity of mung bean fine fractions, which could thus be an explanation for the fact that fibrous products could be formed with the mung bean fine fraction after transglutaminase treatment.

Thus, to shape the meat analogues of the future, it is key to use a combination of ingredients that end up on the Grace curve threshold for optimal elongation of the dispersed phase. Additionally, a high local elasticity of the continuous phase helps to maintain droplet shape after elongation. We have speculated on the ingredient requirements based on results from a mung bean fine fraction, with and without transglutaminase. In the future, this analysis can be performed on other ingredients as well.

7.6.2 Protein quality / fermentation

Plant proteins are often reported to have a lower protein quality than animal proteins, primarily due to the lower amount of essential amino acids and the lower digestibility (Davies & Jakeman, 2020). Meat analogues of the future should be shaped towards providing high quality protein with essential amino acids as a nutritious alternative to animal meat (Jiménez-Munoz, Tavares, & Corredig, 2021). A common strategy to enhance protein quality is blending several types of plant proteins to fill up to a complete

amino acid profile (Dimina, Rémond, Huneau, & Mariotti, 2022; Monnet, Laleg, Michon, & Micard, 2019). A well-known combination of cereal protein with legume protein in meat analogues is wheat gluten with pea protein (Schreuders *et al.*, 2019). As demonstrated in **Chapter 5**, blends with more than one legume protein are also a good starting point to make fibrous products. Another strategy to enhance essential amino acids is fermentation and/or the use of fungi protein. Solid-state fungal fermentation can enhance plant protein quality by improving amino acid composition and protein digestibility (Fawale, Gbadamosi, Ige, & Kadiri, 2017; Giami, 2004; Zwinkels, Wolkers-Rooijackers, & Smid, 2023). We propose two strategies to use fungal protein in meat analogues: (1) using the meat analogue as a substrate for fungal growth or (2) using fungal protein as an ingredient to produce the meat analogues.

Meat analogues produced through shear cell technology or high moisture extrusion cooking typically have a porous structure. If these pores form a network spanning the entire sample, they can be used to facilitate fungal fermentation, resulting in the growth of fungal threads throughout the product (strategy 1). This has both textural and nutritional benefits. From a textural point of view, it may enhance the fibrousness of the product, most likely at a smaller length scales than what we can reach through thermomechanical processing alone. Meat analogues can also directly be produced from the fungal protein source (strategy 2). Potentially, blends of conventional plant proteins, such as soy protein isolate, and fungal proteins can be made. The use of fungal protein was previously shown to improve textural and taste properties of meat analogues compared to meat analogues produced solely from soy protein (Kim *et al.*, 2011). Given that these proteins likely have different water holding and functional properties, they may form different phases in the dough, potentially enabling the formation of a fibrous structure, similar to the ones found by combining two plant proteins in **Chapter 5**. In addition to improving texture, the combination of plant protein with fungal protein can theoretically yield an improved amino acid composition (Zwinkels *et al.*, 2023).

7.6.3 Data driven approaches

Currently, meat analogues do not always mimic animal meat on all length scales. Despite significant advancements, it is still challenging to replicate the fibrous structure of meat accurately, especially on multiple length scales. This is amongst others caused by a knowledge gap on how the fibrousness of meat analogues relates to their mechanical properties and texture, which hinders systematic product development, thereby limiting widespread consumer acceptance. To address this issue, we can take a data driven approach by mapping the fibrousness and mechanical properties of meat analogues onto a multidimensional space, which spans multiple length scales. This multidimensional space can be considered a parameter space covering all the

different aspects of fibrousness, with each axis describing the contribution of a specific parameter. Examples of such parameters are quantitative information on fibrousness on macroscale, anisotropy index of toughness, and quantitative shape parameters extracted from microscopy images. By placing both meat and meat analogues within the space, it can become possible to categorize and compare their similarities and differences systematically. This will reveal on which length scale differences between meat and meat analogues are present, which enables a targeted approach to improving meat analogues. Machine learning techniques will then be used to predict the optimal ingredients and processing to make specific meat analogues with structural properties in the multidimensional space. Moreover, the abundance of data on meat analogues generated over the past years bears a clear opportunity here next to the described AI-driven mapping of fibrousness. For example, in recent years, large amounts of data have been generated on the rheological properties of plant protein ingredients (Schreuders, Sagis, Bodnár, Boom, & van der Goot, 2022). However, we expect that the data carry more undiscovered information. Data driven approaches can help to interpret and correlate these data sets by identifying trends. Eventually, predictive artificial intelligence can be used to extrapolate the findings to other variables, such as other ingredients or processing conditions.

7.7 Concluding remarks

This thesis aimed to engineer custom, protein-rich ingredients tailored for meat analogue applications. Indeed, this thesis describes that dry fractionation in combination with enzyme treatment is a suitable method to produce protein-rich ingredients with excellent structuring properties for meat analogues. Additionally, new insight was created on how to quantify both visual and mechanical fibrousness of meat analogues. In a next step, the multiscale structure of meat analogues should be completely characterized to understand where the differences with real meat originate from. This would also open up the possibility to actively structure towards a designed product texture.



R

References

Reference list

- Adebowale, K. O., & Lawal, O. S. (2003). Foaming, gelation and electrophoretic characteristics of mucuna bean (*Mucuna pruriens*) protein concentrates. *Food Chemistry*, 83(2), 237–246. [https://doi.org/10.1016/S0308-8146\(03\)00086-4](https://doi.org/10.1016/S0308-8146(03)00086-4)
- Aguilera, J. M., & Rojas, E. (1996). Rheological , Thermal and Microstructural Properties of Whey Protein-Cassava Starch Gels. *Journal of Food Science*, 61(5), 962–966.
- Ahmed, J., Al-Ruwaih, N., Mulla, M., & Rahman, M. H. (2018). Effect of high pressure treatment on functional, rheological and structural properties of kidney bean protein isolate. *Lwt*, 91, 191–197. <https://doi.org/10.1016/j.lwt.2018.01.054>
- Aiking, H. (2014). Protein production: Planet, profit, plus people? *American Journal of Clinical Nutrition*, 100(SUPPL. 1), 483–489. <https://doi.org/10.3945/ajcn.113.071209>
- Aiking, H., & de Boer, J. (2020). The next protein transition. *Trends in Food Science and Technology*, 105(May 2018), 515–522. <https://doi.org/10.1016/j.tifs.2018.07.008>
- Ak, M. M., Bogenrief, D., Gunasekaran, S., & Olson, N. F. (1993). Rheological Evaluation of Mozzarella Cheese By Uniaxial Horizontal Extension. *Journal of Texture Studies*, 24(4), 437–453. <https://doi.org/10.1111/j.1745-4603.1993.tb00053.x>
- Ak, M. M., & Gunasekaran, S. (1997). Anisotropy in tensile properties of Mozzarella cheese. *Journal of Food Science*, 62(5), 1031–1033. <https://doi.org/10.1111/j.1365-2621.1997.tb15031.x>
- Alimrani, N. S., & Balazs, G. L. (2023). Toughness and stiffness of fibre reinforced concrete in terms of shear capacity. *Construction and Building Materials*, 389(May), 131711. <https://doi.org/10.1016/j.conbuildmat.2023.131711>
- Anderson, J. W., Baird, P., Davis, R. H., Ferreri, S., Knudtson, M., Koraym, A., ... Williams, C. L. (2009). Health benefits of dietary fiber. *Nutrition Reviews*, 67(4), 188–205. <https://doi.org/10.1111/j.1753-4887.2009.00189.x>
- Anton Paar. (2022). Amplitude Sweeps. Retrieved February 4, 2022, from <https://wiki.anton-paar.com/nl-en/amplitude-sweeps/>
- Araújo, F. S., & Nunes, L. C. S. (2020). Experimental study of the Poynting effect in a soft unidirectional fiber-reinforced material under simple shear. *Soft Matter*, 16(34), 7950–7957. <https://doi.org/10.1039/d0sm00745e>
- Asif, M., Rooney, L. W., Ali, R., & Riaz, M. N. (2013). Application and Opportunities of Pulses in Food System: A Review. *Critical Reviews in Food Science and Nutrition*, 53(11), 1168–1179. <https://doi.org/10.1080/10408398.2011.574804>
- Assatory, A., Vitelli, M., Rajabzadeh, A. R., & Legge, R. L. (2019a). Dry fractionation methods for plant protein, starch and fiber enrichment: A review. *Trends in Food Science and Technology*, 86(November 2018), 340–351. <https://doi.org/10.1016/j.tifs.2019.02.006>
- Assatory, A., Vitelli, M., Rajabzadeh, A. R., & Legge, R. L. (2019b). Dry fractionation methods for plant protein, starch and fiber enrichment: A review. *Trends in Food Science and Technology*, 86(February), 340–351. <https://doi.org/10.1016/j.tifs.2019.02.006>
- Barbut, S. (2015). Chapter 16- Evaluating Texture and Sensory Attributes. In *The Science of Poultry and Meat Processing* (pp. 16-1-16–39).
- Bate, P. S., Ridley, N., & Sotoudeh, K. (2008). Effect of gauge length in superplastic tensile tests. *Materials Science and Technology*, 24(10), 1265–1270. <https://doi.org/10.1179/174328408X323113>
- BeMiller, J., & Whistler, R. (2009). *Starch: Chemistry and Technology* (Third edit). Elsevier.
- Bildstein, M., Lohmann, M., Hennigs, C., Krause, A., & Hilz, H. (2008). An enzyme-based extraction process for the purification and enrichment of vegetable proteins to be applied in bakery products. *European Food Research and Technology*, 228(2), 177–186. <https://doi.org/10.1007/s00217-008-0921-z>
- Blaber, J., Adair, B., & Antoniou, A. (2015). Ncorr: Open-Source 2D Digital Image Correlation Matlab Software. *Experimental Mechanics*, 55(6), 1105–1122. <https://doi.org/10.1007/s11340-015-0009-1>
- Boots, J. N. M., Humblet-Hua, N. P. K., Tonneijck, L., Fokkink, R., van der Gucht, J., & Kodger, T. E. (2021). Characterization of the local mechanical texture of animal meat and meat replacements using multi-point indentation. *Journal of Food Engineering*, 300(January), 110505. <https://doi.org/10.1016/j.j>

- jfoodeng.2021.110505
- Boukid, F., Rosell, C. M., Rosene, S., Bover-Cid, S., & Castellari, M. (2021). Non-animal proteins as cutting-edge ingredients to reformulate animal-free foodstuffs: Present status and future perspectives. *Critical Reviews in Food Science and Nutrition*, 0(0), 1–31. <https://doi.org/10.1080/10408398.2021.1901649>
- Boye, J., Zare, F., & Pletch, A. (2010). Pulse proteins: Processing, characterization, functional properties and applications in food and feed. *Food Research International*, 43, 414–431. <https://doi.org/https://doi.org/10.1016/j.foodres.2009.09.003>
- Boyer, R. A. (1954). US Patent No. 2682466. United States Patent Office. Retrieved from <https://patentimages.storage.googleapis.com/88/d4/e9/06f8fa3be096a5/US2682466.pdf>
- Brishti, F. H., Chay, S. Y., Muhammad, K., Ismail-fitry, M. R., Zarei, M., & Saari, N. (2021). Texturized mung bean protein as a sustainable food source : Effects of extrusion on its physical , textural and protein quality. *Innovative Food Science and Emerging Technologies*, 67(January 2021), 102591. <https://doi.org/10.1016/j.ifset.2020.102591>
- Brishti, F. H., Yea, C. S., Muhammad, K., Ismail-Fitry, M. R., Zarei, M., Karthikeyan, S., & Saari, N. (2020). Effects of drying techniques on the physicochemical, functional, thermal, structural and rheological properties of mung bean (*Vigna radiata*) protein isolate powder. *Food Research International*, 138(PB), 109783. <https://doi.org/10.1016/j.foodres.2020.109783>
- Brishti, F. H., Zarei, M., Muhammad, S. K. S., Ismail-Fitry, M. R., Shukri, R., & Saari, N. (2017). Evaluation of the functional properties of mung bean protein isolate for development of textured vegetable protein. *International Food Research Journal*, 24(4), 1595–1605.
- Buchert, J., Cura, D. E., Ma, H., Gasparetti, C., Monogioudi, E., Faccio, G., ... Kruus, K. (2010). Crosslinking food proteins for improved functionality. *Annual Review of Food Science and Technology*, 1(1), 113–138. <https://doi.org/10.1146/annurev.food.080708.100841>
- Bühler, J. M., Dekkers, B. L., Bruins, M. E., & Goot, A. J. Van Der. (2020). Modifying Faba Bean Protein Concentrate Using Dry Heat to Increase Water Holding Capacity. *Foods*, 1–16. <https://doi.org/10.3390/foods9081077>
- Canal, L. P., González, C., Molina-Aldareguía, J. M., Segurado, J., & Llorca, J. (2012). Application of digital image correlation at the microscale in fiber-reinforced composites. *Composites Part A: Applied Science and Manufacturing*, 43(10), 1630–1638. <https://doi.org/10.1016/j.compositesa.2011.07.014>
- Carneiro da Silva, A., da Costa Santos, D., Lopes Teixeira Junior, D., Bento da Silva, P., Cavalcante dos Santos, R., & Siviero, A. (2019). Cowpea: A Strategic Legume Species for Food Security and Health. *IntechOpen*, (January 2019). <https://doi.org/10.5772/intechopen.79006>
- Chantanuson, R., Nagamine, S., Kobayashi, T., & Nakagawa, K. (2022). Preparation of soy protein-based food gels and control of fibrous structure and rheological property by freezing. *Food Structure*, 32(January), 100258. <https://doi.org/10.1016/j.foostr.2022.100258>
- Chen, Q., Zhang, J., Zhang, Y., Kaplan, D. L., & Wang, Q. (2022). Protein-amylose/amylopectin molecular interactions during high-moisture extruded texturization toward plant-based meat substitutes applications. *Food Hydrocolloids*, 127(September 2021), 107559. <https://doi.org/10.1016/j.foodhyd.2022.107559>
- Chinma, C. E., Ariahu, C. C., & Abu, J. O. (2013). Chemical composition, functional and pasting properties of cassava starch and soy protein concentrate blends. *Journal of Food Science and Technology*, 50(6), 1179–1185. <https://doi.org/10.1007/s13197-011-0451-8>
- Churchill, W. (1931). Fifty Years Hence. *Strand Magazine*.
- Corker, A., Ng, H. C. H., Poole, R. J., & García-Tuñón, E. (2019). 3D printing with 2D colloids: Designing rheology protocols to predict “printability” of soft-materials. *Soft Matter*, 15(6), 1444–1456. <https://doi.org/10.1039/c8sm01936c>
- Cornet, S. H. V., Snel, S. J. E., Schreuders, F. K. G., van der Sman, R. G. M., Beyrer, M., & van der Goot, A. J. (2022). Thermo-mechanical processing of plant proteins using shear cell and high-moisture extrusion cooking. *Critical Reviews in Food Science and Nutrition*, 62(12), 1–18. <https://doi.org/10.1080/10408398.2020.1864618>
- Dabbaghi, M., Namjoshi, S., Panchal, B., Grice, J. E., Prakash, S., Roberts, M. S., & Mohammed, Y. (2021). Viscoelastic and deformation characteristics of structurally different commercial topical systems. *Pharmaceutics*, 13(9), 1–11. <https://doi.org/10.3390/pharmaceutics13091351>
- Davies, R. W., & Jakeman, P. M. (2020). Separating the wheat from the chaff: Nutritional value of plant proteins and their potential contribution to human health. *Nutrients*, 12(8), 1–12. <https://doi.org/10.3390/nui2082410>

-
- Day, L., & Swanson, B. G. (2013). Functionality of protein-fortified extrudates. *Comprehensive Reviews in Food Science and Food Safety*, 12(5), 546–564. <https://doi.org/10.1111/1541-4337.12023>
- de Angelis, D. (2021). New pulses-based ingredients obtained by dry fractionation to improve the nutritional and technological quality of food.
- De Cagny, H. C. G., Vos, B. E., Vahabi, M., Kurniawan, N. A., Doi, M., Koenderink, G. H., ... Bonn, D. (2016). Porosity governs normal stresses in polymer gels. *Physical Review Letters*, 117(21), 1–5. <https://doi.org/10.1103/PhysRevLett.117.217802>
- De Moura, J. M. L. N., Campbell, K., De Almeida, N. M., Glatz, C. E., & Johnson, L. A. (2011). Protein recovery in aqueous extraction processing of soybeans using isoelectric precipitation and nanofiltration. *JAOCS, Journal of the American Oil Chemists' Society*, 88(9), 1447–1454. <https://doi.org/10.1007/s11746-011-1803-2>
- Dekkers, B. L., Boom, R. M., & van der Goot, A. J. (2018). Structuring processes for meat analogues. *Trends in Food Science & Technology*, 81, 25–36. <https://doi.org/10.1016/j.tifs.2018.08.011>
- Dekkers, B. L., Nikiforidis, C. V., & van der Goot, A. J. (2016). Shear-induced fibrous structure formation from a pectin / SPI blend. *Innovative Food Science and Emerging Technologies*, 36, 193–200. <https://doi.org/10.1016/j.ifset.2016.07.003>
- Dimina, L., Rémond, D., Huneau, J. F., & Mariotti, F. (2022). Combining Plant Proteins to Achieve Amino Acid Profiles Adapted to Various Nutritional Objectives—An Exploratory Analysis Using Linear Programming. *Frontiers in Nutrition*, 8(February), 1–11. <https://doi.org/10.3389/fnut.2021.809685>
- Djoullah, A., Djemaoune, Y., Husson, F., & Saurel, R. (2015). Native-state pea albumin and globulin behavior upon transglutaminase treatment. *Process Biochemistry*, 50(8), 1284–1292. <https://doi.org/10.1016/j.procbio.2015.04.021>
- Djoullah, A., Husson, F., & Saurel, R. (2018). Gelation behaviors of denaturated pea albumin and globulin fractions during transglutaminase treatment. *Food Hydrocolloids*, 77, 636–645. <https://doi.org/10.1016/j.foodhyd.2017.11.005>
- Djoullah, A., Krechiche, G., Husson, F., & Saurel, R. (2016). Size measuring techniques as tool to monitor pea proteins intramolecular crosslinking by transglutaminase treatment. *Food Chemistry*, 190, 197–200. <https://doi.org/10.1016/j.foodchem.2015.05.091>
- Dobson, S., Stobbs, J., Laredo, T., & Marangoni, A. G. (2023). A facile strategy for plant protein fiber formation without extrusion or shear processing. *Innovative Food Science and Emerging Technologies*, 86(May), 103385. <https://doi.org/10.1016/j.ifset.2023.103385>
- Du, M., Xie, J., Gong, B., Xu, X., Tang, W., Li, X., ... Xie, M. (2018). Extraction, physicochemical characteristics and functional properties of Mung bean protein. *Food Hydrocolloids*, 76, 131–140. <https://doi.org/10.1016/j.foodhyd.2017.01.003>
- Elzerman, J. E., Hoek, A. C., van Boekel, M. A. J. S., & Luning, P. A. (2011). Consumer acceptance and appropriateness of meat substitutes in a meal context. *Food Quality and Preference*, 22(3), 233–240. <https://doi.org/10.1016/j.foodqual.2010.10.006>
- Fan, F. H., Ma, Q., Ge, J., Peng, Q. Y., Riley, W. W., & Tang, S. Z. (2013). Prediction of texture characteristics from extrusion food surface images using a computer vision system and artificial neural networks. *Journal of Food Engineering*, 118(4), 426–433. <https://doi.org/10.1016/j.jfoodeng.2013.04.015>
- Fawale, O. S., Gbadamosi, S. O., Ige, M. M., & Kadiri, O. (2017). Effects of cooking and fermentation on the chemical composition, functional, and antinutritional properties of kariya (*Hildergardia barteri*) seeds. *Food Science and Nutrition*, 5(6), 1106–1115. <https://doi.org/10.1002/fsn3.501>
- Ferry, J. D. (1980). *Viscoelastic properties of polymers*, 3rd edition. Wiley, New York. Retrieved from <https://www.wiley.com/en-sg/Viscoelastic+Properties+of+Polymers%2C+3rd+Edition-p-9780471048947>
- Flory, P. J., & Rehner, J. (1943). Statistical mechanics of cross-linked polymer networks II. Swelling. *The Journal of Chemical Physics*, 11(11), 521–526. <https://doi.org/10.1063/1.1723792>
- Forghani, Z., Eskandari, M. H., Aminlari, M., & Shekarforoush, S. S. (2017). Effects of microbial transglutaminase on physicochemical properties, electrophoretic patterns and sensory attributes of veggie burger. *Journal of Food Science and Technology*, 54(8), 2203–2213. <https://doi.org/10.1007/s13197-017-2614-8>
- Funke, M., Boom, R., & Weiss, J. (2022). Dry fractionation of lentils by air classification - Composition, interfacial properties and behavior in concentrated O/W emulsions. *Lwt*, 154. <https://doi.org/10.1016/j.lwt.2021.112718>
- Gaspar, A. L. C., & De Góes-Favoni, S. P. (2015, March 15). Action of microbial transglutaminase (MTGase)

- in the modification of food proteins: A review. *Food Chemistry*. Elsevier Ltd. <https://doi.org/10.1016/j.foodchem.2014.09.019>
- Geerts, M. E. J., Dekkers, B. L., van der Padt, A., & van der Goot, A. J. (2018). Aqueous fractionation processes of soy protein for fibrous structure formation. *Innovative Food Science and Emerging Technologies*, 45(September 2017), 313–319. <https://doi.org/10.1016/j.ifset.2017.12.002>
- Gharst, G., Clare, D. A., Davis, J. P., & Sanders, T. H. (2007). The effect of transglutaminase crosslinking on the rheological characteristics of heated peanut flour dispersions. *Journal of Food Science*, 72(7), C369–C375. <https://doi.org/10.1111/j.1750-3841.2007.00442.x>
- Ghorbani, A., Dykstra, D., Coulais, C., Bonn, D., van der Linden, E., & Habibi, M. (2021). Inverted and Programmable Poynting Effects in Metamaterials. *Advanced Science*, 8(20), 1–9. <https://doi.org/10.1002/advs.202102279>
- Giami, S. Y. (2004). Effect of fermentation on the seed proteins, nitrogenous constituents, antinutrients and nutritional quality of fluted pumpkin (*Telfairia occidentalis* Hook). *Food Chemistry*, 88(3), 397–404. <https://doi.org/10.1016/j.foodchem.2004.01.064>
- Giménez-Ribes, G., Oostendorp, M., van der Goot, A. J., van der Linden, E., & Habibi, M. (2024). Effect of fiber properties and orientation on the shear rheology and Poynting effect in meat and meat analogues. *Food Hydrocolloids*, 149(July 2023), 109509. <https://doi.org/10.1016/j.foodhyd.2023.109509>
- Godara, A., Raabe, D., Bergmann, I., Putz, R., & Müller, U. (2009). Influence of additives on the global mechanical behavior and the microscopic strain localization in wood reinforced polypropylene composites during tensile deformation investigated using digital image correlation. *Composites Science and Technology*, 69(2), 139–146. <https://doi.org/10.1016/j.compscitech.2008.08.031>
- Godschalk-Broers, L., Sala, G., & Scholten, E. (2022). Meat Analogues: Relating Structure to Texture and Sensory Perception. *Foods*, 11(15). <https://doi.org/10.3390/foods11152227>
- Goodno, C. C., Swaisgood, H. E., & Catignani, G. L. (1981). A Fluorimetric Assay for Available Lysine in Proteins. *Analytical Biochemistry*, 211, 203–211.
- Grabowska, K. J., Tekidou, S., Boom, R. M., & Goot, A. Van Der. (2014). Shear structuring as a new method to make anisotropic structures from soy – gluten blends. *Food Research International*, 64, 743–751. <https://doi.org/10.1016/j.foodres.2014.08.010>
- Grabowska, K. J., Zhu, S., Dekkers, B. L., De Ruijter, N. C. A., Gieteling, J., & Van Der Goot, A. J. (2016). Shear-induced structuring as a tool to make anisotropic materials using soy protein concentrate. *Journal of Food Engineering*, 188, 77–86. <https://doi.org/10.1016/j.jfoodeng.2016.05.010>
- Grace, H. P. (1982). Dispersion phenomena in high viscosity immiscible fluid systems and application of static mixers as dispersion devices in such systems. *Chemical Engineering Communications*, 14(3–6), 225–277. <https://doi.org/10.1080/00986448208911047>
- Greaves, G. N., Greer, A. L., Lakes, R. S., & Rouxel, T. (2011). Poisson's ratio and modern materials. *Nature Materials*, 10(11), 823–837. <https://doi.org/10.1038/nmat3134>
- Gu, G. H., Kim, Y., Kim, R. E., Seo, M. H., & Kim, H. S. (2023). A New Digital Image Correlation Method for Measuring Wide Strain Range True Stress–Strain Curve of Clad Materials. *Metals and Materials International*, 29(1), 168–173. <https://doi.org/10.1007/s12540-022-01219-3>
- Guo, J., Jin, Y. C., Yang, X. Q., Yu, S. J., Yin, S. W., & Qi, J. R. (2013). Computed microtomography and mechanical property analysis of soy protein porous hydrogel prepared by homogenizing and microbial transglutaminase cross-linking. *Food Hydrocolloids*, 31(2), 220–226. <https://doi.org/10.1016/j.foodhyd.2012.10.023>
- Hampton Creek, I. (2017). US 2017 / 0238590 A1.
- Henshaw, F. O., Mcwatters, K. H., Akingbala, J. O., & Chinnan, M. S. (2003). Thermal properties of cowpea flour : A study by differential scanning calorimetry. *Nahrung - Food*, 47(3), 161–165.
- Hernández-Álvarez, A. J., Mondor, M., & Nosworthy, M. G. (2023). Green Protein Processing Technologies from Plants.
- Hertsberg, R. W. (1996). *Deformation and Fracture Mechanics of Engineering Materials*. John Wiley and Sons Inc.
- Herz, E., Herz, L., Dreher, J., Gibis, M., Ray, J., Pibarot, P., ... Weiss, J. (2021). Influencing factors on the ability to assemble a complex meat analogue using a soy-protein-binder. *Innovative Food Science and Emerging Technologies*, 73(April). <https://doi.org/10.1016/j.ifset.2021.102806>
- Herz, E. M., Schäfer, S., Terjung, N., Gibis, M., & Weiss, J. (2021). Influence of Transglutaminase on Glucono- δ -lactone-Induced Soy Protein Gels. *ACS Food Science & Technology*, 1(8), 1412–1417. <https://doi.org/10.1021/acsf.1c00111>

- Hoover, R., Li, Y. X., Hynes, G., & Senanayake, N. (1997). Physicochemical characterization of mung bean starch. *Food Hydrocolloids*, 11(4), 401–408. [https://doi.org/10.1016/S0268-005X\(97\)80037-9](https://doi.org/10.1016/S0268-005X(97)80037-9)
- Hordijk, D. A. (1991). Local approach to fatigue of concrete.
- Horgan, C. O., & Murphy, J. G. (2017). Fiber orientation effects in simple shearing of fibrous soft tissues. *Journal of Biomechanics*, 64, 131–135. <https://doi.org/10.1016/j.jbiomech.2017.09.018>
- Huang, J., Schols, H. A., van Soest, J. J. G., Jin, Z., Sulmann, E., & Voragen, A. G. J. (2007). Physicochemical properties and amylopectin chain profiles of cowpea, chickpea and yellow pea starches. *Food Chemistry*, 101(4), 1338–1345. <https://doi.org/10.1016/j.foodchem.2006.03.039>
- Huang, W., Li, L., Wang, F., Wan, J., Tilley, M., Ren, C., & Wu, S. (2010). Effects of transglutaminase on the rheological and Mixolab thermomechanical characteristics of oat dough. *Food Chemistry*, 121(4), 934–939. <https://doi.org/10.1016/j.foodchem.2010.01.008>
- Hubalek, S., Post, M. J., & Moutsatsou, P. (2022). Towards resource-efficient and cost-efficient cultured meat. *Current Opinion in Food Science*, 47, 100885. <https://doi.org/10.1016/j.cofs.2022.100885>
- Jahanbakhshian, N., Hamdami, N., & Shahedi, M. (2018). Measurement and prediction of the mechanical properties of a two-component food during freezing. *International Journal of Food Properties*, 20(3), S3088–S3095. <https://doi.org/10.1080/10942912.2016.1247856>
- Jia, W., Curubeto, N., Rodríguez-alonso, E., Keppler, J. K., & van der Goot, A. J. (2021). Rapeseed protein concentrate as a potential ingredient for meat analogues. *Innovative Food Science and Emerging Technologies*, 72(July), 102758. <https://doi.org/10.1016/j.ifset.2021.102758>
- Jiménez-Munoz, L. M., Tavares, G. M., & Corredig, M. (2021). Design future foods using plant protein blends for best nutritional and technological functionality. *Trends in Food Science and Technology*, 113(September 2020), 139–150. <https://doi.org/10.1016/j.tifs.2021.04.049>
- Jong, G. H. a. De, & Koppelman, S. J. (2002). Transglutaminase Catalyzed Reactions: Impact on Food Applications. *Journal of Food Science*, 67(8), 2798–2806.
- Kebede, E., & Bekeko, Z. (2020). Expounding the production and importance of cowpea (*Vigna unguiculata* (L.) Walp.) in Ethiopia. *Cogent Food and Agriculture*, 6(1). <https://doi.org/10.1080/23311932.2020.1769805>
- Keivaninahr, F., Gadkari, P., Zoroufchi Benis, K., Tulbek, M., & Ghosh, S. (2021). Prediction of emulsification behaviour of pea and faba bean protein concentrates and isolates from structure-functionality analysis. *RSC Advances*, 11(20), 12117–12135. <https://doi.org/10.1039/d0ra09302e>
- Kellogg, J. H. (1901). US Patent No. 670283. United States Patent Office. <https://doi.org/10.1145/178951.178972>
- Kethireddipalli, P., Hung, Y. C., McWatters, K. H., & Philips, R. D. (2002). Effect of milling method (wet and dry) on the functional properties of cowpea (*Vigna unguiculata*) pastes and end product (akara) quality. *Journal of Food Science*, 67(1), 48–52. <https://doi.org/10.1111/j.1365-2621.2002.tb11357.x>
- Kim, K., Choi, B., Lee, I., Lee, H., Kwon, S., Oh, K., & Kim, A. Y. (2011). Bioproduction of mushroom mycelium of *Agaricus bisporus* by commercial submerged fermentation for the production of meat analogue. *Journal of the Science of Food and Agriculture*, 91(9), 1561–1568. <https://doi.org/10.1002/jsfa.4348>
- Kornet, R., Veenemans, J., Venema, P., van der Goot, A. J., Meinders, M., Sagis, L., & van der Linden, E. (2021). Less is more: Limited fractionation yields stronger gels for pea proteins. *Food Hydrocolloids*, 112, 106285. <https://doi.org/10.1016/j.foodhyd.2020.106285>
- Krintiras, G. A., Göbel, J., Van Der Goot, A. J., & Stefanidis, G. D. (2015). Production of structured soy-based meat analogues using simple shear and heat in a Couette Cell. *Journal of Food Engineering*, 160, 34–41. <https://doi.org/10.1016/j.jfoodeng.2015.02.015>
- Kyriakopoulou, K., Dekkers, B., & van der Goot, A. J. (2019). Plant-Based Meat Analogues. *Sustainable Meat Production and Processing*. Elsevier Inc. <https://doi.org/10.1016/B978-0-12-814874-7.00006-7>
- Kyriakopoulou, K., Keppler, J. K., van der Goot, A. J., & Boom, R. M. (2021). Alternatives to Meat and Dairy. *Annual Review of Food Science and Technology*, 12(1), 1–22. <https://doi.org/10.1146/annurev-food-062520-101850>
- Lam, A. C. Y., Can Karaca, A., Tyler, R. T., & Nickerson, M. T. (2018, February 17). Pea protein isolates: Structure, extraction, and functionality. *Food Reviews International*. Taylor and Francis Inc. <https://doi.org/10.1080/87559129.2016.1242135>
- Lam, M., Paulsen, P., & Corredig, M. (2008). Interactions of soy protein fractions with high-methoxyl pectin. *Journal of Agricultural and Food Chemistry*, 56(12), 4726–4735. <https://doi.org/10.1021/jf073375d>

- Lamsal, B. P., Jung, S., & Johnson, L. A. (2007). Rheological properties of soy protein hydrolysates obtained from limited enzymatic hydrolysis. *LWT - Food Science and Technology*, 40(7), 1215–1223. <https://doi.org/10.1016/j.lwt.2006.08.021>
- Lan, Y., Xu, M., Ohm, J. B., Chen, B., & Rao, J. (2019). Solid dispersion-based spray-drying improves solubility and mitigates beany flavour of pea protein isolate. *Food Chemistry*, 278(November 2018), 665–673. <https://doi.org/10.1016/j.foodchem.2018.11.074>
- Lee, D. J., Ahn, D. H., Yoon, E. Y., Hong, S. I., Lee, S., & Kim, H. S. (2013). Estimating interface bonding strength in clad metals using digital image correlation. *Scripta Materialia*, 68(11), 893–896. <https://doi.org/10.1016/j.scriptamat.2013.02.021>
- Lee, H., Choi, M. K., & Kim, B. J. (2023). Structural and functional properties of fiber reinforced concrete composites for construction applications. *Journal of Industrial and Engineering Chemistry*, 125, 38–49. <https://doi.org/10.1016/j.jiec.2023.05.019>
- Lerdwijitjarud, W., Sirivat, A., & Larson, R. G. (2002). Influence of elasticity on dispersed-phase droplet size in immiscible polymer blends in simple shearing flow. *Polymer Engineering & Science*, 42(4), 798–809. <https://doi.org/10.1002/PEN.10992>
- Lie-Piang, A., Braconi, N., Boom, R. M., & van der Padt, A. (2021). Less refined ingredients have lower environmental impact – A life cycle assessment of protein-rich ingredients from oiland starch-bearing crops. *J. Clean. Prod.*, 292. Retrieved from <https://doi.org/10.1016/j.jclepro.2021.126046>
- Liu, H., Shen, Y., Yang, S., Zheng, P., & Zhang, L. (2017). A comprehensive solution to miniaturized tensile testing: Specimen geometry optimization and extraction of constitutive behaviors using inverse FEM procedure. *Fusion Engineering and Design*, 121, 188–197. <https://doi.org/10.1016/j.fusengdes.2017.07.016>
- Liu, Y., Zhang, Y., Guo, Z., Wang, C., Kang, H., Li, J., ... Liu, Y. (2021). Enhancing the functional characteristics of soy protein isolate via cross-linking catalyzed by *Bacillus subtilis* transglutaminase. *Journal of the Science of Food and Agriculture*, 101(10), 4154–4160. <https://doi.org/10.1002/jsfa.11052>
- Lu, R., & Abbott, J. A. (2004). Force/deformation techniques for measuring texture. *Texture in Food* (Vol. 2). Woodhead Publishing Limited. <https://doi.org/10.1533/978185538362.2.109>
- Luyckx, T., Verstraete, M., De Roo, K., De Waele, W., Bellemans, J., & Victor, J. (2014). Digital image correlation as a tool for three-dimensional strain analysis in human tendon tissue. *Journal of Experimental Orthopaedics*, 1(1), 1–9. <https://doi.org/10.1186/s40634-014-0007-8>
- Luyten, H., Van Vliet, T., & Walstra, P. (1992). Comparison of Various Methods To Evaluate Fracture Phenomena in Food Materials. *Journal of Texture Studies*, 23(3), 245–266. <https://doi.org/10.1111/j.1745-4603.1992.tb00524.x>
- Ma, Y., Potappel, J., Chauhan, A., Schutyser, M. A. I., Boom, R. M., & Zhang, L. (2023). Improving 3D food printing performance using computer vision and feedforward nozzle motion control. *Journal of Food Engineering*, 339, 11277. <https://doi.org/https://doi.org/10.1016/j.jfoodeng.2022.11277>
- Ma, Y., Potappel, J., Schutyser, M. A. I., Boom, R. M., & Zhang, L. (2023). Quantitative analysis of 3D food printing layer extrusion accuracy: Contextualizing automated image analysis with human evaluations: Quantifying 3D food printing accuracy. *Current Research in Food Science*, 6(February), 100511. <https://doi.org/10.1016/j.crfs.2023.100511>
- Malik, M. A., & Saini, C. S. (2017). Polyphenol removal from sunflower seed and kernel: Effect on functional and rheological properties of protein isolates. *Food Hydrocolloids*, 63, 705–715. <https://doi.org/10.1016/j.foodhyd.2016.10.026>
- Marlow, P. J., Gegenfurtner, K. R., & Anderson, B. L. (2022). The role of color in the perception of three-dimensional shape. *Current Biology*, 32(6), 1387–1394.e3. <https://doi.org/10.1016/j.cub.2022.01.026>
- Marques, S. P. C., & Creus, G. J. (2012). *Computational Viscoelasticity*. Computational Mechanics (Vol. 6). Springer.
- Mattice, K. D., & Marangoni, A. G. (2021). Physical properties of zein networks treated with microbial transglutaminase. *Food Chemistry*, 338(September 2020), 128010. <https://doi.org/10.1016/j.foodchem.2020.128010>
- McClements, D. J., & Grossmann, L. (2022). Next-Generation Plant-based Foods Design, Production, and Properties. Springer.
- McClements, D. J., Weiss, J., Kinchla, A. J., Nolden, A. A., & Grossmann, L. (2021). Methods for Testing the Quality Attributes of Plant-Based Foods : Meat- and Processed-Meat Analogs, 1–30.
- McWatters, K. H. (1983). Compositional, physical, and sensory characteristics of akara processed from cowpea paste and nigerian cowpea flour. *American Association of Cereal Chemists*, 60(5), 333–336.

-
- Mession, J. L., Sok, N., Assifaoui, A., & Saurel, R. (2013). Thermal denaturation of pea globulins (*Pisum sativum* L.) - Molecular interactions leading to heat-induced protein aggregation. *Journal of Agricultural and Food Chemistry*, 61(6), 1196–1204. <https://doi.org/10.1021/jf303739n>
- Michel, F., Hartmann, C., & Siegrist, M. (2021). Consumers' associations, perceptions and acceptance of meat and plant-based meat alternatives. *Food Quality and Preference*, 87(August 2020), 104063. <https://doi.org/10.1016/j.foodqual.2020.104063>
- Mighri, F., Carreau, P. J., & Ajji, A. (1998). Influence of elastic properties on drop deformation and breakup in shear flow. *Journal of Rheology*, 42(6), 1477–1490. <https://doi.org/10.1122/1.550897>
- Mofoluke, A. A., Olusegun, A. S., Adeoye, O. S., Ramota, K. O., & Toyin, O. A. (2013). Physico-chemical Properties and akara making potentials of pre-processed Jack Beans (*Canavalia ensiformis*) and Cowpea (*Vigna unguiculata* L. Walp) Composite Flour. *Croatian Journal of Food Technology, Biotechnology and Nutrition*, 8(3–4), 102–110.
- Möller, A. C., van der Padt, A., & van der Goot, A. J. (2021). From raw material to mildly refined ingredient – Linking structure to composition to understand fractionation processes. *Journal of Food Engineering*, 291. <https://doi.org/10.1016/j.jfoodeng.2020.110321>
- Monnet, A. F., Laleg, K., Michon, C., & Micard, V. (2019). Legume enriched cereal products: A generic approach derived from material science to predict their structuring by the process and their final properties. *Trends Food Sci. Technol.* Retrieved from <https://doi.org/10.1016/j.tifs.2019.02.027>
- Moreno, H. M., Tovar, C. A., Domínguez-Timón, F., Cano-Báez, J., Díaz, M. T., Pedrosa, M. M., & Borderías, A. J. (2020). Gelation of commercial pea protein isolate: Effect of microbitransglutaminase and thermal processing. *Food Science and Technology*, 40(4), 800–809. <https://doi.org/10.1590/fst.19519>
- Motoki, M., & Kumazawa, Y. (2000). Recent Research Trends in Transglutaminase Technology for Food Processing. *Food Science and Technology Research*, 6(3), 151–160. <https://doi.org/10.3136/fstr.6.151>
- Mubarak, A. E. (2005). Nutritional composition and antinutritional factors of mung bean seeds (*Phaseolus aureus*) as affected by some home traditional processes. *Food Chemistry*, 89(4), 489–495. <https://doi.org/10.1016/j.foodchem.2004.01.007>
- Mukherjee, S., & Sarkar, K. (2009). Effects of viscosity ratio on deformation of a viscoelastic drop in a Newtonian matrix under steady shear. *J. Non-Newtonian Fluid Mech*, 160, 104–112. <https://doi.org/10.1016/j.jnnfm.2009.03.007>
- Nežerka, V., Antoš, J., Sajdllová, T., & Tesárek, P. (2016). Use of Open Source DIC Tools for Analysis of Multiple Cracking in Fiber-Reinforced Concrete. *Applied Mechanics and Materials*, 827(February), 336–339. <https://doi.org/10.4028/www.scientific.net/amm.827.336>
- Nieuwland, M., Heijnis, W., van der Goot, A. J., & Hamoen, R. (2023). XRT for visualizing microstructure of extruded meat replacers. *Current Research in Food Science*, 6(December 2022), 100457. <https://doi.org/10.1016/j.crfs.2023.100457>
- Nivala, O., Mäkinen, O. E., Kruus, K., Nordlund, E., & Ercili-Cura, D. (2017). Structuring colloidal oat and faba bean protein particles via enzymatic modification. *Food Chemistry*, 231, 87–95. <https://doi.org/10.1016/j.foodchem.2017.03.114>
- Nivala, O., Nordlund, E., Kruus, K., & Ercili-Cura, D. (2021). The effect of heat and transglutaminase treatment on emulsifying and gelling properties of faba bean protein isolate. *Lwt*, 139(July 2020), 110517. <https://doi.org/10.1016/j.lwt.2020.110517>
- Opazo-Navarrete, M., Schutyser, M. A. I., Boom, R. M., & Janssen, A. E. M. (2018). Effect of pre-treatment on in vitro gastric digestion of quinoa protein (*Chenopodium quinoa* Willd.) obtained by wet and dry fractionation. *International Journal of Food Sciences and Nutrition*, 69(1), 1–11. <https://doi.org/10.1080/09637486.2017.1332171>
- Osen, R., Toelstede, S., Wild, F., Eisner, P., & Schweiggert-Weisz, U. (2014). High moisture extrusion cooking of pea protein isolates: Raw material characteristics, extruder responses, and texture properties. *Journal of Food Engineering*, 127, 67–74. <https://doi.org/10.1016/j.jfoodeng.2013.11.023>
- Paredes-Lopez, O., Ordorica-Falomir, C., & Olivarez-Vazquez, M. R. (1991). Chickpea Protein Isolates: Nutritional Characterization Functional and Nutritional Characterization. *Journal of Food Science*, 56(3), 3–6.
- Park, H. W., Park, J. W., & Yoon, W. B. (2023). The Relationship between Penetration, Tension, and Torsion for the Fracture of Surimi Gels: Application of Digital Image Correlation (DIC). *Processes*, 11(265).
- Pelgrom, P. J. M., Boom, R. M., & Schutyser, M. A. I. (2015a). Functional analysis of mildly refined fractions from yellow pea. *Food Hydrocolloids*, 44, 12–22. <https://doi.org/10.1016/j.foodhyd.2014.09.001>

- Pelgrom, P. J. M., Boom, R. M., & Schutyser, M. A. I. (2015b). Method Development to Increase Protein Enrichment During Dry Fractionation of Starch-Rich Legumes. *Food and Bioprocess Technology*, 8(7), 1495–1502. <https://doi.org/10.1007/s11947-015-1513-0>
- Pelgrom, P. J. M., Vissers, A. M., Boom, R. M., & Schutyser, M. A. I. (2013). Dry fractionation for production of functional pea protein concentrates. *Food Research International*, 53(1), 232–239. <https://doi.org/10.1016/j.foodres.2013.05.004>
- Pietsch, V. L., Werner, R., Karbstein, H. P., & Emin, M. A. (2019). High moisture extrusion of wheat gluten: Relationship between process parameters, protein polymerization, and final product characteristics. *Journal of Food Engineering*, 259(January 2018), 3–11. <https://doi.org/10.1016/j.jfoodeng.2019.04.006>
- Plant, A.R., & Moore, K.G. (1983). The protein, lipid and carbohydrate composition of protein bodies from *Lupinus angustifolius* seeds. *Phytochemistry*, 22(11), 2359–2363.
- Poynting, J. H. (1909). On Pressure Perpendicular to the Shear Planes in Finite Pure Shears, and on the Lengthening of Loaded Wires when Twisted. *Proceedings of the Royal Society A: Mathematical, Physical and Engineering Sciences*, 82, 546–559.
- Prinyawiwatkul, W., McWatters, K. H., Beuchat, L. R., & Phillips, R. D. (1996). Cowpea Flour: A Potential Ingredient in Food Products. *Critical Reviews in Food Science and Nutrition*, 36(5), 413–436. <https://doi.org/10.1080/10408399609527734>
- Qiu, Y., McClements, D. J., Chen, J., Li, C., Liu, C., & Dai, T. (2023). Construction of 3D printed meat analogs from plant-based proteins: Improving the printing performance of soy protein- and gluten-based pastes facilitated by rice protein. *Food Research International*, 167(September 2022), 112635. <https://doi.org/10.1016/j.foodres.2023.112635>
- Rahma, E. H., Dudek, S., Mothes, R., Görnitz, E., & Schwenke, K. D. (2000). Physicochemical characterization of mung bean (*Phaseolus aureus*) protein isolates. *Journal of the Science of Food and Agriculture*, 80(4), 477–483. [https://doi.org/10.1002/\(SICI\)1097-0010\(200003\)](https://doi.org/10.1002/(SICI)1097-0010(200003)477-483)
- Ranasinghesagara, J., Hsieh, F.-H., Huff, H., & Yao, G. (2009). Laser Scanning System for Real-Time Mapping of Fiber Formations in Meat. *Food Engineering and Physical Properties*, 74(2). <https://doi.org/10.1111/j.1750-3841.2008.01032.x>
- Ranasinghesagara, J., Hsieh, F., & Yao, G. (2005). An Image Processing Method for Quantifying Fiber Formation in Meat Analogs Under High Moisture Extrusion. *Food Engineering and Physical Properties*, 70(8), 450–454.
- Ranasinghesagara, J., Hsieh, F., & Yao, G. (2006). A photon migration method for characterizing fiber formation in meat analogs. *Journal of Food Science*, 71(5). <https://doi.org/10.1111/j.1750-3841.2006.00038.x>
- Ratnayake, W. S., Hoover, R., & Warkentin, T. (2002). Pea starch: Composition, structure and properties - A review. *Starch/Stärke*, 54(6), 217–234. [https://doi.org/10.1002/1521-379X\(200206\)54:6<217::AID-STAR217>3.0.CO;2-R](https://doi.org/10.1002/1521-379X(200206)54:6<217::AID-STAR217>3.0.CO;2-R)
- Ridout, M. S., & Linkie, M. (2009). Estimating overlap of daily activity patterns from camera trap data. *Journal of Agricultural, Biological, and Environmental Statistics*, 14(3), 322–337. <https://doi.org/10.1198/jabes.2009.08038>
- Rivera, J., Siliveru, K., & Li, Y. (2022). A comprehensive review on pulse protein fractionation and extraction: processes, functionality, and food applications. *Critical Reviews in Food Science and Nutrition*, 62(1), 1–23. <https://doi.org/10.1080/10408398.2022.2139223>
- Ruzengwe, F. M., Amonsou, E. O., & Kudanga, T. (2020). Transglutaminase-mediated crosslinking of Bambara groundnut protein hydrogels: Implications on rheological, textural and microstructural properties. *Food Research International*, 137(May), 109734. <https://doi.org/10.1016/j.foodres.2020.109734>
- Saldanha do Carmo, C., Silventoinen, P., Nordgård, C. T., Poudroux, C., Dessev, T., Zobel, H., ... Sahlström, S. (2020). Is dehulling of peas and faba beans necessary prior to dry fractionation for the production of protein- and starch-rich fractions? Impact on physical properties, chemical composition and technological properties. *Journal of Food Engineering*, 278. <https://doi.org/10.1016/j.jfoodeng.2020.109937>
- Saldanha do Carmo, C., Knutsen, S. H., Malizia, G., Dessev, T., Geny, A., Zobel, H., Myhrer, K. S., Varela, P., Sahlström, S. (2021). Meat analogues from a faba bean concentrate can be generated by high moisture extrusion. *Future Foods*, 3: 100014. <https://doi.org/10.1016/j.fufo.2021.100014>
- Salimi, A., Abbassi-Sourki, F., Karrabi, M., & Reza Ghoreishy, M. H. (2021). Investigation on viscoelastic behavior of virgin EPDM/ reclaimed rubber blends using Generalized Maxwell Model (GMM). *Polymer Testing*, 93, 106989. <https://doi.org/10.1016/j.polymertesting.2020.106989>
- Samard, S., & Ryu, G. H. (2019). Physicochemical and functional characteristics of plant protein-based meat analogs. *Journal of Food Processing and Preservation*, 43(10), 1–11. <https://doi.org/10.1111/jfpp.14123>

-
- Schab, D., Tiedemann, L., Rohm, H., & Zahn, S. (2022). Application of a Tensile Test Method to Identify the Ductile-Brittle Transition of Caramel. *Foods*, 11(20). <https://doi.org/10.3390/foods11203218>
- Schäfer, C., Zacherl, C., Engel, K.-H. H., Neidhart, S., & Carle, R. (2007). Comparative study of gelation and cross-link formation during enzymatic texturisation of leguminous proteins. *Innovative Food Science & Emerging Technologies*, 8(2), 269–278. <https://doi.org/10.1016/j.ifset.2007.01.005>
- Schlangen, M., Dinani, S. T., Schutyser, M. A. I., & van der Goot, A. J. (2022). Dry fractionation to produce functional fractions from mung bean, yellow pea and cowpea flour. *Innovative Food Science and Emerging Technologies*, 78(103018), 1–11. <https://doi.org/https://doi.org/10.1016/j.ifset.2022.103018>
- Schlangen, M., Ribberink, M. A., Taghian, S., Sagis, L. M. C., & van der Goot, A. J. (2023). Mechanical and rheological effects of transglutaminase treatment on dense plant protein blends. *Food Hydrocolloids*, 136(PA), 108261. <https://doi.org/10.1016/j.foodhyd.2022.108261>
- Schlangen, M., Schlangen, E., & van der Goot, A. J. (2023). Advanced tensile testing as a new tool to quantify properties of food. *Current Research in Food Science*, 7(May), 100577. <https://doi.org/10.1016/j.crfs.2023.100577>
- Schreuders, F.K.G., Sagis, L. M. C., Bodnar, I., Erni, P., Boom, R. M., & Goot, A. J. Van Der. (2021). Small and large oscillatory shear properties of concentrated proteins. *Food Hydrocolloids*, 110(June 2020). <https://doi.org/10.1016/j.foodhyd.2020.106172>
- Schreuders, F. K. G., Dekkers, B. L., Bodnár, I., Erni, P., Boom, R. M., & van der Goot, A. J. (2019). Comparing structuring potential of pea and soy protein with gluten for meat analogue preparation. *Journal of Food Engineering*, 261(April), 32–39. <https://doi.org/10.1016/j.jfoodeng.2019.04.022>
- Schreuders, F. K. G., Bodnár, I., Erni, P., Boom, R. M. & van der Goot, A. J. (2020). Water redistribution determined by time domain NMR explains rheological properties of dense fibrous protein blends at high temperature. *Food Hydrocolloids*. 101: 105562. <https://doi.org/10.1016/j.foodhyd.2019.105562>
- Schreuders, F. K. G., Sagis, L. M. C., Bodnár, I., Boom, R. M., & van der Goot, A. J. (2022). Non-linear rheology reveals the importance of elasticity in meat and meat analogues. *Scientific Reports*, 12(1), 1–11. <https://doi.org/10.1038/s41598-021-04478-z>
- Schreuders, F. K. G., Sagis, L. M. C., Bodnár, I., Erni, P., Boom, R. M., & van der Goot, A. J. (2021). Mapping the texture of plant protein blends for meat analogues. *Food Hydrocolloids*, 118(February). <https://doi.org/10.1016/j.foodhyd.2021.106753>
- Schreuders, F. K.G., Schlangen, M., Bodnár, I., Erni, P., Boom, R. M., & van der Goot, A. J. (2021). Structure formation and non-linear rheology of blends of plant proteins with pectin and cellulose. *Food Hydrocolloids*, 124(September 2021), 107327. <https://doi.org/10.1016/j.foodhyd.2021.107327>
- Schreuders, F. K.G., Schlangen, M., Kyriakopoulou, K., Boom, R. M., & van der Goot, A. J. (2021). Texture methods for evaluating meat and meat analogue structures: A review. *Food Control*, 127(April), 108103. <https://doi.org/10.1016/j.foodcont.2021.108103>
- Schreuders, F. K. G. (2021). PhD thesis Structuring pea towards meat analogues.
- Schutyser, M. A. I., Pelgrom, P. J. M., van der Goot, A. J., & Boom, R. M. (2015). Dry fractionation for sustainable production of functional legume protein concentrates. *Trends in Food Science & Technology*, 45(2), 327–335. <https://doi.org/10.1016/j.tifs.2015.04.013>
- Schutyser, M. A. I., & van der Goot, A. J. (2011). The potential of dry fractionation processes for sustainable plant protein production. *Trends in Food Science and Technology*, 22(4), 154–164. <https://doi.org/10.1016/j.tifs.2010.11.006>
- Shand, P. J. J., Ya, H., Pietrasik, Z., & Wanasundara, P. K. J. P. D. K. J. P. D. (2008). Transglutaminase treatment of pea proteins: Effect on physicochemical and rheological properties of heat-induced protein gels. *Food Chemistry*, 107(2), 692–699. <https://doi.org/https://doi.org/10.1016/j.foodchem.2007.08.095>
- Sharma, R., Kumar, M., & Alam, M. S. (2021). Image processing techniques to estimate weight and morphological parameters for selected wheat refractions. *Scientific Reports*, 11(1), 1–12. <https://doi.org/10.1038/s41598-021-00081-4>
- Shurtleff, W., & Aoyagi, A. (2013). History of Meat Alternatives.
- Silventoinen, P., Rommi, K., Holopainen-Mantila, U., Poutanen, K., & Nordlund, E. (2019). Biochemical and Techno-Functional Properties of Protein- and Fibre-Rich Hybrid Ingredients Produced by Dry Fractionation from Rice Bran. *Food and Bioprocess Technology*, 12(9), 1487–1499. <https://doi.org/10.1007/s11947-019-02307-w>
- Silventoinen, P., Sipponen, M. H., Holopainen-Mantila, U., Poutanen, K., & Sozer, N. (2018). Use of air classification technology to produce protein-enriched barley ingredients. *Journal of Food Engineering*,

- 222, 169–177. <https://doi.org/10.1016/j.jfoodeng.2017.11.016>
- Singh, H. (1991). Modification of food proteins by covalent crosslinking. *Trends in Food Science and Technology*, 2(C), 196–200. [https://doi.org/10.1016/0924-2244\(91\)90683-A](https://doi.org/10.1016/0924-2244(91)90683-A)
- Singh, N., Nakaura, Y., Inouchi, N., & Nishinari, K. (2008). Structure and viscoelastic properties of starches separated from different legumes. *Starch/Staerke*, 60(7), 349–357. <https://doi.org/10.1002/star.200800689>
- Sliwinski, E. L., Kolster, P., & van Vliet, T. (2004). Large-deformation properties of wheat dough in uni- and biaxial extension. Part I. Flour dough. *Rheologica Acta*, 43(4), 306–320. <https://doi.org/10.1007/s00397-003-0344-5>
- Snel, S. J. E., Bellwald, Y., van der Goot, A. J., & Beyrer, M. (2022). Novel rotating die coupled to a twin-screw extruder as a new route to produce meat analogues with soy, pea and gluten. *Innovative Food Science and Emerging Technologies*, 81(May), 103152. <https://doi.org/10.1016/j.ifset.2022.103152>
- Steffe, J. F. (1992). *Rheological Methods in Food Process Engineering*. Freeman Press (Second edi). Freeman Press. <https://doi.org/10.1016/b978-1-4832-3245-4.50016-9>
- Sun, X. D., & Arntfield, S. D. (2011). Gelation properties of salt-extracted pea protein isolate catalyzed by microbial transglutaminase cross-linking. *Food Hydrocolloids*, 25(1), 25–31. <https://doi.org/10.1016/j.foodhyd.2010.05.002>
- Svihus, B., & Hervik, A. K. (2016). Digestion and metabolic fates of starch and its relation to major nutrition-related health. *Starch*, 68, 302–313. <https://doi.org/10.1002/star.201500295>
- Taghian Dinani, S., Charles Carrillo, M. F., Boom, R., & van der Goot, A. J. (2023). Quality improvement of plant-based meat alternatives by addition of iota carrageenan to pea protein–wheat gluten blend. *European Food Research and Technology*, (0123456789). <https://doi.org/10.1007/s00217-023-04244-7>
- Taghian Dinani, S., van der Harst, J. P., Boom, R., & van der Goot, A. J. (2023). Effect of L-cysteine and L-ascorbic acid addition on properties of meat analogues. *Food Hydrocolloids*, 134(August 2022). <https://doi.org/10.1016/j.foodhyd.2022.108059>
- Taheri-Garavand, A., Fatahi, S., Omid, M., & Makino, Y. (2019). Meat quality evaluation based on computer vision technique: A review. *Meat Science*, 156(December 2018), 183–195. <https://doi.org/10.1016/j.meatsci.2019.06.002>
- Tamayo Tenorio, A., Kyriakopoulou, K. E., Suarez-Garcia, E., van den Berg, C., & van der Goot, A. J. (2018). Understanding differences in protein fractionation from conventional crops, and herbaceous and aquatic biomass - Consequences for industrial use. *Trends in Food Science and Technology*, 71(August 2017), 235–245. <https://doi.org/10.1016/j.tifs.2017.11.010>
- Tang, C. H., & Sun, X. (2010). Physicochemical and structural properties of 8S and/or 11S globulins from mungbean [*Vigna radiata* (L.) Wilczek] with various polypeptide constituents. *Journal of Agricultural and Food Chemistry*, 58(10), 6395–6402. <https://doi.org/10.1021/jf904254f>
- Tolstoguzov, V. B. (2006). Texturising by phase separation. *Biotechnology Advances*, 24, 626–628. <https://doi.org/10.1016/j.biotechadv.2006.07.001>
- Tombs, M. P. (1967). Protein bodies of the soybean. *Plant physiology*, 42(6), 797–813.
- Tomić, J., Torbica, A., & Belović, M. (2020). Effect of non-gluten proteins and transglutaminase on dough rheological properties and quality of bread based on millet (*Panicum miliaceum*) flour. *Lwt*, 118(June 2019). <https://doi.org/10.1016/j.lwt.2019.108852>
- Tyler, R. T., Youngs, C. G., & Sosulski, F. W. (1981). Air classification of legumes. I. Separation efficiency, yield and composition of the starch and protein fractions. *Cereal Chemistry*. Retrieved from https://www.aaccnet.org/publications/cc/backissues/1981/Documents/chem58_144.pdf
- van der Sman, R. G. M., & van der Goot, A. J. (2023). Hypotheses concerning structuring of extruded meat analogs. *Current Research in Food Science*, 6(April), 100510. <https://doi.org/10.1016/j.crfs.2023.100510>
- van Mier, J. G. M. (1997). *Fracture Processes of Concrete*. Taylor & Francis.
- van Mier, J. G. M., & van Vliet, M. R. A. (2002). Uniaxial tension test for the determination of fracture parameters of concrete : state of the art. *Engineering Fracture Mechanics*, 69, 235–247.
- van Vliet, T. (1996). Large deformation and fracture behaviour of gels. *Current Opinion in Colloid & Interface Science*, 1(6), 740–745. [https://doi.org/10.1016/s1359-0294\(96\)80075-6](https://doi.org/10.1016/s1359-0294(96)80075-6)
- van Vliet, T. (2013). Rheology and fracture mechanics of foods. *Rheology and Fracture Mechanics of Foods*. <https://doi.org/10.1201/b15681>
- Vatansever, S., Tulbek, M. C., & Riaz, M. N. (2020). Low- and High-Moisture Extrusion of Pulse Proteins as

- Plant-Based Meat Ingredients: A Review. *Cereal Foods World*, 65(4). <https://doi.org/10.1094/cfw-65-4-0038>
- Vogelsang-O'Dwyer, M., Petersen, I. L., Joehnke, M. S., Sørensen, J. C., Bez, J., Detzel, A., ... Zannini, E. (2020). Comparison of Faba bean protein ingredients produced using dry fractionation and isoelectric precipitation: Techno-functional, nutritional and environmental performance. *Foods*, 9(3), 1–25. <https://doi.org/10.3390/foods9030322>
- Vogelsang-O'Dwyer, M., Zannini, E., & Arendt, E. K. (2021). Production of pulse protein ingredients and their application in plant-based milk alternatives. *Trends in Food Science and Technology*, 110(January), 364–374. <https://doi.org/10.1016/j.tifs.2021.01.090>
- Wang, Z., Tian, B., Boom, R., & Goot, A. J. Van Der. (2019). Air bubbles in calcium caseinate fibrous material enhances anisotropy. *Food Hydrocolloids*, 87(May 2018), 497–505. <https://doi.org/10.1016/j.foodhyd.2018.08.037>
- Warhawk Air Museum. (2019). From meatless Monday to Chef Boyardee. Retrieved October 31, 2023, from <https://warhawkairmuseum.org/blog/from-meatless-monday-to-chef-boyardee-the-surprising-lasting-effects-of-wartime-rationing/>
- Webb, D., Dogan, H., & Li, Y. (2023). Physico-Chemical Properties and Texturization of Pea, Wheat and Soy Proteins Using Extrusion and Their Application in Plant-Based Meat. *Foods*, 12(8). <https://doi.org/10.3390/foods12081586>
- Wittek, P., Karbstein, H. P., & Emin, M. A. (2021). Blending proteins in high moisture extrusion to design meat analogues: Rheological properties, morphology development and product properties. *Foods*, 10(7). <https://doi.org/10.3390/foods10071509>
- Wittek, P., Zeiler, N., Karbstein, H. P., & Emin, M. A. (2020). Analysis of the complex rheological properties of highly concentrated proteins with a closed cavity rheometer. *Applied Rheology*, 30(1), 64–76. <https://doi.org/10.1515/arh-2020-0107>
- Xia, H., Li, L., Tan, C., Yang, J., Li, H., Song, W., ... Ma, N. (2022). In situ SEM study on tensile fractured behavior of Al/steel laser welding-brazing interface. *Materials and Design*, 224, 11320. <https://doi.org/10.1016/j.matdes.2022.11320>
- Xing, Q., Utami, D. P., Dematthey, M. B., Kyriakopoulou, K., de Wit, M., Boom, R. M., & Schutyser, M. A. I. (2020). A two-step air classification and electrostatic separation process for protein enrichment of starch-containing legumes. *Innovative Food Science and Emerging Technologies*, 66(August), 102480. <https://doi.org/10.1016/j.ifset.2020.102480>
- Yi-Shen, Z., Shuai, S., & Fitzgerald, R. (2018). Mung bean proteins and peptides: Nutritional, functional and bioactive properties. *Food and Nutrition Research*, 62, 1–11. <https://doi.org/10.29219/fnr.v62.1290>
- Yousfi, M., Dadouche, T., Chomat, D., Samuel, C., Soulestin, J., Lacrampe, M. F., & Krawczak, P. (2018). Development of nanofibrillar morphologies in poly(l-lactide)/poly(amide) blends: Role of the matrix elasticity and identification of the critical shear rate for the nodular/fibrillar transition. *RSC Advances*, 8(39), 22023–22041. <https://doi.org/10.1039/c8ra03339k>
- Yu, W., Bousmina, M., Zhou, C., & Tucker, C. L. (2004). Theory for drop deformation in viscoelastic systems. *Journal of Rheology*, 48(2), 417–438. <https://doi.org/10.1122/1.1647559>
- Zapotoczny, P., Zielinska, M., & Nita, Z. (2008). Application of image analysis for the varietal classification of barley: Morphological features. *Journal of Cereal Science*, 48(1), 104–110. <https://doi.org/10.1016/j.jcs.2007.08.006>
- Zayas, J. F. (1997). *Functionality of Proteins in Food*. Springer. Springer.
- Zhang, J., Chen, Q., Liu, L., Zhang, Y., He, N., & Wang, Q. (2021). High-moisture extrusion process of transglutaminase-modified peanut protein: Effect of transglutaminase on the mechanics of the process forming a fibrous structure. *Food Hydrocolloids*, 112(September 2020), 106346. <https://doi.org/10.1016/j.foodhyd.2020.106346>
- Zhang, Y., Zheng, J., Xia, Y., Shou, H., Tan, W., Han, W., & Liu, Q. (2020). Porosity quantification for ductility prediction in high pressure die casting AM60 alloy using 3D X-ray tomography. *Materials Science and Engineering: A*, 772(December 2019), 138781. <https://doi.org/10.1016/j.msea.2019.138781>
- Zhong, Z., & Xiong, Y. L. (2020). Thermo-sonication-induced structural changes and solution properties of mung bean protein. *Ultrasonics Sonochemistry*, 62(August 2019), 104908. <https://doi.org/10.1016/j.ultsonch.2019.104908>
- Zhou, J. W., Liu, D. H., Shao, L. Y., & Wang, Z. L. (2013). Application of digital image correlation to measurement of packaging material mechanical properties. *Mathematical Problems in Engineering*, 2013(Dic). <https://doi.org/10.1155/2013/204875>

- Zhu, H. G., Tang, H. Q., Cheng, Y. Q., Li, Z. G., & Tong, L. T. (2021). Potential of preparing meat analogue by functional dry and wet pea (*Pisum sativum*) protein isolate. *Lwt*, 148(January), 111702. <https://doi.org/10.1016/j.lwt.2021.111702>
- Zhu, H. G., Wang, Y., Cheng, Y. Q., Li, Z. G., & Tong, L. T. (2020). Optimization of the powder state to enhance the enrichment of functional mung bean protein concentrates obtained by dry separation. *Powder Technology*, 373, 681–688. <https://doi.org/10.1016/j.powtec.2020.07.023>
- Zink, J. I., Zeneli, L., Windhab, E. J. (2023). Micro-foaming of plant protein based meat analogues for tailored textural properties. *Current Research in Food Science*. 7: 100580. <https://doi.org/10.1016/j.crfs.2023.100580>
- Zwinkels, J., Wolkers-Rooijackers, J., & Smid, E. J. (2023). Solid-state fungal fermentation transforms low-quality plant-based foods into products with improved protein quality. *Lwt*, 184(June), 114979. <https://doi.org/10.1016/j.lwt.2023.114979>



S

Summary

Meat analogues, with high similarity to texture of animal meat, are a route to help consumers to lower their meat intake. Most commercial meat analogues are currently produced from highly refined protein ingredients made from soy or pea. However, the process to obtain these ingredients requires large amounts of water, energy, and chemicals. As an alternative, dry fractionation methods can be used to obtain protein-rich ingredients. The overall aim of this thesis therefore was to investigate the potential of dry fractionation as a route to produce protein-rich ingredients for meat analogue product applications. Specifically mung bean was targeted as a crop to produce protein-rich ingredients, due to its recognized protein functionality.

Chapter 1 gives an overview of the history of meat analogues from the first meat analogue based on tofu in 965, to the first commercial meat analogue in 1890, and the new structuring technologies being developed nowadays. Furthermore, we outlined the fractionation procedures, functionality, and modification of meat analogue ingredients and the texture characterization of meat analogue products.

In **Chapter 2**, dry fractionation of mung bean, yellow pea, and cowpea was explored as a method to obtain functional protein-rich ingredients. Dry fractionation yielded fine fractions with 42 to 58 wt.% protein, depending on crop and air classification processing settings. In addition to protein content, functional properties of the ingredients were also investigated. We highlighted that fine fractions formed stronger gels after heating than flours and coarse fractions. Furthermore, the water holding capacity of the resulting fractions was correlated to protein content. Dry fractionated fine fractions from mung bean exhibited specifically high water holding capacity, low least gelation concentration, and favourable rheological properties. Therefore, mung bean fine fractions were considered as promising candidates for incorporation into meat analogues.

We studied the potential of enzymatic crosslinking to enhance functional properties of mung bean protein and pea protein in **Chapter 3** and **Chapter 4**. In **Chapter 3**, transglutaminase was added to mung bean protein isolate and pea protein isolate and processed into gels and meat analogues with the high temperature shear cell. We showed that transglutaminase affected pea protein isolate to a larger extent than mung bean protein isolate. In pea protein isolate gels, transglutaminase improved tensile strength and extended the linear viscoelastic regime. In both proteins, the extent of transglutaminase crosslinking was related to incubation temperature and transglutaminase concentration, with 0.5 wt.% transglutaminase and 50 °C being optimal. Enzymatic crosslinking negatively influenced the macrostructure of the produced meat analogues. Given that enzyme kinetics are highly dependent on protein structure, we studied the relation between protein fractionation procedure and the ability of transglutaminase to crosslink the proteins in **Chapter 4**. Four dispersions of

4 wt.% mung bean protein were incubated with transglutaminase: (1) a fine fraction, (2) a heated fine fraction, (3) lab-scale wet fractioned isolate, and (4) a commercial protein isolate. Molecular crosslinking induced by transglutaminase occurred irrespective of the fractionation procedure, but the extent of crosslinking depended on the fraction used, as shown with gel electrophoresis. Molecular changes also resulted in colloidal changes for the fine fraction and heated fine fraction, such as increased particle size distribution and decreased dispersibility. Transglutaminase crosslinking improved the rheological properties of dispersions of the fractions, with the exception of the commercial protein isolate. Three crosslinking mechanisms were proposed to explain the different crosslinking effects of transglutaminase on the protein fractions. The commercial protein isolate mostly belongs to the first mechanism; a dense particle that does not swell upon hydration and remains rather inert. The fine fraction and heated fine fraction mostly belong to the second mechanism: swollen particles in which transglutaminase can diffuse, leading to both intra- and intermolecular crosslinks. The wet fractionated isolate belongs to the third mechanism; soluble proteins that can be readily crosslinked leading to still soluble aggregates or swollen particles.

The quantification of textural and mechanical properties of fibrous meat analogues was studied in **Chapter 5** and **Chapter 6**. **Chapter 5** describes the quantification of the visual internal structure of meat analogues through computer vision. Quantitative assessment of visual fibrousness of meat analogues relies on sensory data and is resource-intensive and time-consuming. We found that by segmentation and shape feature extraction of 2D meat analogue images we could characterize their fibrous structures. A strong correlation ($R^2 = 0.93$) was found between computed fibre scores (the ratio between fibre length and width) and expert panel evaluations. Structural similarity of meat analogues was compared to cooked chicken as a benchmark based on the extracted fibre shape features, such as fibre score, fibre area, and the number of fibre branches. Quantification of the visual fibrousness of meat analogues was thus deemed possible through computer vision. **Chapter 6** describes how advanced tensile testing can be used to quantify properties of food, more specifically, of meat analogues. Optimization of the tensile testing protocol was found to improve the interpretation of the resulting data due to prevention of rapid crack propagation. For example, a shorter tensile gauge length and a slower deformation rate provided additional insights in the fracture properties of the product. Additionally, digital image correlation, an image analysis technique, was used to obtain true distance data and a dynamic Poisson's ratio. Anisotropic products were found to exhibit heterogeneous, multi-stage fracture patterns, while isotropic products exhibited homogeneous fracture patterns.

Finally, in **Chapter 7**, we reflect on the results obtained in this thesis and take a look into the future. We demonstrated that dry fractionated protein-rich ingredients combined with transglutaminase can be successfully structured into fibrous meat analogues.

Thus, dry fractionation is a promising choice for the production of protein-rich meat analogue ingredients. Concerning the quantification of the structures formed, texture analyses of meat analogues so far was considered to comprise two elements: visual fibrousness and mechanical anisotropy. We found correlations between visual fibrousness (as characterized by computer vision) and fracture strain (as characterized by tensile testing). Additionally, we propose that fibrousness exists across multiple length scales. Finally, an outlook is given of how to shape the meat analogues of the future. Three opportunities were identified: ingredient requirements, protein quality, and data-driven solutions.

Acknowledgements

At the start of my PhD, I remember saying “the acknowledgements must be one of the most rewarding parts of the PhD thesis to write”. I still believe that now, perhaps I should have submitted that as one of my propositions. Over the past four years, many people have supported me in the PhD journey, be it through help in the lab, advice, fruitful discussions, or sports and leisure activities. I am grateful to each and every one of those people. There are some people that I would like to thank in particular.

To my promotor, **Atze Jan**, thank you for your supervision, advice, guidance, help, and patience over the past years. I truly value how you have given me the freedom to find and explore my own line of research, but at the same time you have given me enough guidance and gentle pushes in the right direction. That started with your belief and trust in me to let me write my own grant proposal for my PhD project. I have always appreciated your honesty and enthusiasm. I hope we can continue to work together in the future.

To my daily supervisors, **Konstantina & Somayeh**, thank you. **Konstantina**, thank you for guiding me throughout the first months of my PhD. **Somayeh**, thank you for your help, supervision, and crash course on statistical analyses during year two and three of my PhD journey.

To my supervisors in Aarhus, **Norbert & Milena**, it was great collaborating with you. **Norbert**, thank you for your help in the lab and many hours of advice on my research. I hope to see you soon in Denmark! **Milena**, thank you for opening up your lab and group to me, challenging me to rethink the concept of “solubility”, and teaching me about the physical-chemistry side of food.

To my non-promoting co-authors and collaborators, **Floor, Jan, Anna, Maarten, Lu, Leonard, and Remko**, thank you for your help and valuable suggestions over the years. I learned a lot from you! **Tom**, your unique vision on material science is inspiring. Thank you for the guidance and critical feedback you have given me. I also enjoyed co-supervising several students with you.

Good lab technicians are essential during a PhD project, fortunately we are very lucky within FPE. **Jarno**, thank you for all your help in the shear cell lab. **Jos**, thank you for your help with the Instron, multi-mill, and CCR, and the “goedemorgen” every morning at 7 AM. **Maurice**, thank you for your help with the SEM images of my powders and the fun collaboration in the DIPP practical. It was great to have a fellow bird watcher within FPE! **Martin**, thank you for taking care of the financial side of my project. **Wouter**, thank you for your help with the Mastersizer and Dumas. **Lyneth**, even though we have not really worked together, I am happy that you joined the lab technician team, you are a true addition!

Evelyn & Ilone, thank you for taking care of the administrative and organizational side of my project. Thanks to you the group runs like a well-oiled machine.

During my PhD project, I realized that there is a very fine line between colleagues and friends. To my colleagues who became my friends and to my friends who also became my colleagues, I am very grateful for your support over the past years.

Kieke & Melanie, bedankt dat jullie mijn paranimfen willen zijn. Ik vergeet niet snel de dag waarop we alle drie speciaal naar kantoor waren gekomen om 4 uur lang bij te praten over vakanties en belangrijke gebeurtenissen. Wanneer we iedere dag vanaf 11:30 uur al met smacht klaar zitten voor onze lunch besef ik maar weer wat een leuke en lieve collega's en vriendinnen jullie zijn! **Kieke**, naast dat wij letterlijk van kledingkast kunnen ruilen, zijn wij ook heel erg gelijk in doen en laten, fijn om altijd met jou te kunnen praten. Daarnaast is het meer dan het benoemen waard dat jouw doorzettingsvermogen inspirerend is. **Melanie**, ik waardeer al je advies over educatie, uitleg over racefietsen en uitgebreide routebeschrijvingen van skigebieden enorm. Bedankt dat je er altijd voor me bent. Ik kijk nu al uit naar ons 10-jaren plan.

Yizhou, being part of the “dream-team” with you was great. You always challenged me to think outside the box. I admire your creativity and problem-solving skills. Thank you for teaching me about coding and developing the Fiberlyzer with me. I will miss our weekly chats about science, pet projects, the academic world, and career aspirations. All the best for finishing up your own PhD project, I am sure you will nail it! **Silvia & Aadi**, thank you for being my vegan buddies in FPE! **Silvia**, ik vond het heel erg fijn dat ik jou heb leren kennen in het eerste jaar van mijn PhD, want wat heb ik veel aan jou gehad! Ik heb altijd erg uitgekeken naar de weken dat jij hier in Wageningen was. Ik hoop dat onze dagelijkse whatsappgesprekken over onze onderzoeken, vegan eten en nog veel meer nog lang zo doorgaan. **Aadi**, thank you for being you and the check-ins every once in a while! I enjoyed our chats a lot and will forever crave your Indian food, in particular idli! **Floor**, dankjewel voor je hulp, advies en gezelligheid tijdens de eerste maanden van mijn project. Wat heb ik veel geleerd van jou! **Yafei**, thank you for always being there for a chat and introducing me to my new favorite food: hotpot. **Silvia, Sten**, and **Loes**, ons tripje naar Maleisië na de PhD trip in Singapore blijft toch wel echt een highlight voor mij! **Sten**, bedankt dat je vroeg op wilde staan om wild en vogels te zoeken met mij!

Kieke, Melanie, Julia, Yhan, Aryo, Ruihao, Stefan, thank you for being the best office-mates! Our office is being referred to as “het gezellige kantoor” for a reason. **Julia**, thank you for turning my PhD thesis submission day into a small party.

Nienke K., Jolien, Yafei, Silvia, Steven, Jan, Anna, Floor, Atze Jan, Jarno, Wanqing, Punpun, Konstantina, and Somayeh, thank you for sharing your passion

and knowledge on plant proteins and meat analogues with me. It was a pleasure being part of the Food Structuring group. **Luc, Regina, Anneloes, Jolien, Murat, Sten, Solange, Nienke K., Nienke E., Martijn, Suzan, Judith, Yifeng, Lingfeng, Anouk, Laurens, Patrick, Zulhaj, Sybren, Joanne**, thank you for all the fun chats, lunch breaks, and sport activities!

One can learn a lot from a research visit abroad. **Julie, Katt, Simone, Dionysios, Gökhan, Sandra, Norbert, Milena**, tak til den varme velkomst på AU FOOD, masser af kaffe- og frokostpauser, gode snakke, og hjælp i lab. Vi ses!

To my talented students, **Aaron, Karlijn, Marieke, Stijn, Kimberly, Mike, Janneke, Merel, Rosanne, Jelle, Dylan, and Iris**, thank you for your motivation and contributions to my project. Your help has been essential to this PhD thesis. It was truly exciting to see all of you grow over the course of your thesis and I learned a lot from each of you!

Pien, Ward, Jasper Z., JW, bedankt voor alle gezamenlijke lunchpauzes op het Axis. **Pien**, dankjewel voor je vriendschap, steun, alle rondjes wandelen over campus, ritjes naar Arnhem om te boulderen en etentjes. Ik heb heel veel aan je gehad de afgelopen jaren. **Ward**, bedankt voor je eerlijkheid en alle interessante discussies over de meest willekeurige onderwerpen. Jouw gedachtegang is indrukwekkend. Met jouw hulp zijn mijn stellingen een stuk scherper geworden! **Jasper**, ook al liep het niet gelijk uit op een geweldig resultaat, ik vond het erg leuk om onze onderzoeken samen te combineren in het lab. **JW**, fijn om met jou samen in de Wageningen PhD Council te hebben gezeten, we waren een goed team!

Tot slot wil ik graag mijn familie en vrienden van buiten Wageningen bedanken. **Barbara**, bedankt voor alle spelletjesmiddagen, al het lekkere vegan eten, en onze nooit eindigende whatsappgesprekken! **Rebecca**, in een net ander veld, maar toch redelijk hetzelfde pad bewandeld door de jaren heen. Ik vond het erg leuk elkaar wat vaker te zien tijdens de weken dat je in Wageningen was voor onderzoek! **Emi & Jasper L.**, bedankt dat jullie altijd voor mij klaar staan! **Emi**, dankjewel voor je steun de afgelopen jaren. Wat is het fijn om jou als vriendin te hebben! Jij snapt mij door en door. **Jasper**, bedankt voor alle vogeltripjes, hulp bij het determineren en geklets over de academische wereld. **Petra & Erik**, bedankt voor alle wandelingen met de hond, het lekkere eten, de goede gesprekken, de inspiratie voor nieuwe onderzoeken, spelletjes en weekendjes weg de afgelopen jaren. **Bram**, bedankt voor je hulp bij het ontwerpen van mijn voorkant, interesse in mijn onderzoek en gezamenlijk snowboard- en bouldertripjes. Lieve **Koen**, jij hebt het laatste jaar van mijn PhD heel erg bijzonder gemaakt. Bedankt voor je steun, liefde, sportiviteit en alles wat je me biedt. Ik kijk enorm uit naar onze volgende stappen samen.

About the author

Miek Schlangen was born on the 22th of August 1996 in Delft, the Netherlands. She obtained her high school diploma in 2014 at Grotius College in Delft. Miek started her BSc in Food Technology at Wageningen University in 2014. In 2016, she took several food science related courses to complete a minor at the University of Copenhagen. Her dedication to science developed in 2017 when she finalized her BSc study with a thesis at the Food Process Engineering department about iron-fortification related protein oxidation in meat analogues.

Miek started her master in Food Technology with a specialisation in Product Design at Wageningen University in 2017. During her MSc thesis she returned to the Food Process Engineering department to study the role of biopolymers on structure formation of pea protein isolate with the shear cell technology. It was during this thesis that she found her true passion for this research field. Miek then finished her MSc degree in 2019 with an internship at De Vegetarische Slager in Breda by studying the difference in structuring behaviour between shear cell technology and extrusion.



After her MSc degree, Miek was certain that she wanted to continue in academia. She wrote a successful grant proposal for an international funding call to start her PhD project at the Food Process Engineering department at Wageningen University. Miek started as a PhD candidate in 2020 and studied the ingredients and texture of meat analogues. The results of her research are described in this thesis.

List of publications

This thesis:

M. Schlangen, S. Taghian Dinani, M.A.I. Schutyser, A.J. van der Goot. Dry fractionation to produce functional fractions from mung bean, yellow pea, and cowpea flour. *Innovative Food Science and Emerging Technologies*. (2022). 78: 103018.

M. Schlangen, M.A. Ribberink, S. Taghian Dinani, L.M.C. Sagis, A.J. van der Goot. Mechanical and rheological effects of transglutaminase treatment on dense plant protein blends. *Food Hydrocolloids*. (2023). 136: 108261.

M. Schlangen, N. Raak, S. Taghian Dinani, M. Corredig, A.J. van der Goot. How fractionation procedure of mung bean protein affects transglutaminase crosslinking. *Food Hydrocolloids*. (2023). 145: 109067.

Y. Ma¹, **M. Schlangen**¹, J. Potappel, L. Zhang, A.J. van der Goot. Quantitative characterizations of visual fibrousness in meat analogues using automated image analysis. *Journal of Texture Studies*. (2024). 55: e12806. ¹: joint first authors.

M. Schlangen, E. Schlangen, A.J. van der Goot. Advanced tensile testing as a new tool to quantify properties of food. *Current Research in Food Science*. (2023). 7: 100577.

Other publications:

P. Duque Estrada, C.C. Berton-Carabin, **M. Schlangen**, A. Haagsma, A.P.T.R. Pierucci, A.J. van der Goot. Protein oxidation in plant protein-based fibrous products: Effects of encapsulated iron and process conditions. *Journal of Agricultural and Food Chemistry*. (2018). 66: 11105.

F.K.G. Scheuders, **M. Schlangen**, K. Kyriakopoulou, R.M. Boom, A.J. van der Goot. Texture methods for evaluating meat and meat analogue structures: A review. *Food Control*. (2021). 127: 108103.

J.M. Bühler, **M. Schlangen**, A.C. Möller, M.E. Bruins, A.J. van der Goot. Starch in plant-based meat analogues: A new approach to using endogenous starch from cereals and legumes. *Starch-Stärke*. (2022). 74: 2100157.

F.K.G. Schreuders, **M. Schlangen**, I. Bodnár, P. Erni, R.M. Boom, A.J. van der Goot. Structure formation and non-linear rheology of blends of plant proteins with pectin and cellulose. *Food Hydrocolloids*. (2022). 124: 107327.

S.J.E. Snel, K. Otto, **M. Schlangen**, M. Beyrer, A.J. van der Goot. Type of pectin determines structuring potential of soy proteins into meat analogue applications. *Food Hydrocolloids*. (2024). 146: 109262.

Overview of completed training activities

Discipline specific activities	Organizer	Year
NIZO Plant Protein Conference	NIZO	2020
Food Proteins	University of Copenhagen	2020
Rheology do's and don'ts	VLAG	2020
7th Conference on FoodTech ^a	Tel Hai College	2020
High moisture extrusion cooking	Foodstream	2021
European School on Rheology	KU Leuven	2021
Science and Technology for Meat Analogues Conference ^a	Wageningen University	2021
Hebrew University course plant-based meat ^a	Hebrew University & GFI	2021
Good Food Conference ^a	GFI	2021
35 th EFFoST International Conference ^a	EFFoST	2021
2 nd Edible Soft Matter Conference ^b	Wageningen University	2022
Summer School Jiangnan University ^a	Jiangnan University	2022
Food Structure & Functionality Symposium ^a	Cork University	2022
Visiting researcher/secondment at Aarhus University	Aarhus University	2022
GFI: The Science of Alt Protein ^a	GFI	2022
Nordic Rheology Conference ^a	Aarhus University	2023
International Symposium on Food Rheology & Structure ^a	Wageningen University	2023
Food Fracture Symposium ^a	Wageningen University	2023
Meat Analogues Technology & Science Course ^a	Wageningen Academy	2023
Free From Food Conference ^a	RAI	2023

General courses	Organizer	Year
Research Data Management	WGS	2020
Scientific Publishing	WGS	2020
Brain Friendly Working	WGS	2020
Competence Assessment	WGS	2020
Scientific Writing	WGS	2021
Supervising BSc & MSc thesis students	WGS	2021
Effective and efficient communication in academia and beyond	WGS	2021
PhD carousel	WGS	2021
Scientific Artwork, Data Visualization, and Inforgraphics with Adobe Illustrator	WGS	2022
Grant Application Course	BCF Courses	2022
Other activities		
Preparation of research proposal	WUR-FPE	2020
Journal club	WUR-FPE	2020
Weekly group meetings ^a	WUR-FPE	2020
GFI project meetings ^a	GFI	2020- 2022
Secretary of Wageningen PhD Council	WPC	2020- 2021
Member of VLAG PhD Council	VLAG	2020- 2022
VLAG PhD Council coaching session	VLAG	2021
Organisation committee Young Scientist Event during the Science & Technology for Meat Analogues Conference	WUR-FPE	2021
PhD study tour ^{a,b}	WUR-FPE	2022

^a Oral presentation

^b Poster presentation

The research described in this thesis was financially supported by The Good Food Institute and VLAG Graduate School.

Cover design by Bram Schlangen and Miek Schlangen

Printed by Proefschriftmaken on recycled paper || www.proefschriftmaken.nl